Title

Testing and Evaluation of Robust Fault Detection and Identification for a Fault Tolerant Automated Highway System: Final Report

Authors
Chen, Robert H.
Ng, Hok K.
Speyer, Jason L.
et al.

Publication Date
2004-11-01

CALIFORNIA PATH PROGRAM
INSTITUTE OF TRANSPORTATION STUDIES
UNIVERSITY OF CALIFORNIA, BERKELEY

Testing and Evaluation of Robust Fault Detection and Identification for a Fault Tolerant Automated Highway System: Final Report

Robert H. Chen, Hok K. Ng,
Jason L. Speyer, D. Lewis Mingori

California PATH Research Report
UCB-ITS-PRR-2004-46

This work was performed as part of the California PATH Program of the University of California, in cooperation with the State of California Business, Transportation, and Housing Agency, Department of Transportation; and the United States Department of Transportation, Federal Highway Administration.

Report for Task Order 4209

November 2004

ISSN 1055-1425

Final Report

Testing and Evaluation of Robust Fault Detection and Identification for a Fault Tolerant Automated Highway System

Agreement No. 65A0071, Task Order 4209

Robert H. Chen, Hok K. Ng, Jason L. Speyer and D. Lewis Mingori

Mechanical and Aerospace Engineering Department
University of California, Los Angeles
Los Angeles, California 90095

Testing and Evaluation of Robust Fault Detection and Identification for a Fault Tolerant Automated Highway System

Agreement No. 65A0071, Task Order 4209

Robert H. Chen, Hok K. Ng, Jason L. Speyer and D. Lewis Mingori

Mechanical and Aerospace Engineering Department
University of California, Los Angeles
Los Angeles, California 90095

September 1, 2004

Summary

This report concerns vehicle fault detection and identification. The design of a vehicle health monitoring system based on analytical redundancy approach is described. A residual generator and a residual processor are designed to detect and identify actuator and sensor faults of the PATH Buick LeSabre. The residual generator, which includes fault detection filters and parity equations, uses the control commands and sensor measurements to generate the residuals which have a unique static pattern in response to each fault. Then, the residual processor interrogates the residuals by matching the residuals to one of several known patterns and computes the probability of each pattern defined hypothesis. The vehicle health monitoring system is first evaluated using simulated data generated by a high-fidelity vehicle simulation. Then, it is evaluated using empirical data recorded when driving a PATH Buick LeSabre at Crow's Landing. Finally, a real-time testing environment is developed using Linux operating system and C language. This allows the vehicle health monitoring system to be evaluated in real-time on a PATH Buick LeSabre. The real-time evaluation at Crow's Landing demonstrates that the vehicle health monitoring system can detect and identify actuator and sensor faults as expected even under various disturbances and uncertainties including sensor noise, road noise, system parameter variations, unmodeled dynamics and nonlinearities.

Contents

List of Figures

Chapter 1

Introduction

This report concerns vehicle fault detection and identification. A vehicle health monitoring approach based on analytical redundancy is described. A system view of vehicle health monitoring is summarized by Figure 1.1. Vehicle dynamics are driven by throttle, brake and steering commands, and various unmeasured exogenous influences such as road noise and actuator faults. Sensors measure a possible nonlinear function of the dynamic states and are corrupted by noise, biases and faults of their own. The vehicle health monitoring system uses the control commands and sensor measurements to generate the conditional probability of each fault hypothesis. The fault hypothesis probabilities are generated in two stages. In the first stage, a residual generator formed as a combination of fault detection filters and parity equations generates the residuals which have a unique static pattern with a given fault or no-fault condition. In the second stage, a residual processor interrogates the residuals by matching the residuals to one of several known patterns. The pattern matching is done with a probabilistically based algorithm so the residual processor generates the fault hypothesis probabilities rather than a simple binary announcement. A simple threshold mapping could be added very easily to produce a binary announcement if that were needed. The fault hypothesis probabilities are passed to a vehicle health management system developed by the UC Berkeley team. The vehicle health management system determines the impact of the possible fault on safe vehicle operation and adjusts control laws if necessary to accommodate a degraded operating condition.

In the previous report, residual generator is developed for the longitudinal dynamics of the vehicle and evaluated in real time on a PATH Buick LeSabre. The result is also included here. In this report, the brake actuator and longitudinal accelerometer fault detection filters are redesigned to enhance the performance. In addition, the residual generator for the lateral dynamics of the ve-

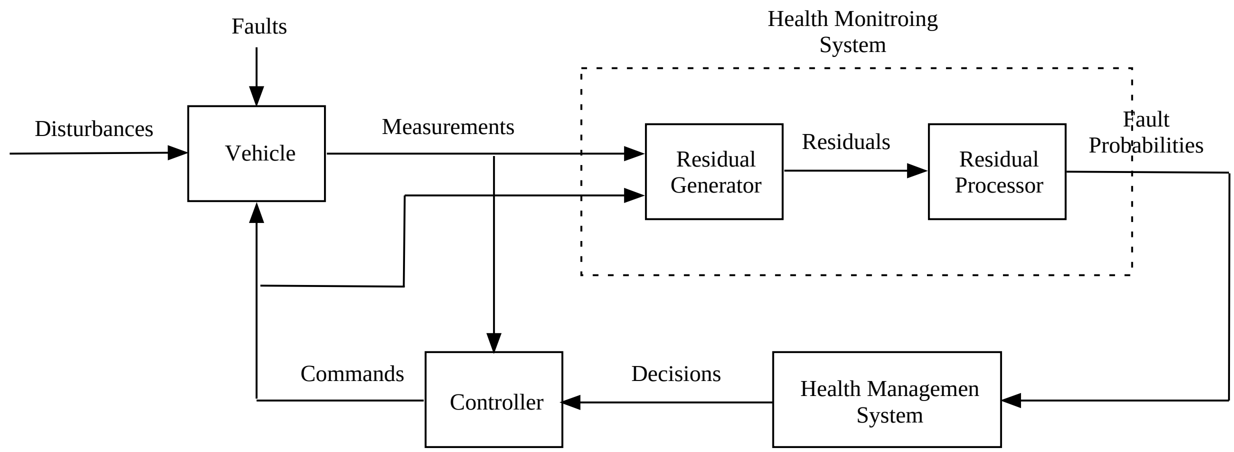

Figure 1.1: A system view of vehicle health monitoring and management

hicle and the residual processor are also developed. Then, the completed vehicle health monitoring system is evaluated in real time on a PATH Buick LeSabre at Crow's Landing.

In Chapter 2, the background of the fault detection filter is briefly discussed. The idea of the fault detection filter is to combine control commands and sensor measurements with known system dynamics to obtain an analytical redundancy. The fault detection filter is designed to have an invariant subspace structure that forces the residual to take on a prescribed and fixed direction in response to a fault. References (Massoumnia, 1986; White and Speyer, 1987; Douglas and Speyer, 1996, 1999) describe the fault detection filter in detail and some of our early results in defining fault detection filter design algorithms.

In Chapter 3, the nonlinear vehicle simulation of the PATH Buick LeSabre is briefly discussed. The PATH Buick LeSabre has two actuators (throttle actuator and brake actuator) and seven sensors (manifold pressure sensor, engine speed sensor, longitudinal accelerometer, front wheel speed sensors, rear wheel speed sensors, throttle sensor and brake sensor) that control or measure the longitudinal dynamics of the vehicle. There are one actuator (steering actuator) and four sensors (lateral accelerometer, yaw rate sensor, front wheel speed sensors and rear wheel speed sensors) that control or measure the lateral dynamics of the vehicle. Since the fault detection filter is model-based, linear vehicle models are derived for the purpose of fault detection filter design.

In Chapter 4, fault detection filters are developed for the longitudinal dynamics of the vehicle to detect and identify the brake actuator, engine speed sensor, longitudinal accelerometer, front wheel speed sensor and rear wheel speed sensor faults. In Chapter 5, fault detection filters are developed for the lateral dynamics of the vehicle to detect and identify the steering actuator, lateral accelerometer, front wheel speed sensor and rear wheel speed sensor faults. In Chapter 6, brake actuator fault detection filters and longitudinal accelerometer fault detection filters are redesigned. Chapter 7, parity equations are developed to detect the throttle actuator, throttle sensor, brake actuator, brake sensor, manifold pressure sensor and engine speed sensor faults. By combining the residuals generated by the fault detection filters and parity equations, the residuals have a unique static pattern in response to each fault. The pattern constructed by the fault detection filters can be used to define fault conditioned hypothesis when the residual processor is designed in Chapter 8. Therefore, a fault in any actuators or sensors on the PATH Buick LeSabre can be detected and identified with probability.

In Chapters 9 and 10, fault detection filters and parity equations designed for the vehicle longitudinal dynamics are first evaluated using simulated data generated by the vehicle simulation. Then, fault detection filters and parity equations are evaluated using empirical data recorded when driving a PATH Buick LeSabre at Crow's Landing. Finally, a real-time testing environment is developed using Linux operating system and C language to evaluate fault detection filters in real-time on a PATH Buick LeSabre. The real-time evaluation at Crow's Landing demonstrates that the fault detection filters can detect and identify actuator and sensor faults as expected even under various disturbances and uncertainties including sensor noise, road noise, system parameter variations, unmodeled dynamics and nonlinearities.

In Chapters 11, the completed vehicle health monitoring system composed of a residual generator and residual processor are first evaluated using simulated data generated by the vehicle simulation and empirical data recorded at Crow' landing. Second, the health monitoring system is evaluated in real-time on a PATH Buick LeSabre when the actuator and sensor faults are simulated and imposed by UCLA laptop. Then, the health monitoring system is evaluated in real-time on a PATH Buick LeSabre when the actuator and sensor faults are directly injected by PATH vehicle computer. In this case, the reaction of the vehicle controller to each fault is encountered when evaluating the health monitoring system. Finally, real steering actuator and real brake actuator faults are created by the driver and the performance of the health monitoring system is evaluated. The real-time evaluation at Crow's Landing demonstrates that the vehicle health monitoring system can detect and identify actuator and sensor fault under various disturbances and uncertainties.

In Chapter 12, the fault detection filter design algorithm (Chen and Speyer, 1999a; Chen *et al.*, 2002) used in Chapter 4 is discussed in detail. The design algorithm is based on an optimization problem where the transmission from the target fault, the fault to be detected, is maximized and the transmission from the nuisance faults, the faults to be blocked, is minimized. Furthermore, the transmission from the sensor noise, process noise and plant uncertainties is minimized. Therefore, the geometric structure of the fault detection filter is approximated in the presence of these disturbances to any degree determined by the designer by using the weightings of the transmissions.

Chapter 2

Fault Detection Filter Background

Any system under automatic control demands a high degree of reliability in order to operate properly. If a fault develops in the plant, the controller will not work properly because it is designed based on the nominal plant. The controller also relies on the health of the sensors and actuators. If a sensor fails, the controller's command will be generated using incorrect measurements. If an actuator fails, the controller's command will not be applied properly to the plant. To avoid these situations, one needs a health monitoring system capable of detecting a fault as it occurs and identifying the faulty component. This process is called fault detection and identification.

The most common approach to fault detection and identification is hardware redundancy which is the direct comparison of the outputs from identical components. This approach requires very little computation. However, hardware redundancy is expensive and limited by space and weight. An alternative is analytical redundancy which uses the modeled dynamic relationship between system inputs and measured system outputs to form a residual process. Nominally, the residual is nonzero only when a fault has occurred and is zero at other times. Therefore, no redundant components are needed. However, additional computation is required.

A popular approach to analytical redundancy is the detection filter which was first introduced by (Beard, 1971) and refined by (Jones, 1973). It is also known as Beard-Jones detection filter. A geometric interpretation and a spectral analysis of the detection filter are given in (Massoumnia, 1986) and (White and Speyer, 1987), respectively. Design algorithms have been developed (Douglas and Speyer, 1996, 1999; Chen and Speyer, 2002) which improve the detection filter robustness. The idea of a detection filter is to place the reachable subspace of each fault into invariant subspaces which do not overlap each other. Then, when a nonzero residual is detected, a fault can be announced and identified by projecting the residual onto each of the invariant subspaces. In this way, multiple faults can be monitored in one filter.

In a related approach, the unknown input observer (Massoumnia *et al.*, 1989; Frank, 1990; Patton and Chen, 1992) simplifies the detection filter problem by dividing the faults into two groups: a single target fault and possibly several nuisance faults. The nuisance faults are placed in an invariant subspace which is unobservable to the residual. Therefore, the residual is only sensitive to the target fault, but not to the nuisance faults. Although only one fault can be monitored in each unknown input observer, there are some benefits. For example, one gains additional flexibility which can be used to improve robustness and time-varying systems can be treated (Chung and Speyer, 1998; Chen and Speyer, 1999a,b, 2000).

In this chapter, the background of the fault detection filter is given. In Section 2.1, the fault models are given. In Section 2.2, the detection filter is briefly discussed. In Section 2.3, the unknown input observer is briefly discussed.

2.1 Fault Modeling

In this section, the models of the plant, actuator and sensor faults are given (Beard, 1971; White and Speyer, 1987; Chung and Speyer, 1998). Consider a linear time-invariant system,

$$\dot{x} = Ax + Bu \tag{2.1a}$$

$$y = Cx \tag{2.1b}$$

where u is the control input and y is the measurement. The ith actuator fault can be modeled as an additive term in the state equation (2.1a) (Beard, 1971; White and Speyer, 1987).

$$\dot{x} = Ax + Bu + F_a\mu_a$$

where F_a is the ith column of B and μ_a is an unknown and arbitrary scalar function of time that is zero when there is no fault. The failure mode μ_a models the time-varying amplitude of the actuator fault while the failure signature F_a models the directional characteristics of the actuator fault. For example, a stuck ith actuator fault can be modeled as $u_i + \mu_a = c$ where u_i is the control command of the ith actuator and c is the position where the ith actuator is stuck. A bias ith actuator fault can be modeled as $\mu_a = c$ where c is the bias. The plant fault can be modeled similarly to the actuator fault by pulling out the corresponding entries in the A matrix.

The ith sensor fault can be modeled as an additive term in the measurement equation (2.1b) (Beard, 1971; White and Speyer, 1987).

$$y = Cx + E_s\mu_s \tag{2.2}$$

where E_s is a column of zeros except a one in the ith position and μ_s is an unknown and arbitrary scalar function of time that is zero when there is no fault. The failure mode μ_s models the time-varying amplitude of the sensor fault while the failure signature E_s models the directional characteristics of the sensor fault. For the purpose of fault detection filter design, an input to the state equation (2.1a) which drives the measurement in the same way that μ_s does in (2.2) is obtained as in (Chung and Speyer, 1998). Define a new state $\bar{x}$,

$$\bar{x} = x + f_s\mu_s$$

where $E_s = Cf_s$. Assume C has full row rank. Then, $f_s = C^{-r}E_s$ where C^{-r} is the right inverse of C. Then, (2.2) can be written as

$$y = C\bar{x}$$

and the dynamic equation of $\bar{x}$ is

$$\dot{\bar{x}} = A\bar{x} + Bu + \begin{bmatrix} f_s & \bar{f}_s \end{bmatrix} \begin{bmatrix} \dot{\mu}_s \\ -\mu_s \end{bmatrix} \tag{2.3}$$

where $\bar{f}_s = Af_s$. Therefore, for fault detection filter design, the sensor fault is modeled as a two-dimensional additive term in the state equation as in (2.3). The interpretation of (2.3) is that $\bar{f}_s$ represents the sensor fault magnitude direction and f_s represents the sensor fault rate direction. This suggests that a possible simplification when information about the spectral content of the sensor fault is available. If it is known that the sensor fault has persistent and significant high frequency components, the fault direction could be approximated by the f_s direction. Or, if it is known that the sensor fault has only low frequency components, such as in the case of a bias, the fault direction could be approximated by the $\bar{f}_s$ direction.

2.2 Beard-Jones Detection Filter

In this section, the detection filter is briefly discussed from the geometric point of view (Massoumnia, 1986; Douglas, 1993). Following the development in Section 2.1, any plant, actuator and sensor fault can be modeled as an additive term in the state equation. Therefore, a linear time-invariant system with q faults can be modeled as

$$\dot{x} = Ax + Bu + \sum_{i=1}^{q} F_i \mu_i \tag{2.4a}$$

$$y = Cx \tag{2.4b}$$

Assume F_i are monic so that $\mu_i \neq 0$ imply $F_i \mu_i \neq 0$.

The detection filter is a linear observer in the form of

$$\dot{\hat{x}} = A\hat{x} + Bu + L(y - C\hat{x}) \tag{2.5}$$

and the residual is

$$r = y - C\hat{x}$$

By using (2.4) and (2.5), the dynamic equation of the error $e = x - \hat{x}$ is

$$\dot{e} = (A - LC)e + \sum_{i=1}^{q} F_i \mu_i$$

and the residual can be written as

$$r = Ce$$

The detection filter gain L is chosen such that $A - LC$ is stable and there exists an invariant subspace $\mathcal{T}_i$ for each fault F_i. $\mathcal{T}_i$ is called the minimal (C, A)-unobservability subspace or the detection space of F_i. Assume (C, A) is observable and the invariant zeros of (C, A, F_i) have the same geometric and algebraic multiplicities. $\mathcal{T}_i$ can be found by

$$\mathcal{T}_i = \mathcal{W}_i \oplus \mathcal{V}_i \tag{2.6}$$

where $\mathcal{W}_i$ is the minimal (C, A)-invariant subspace of F_i given by the recursive algorithm

$$\mathcal{W}_i^0 = 0 \tag{2.7a}$$

$$\mathcal{W}_i^{k+1} = \mathrm{Im} F_i \oplus A(\mathcal{W}_i^k \bigcap \mathrm{Ker}\, C) \tag{2.7b}$$

and $\mathcal{V}_i$ is spanned by the invariant zero directions of (C, A, F_i). When $\dim F_i = 1$, the recursive algorithm (2.7) implies

$$\mathcal{W}_i = \mathrm{Im} \begin{bmatrix} F_i & AF_i & \cdots & A^{k_i} F_i \end{bmatrix}$$

where k_i is the smallest non-negative integer such that $CA^{k_i}F_i \neq 0$.

It is assumed that $C\mathcal{T}_1 \cdots C\mathcal{T}_q$ are independent, that is,

$$C\mathcal{T}_i \cap \sum_{j \neq i} C\mathcal{T}_j = 0$$

If they are not independent, the faults can only be detected, but not identified. This condition is called output separability. If the faults are not output separable, then usually, the designer needs to discard some faults from the design set. It is also assumed that $(C, A, [\,F_1 \cdots F_q\,])$ does not have more invariant zeros than $(C, A, F_1) \cdots (C, A, F_q)$. If it does, the extra invariant zeros will become part of the eigenvalues of $A - LC$. This condition is called mutual detectability. For more details, please refer to (Massoumnia, 1986; Douglas, 1993). For the design algorithms to form the detection filter gain L, please refer to (White and Speyer, 1987; Douglas and Speyer, 1996, 1999; Chen and Speyer, 2002).

When there is no fault, the residual generated by the detection filter is zero after the transient response due to the initial condition error because $A - LC$ is stable. When the fault μ_i occurs, the residual becomes nonzero, but only in the direction of $C\mathcal{T}_i$ because

$$\mathrm{Im} F_i \subseteq \mathcal{T}_i$$

$$(A - LC)\mathcal{T}_i \subseteq \mathcal{T}_i$$

Hence, the fault can be identified by projecting the residual onto each $C\mathcal{T}_i$ by using a projector $\hat{H}_i$ that annihilates $[\,C\mathcal{T}_1 \;\cdots\; C\mathcal{T}_{i-1} \;\; C\mathcal{T}_{i+1} \;\cdots\; C\mathcal{T}_q\,] \stackrel{\triangle}{=} C\hat{\mathcal{T}}_i$.

$$\hat{H}_i : \mathcal{Y} \to \mathcal{Y}\,, \quad \mathrm{Ker}\,\hat{H}_i = C\hat{\mathcal{T}}_i\,, \quad \hat{H}_i = I - C\hat{\mathcal{T}}_i[(C\hat{\mathcal{T}}_i)^T C\hat{\mathcal{T}}_i]^{-1}(C\hat{\mathcal{T}}_i)^T$$

where $\mathcal{Y}$ is the output space. The projected residual $\hat{H}_i r$ is nonzero only when the fault μ_i is nonzero and is zero even when other faults $\mu_{j \neq i}$ are nonzero. Therefore, by monitoring $\hat{H}_1 r \cdots \hat{H}_q r$, every fault can be detected and identified.

2.3 Unknown Input Observer

In this section, the unknown input observer is briefly discussed (Massoumnia *et al.*, 1989). The unknown input observer simplifies the detection filter problem by dividing the faults into two groups: a single target fault and possibly several nuisance faults. Consider a linear time-invariant system with q faults,

$$\dot{x} = Ax + Bu + \sum_{i=1}^{q} \bar{F}_i \bar{\mu}_i \tag{2.8a}$$

$$y = Cx \tag{2.8b}$$

Let $\mu_1 = \bar{\mu}_i$ be the target fault and $\mu_2 = [\,\bar{\mu}_1^T \ \cdots \ \bar{\mu}_{i-1}^T \ \ \bar{\mu}_{i+1}^T \ \cdots \ \bar{\mu}_q^T\,]^T$ be the nuisance fault. Then, (2.8) can be rewritten as

$$\dot{x} = Ax + Bu + F_1\mu_1 + F_2\mu_2 \tag{2.9a}$$

$$y = Cx \tag{2.9b}$$

where $F_1 = \bar{F}_i$ and $F_2 = [\,\bar{F}_1 \ \cdots \ \bar{F}_{i-1} \ \ \bar{F}_{i+1} \ \cdots \ \bar{F}_q\,]$.

The unknown input observer is a linear observer in the form of

$$\dot{\hat{x}} = A\hat{x} + Bu + L(y - C\hat{x}) \tag{2.10}$$

and the residual is

$$r = \hat{H}(y - C\hat{x})$$

By using (2.9) and (2.10), the dynamic equation of the error $e = x - \hat{x}$ is

$$\dot{e} = (A - LC)e + F_1\mu_1 + F_2\mu_2$$

and the residual can be written as

$$r = \hat{H}Ce$$

The unknown input observer gain L is chosen such that $A - LC$ is stable and there exists a detection space $\mathcal{T}_2$ for the nuisance fault F_2. The projector $\hat{H}$ is chosen to annihilate $C\mathcal{T}_2$, i.e.,

$$\hat{H} : \mathcal{Y} \to \mathcal{Y}\,, \quad \operatorname{Ker} \hat{H} = C\mathcal{T}_2\,, \quad \hat{H} = I - C\mathcal{T}_2[(C\mathcal{T}_2)^T C\mathcal{T}_2]^{-1}(C\mathcal{T}_2)^T$$

When there is no fault, the residual generated by the unknown input observer is zero after the transient response due to the initial condition error because $A - LC$ is stable. When the nuisance fault occurs, the residual is still zero because the nuisance fault is contained in $\mathcal{T}_2$ which is unobservable to the residual. When the target fault occurs, the residual is nonzero if F_1 and $\mathcal{T}_2$ are independent. If $\operatorname{Im} F_1 \subseteq \mathcal{T}_2$, the target fault cannot be detected. This condition is similar to the output separability condition, but less restrictive because there is no detection space formed for the target fault. Furthermore, mutual detectability condition is not required because there is only one detection space formed. Therefore, by monitoring the residual, the target fault can be detected. Although only one fault can be monitored in each unknown input observer, there are some benefits. For example, one gains additional flexibility which can be used to improve robustness and time-varying systems can be treated (Chung and Speyer, 1998; Chen and Speyer, 1999a,b, 2000). Note that multiple unknown input observers are needed to detect multiple faults.

2.4 Generalized Shiryayev Sequential Probability Ratio Test

In this section, the Generalized Shiryayev sequential probability ratio test (GSSPRT) (Malladi and Speyer, 1999) is briefly discussed. This test is a generalized result of Speyer and White (Speyer and White, 1984) who approached the change detection problem based on the results of Shiryayev (Shiryayev, 1977) and using a dynamic programming formulation. Under certain condition, this Generalized Shiryayev SPRT detects the change in hypothesis (i.e., occurrence of a disruption) in a sequence of conditionally independent measurements in minimum time. In the dynamic programming formulation, the measurement cost, the cost of false alarm and the cost of miss-alarm are considered. The algorithm is shown to be optimal in infinite time case.

Here, the propagation equation for the posterior probability of disruption conditioned on the measurement sequence will be introduced first. This recursive formula provides the posterior probability of each hypothesis online and also plays a central role in the dynamic programming analysis. Then, the assumptions that made behind the derivation are discussed and investigated when the recursive formula is applied to our application. The propagation equation of the probability of each hypothesis based on the measurement history is shown below.

$$F_{k+1,i} = \frac{P(\theta_i \leq t_{k+1}/X_k) \cdot f_i(x_{k+1})}{\sum_{i=0}^{m} P(\theta_i \leq t_{k+1}/X_k) \cdot f_i(x_{k+1})} \tag{2.11}$$

$$P(\theta_i \leq t_{k+1}/X_k) = F_{ki} + \tilde{p}_i(1 - F_{ki}) \qquad \forall i \neq 0 \tag{2.12}$$

$$P(\theta_0 \leq t_{k+1}/X_k) = \prod_i (1 - P(\theta_i \leq t_{k+1}/X_k)) \qquad \forall i \neq 0 \tag{2.13}$$

$$F_{0,i} = \pi_i \tag{2.14}$$

where

$$
\begin{aligned}
F_{ki}: &\quad P(\theta_i \leq t_k/X_k), \\
\theta_i: &\quad \text{Time of transition to hypothesis } \mathcal{H}_i, \\
X_k: &\quad \text{Measurement history up to } t_k, \\
\tilde{p}_i: &\quad \text{A priori probability of transition to hypothesis } \mathcal{H}_i \text{from } t_k \text{to } t_{k+1} \forall k, \\
f_i(\cdot): &\quad \text{Probability density function of x given } \mathcal{H}_i, \\
m+1: &\quad \text{Number of hypothesis}, \\
\pi_i: &\quad P(\theta_i \leq t_0).
\end{aligned}
$$

The propagation equation (2.11) is derived from Bayes Rule under the following assumptions: The measurement sequence x_k is conditionally independent or equivalently, $P(X_k/\theta_i \leq t_k) = P(x_k/\theta_i \leq t_k)P(x_{k-1}/\theta_i \leq t_k) \cdots P(x_1/\theta_i \leq t_k)$. Which means that the measurement sequence is assumed to be independent when a disruption occured. Furthermore, the statistical properties of the measurements (i.e., the probability density function $f_i(\cdot)$) are assumed known before and after disruption for all hypotheses. The priori transition probability $\tilde{p}_i$ is assumed to be known and constant for all stage. However, the analysis remains the same even if the transition probability is stage dependent. Finally, the a priori probability π_i is also assumed to be known for all hypotheses.

The validity of the above assumptions are investigated when the recursive formula is applied to our application. First, it is likely that each of the residual process generated by the fault detection filter is time correlated. In our application, the collection of residuals generated at each time instant is considered independent static pattern which can be associated to one of the pre-defined hypothesis.

Second, the distribution of the measurement sequence is assumed to be known before and after disruption. In practice, the magnitude of the failure is not known priori. The statistical properties of the distribution defined for all failure hypotheses may not be completely known. To deal with this uncertainty, if one of the parameters α of the density function $f_i(\cdot)$ is not known and assumed to follow its own distribution (i.e., a density function $\psi_\alpha(\cdot)$ defined over Ω), the conditional density function $f_i(\cdot)$ can be formulated as

$$f_i(\cdot) \quad = \quad \int_\Omega f_i(x/\eta) \cdot \psi_\alpha(\eta) \cdot d\eta \tag{2.15}$$

Third, the probability of transition $\tilde{p}_i$ and the a priori probability π_i are not known. Both of them are treated as design parameters. In general, a smaller $\tilde{p}_i$ is chosen when noisy measurement sequence is processed. The a priori probability π_i is assumed to be a small number. These two parameters are not sensitive in the algorithm and should not affect the performance when reasonable values are assumed.

Chapter 3

Vehicle Dynamics

In this chapter, the nonlinear vehicle simulation of the PATH Buick LeSabre is discussed. Since the fault detection filter is model-based, linear vehicle models are derived for the purpose of fault detection filter design. In Section 3.1, the nonlinear vehicle simulation is briefly discussed. In Section 3.2, linear vehicle models are derived numerically from the nonlinear vehicle simulation. In Section 3.3, the sensors installed on the PATH Buick LeSabre and the measurements of the linear vehicle models are listed. In Section 3.4, model reduction is applied to the linear vehicle models. In Section 3.5, the actuator and sensor fault models are derived.

3.1 Nonlinear Vehicle Simulation

A high-fidelity six degree-of-freedom nonlinear vehicle model described in (Douglas *et al.*, 1996, 1997) is used as a starting point. The nonlinear vehicle model has twenty-five states and three control inputs.

States:

x_{m_a} : Manifold air mass.

x_{w_e} : Engine speed.

x_x : Longitudinal position.

x_{v_x} : Longitudinal velocity.

x_y : Lateral position.

x_{v_y} : Lateral velocity.

x_z : Vertical position.

x_{v_z} : Vertical velocity.

x_ϕ : Roll angle.

x_p : Roll rate.

x_θ : Pitch angle.

x_q : Pitch rate.

x_ψ : Yaw angle.

x_r : Yaw rate.

$x_{w_{fl}}$: Front left wheel speed.

$x_{w_{fr}}$: Front right wheel speed.

$x_{w_{rl}}$: Rear left wheel speed.

$x_{w_{rr}}$: Rear right wheel speed.

$x_{l_{fl}}$: Front left suspension length.

$x_{l_{fr}}$: Front right suspension length.

$x_{l_{rl}}$: Rear left suspension length.

$x_{l_{rr}}$: Rear right suspension length.

x_α : Throttle state.

x_{T_b} : Brake state.

x_γ : Steering state.

Control inputs: u_α : Throttle command.

u_{T_b} : Brake command.

u_γ : Steering command.

A computer simulation of this nonlinear vehicle model is implemented in C++ with vehicle parameters chosen for the PATH Buick LeSabre.

3.2 Linear Vehicle Model

Since the fault detection filter is model-based, linear vehicle models are derived for the purpose of fault detection filter design. The linearized dynamics of the vehicle are derived numerically from the nonlinear vehicle simulation using a central differences method. An analytical approach taking partial derivatives is impractical because the nonlinear vehicle model is too complicate. The central differences method is described in detail in (Douglas *et al.*, 1996, 1997). Two linear vehicle models are derived at different nominal operating points where the vehicle is travelling straight ahead on a flat road. The first linearization is done at 20 meters per second which is 45 miles per hour. The second linearization is done at 24 meters per second which is 54 miles per hour. The vehicle is in the third gear for both linearizations.

Since the vehicle is not in a turn, the linear longitudinal dynamics decouple completely from the linear lateral dynamics. The linear longitudinal vehicle model has fourteen states and two control inputs.

States:	x_{m_a}	: Manifold air mass.
	x_{w_e}	: Engine speed.
	x_x	: Longitudinal position.
	x_{v_x}	: Longitudinal velocity.
	x_z	: Vertical position.
	x_{v_z}	: Vertical velocity.
	x_θ	: Pitch angle.
	x_q	: Pitch rate.
	$x_{\bar{w}_f}$	: Sum of front wheel speeds.
	$x_{\bar{w}_r}$	: Sum of rear wheel speeds.
	$x_{\bar{l}_f}$	: Sum of front suspension lengths.
	$x_{\bar{l}_r}$	: Sum of rear suspension lengths.
	x_α	: Throttle state.
	x_{T_b}	: Brake state.
Control inputs:	u_α	: Throttle command.
	u_{T_b}	: Brake command.

The linear lateral vehicle model has eleven states and one control input.

States: x_y : Lateral position.

x_{v_y} : Lateral velocity.

x_ϕ : Roll angle.

x_p : Roll rate.

x_ψ : Yaw angle.

x_r : Yaw rate.

$x_{\tilde{w}_f}$: Difference of front wheel speeds.

$x_{\tilde{w}_r}$: Difference of rear wheel speeds.

$x_{\tilde{l}_f}$: Difference of front suspension lengths.

$x_{\tilde{l}_r}$: Difference of rear suspension lengths.

x_γ : Steering state.

Control input: u_γ : Steering command.

In this report, the fault detection filter is developed for the longitudinal dynamics and lateral dynamics of the vehicle.

3.3 Vehicle Measurements

There are nine sensors installed on the PATH Buick LeSabre that measure the longitudinal dynamics of the vehicle.

y_{m_p} : Manifold pressure sensor.

y_{ω_e} : Engine speed sensor.

y_{a_x} : Longitudinal accelerometer.

$y_{\omega_{fl}}$: Front left wheel speed sensor.

$y_{\omega_{fr}}$: Front right wheel speed sensor.

$y_{\omega_{rl}}$: Rear left wheel speed sensor.

$y_{\omega_{rr}}$: Rear right wheel speed sensor.

y_{α} : Throttle sensor.

y_{T_b} : Brake sensor.

Since the dynamics of the vehicle naturally decompose into longitudinal and lateral components, the following processed wheel speed sensors form a more natural set of measurements:

$y_{\bar{\omega}_f}$: Sum of front wheel speed sensors.

$y_{\bar{\omega}_r}$: Sum of rear wheel speed sensors.

$y_{\tilde{\omega}_f}$: Difference of front wheel speed sensors.

$y_{\tilde{\omega}_r}$: Difference of rear wheel speed sensors.

For the longitudinal dynamics of the vehicle, the wheel speed difference measurements, $y_{\tilde{\omega}_f}$ and $y_{\tilde{\omega}_r}$, are not relevant. Therefore, there are seven measurements associated with the longitudinal dynamics of the vehicle.

y_{m_p} : Manifold pressure sensor.

y_{ω_e} : Engine speed sensor.

y_{a_x} : Longitudinal accelerometer.

$y_{\bar{\omega}_f}$: Sum of front wheel speed sensors.

$y_{\bar{\omega}_r}$: Sum of rear wheel speed sensors.

y_{α} : Throttle sensor.

y_{T_b} : Brake sensor.

Since throttle and brake sensors, y_{α} and y_{T_b}, measure control inputs rather than states, the linear longitudinal vehicle model has only five measurements:

y_{m_p} : Manifold pressure sensor.

y_{ω_e} : Engine speed sensor.

y_{a_x} : Longitudinal accelerometer.

$y_{\bar{\omega}_f}$: Sum of front wheel speed sensors.

$y_{\bar{\omega}_r}$: Sum of rear wheel speed sensors.

There are seven sensors installed on the PATH Buick LeSabre that measure the lateral dynamics of the vehicle.

$$
\begin{aligned}
y_r &: \text{Yaw rate sensor.} \\
y_{a_y} &: \text{Lateral accelerometer.} \\
y_{\omega_{fl}} &: \text{Front left wheel speed sensor.} \\
y_{\omega_{fr}} &: \text{Front right wheel speed sensor.} \\
y_{\omega_{rl}} &: \text{Rear left wheel speed sensor.} \\
y_{\omega_{rr}} &: \text{Rear right wheel speed sensor.} \\
y_\gamma &: \text{Steering sensor.}
\end{aligned}
$$

Since the dynamics of the vehicle naturally decompose into longitudinal and lateral components, the following processed wheel speed sensors form a more natural set of measurements:

$$
\begin{aligned}
y_{\bar{\omega}_f} &: \text{Sum of front wheel speed sensors.} \\
y_{\bar{\omega}_r} &: \text{Sum of rear wheel speed sensors.} \\
y_{\tilde{\omega}_f} &: \text{Difference of front wheel speed sensors.} \\
y_{\tilde{\omega}_r} &: \text{Difference of rear wheel speed sensors.}
\end{aligned}
$$

For the lateral dynamics of the vehicle, the sum of wheel speed measurements, $y_{\bar{\omega}_f}$ and $y_{\bar{\omega}_r}$, are not relevant. Therefore, there are five measurements associated with the lateral dynamics of the vehicle.

$$
\begin{aligned}
y_{a_y} &: \text{Lateral accelerometer.} \\
y_r &: \text{Yaw rate sensor.} \\
y_{\tilde{\omega}_f} &: \text{Difference of front wheel speed sensors.} \\
y_{\tilde{\omega}_r} &: \text{Difference of rear wheel speed sensors.} \\
y_\gamma &: \text{Steering sensor.}
\end{aligned}
$$

Since steering sensors, y_γ, measure control inputs rather than states, the linear lateral vehicle model has only four measurements:

y_{a_y} : Lateral accelerometer.

y_r : Yaw rate sensor.

$y_{\tilde{\omega}_f}$: Difference of front wheel speed sensors.

$y_{\tilde{\omega}_r}$: Difference of rear wheel speed sensors.

3.4 Linear Model Reduction

By examining the linear longitudinal model derived when the vehicle is travelling at 20 m/s, the longitudinal position state x_x is unobservable and therefore is truncated. After the truncation, the thirteenth-order model has eigenvalues: -313.77, -201.40, -90.91, -53.29, -26.95, $-10.12 \pm 15.99i$, $-5.01 \pm 7.59i$, -14.44, -9.75, -1.25 and -0.032. Observe that three of these eigenvalues are significantly faster than the rest. By inspection of the eigenvectors, it is determined that the fast eigenvalues are associated with the states $x_{\bar{\omega}_f}$, $x_{\bar{\omega}_r}$ and x_α. A model reduction is applied by dynamic truncation with a steady-state correction (Prakash, 1994). First, the derivatives of the fast states $x_{\bar{\omega}_f}$, $x_{\bar{\omega}_r}$ and x_α are set to zero. Then, these linear equations are solved for the fast states in terms of the remaining states: x_{m_a}, x_{ω_e}, x_{v_x}, x_z, x_{v_z}, x_θ, x_q, $x_{\bar{l}_f}$, $x_{\bar{l}_r}$ and x_{T_b}. Finally, the result is substituted into the state equations of the remaining states. This process is described in more detail in (Douglas *et al.*, 1996, 1997). The eigenvalues of the reduced-order model are -53.43, -28.37, $-9.43 \pm 16.84i$, $-5.04 \pm 7.42i$, -13.79, -9.74, -1.25 and -0.034 which are close to the eigenvalues of the full-order model. Also, the frequency responses of the reduced-order and full-order models are close to each other. The same procedure is also applied to the linear longitudinal model derived when the vehicle is travelling at 24 m/s. Both reduced-order models are given in Appendix A.

By examining the linear lateral model derived when the vehicle is travelling at 20 m/s, the lateral position state x_y and the yaw angle x_ψ are unobservable and therefore are truncated. After the truncation, the ninth-order model has eigenvalues: -283.30, -198.03, -80.00, $-22.18 \pm 22.45i$, -36.17, $-5.45 \pm 4.46i$, and -8.50. Observe that three of these eigenvalues are significantly faster than the rest. By inspection of the eigenvectors, it is determined that the fast eigenvalues are associated with the states $x_{\tilde{w}_f}$, $x_{\tilde{w}_r}$ and x_γ. A model reduction is applied by dynamic truncation with a steady-state correction (Prakash, 1994). First, the derivatives of the fast states $x_{\tilde{w}_f}$, $x_{\tilde{w}_r}$ and x_γ are set to zero. Then, these linear equations are solved for the fast states in terms of the remaining states:x_{v_y}, x_ϕ, x_p, x_r, $x_{\tilde{l}_f}$ and $x_{\tilde{l}_r}$. Finally, the result is substituted into the state equations of the remaining states. This process is described in more detail in (Douglas *et al.*, 1996, 1997). The eigenvalues of the reduced-order model are $22.64 \pm 22.73i$, -36.16, $-5.12 \pm 4.83i$, -8.41 which are close to the eigenvalues of the full-order model. Also, the frequency responses of the reduced-order and full-order models are close to each other. All the lateral fault detection filters are designed using the linear lateral model derived when the vehicle is travelling at 20 m/s. However, an additional model, which is obtained by modifing this reduced order model, is used to design lateral accelerometer fault detection filter. Both models are given in Appendix A.

3.5 Actuator and Sensor Fault Models

From Section 3.4, the longitudinal dynamics of the vehicle is represented by a tenth-order linear model.

$$\dot{x} = Ax + Bu$$
$$y = Cx$$

where u has two control inputs and y has five measurements. From Section 2.1, the longitudinal dynamics of the vehicle with two actuator and five sensor faults can be modeled as

$$\dot{x} = Ax + Bu + F_{u_\alpha}\mu_{u_\alpha} + F_{u_{T_b}}\mu_{u_{T_b}} + F_{y_{mp}}\mu_{y_{mp}} + F_{y_{we}}\mu_{y_{we}} + F_{y_{a_x}}\mu_{y_{a_x}} + F_{y_{\bar{w}_f}}\mu_{y_{\bar{w}_f}} + F_{y_{\bar{w}_r}}\mu_{y_{\bar{w}_r}}$$
$$y = Cx$$

where $F_{u_\alpha}\mu_{u_\alpha}$ represents the throttle actuator fault, $F_{u_{T_b}}\mu_{u_{T_b}}$ represents the brake actuator fault, $F_{y_{mp}}\mu_{y_{mp}}$ represents the manifold pressure sensor fault, $F_{y_{we}}\mu_{y_{we}}$ represents the engine speed sensor fault, $F_{y_{a_x}}\mu_{y_{a_x}}$ represents the longitudinal accelerometer fault, $F_{y_{\bar{w}_f}}\mu_{y_{\bar{w}_f}}$ represents the front wheel speed sensor fault and $F_{y_{\bar{w}_r}}\mu_{y_{\bar{w}_r}}$ represents the rear wheel speed sensor fault. The actuator fault directions F_{u_α} and $F_{u_{T_b}}$ are one-dimensional. F_{u_α} is the first column of the B matrix and $F_{u_{T_b}}$ is the second column of the B matrix. The sensor fault directions $F_{y_{mp}}$, $F_{y_{we}}$, $F_{y_{a_x}}$, $F_{y_{\bar{w}_f}}$ and $F_{y_{\bar{w}_r}}$ are two-dimensional and obtained by using (2.3). The actuator and sensor fault directions are given in Appendix A.

From Section 3.4, the lateral dynamics of the vehicle is represented by a sixth-order linear model.

$$\dot{x} = Ax + Bu$$
$$y = Cx + Du$$

where u has one control inputs and y has four measurements. Note that the system matrix D of the reduced order model is non zero after the model reduction technique is applied. From Section 2.1, the lateral dynamics of the vehicle with one actuator and four sensor faults can be modeled as

$$\begin{aligned}\dot{x} &= Ax+Bu+F_{u_\gamma}\mu_{u_\gamma}+F_{y_{a_y}}\mu_{y_{a_y}}+F_{y_r}\mu_{y_r}+F_{y_{\tilde{w}_f}}\mu_{y_{\tilde{w}_f}}+F_{y_{\tilde{w}_r}}\mu_{y_{\tilde{w}_r}}\\ y &= Cx + Du\end{aligned}$$

where $F_{u_\gamma}\mu_{u_\gamma}$ represents the steering actuator fault, $F_{y_{a_y}}\mu_{y_{a_y}}$ represents the lateral accelerometer fault, $F_{y_r}\mu_{y_r}$ represents the yaw rate sensor fault, $F_{y_{\tilde{w}_f}}\mu_{y_{\tilde{w}_f}}$ represents the front wheel speed sensor fault and $F_{y_{\tilde{w}_r}}\mu_{y_{\tilde{w}_r}}$ represents the rear wheel speed sensor fault. Since the D matrix is non-zero, the actuator fault directions F_{u_γ} is two-dimensional and obtained by combining the column of the B matrix and direction obtained from (2.3). The sensor fault directions $F_{y_{a_y}}$, F_{y_r}, $F_{y_{\tilde{w}_f}}$ and $F_{y_{\tilde{w}_r}}$ are two-dimensional and obtained by using (2.3). The actuator and sensor fault directions are given in Appendix A.

Chapter 4

Longitudinal Fault Detection Filter Design

In this chapter, fault detection filters are designed to detect and identify actuator and sensor faults for the longitudinal dynamics of the vehicle. From Sections 3.2 and 3.3, there are two actuators and seven sensors on the PATH Buick LeSabre that control or measure the longitudinal dynamics of the vehicle.

Actuators:	u_α	: Throttle actuator.
	u_{T_b}	: Brake actuator.
Sensors:	y_{m_p}	: Manifold pressure sensor.
	y_{w_e}	: Engine speed sensor.
	y_{a_x}	: Longitudinal accelerometer.
	$y_{\bar{w}_f}$	: Sum of front wheel speed sensors.
	$y_{\bar{w}_r}$	: Sum of rear wheel speed sensors.
	y_α	: Throttle sensor.
	y_{T_b}	: Brake sensor.

Since throttle and brake sensors measure control inputs rather than states, the linear longitudinal vehicle model has only five measurements. Therefore, throttle and brake sensor faults cannot be detected by using the fault detection filter. However, they will be detected by using the parity equation in Chapter 7.

From Section 3.5, the linear longitudinal vehicle model with two actuator and five sensor faults is

$$\dot{x} = Ax + Bu + F_{u_\alpha}\mu_{u_\alpha} + F_{u_{T_b}}\mu_{u_{T_b}} + F_{y_{m_p}}\mu_{y_{m_p}} + F_{y_{w_e}}\mu_{y_{w_e}} + F_{y_{a_x}}\mu_{y_{a_x}} + F_{y_{\bar{w}_f}}\mu_{y_{\bar{w}_f}} + F_{y_{\bar{w}_r}}\mu_{y_{\bar{w}_r}}$$
$$y = Cx$$

Fault detection filters were designed based on this vehicle model to detect and identify these seven faults. However, as explained in Section 4.2, fault detection filters designed for the throttle actuator and manifold pressure sensor are not robust when the vehicle operates far from the nominal point. Therefore, fault detection filters are designed to detect and identify only five faults: brake actuator, engine speed sensor, longitudinal accelerometer, front wheel speed sensor and rear wheel speed sensor faults. The throttle actuator and manifold pressure sensor faults will be detected by using the parity equation in Chapter 7.

In Section 4.1, two design considerations that are specific to the fault detection filter design for the longitudinal dynamics of the vehicle are discussed. In Section 4.2, the robustness of the fault detection filter is enhanced through two approaches. In Section 4.3, the five faults to be detected and identified by the fault detection filter are grouped into three sets. In Section 4.4, the design algorithm of the fault detection filter is given. In Section 4.5, the reduced-order fault detection filter is discussed. In Section 4.6, fault detection filters are designed for each set of faults.

4.1 Special Design Considerations

Two design considerations arise that are specific to the fault detection filter design for the longitudinal dynamics of the vehicle. In Section 4.1.1, it is a conditioning problem that arises from the model reduction done in Section 3.4. In Section 4.1.2, it is an output separability problem.

4.1.1 Ill-Conditioned Fault Direction

The first step of the fault detection filter design is to check if the two actuator and five sensor faults are output separable. If the faults are not output separable, they can only be detected, but not identified. In order to check the output separability, the detection space of each fault is obtained by using (2.6). For the throttle actuator and five sensor faults, the detection spaces are given by the fault directions themselves, that is,

$$\mathcal{T}_i = \mathrm{Im} F_i$$

because $CF_i \neq 0$ and (C, A, F_i) does not have any invariant zero. For the brake actuator fault, $CF_{u_{T_b}} \neq 0$ only holds for the reduced-order vehicle model. For the full-order vehicle model, $CF_{u_{T_b}} = 0$. Therefore, $F_{u_{T_b}}$ should be considered as a very weakly observable direction. For the fault detection filter design, a second fault direction $AF_{u_{T_b}}$ is added to the brake actuator fault and its detection space becomes

$$\mathcal{T}_{u_{T_b}} = \text{Im} \begin{bmatrix} F_{u_{T_b}} & AF_{u_{T_b}} \end{bmatrix}$$

The modified brake actuator fault direction is given in Appendix A. Therefore, the dimension of the detection space of the throttle actuator fault is one. The dimension of the detection spaces of the brake actuator and five sensor faults is two.

4.1.2 Output Separability

In order to check the output separability, $C\mathcal{T}_i$ is obtained for each fault. The dimension of $C\mathcal{T}_{u_\alpha}$ is one. The dimension of $C\mathcal{T}_{u_{T_b}}$, $C\mathcal{T}_{y_{mp}}$, $C\mathcal{T}_{y_{we}}$, $C\mathcal{T}_{y_{ax}}$, $C\mathcal{T}_{y_{\bar{w}_f}}$ and $C\mathcal{T}_{y_{\bar{w}_r}}$ is two. The sum of the dimension of each $C\mathcal{T}_i$ is thirteen. Since it is larger than the dimension of the output space which is five, these seven faults are not output separable. Therefore, they are grouped into several sets where the faults in each set are output separable in Section 4.3. Then, fault detection filters are designed for each set of faults in Section 4.6.

Before grouping the faults into several sets, the output separability between each fault is examined, that is,

$$C\mathcal{T}_i \cap C\mathcal{T}_{j \neq i} = 0$$

By examining the singular values of $[\, C\mathcal{T}_i \;\; C\mathcal{T}_{j\neq i} \,]$, every pair of faults is output separable except two pairs. The longitudinal accelerometer fault and rear wheel speed sensor fault are not output separable because $C\mathcal{T}_{y_{ax}}$ and $C\mathcal{T}_{y_{wr}}$ are not independent. Since $C\mathcal{T}_{y_{ax}} \not\subseteq C\mathcal{T}_{y_{wr}}$ and $C\mathcal{T}_{y_{wr}} \not\subseteq C\mathcal{T}_{y_{ax}}$, these two faults can be detected and identified by grouping them into different sets.

The throttle actuator fault and manifold pressure sensor fault are not output separable either. From (2.3), $F_{y_{mp}} = [\, f_{y_{mp}} \;\; \bar{f}_{y_{mp}} \,]$ where $f_{y_{mp}}$ represents the fault rate direction and $\bar{f}_{y_{mp}}$ represents the fault magnitude direction. These two faults are not output separable because $\text{Im}\, F_{u_\alpha} = \text{Im}\, f_{y_{mp}}$. Since $C\mathcal{T}_{u_\alpha} \subset C\mathcal{T}_{y_{mp}}$, grouping these two faults into different sets will not work. One solution is to model the manifold pressure sensor fault as $F_{y_{mp}} = \bar{f}_{y_{mp}}$. Then, these two faults become output separable. However, this design decision could make it difficult to detect a manifold pressure sensor fault that is noisy but with small amplitude. Also, a manifold pressure sensor fault rate will stimulate the throttle actuator residual. However, a throttle actuator fault could never stimulate the manifold pressure sensor residual. In summary, as long as the manifold pressure sensor fault spectral components are low frequency, the throttle actuator fault and manifold pressure sensor fault can be identified.

4.2 Fault Detection Filter Robustness Enhancement

Since the fault detection filter is designed based on the linear model linearized from the nonlinear model at a single nominal point, the filter might not be robust when the vehicle is operating far from the nominal point. In Section 4.2.1, the nonlinearity is modeled as an additive term in the state equation. In Section 4.2.2, the robustness of the fault detection filter is enhanced by considering the nonlinearity as a fault. In Section 4.2.3, the robustness of the fault detection filter is enhanced by decoupling the nonlinearity from the linear model.

4.2.1 Nonlinearity Direction Identification

In this section, the nonlinearity is modeled as an additive term in the state equation (Patton and Chen, 1992; Douglas *et al.*, 2004).

$$\dot{x} = Ax + Bu + F_n\mu_n$$

where F_n represents the nonlinearity direction to be determined and μ_n represents the nonlinearity amplitude. Define $w \triangleq F_n\mu_n$ and assume w is slowly time-varying. Then, the following system can be formed.

$$\begin{bmatrix} \dot{x} \\ \dot{w} \end{bmatrix} = \begin{bmatrix} A & I \\ 0 & 0 \end{bmatrix} \begin{bmatrix} x \\ w \end{bmatrix} + \begin{bmatrix} B \\ 0 \end{bmatrix} u$$
$$x = \begin{bmatrix} I & 0 \end{bmatrix} \begin{bmatrix} x \\ w \end{bmatrix}$$

An observer based on this system can be obtained.

$$\begin{bmatrix} \dot{\hat{x}} \\ \dot{\hat{w}} \end{bmatrix} = \begin{bmatrix} A & I \\ 0 & 0 \end{bmatrix} \begin{bmatrix} \hat{x} \\ \hat{w} \end{bmatrix} + \begin{bmatrix} B \\ 0 \end{bmatrix} u + L\left(x - \begin{bmatrix} I & 0 \end{bmatrix} \begin{bmatrix} \hat{x} \\ \hat{w} \end{bmatrix}\right)$$

where the observer gain L is chosen to make the observer stable. The inputs of the observer, u and x, are determined as followed. First, the control input u is chosen as a step. Then, this control input is applied to the nonlinear vehicle simulation to obtain the state x. Finally, u and x are applied to the observer to estimate w. After the transient response, $\hat{w}$ becomes a constant vector and F_n is the normalized $\hat{w}$. By choosing u as different step and sinusoidal functions, several F_n's are obtained. By examining all F_n's, it seems that the most important directions are

$$F_{n_2} = \begin{bmatrix} 1 & 0 & 0 & 0 & 0 & 0 & 0 & 0 & 0 & 0 \\ 0 & 1 & 0 & 0 & 0 & 0 & 0 & 0 & 0 & 0 \end{bmatrix}^T \tag{4.1}$$

This indicates that the state equations of the manifold air mass and engine speed states are most nonlinear among the ten states. It also indicates that the dynamics of the engine are more nonlinear than the rest of the longitudinal dynamics of the vehicle.

4.2.2 Nonlinearity Fault

In this section, the robustness of the fault detection filter is enhanced by considering the nonlinearity as a fault.

$$\dot{x} = Ax + Bu + F_n \mu_n$$

where $F_n = F_{n_2}$ represents the apriori known nonlinearity fault direction and μ_n represents the unknown and arbitrary nonlinearity fault amplitude. Since the nonlinearity is considered as a fault, the fault detection filter will place the nonlinearity into an invariant subspace. Hence, the nonlinearity is isolated from the actuator and sensor faults and does not affect the residuals used for detecting and identifying these faults. Therefore, the robustness of the fault detection filter is enhanced.

It is desired to model the nonlinearity as a fault whose dimension is as small as possible because the number of the faults that can be identified by a fault detection filter is limited due to the output separability condition. Therefore, it is desired to obtain a one-dimensional nonlinearity fault direction from (4.1). Different linear combinations of the two directions in (4.1) have been used to represent the nonlinearity for the fault detection filter design. It is found that by using F_n as

$$F_{n_1} = \begin{bmatrix} 1 & 0 & 0 & 0 & 0 & 0 & 0 & 0 & 0 & 0 \end{bmatrix}^T \tag{4.2}$$

the fault detection filter is most robust. However, the nonlinearity fault and throttle actuator fault are not output separable because $\operatorname{Im} F_{n_1} = \operatorname{Im} F_{u_\alpha}$. Therefore, this approach can only be used to enhance the robustness of the fault detection filter that detects and identifies the brake actuator and five sensor faults. (4.2) indicates that the state equation of the manifold air mass state is most nonlinear among the ten states. It also indicates that the nonlinearity affects the longitudinal dynamics of the vehicle in a way similar to the throttle actuator fault. Hence, it is difficult to identify the throttle actuator fault from the nonlinearity by using the fault detection filter. Therefore, the throttle actuator fault will be detected by using the parity equation in Chapter 7.

For fault detection filters that detect the brake actuator and manifold pressure sensor faults, they are still not robust even with the nonlinearity modeled by F_{n_1}. For the brake actuator fault, the robustness of the fault detection filter can further be enhanced by modeling the nonlinearity with F_{n_2} which includes F_{n_1}. Now the fault detection filter that detects the brake actuator fault becomes robust. For manifold pressure sensor fault, the nonlinearity cannot be modeled by F_{n_2} because these two faults are not output separable, i.e., $\operatorname{Im} F_{n_2} = \operatorname{Im} F_{y_{mp}}$. (4.1) indicates that the nonlinearity affects the longitudinal dynamics of the vehicle in a way similar to the manifold pressure sensor fault which includes the throttle actuator fault. Hence, it is difficult to identify the manifold pressure sensor fault from the nonlinearity by using the fault detection filter. Therefore, the manifold pressure sensor fault will be detected by using the parity equation in Chapter 7.

In summary, fault detection filters will be designed to detect and identify five faults: brake actuator, engine speed sensor, longitudinal accelerometer, front wheel speed sensor and rear wheel speed sensor faults. For the four sensor faults, the nonlinearity is modeled as the fault F_{n_1}. For the brake actuator fault, the nonlinearity is modeled as the fault F_{n_2}. The throttle actuator and manifold pressure sensor faults will be detected by using the parity equation in Chapter 7.

4.2.3 Nonlinearity Decoupling

In this section, the robustness of the fault detection filter is enhanced by decoupling the nonlinearity from the linear model. From Section 3.4, the longitudinal dynamics of the vehicle is represented by a tenth-order linear model.

$$\dot{x} = Ax + Bu \tag{4.3a}$$

$$y = Cx \tag{4.3b}$$

Since (4.2) indicates that the state equation of the manifold air mass state is most nonlinear among the ten states, (4.3) is rewritten as

$$\begin{bmatrix} \dot{x}_{m_a} \\ \dot{\bar{x}} \end{bmatrix} = \begin{bmatrix} A_{11} & A_{12} \\ A_{21} & A_{22} \end{bmatrix} \begin{bmatrix} x_{m_a} \\ \bar{x} \end{bmatrix} + \begin{bmatrix} B_1 & 0 \\ 0 & B_2 \end{bmatrix} \begin{bmatrix} u_\alpha \\ u_{T_b} \end{bmatrix} \tag{4.4a}$$

$$\begin{bmatrix} y_{m_p} \\ \bar{y} \end{bmatrix} = \begin{bmatrix} C_1 & 0 \\ 0 & C_2 \end{bmatrix} \begin{bmatrix} x_{m_a} \\ \bar{x} \end{bmatrix} \tag{4.4b}$$

where $\bar{x}$ and $\bar{y}$ contain all the states and measurements except manifold air mass and manifold pressure, respectively. Note that C_1 is a scalar. From the second row of (4.4a) and (4.4b), a subsystem that is decoupled from the nonlinearity associated with the manifold air mass state is formed.

$$\dot{\bar{x}} = A_{22}\bar{x} + \begin{bmatrix} \frac{A_{21}}{C_1} & B_2 \end{bmatrix} \begin{bmatrix} y_{m_p} \\ u_{T_b} \end{bmatrix} \tag{4.5a}$$

$$\bar{y} = C_2\bar{x} \tag{4.5b}$$

Note that the throttle command is no longer an input and the manifold pressure measurement is now an input. Since the nonlinearity associated with the manifold air mass state is completely decoupled, the robustness of the fault detection filter designed based on this subsystem should improve. However, the throttle actuator fault cannot be detected because this subsystem is independent of the throttle command. Therefore, this subsystem can only be used to design fault detection filters that detect and identify the brake actuator and five sensor faults. Note that this approach of enhancing the robustness of the fault detection filter is similar to the approach of considering the nonlinearity as the fault F_{n_1} in the sense that both approaches reduce the effect of the nonlinearity associated with the manifold air mass state. However, there is no output separability issue between the throttle actuator fault and manifold pressure sensor fault if (4.5) is used.

Since (4.1) indicates that the state equation of the engine speed state is second most nonlinear after the manifold air mass state, it may be desired to decouple the nonlinearity associated with the engine speed state in addition to the manifold air mass state from the linear model. Therefore, (4.3) is rewritten as

$$\begin{bmatrix} \dot{x}_1 \\ \dot{x}_2 \end{bmatrix} = \begin{bmatrix} \tilde{A}_{11} & \tilde{A}_{12} \\ \tilde{A}_{21} & \tilde{A}_{22} \end{bmatrix} \begin{bmatrix} x_1 \\ x_2 \end{bmatrix} + \begin{bmatrix} \tilde{B}_1 & 0 \\ 0 & \tilde{B}_2 \end{bmatrix} \begin{bmatrix} u_\alpha \\ u_{T_b} \end{bmatrix} \tag{4.6a}$$

$$\begin{bmatrix} y_1 \\ y_2 \end{bmatrix} = \begin{bmatrix} \tilde{C}_1 & 0 \\ 0 & \tilde{C}_2 \end{bmatrix} \begin{bmatrix} x_1 \\ x_2 \end{bmatrix} \tag{4.6b}$$

where

$$
\begin{aligned}
x_1 &= \left[\begin{array}{cc} x_{m_a} & x_{w_e} \end{array} \right]^T \\
x_2 &= \left[\begin{array}{cccccccc} x_{v_x} & x_z & x_{v_z} & x_\theta & x_q & x_{\bar{l}_f} & x_{\bar{l}_r} & x_{T_b} \end{array} \right]^T \\
y_1 &= \left[\begin{array}{cc} y_{m_p} & y_{w_e} \end{array} \right]^T \\
y_2 &= \left[\begin{array}{ccc} y_{a_x} & y_{\bar{l}_f} & y_{\bar{l}_r} \end{array} \right]^T
\end{aligned}
$$

From the second row of (4.6a) and (4.6b), a subsystem that is decoupled from the nonlinearity associated with the manifold air mass and engine speed states is formed.

$$\dot{x}_2 = \tilde{A}_{22}x_2 + \left[\begin{array}{cc} \tilde{A}_{21}\tilde{C}_1^{-1} & \tilde{B}_2 \end{array} \right] \left[\begin{array}{c} y_1 \\ u_{T_b} \end{array} \right] \tag{4.7a}$$

$$y_2 = \tilde{C}_2 x_2 \tag{4.7b}$$

Note that the throttle command is no longer an input and the engine speed measurements is now an input. The manifold pressure measurement is not an input because the first column of $\tilde{A}_{21}\tilde{C}_1^{-1}$ is zero. Since the nonlinearity associated with the manifold air mass and engine speed states is completely decoupled, the robustness of the fault detection filter designed based on this subsystem should further improve. However, the throttle actuator and manifold pressure sensor faults cannot be detected because this subsystem is independent of the throttle command and manifold pressure measurement. Furthermore, the fault detection filter designed based on this subsystem can identify less number of faults than the fault detection filter designed based on (4.5) because (4.7) has less number of measurements than (4.5). Note that this approach of enhancing the robustness of the fault detection filter is similar to the approach of considering the nonlinearity as the fault F_{n_2} in the sense that both approaches reduce the effect of the nonlinearity associated with the manifold air mass and engine speed states.

4.3 Fault Configuration

In this section, the approach in Section 4.2.2 is used to enhance the robustness of the fault detection filter, i.e., to consider the nonlinearity as a fault. There are five faults to be detected and identified by the fault detection filter: brake actuator, engine speed sensor, longitudinal accelerometer, front wheel speed sensor and rear wheel speed sensor faults. Since the sum of the dimensions of $C\mathcal{T}_{u_{T_b}}$, $C\mathcal{T}_{y_{w_e}}$, $C\mathcal{T}_{y_{a_x}}$, $C\mathcal{T}_{y_{\bar{w}_f}}$ and $C\mathcal{T}_{y_{\bar{w}_r}}$ is ten which is larger than the dimension of the output space which is five, these five faults are not output separable. Therefore, they are grouped into several sets where the faults in each set are output separable. Note that the nonlinearity is modeled as the fault F_{n_1} for the four sensor faults and F_{n_2} for the brake actuator fault.

Since $C\mathcal{T}_{F_{n_1}} = 1$, the four sensor faults are grouped into two sets where each set has two sensor faults and F_{n_1}. From Section 4.1.2, the longitudinal accelerometer fault and rear wheel speed sensor fault cannot be in the same set because they are not output separable. Then, there are two possible combinations to group these four faults. The first combination is to put F_{w_e} and F_{a_x} in one set; F_{w_f} and F_{w_r} in the other. The other combination is to put F_{w_e} and F_{w_r} in one set; F_{a_x} and F_{w_f} in the other. Note that all four sets of faults are not mutually detectable, but with the extra invariant zeros in the left-half plane. In next section, fault detection filters are designed using the first combination for no particular reason.

Since $C\mathcal{T}_{F_{n_2}} = 2$, the brake actuator fault cannot be grouped with any of the sensor faults because of the output separability condition. Therefore, the brake actuator fault is paired with a sensor fault which is modeled only by its fault magnitude direction. The rear wheel speed sensor fault is chosen for no particular reason. This design decision could allow the rear wheel speed sensor fault rate to stimulate the brake actuator residual because it is not placed in an invariant subspace. However, since the rear wheel speed sensor fault is also detected by another fault detection filter, the brake actuator fault can be detected and identified.

In summary, the three fault detection filter sets are

Fault detection filter set no. 1	y_{w_e}	: Engine speed sensor.
	y_{a_x}	: Longitudinal accelerometer.
	n_1	: Nonlinearity.
Fault detection filter set no. 2	$y_{\bar{\omega}_f}$	: Front wheel speed sensors.
	$y_{\bar{\omega}_r}$	: Rear wheel speed sensors.
	n_1	: Nonlinearity.
Fault detection filter set no. 3	u_{T_b}	: Brake actuator.
	$y_{\bar{\omega}_r}$	: Rear wheel speed sensors (magnitude direction only).
	n_2	: Nonlinearity.

This fault configuration can also be used for the fault detection filter design by not including the nonlinearity if the approach in Section 4.2.3 is used to enhance the robustness of the fault detection filter, i.e., to decouple the nonlinearity from the linear model.

4.4 Fault Detection Filter Design Algorithm

In this section, a design algorithm of the fault detection filter is given. The fault detection filter designed for the PATH Buick LeSabre is the unknown input observer because it is more robust than Beard-Jones detection filter with respect to the nonlinearity that occurs when the vehicle operates far from the nominal point. However, one unknown input observer is needed for detecting one fault.

From Section 2.3, consider a linear time-invariant system,

$$\dot{x} = Ax + Bu + F_1\mu_1 + F_2\mu_2 \tag{4.8a}$$

$$y = Cx \tag{4.8b}$$

where F_1 is the target fault to be detected and F_2 is the nuisance fault to be blocked. The unknown input observer is a linear observer in the form of

$$\dot{\hat{x}} = A\hat{x} + Bu + L(y - C\hat{x}) \tag{4.9a}$$

and the residual is

$$r = \hat{H}(y - C\hat{x}) \tag{4.9b}$$

One design algorithm (Chen and Speyer, 1999a; Chen *et al.*, 2002) for the unknown input observer is to maximize the sensitivity of the residual to the target fault using the weighting Q_1 and minimize the sensitivity of the residual to the nuisance fault using the weightings Q_2 and γ. Furthermore, the sensitivity of the residual to the sensor noise is minimized using the weighting V. The unknown input observer gain L is derived by solving an algebraic Riccati equation

$$0 = AP + PA^T - PC^TV^{-1}CP + \frac{1}{\gamma}F_2Q_2F_2^T - F_1Q_1F_1^T \tag{4.10}$$

and

$$L = PC^TV^{-1} \tag{4.11}$$

The projector $\hat{H}$ is obtained by

$$\hat{H} = I - C\mathcal{T}_2[(C\mathcal{T}_2)^T C\mathcal{T}_2]^{-1}(C\mathcal{T}_2)^T \tag{4.12}$$

where $\mathcal{T}_2$ is the detection space of the nuisance fault. More details of this design algorithm are given in Chapter 12.

4.5 Reduced-Order Fault Detection Filter

In this section, the reduced-order fault detection filter is derived for (4.9). From Chapter 12, the unknown input observer places the nuisance fault into its detection space which is unobservable to the residual in the limit when $\gamma \to 0$. Therefore, the nuisance fault is completely blocked from the residual. Furthermore, a reduced-order unknown input observer can be obtained by truncating the unobservable subspace. Note that the eigenvalues of the unknown input observer associated with the unobservable subspace go to $-\infty$. When it is not in the limit (i.e., γ is small), the nuisance fault is partially blocked and the unknown input observer has some fast eigenvalues associated with some weakly observable states. These weakly observable states approximate the detection space of the nuisance fault. Therefore, model reduction is needed to reduce the order of the unknown input observer when it is not in the limit. In Section 4.5.1, the reduced-order unknown input observer is derived by identifying and truncating the weakly observable states. In Section 4.5.2, the reduced-order unknown input observer is derived by using balance realization.

4.5.1 Weakly Observable State Truncation

In this section, the reduced-order unknown input observer is derived for (4.9) by identifying and truncating the weakly observable states. The unknown input observer (4.9a) and the residual (4.9b) are rewritten as

$$\dot{\hat{x}} = \bar{A}\hat{x} + \bar{B}\begin{bmatrix} u \\ y \end{bmatrix} \tag{4.13a}$$

$$r = \bar{C}\hat{x} + \bar{D}\begin{bmatrix} u \\ y \end{bmatrix} \tag{4.13b}$$

where $\bar{A} = A - LC$, $\bar{B} = [\, B \;\; L \,]$, $\bar{C} = -\hat{H}C$ and $\bar{D} = [\, 0 \;\; \hat{H} \,]$. By applying a state transformation

$$\hat{x}_T = T\hat{x}$$

where $T = U^T$ and U is the left singular vectors of the observability grammian of $(\bar{C}, \bar{A})$, i.e.,

$$W_o = \int_0^\infty e^{\bar{A}^T t}\bar{C}^T\bar{C}e^{\bar{A}t}\,dt \triangleq U\Sigma U^T$$

(4.13) becomes

$$\dot{\hat{x}}_T = T\bar{A}T^T\hat{x}_T + T\bar{B}\begin{bmatrix} u \\ y \end{bmatrix} \tag{4.14a}$$

$$r = \bar{C}T^T\hat{x}_T + \bar{D}\begin{bmatrix} u \\ y \end{bmatrix} \tag{4.14b}$$

and its observability grammian is

$$\begin{aligned}&\int_0^\infty e^{T\bar{A}^T T^T t}T\bar{C}^T\bar{C}T^T e^{T\bar{A}T^T t}\,dt = \int_0^\infty Te^{\bar{A}^T t}T^T T\bar{C}^T\bar{C}T^T Te^{\bar{A}t}T^T\,dt \\ &= T\int_0^\infty e^{\bar{A}^T t}\bar{C}^T\bar{C}e^{\bar{A}t}\,dtT^T = TW_oT^T = \Sigma\end{aligned}$$

Therefore, the states of the unknown input observer are rearranged in the order from most observable to least observable. The degrees of the observability of the states are indicated by the singular values of W_o, i.e., the diagonal elements of Σ. If some singular values are significant smaller than the others, the states associated with the small singular values are weakly observable and might be truncated. Therefore, (4.14) is partitioned as

$$\begin{bmatrix} \dot{\hat{x}}_{T1} \\ \dot{\hat{x}}_{T2} \end{bmatrix} = \begin{bmatrix} \bar{A}_{11} & \bar{A}_{12} \\ \bar{A}_{21} & \bar{A}_{22} \end{bmatrix}\begin{bmatrix} \hat{x}_{T1} \\ \hat{x}_{T2} \end{bmatrix} + \begin{bmatrix} \bar{B}_1 \\ \bar{B}_2 \end{bmatrix}\begin{bmatrix} u \\ y \end{bmatrix}$$

$$r = \begin{bmatrix} \bar{C}_1 & \bar{C}_2 \end{bmatrix}\begin{bmatrix} \hat{x}_{T1} \\ \hat{x}_{T2} \end{bmatrix} + \bar{D}\begin{bmatrix} u \\ y \end{bmatrix}$$

where $\hat{x}_{T1}$ is the states associated with the large singular values and $\hat{x}_{T2}$ is the states associated with the small singular values. Then, the reduced-order unknown input observer is derived by truncating the states $\hat{x}_{T2}$.

$$\dot{\hat{x}}_{T1} = \bar{A}_{11}\hat{x}_{T1} + \bar{B}_1\begin{bmatrix} u \\ y \end{bmatrix}$$

$$r = \bar{C}_1\hat{x}_{T1} + \bar{D}\begin{bmatrix} u \\ y \end{bmatrix}$$

4.5.2 Balance Realization

In this section, the reduced-order unknown input observer is derived for (4.9) by using balance realization (Moore, 1981). Instead of only considering the system observability as in Section 4.5.1, balance realization considers both system controllability and observability. The use of balance realization to the unknown input observer is different from the use of balance realization to the plant. For the plant, the controllability is associated with the control inputs for the purpose of the controller design and the observability is associated with the measurements for the purpose of the observer design. However, the unknown input observer is already a design product whose purpose is to detect the target fault using the residual. Therefore, for the unknown input observer, the controllability should be associated with the target fault and the observability should be associated with the residual even though the inputs of the unknown input observer are control commands and measurements. This becomes clear when the residual is written in terms of the error $e = x - \hat{x}$ by using (4.8) and (4.9) in the absence of the nuisance fault.

$$\dot{e} = (A - LC)e + F_1\mu_1 \tag{4.15a}$$

$$r = \hat{H}Ce \tag{4.15b}$$

Therefore, balance realization is applied to (4.15) which becomes

$$\begin{aligned} \dot{e}_T &= T(A - LC)T^T e_T + TF_1\mu_1 \\ r &= \hat{H}CT^T e_T \end{aligned}$$

where $e_T = Te$ and T is the transformation that makes the controllability grammian of $(T(A - LC)T^T, TF_1)$ and the observability grammian of $(\hat{H}CT^T, T(A - LC)T^T)$ equal and diagonal. T can be found by using the function "balreal" in MATLAB. The error is rearranged in the order from most controllable and observable to least controllable and observable. The degree of the controllability and observability of the error is indicated by the hankel singular values, i.e., the diagonal elements of the controllability and observability grammians. If some hankel singular values are significantly smaller than the others, the error associated with the small hankel singular values is weakly controllable and observable, and might be truncated. Therefore, the transformation T is applied to the unknown input observer (4.13) and the last few states associated with the smallest hankel singular values can be truncated by following the same procedure in Section 4.5.1.

4.6 Fault Detection Filter Design

In this section, fault detection filters are designed for the three sets of faults determined in Section 4.3 by using the design algorithm in Section 4.4 and the model reduction techniques in Section 4.5. In Section 4.6.1, two unknown input observers are designed for the first set of faults which are the engine speed sensor and longitudinal accelerometer faults. In Section 4.6.2, two unknown input observers are designed for the second set of faults which are the front wheel speed sensor and rear wheel speed sensor faults. In Section 4.6.3, two unknown input observers are designed for the third set of faults which are the brake actuator and rear wheel speed sensor magnitude faults.

4.6.1 Fault Detection Filter Set No. 1

In this section, one unknown input observer is designed to detect the engine speed sensor fault and one unknown input observer is designed to detect the longitudinal accelerometer fault. From Sections 3.5 and 4.2.2, the linear longitudinal vehicle model with engine speed sensor, longitudinal accelerometer and nonlinearity faults is

$$\begin{aligned} \dot{x} &= Ax + Bu + F_{y_{w_e}}\mu_{y_{w_e}} + F_{y_{a_x}}\mu_{y_{a_x}} + F_{n_1}\mu_{n_1} \\ y &= Cx \end{aligned}$$

where A, B, C, $F_{y_{w_e}}$ and $F_{y_{a_x}}$ are derived when the vehicle is travelling at 24 m/s and given in Appendix A.2. F_{n_1} is given by (4.2).

For the first unknown input observer,

$$\begin{aligned} \dot{\hat{x}} &= A\hat{x} + Bu + L(y - C\hat{x}) \\ r &= \hat{H}(y - C\hat{x}) \end{aligned}$$

The target fault is the engine speed sensor fault $F_1 = F_{y_{w_e}}$ and the nuisance fault is the nonlinearity and longitudinal accelerometer faults $F_2 = [\, F_{n_1} \;\; F_{y_{a_x}} \,]$. For the unknown input observer design, $F_2 = [\, F_{u_\alpha} \;\; F_{y_{a_x}} \,]$ is used because $\operatorname{Im} F_{n_1} = \operatorname{Im} F_{u_\alpha}$. The weighting of the target fault is chosen as $Q_1 = 0.1 I_2$. The weightings of the nuisance fault are chosen as $Q_2 = I_3$ and $\gamma = 10^{-8}$. The weighting of the sensor noise is chosen as $V = I_5$. The unknown input observer gain L is obtained by solving the Riccati equation (4.10) and (4.11). The projector $\hat{H}$ is obtained by using (4.12) where $\mathcal{T}_2 = [\, \mathcal{T}_{u_\alpha} \;\; \mathcal{T}_{y_{a_x}} \,]$. The Riccati matrix P, unknown input observer gain L and projector $\hat{H}$ are given in Appendix B.1.

The eigenvalues of the unknown input observer are $-1.826 \cdot 10^8$, $-5.044 \cdot 10^5$, $-9.998 \cdot 10^3$, -59.386, -25.301, $-7.175 \pm 8.948i$, -6.926, -4.003 and -1.250. Observe that three of these eigenvalues are significantly faster than the rest because γ is very small and the dimension of the detection space of the nuisance fault is three. Furthermore, the singular values of the observability grammian of the unknown input observer are $4.04 \cdot 10^4$, $1.44 \cdot 10^4$, 45.11, 12.87, 0.17, $6.29 \cdot 10^{-3}$, $6.10 \cdot 10^{-7}$, $1.31 \cdot 10^{-13}$, $1.40 \cdot 10^{-15}$ and $6.73 \cdot 10^{-21}$. Observe that three of these singular values are significantly smaller than the rest. Therefore, the model reduction technique in Section 4.5.1 is used to truncate the three least observable states of the unknown input observer. The reduced-order unknown input observer is

$$\begin{aligned} \dot{\hat{x}}_r &= A_r \hat{x}_r + B_r \begin{bmatrix} u \\ y \end{bmatrix} \\ r &= C_r \hat{x}_r + D_r \begin{bmatrix} u \\ y \end{bmatrix} \end{aligned}$$

where A_r, B_r, C_r, and D_r are given in Appendix B.1. The eigenvalues of the reduced-order observer are -59.387, -25.301, $-7.175 \pm 8.948i$, -6.926, -4.003 and -1.250 which are closed to the full-order observer. The frequency response from the engine speed sensor and longitudinal accelerometer faults to the residuals is shown in Figure 4.1. The left figure is the full-order observer and the right figure is the reduced-order observer. The solid line represents the engine speed sensor fault and the dotted line represents the longitudinal accelerometer fault. Figure 4.1 shows that both observers can detect the engine speed sensor fault and block the longitudinal accelerometer fault.

For the second unknown input observer, the target fault is the longitudinal accelerometer fault $F_1 = F_{y_{a_x}}$ and the nuisance fault is the nonlinearity and engine speed sensor faults $F_2 = [\, F_{u_\alpha} \;\; F_{y_{w_e}} \,]$ because $\operatorname{Im} F_{n_1} = \operatorname{Im} F_{u_\alpha}$. The weightings are chosen as

$$Q_1 = 0I_2\,, \quad Q_2 = I_3\,, \quad \gamma = 10^{-8}\,, \quad V = \begin{bmatrix} 1 & 0 & 0 & 0 & 0 \\ 0 & 1 & 0 & 0 & 0 \\ 0 & 0 & 10^{-2} & 0 & 0 \\ 0 & 0 & 0 & 10^3 & 0 \\ 0 & 0 & 0 & 0 & 10^5 \end{bmatrix}$$

The unknown input observer gain L is obtained by solving the Riccati equation (4.10) and (4.11). The projector $\hat{H}$ is obtained by using (4.12) where $\mathcal{T}_2 = [\, \mathcal{T}_{u_\alpha} \;\; \mathcal{T}_{y_{w_e}} \,]$. The Riccati matrix P, unknown input observer gain L and projector $\hat{H}$ are given in Appendix B.1.

The eigenvalues of the unknown input observer are $-2.030 \cdot 10^6$, $-5.044 \cdot 10^5$, $-9.595 \cdot 10^3$, -14.229, $-10.790 \pm 17.647i$, $-7.597 \pm 0.591i$, -1.370 and -1.216. Observe that three of these eigenvalues are significantly faster than the rest because γ is very small and the dimension of the

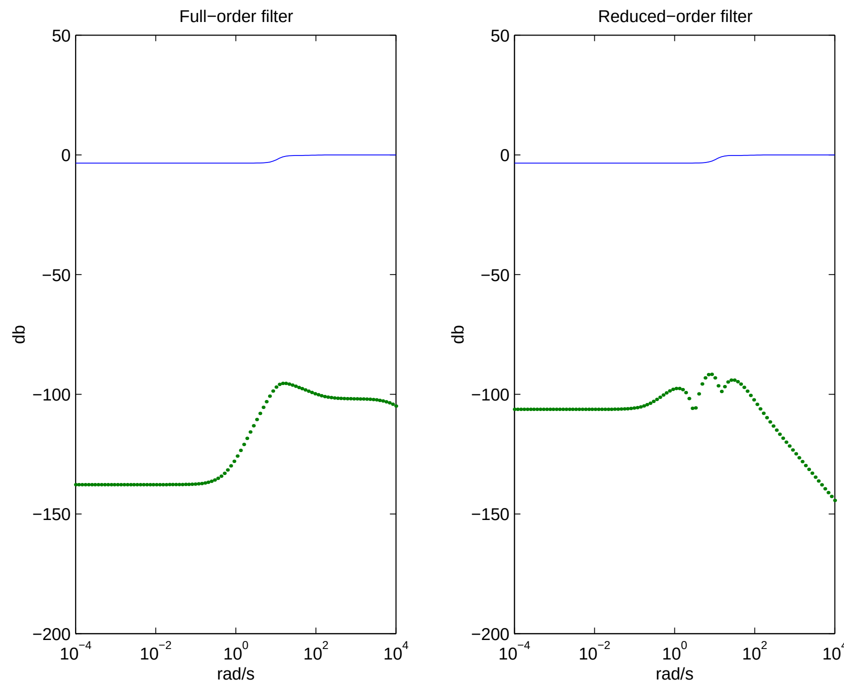

Figure 4.1: Frequency response of the unknown input observer that detects the engine speed sensor fault

detection space of the nuisance fault is three. Furthermore, the singular values of the observability grammian of the unknown input observer are $1.50 \cdot 10^4$, $5.99 \cdot 10^3$, 16.33, 4.22, 0.24, $5.57 \cdot 10^{-2}$, $2.64 \cdot 10^{-3}$, $3.28 \cdot 10^{-11}$, $3.75 \cdot 10^{-13}$ and $9.82 \cdot 10^{-16}$. Observe that three of these singular values are significantly smaller than the rest. Therefore, the model reduction technique in Section 4.5.1 is used to truncate the three least observable states of the unknown input observer. However, the eigenvalues of the reduced-order observer are not close to the full-order observer. Therefore, only the two least observable states are truncated. Then, one more state is truncated by using the model reduction technique in Section 4.5.2. The reduced-order unknown input observer is given in Appendix B.1. The eigenvalues of the reduced-order observer are -14.229, $-10.790 \pm 17.646i$, $-7.598 \pm 0.583i$, -1.371 and -1.215 which are closed to the full-order observer. The frequency response from the engine speed sensor and longitudinal accelerometer faults to the residuals is shown in Figure 4.2. The left figure is the full-order observer and the right figure is the reduced-order observer. The solid line represents the engine speed sensor fault and the dotted line represents the longitudinal accelerometer fault. Figure 4.2 shows that both observers can detect the longitudinal accelerometer fault and block the engine speed sensor fault.

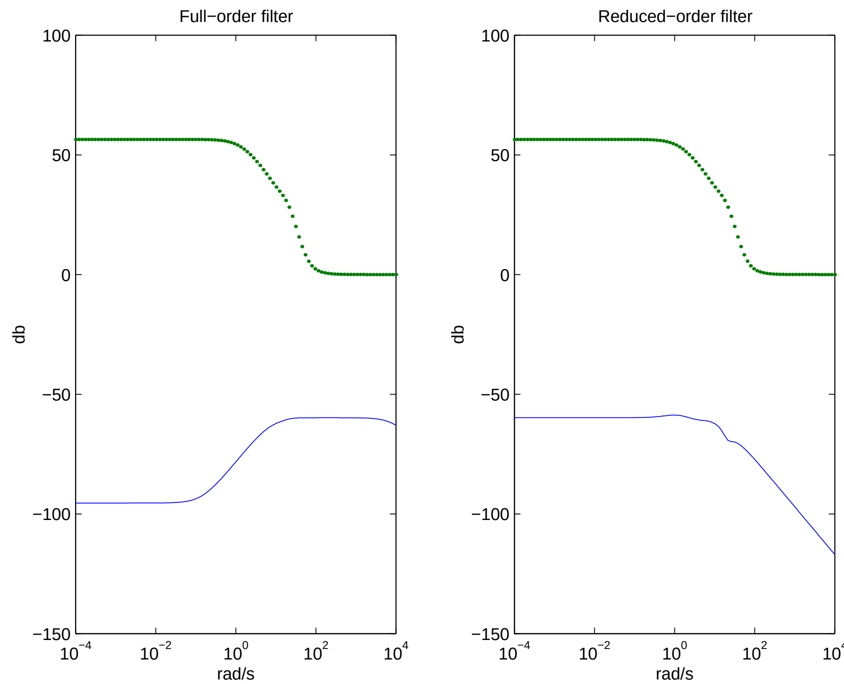

Figure 4.2: Frequency response of the unknown input observer that detects the longitudinal accelerometer fault

4.6.2 Fault Detection Filter Set No. 2

In this section, one unknown input observer is designed to detect the front wheel speed sensor fault and one unknown input observer is designed to detect the rear wheel speed sensor fault. From Sections 3.5 and 4.2.2, the linear longitudinal vehicle model with front wheel speed sensor, rear wheel speed sensor and nonlinearity faults is

$$\begin{aligned}\dot{x} &= Ax + Bu + F_{y_{\bar{w}_f}}\mu_{y_{\bar{w}_f}} + F_{y_{\bar{w}_r}}\mu_{y_{\bar{w}_r}} + F_{n_1}\mu_{n_1} \\ y &= Cx\end{aligned}$$

where A, B, C, $F_{y_{\bar{w}_f}}$ and $F_{y_{\bar{w}_r}}$ are derived when the vehicle is travelling at 20 m/s and given in Appendix A.1. F_{n_1} is given by (4.2).

For the first unknown input observer, the target fault is the front wheel speed sensor fault $F_1 = F_{y_{\bar{w}_f}}$ and the nuisance fault is the nonlinearity and rear wheel speed sensor faults $F_2 =$

$[\, F_{u_\alpha} \;\; F_{y_{\bar{w}_r}} \,]$ because $\operatorname{Im} F_{n_1} = \operatorname{Im} F_{u_\alpha}$. The weightings are chosen as

$$Q_1 = 0.1 I_2\,, \quad Q_2 = I_3\,, \quad \gamma = 10^{-8}\,, \quad V = \begin{bmatrix} 1 & 0 & 0 & 0 & 0 \\ 0 & 1 & 0 & 0 & 0 \\ 0 & 0 & 1 & 0 & 0 \\ 0 & 0 & 0 & 0.01 & 0 \\ 0 & 0 & 0 & 0 & 0.01 \end{bmatrix}$$

The unknown input observer gain L is obtained by solving the Riccati equation (4.10) and (4.11). The projector $\hat{H}$ is obtained by using (4.12) where $\mathcal{T}_2 = [\, \mathcal{T}_{u_\alpha} \;\; \mathcal{T}_{y_{\bar{w}_r}} \,]$. The Riccati matrix P, unknown input observer gain L and projector $\hat{H}$ are given in Appendix B.2.

The eigenvalues of the unknown input observer are $-3.879 \cdot 10^6$, $-5.034 \cdot 10^5$, $-3.215 \cdot 10^4$, -53.312, -14.011, $-8.588 \pm 16.082i$, -4.066, -1.250 and -1.035. Observe that three of these eigenvalues are significantly faster than the rest because γ is very small and the dimension of the detection space of the nuisance fault is three. Furthermore, the singular values of the observability grammian of the unknown input observer are 8.87, 0.50, 0.43, 0.20, $9.38 \cdot 10^{-3}$, $2.57 \cdot 10^{-4}$, $1.25 \cdot 10^{-7}$, $2.33 \cdot 10^{-12}$, $3.13 \cdot 10^{-17}$ and $3.92 \cdot 10^{-20}$. Observe that three of these singular values are significantly smaller than the rest. Therefore, the model reduction technique in Section 4.5.1 is used to truncate the three least observable states of the unknown input observer. The reduced-order unknown input observer is given in Appendix B.2. The eigenvalues of the reduced-order observer are -53.312, -14.011, $-8.588 \pm 16.082i$, -4.065, -1.250 and -1.035 which are closed to the full-order observer. The frequency response from the front wheel speed sensor and rear wheel speed sensor faults to the residuals is shown in Figure 4.3. The left figure is the full-order observer and the right figure is the reduced-order observer. The solid line represents the front wheel speed sensor fault and the dotted line represents the rear wheel speed sensor fault. Figure 4.3 shows that both observers can detect the front wheel speed sensor fault and block the rear wheel speed sensor fault.

For the second unknown input observer, the target fault is the rear wheel speed sensor fault $F_1 = F_{y_{\bar{w}_r}}$ and the nuisance fault is the nonlinearity and front wheel speed sensor faults $F_2 = [\, F_{u_\alpha} \;\; F_{y_{\bar{w}_f}} \,]$ because $\operatorname{Im} F_{n_1} = \operatorname{Im} F_{u_\alpha}$. The weightings are chosen as

$$Q_1 = 0 I_2\,, \quad Q_2 = I_3\,, \quad \gamma = 10^{-8}\,, \quad V = \begin{bmatrix} 10^{-4} & 0 & 0 & 0 & 0 \\ 0 & 10^{-4} & 0 & 0 & 0 \\ 0 & 0 & 10^{-5} & 0 & 0 \\ 0 & 0 & 0 & 10^3 & 0 \\ 0 & 0 & 0 & 0 & 10^4 \end{bmatrix}$$

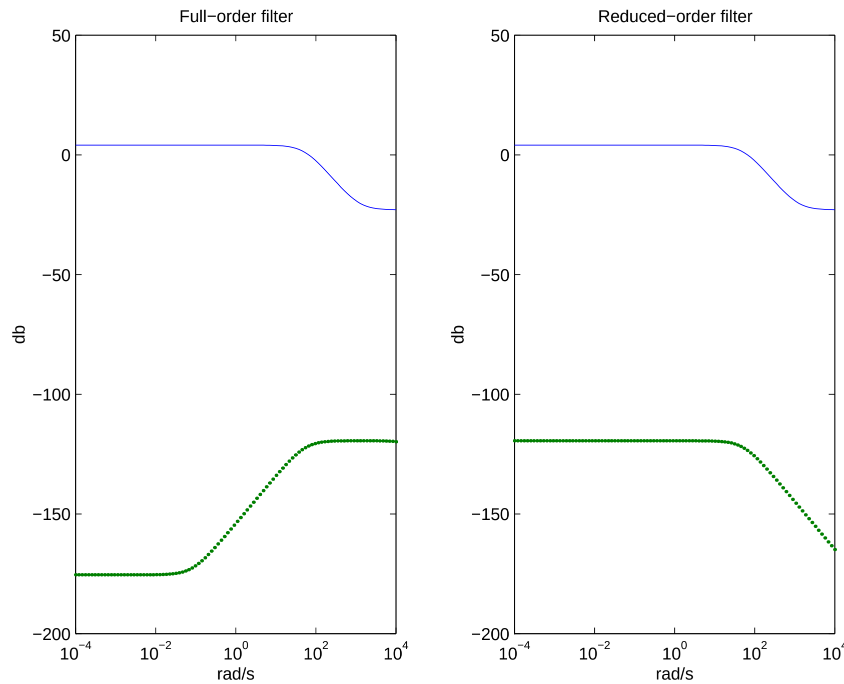

Figure 4.3: Frequency response of the unknown input observer that detects the front wheel speed sensor fault

The unknown input observer gain L is obtained by solving the Riccati equation (4.10) and (4.11). The projector $\hat{H}$ is obtained by using (4.12) where $\mathcal{T}_2 = [\,\mathcal{T}_{u_\alpha} \;\; \mathcal{T}_{y_{\bar{w}_f}}\,]$. The Riccati matrix P, unknown input observer gain L and projector $\hat{H}$ are given in Appendix B.2.

The eigenvalues of the unknown input observer are $-8.583 \cdot 10^7$, $-5.034 \cdot 10^7$, -316.23, -49.565, -13.880, $-9.033 \pm 16.665i$, $-1.652 \pm 1.297i$ and -1.250. Observe that three of these eigenvalues are significantly faster than the rest because γ is very small and the dimension of the detection space of the nuisance fault is three. Furthermore, the singular values of the observability grammian of the unknown input observer are $1.59 \cdot 10^4$, $7.38 \cdot 10^2$, 53.26, 6.72, 2.03, 0.18, $4.83 \cdot 10^{-7}$, $3.02 \cdot 10^{-13}$, $2.00 \cdot 10^{-13}$ and $8.02 \cdot 10^{-19}$. Observe that three of these singular values are significantly smaller than the rest. Therefore, the model reduction technique in Section 4.5.1 is used to truncate the three least observable states of the unknown input observer. The reduced-order unknown input observer is given in Appendix B.2. The eigenvalues of the reduced-order observer are -49.565, -13.880, $-9.033 \pm 16.652i$, $-1.652 \pm 1.297i$ and -1.250 which are closed to the full-order observer. The frequency response from the front wheel speed sensor and rear wheel speed sensor faults to the residuals is shown in Figure 4.4. The left figure is the full-order observer and the right figure is the reduced-order observer. The solid line represents the front wheel speed sensor fault and the

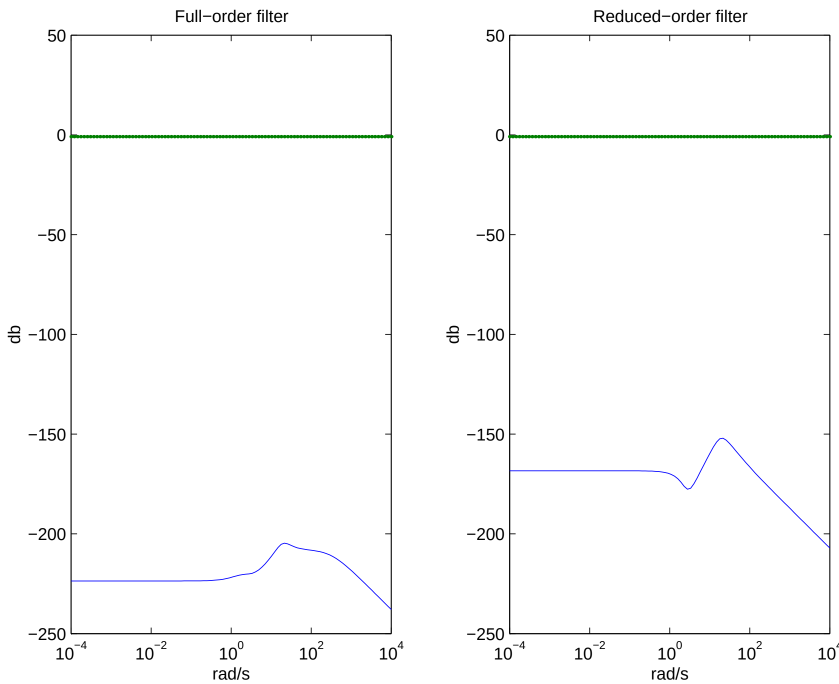

Figure 4.4: Frequency response of the unknown input observer that detects the rear wheel speed sensor fault

dotted line represents the rear wheel speed sensor fault. Figure 4.4 shows that both observers can detect the rear wheel speed sensor fault and block the front wheel speed sensor fault.

4.6.3 Fault Detection Filter Set No. 3

In this section, one unknown input observer is designed to detect the brake actuator fault and one unknown input observer is designed to detect the rear wheel speed sensor magnitude fault. From Sections 3.5, 4.2.2 and 4.3, the linear longitudinal vehicle model with brake actuator, rear wheel speed sensor magnitude and nonlinearity faults is

$$\dot{x} = Ax + Bu + F_{u_{T_b}} \mu_{u_{T_b}} + \bar{f}_{y_{\bar{w}_r}} \bar{\mu}_{y_{\bar{w}_r}} + F_{n_2} \mu_{n_2}$$
$$y = Cx$$

where A, B, C, $F_{u_{T_b}}$ and $\bar{f}_{y_{\bar{w}_r}}$ (the second column of $F_{y_{\bar{w}_r}}$) are derived when the vehicle is travelling at 24 m/s and given in Appendix A.2. F_{n_2} is given by (4.1).

For the first unknown input observer, the target fault is the brake actuator fault $F_1 = F_{u_{T_b}}$ and the nuisance fault is the nonlinearity and rear wheel speed sensor magnitude faults $F_2 = [\, F_{n_2} \quad \bar{f}_{y_{\bar{w}_r}} \,]$. For the unknown input observer design, $F_2 = [\, F_{y_{m_p}} \quad \bar{f}_{y_{\bar{w}_r}} \,]$ is used because $\operatorname{Im} F_{n_2} = \operatorname{Im} F_{y_{m_p}}$. The weightings are chosen as $Q_1 = 1500I_2$, $\gamma = 10^{-4}$ and

$$Q_2 = \begin{bmatrix} 1 & 0 & 0 \\ 0 & 1 & 0 \\ 0 & 0 & 10000 \end{bmatrix}, \quad V = \begin{bmatrix} 4\cdot 10^5 & 0 & 0 & 0 & 0 \\ 0 & 4\cdot 10^6 & 0 & 0 & 0 \\ 0 & 0 & 4\cdot 10^4 & 0 & 0 \\ 0 & 0 & 0 & 2\cdot 10^4 & 0 \\ 0 & 0 & 0 & 0 & 2\cdot 10^4 \end{bmatrix}$$

The unknown input observer gain L is obtained by solving the Riccati equation (4.10) and (4.11). The projector $\hat{H}$ is obtained by using (4.12) where $\mathcal{T}_2 = [\, \mathcal{T}_{y_{m_p}} \;\; \bar{f}_{y_{\bar{w}_r}} \,]$ because $C\bar{f}_{y_{\bar{w}_r}} \neq 0$ and $(C, A, \bar{f}_{y_{\bar{w}_r}})$ does not have any invariant zero. The Riccati matrix P, unknown input observer gain L and projector $\hat{H}$ are given in Appendix B.3.

The eigenvalues of the unknown input observer are $-1.921\cdot 10^3$, -54.966, -21.653, -14.468, $-13.163 \pm 7.956i$, $-5.461 \pm 6.727i$, -1.250 and -0.323. Observe that only one of these eigenvalues is significantly faster than the rest because γ is not small enough to approximately induce the whole detection space of the nuisance fault. Note that the dimension of the detection space is three. Therefore, the model reduction technique in Section 4.5.1 is used to truncate the least observable state of the unknown input observer. However, the eigenvalues of the reduced-order observer are not close to the full-order observer. Therefore, the model reduction technique in Section 4.5.2 is used to truncate the least controllable and observable state of the unknown input observer. The reduced-order unknown input observer is given in Appendix B.3. The eigenvalues of the reduced-order observer are -54.878, -21.654, -14.534, $-13.162 \pm 7.957i$, $-5.461 \pm 6.727i$, -1.250 and -0.323 which are closed to the full-order observer. The frequency response from the brake actuator and rear wheel speed sensor faults to the residuals is shown in Figure 4.5. The left figure is the full-order observer and the right figure is the reduced-order observer. The solid line represents the brake actuator fault and the dotted line represents the rear wheel speed sensor fault. Figure 4.5 shows that the residuals are sensitive to the rear wheel speed sensor fault in the high frequency because only the magnitude direction is used to model the rear wheel speed sensor fault. Therefore, the unknown input observer cannot identify the brake actuator and rear wheel speed sensor faults if the spectral components of the faults are high frequency. However, since the rear wheel speed sensor fault is also detected by another unknown input observer in Section 4.6.2, these two faults can be detected and identified by using the unknown input observers for both sets.

For the second unknown input observer, the target fault is the rear wheel speed sensor magnitude fault $F_1 = \bar{f}_{y_{\bar{w}_r}}$ and the nuisance fault is the nonlinearity and brake actuator faults $F_2 =$

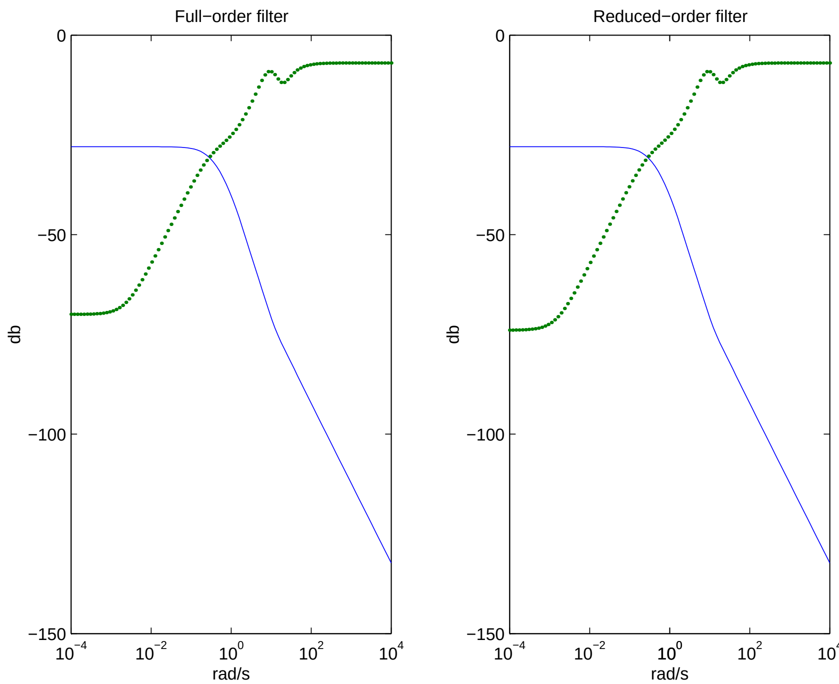

Figure 4.5: Frequency response of the unknown input observer that detects the brake actuator fault

$[\,F_{y_{m_p}} \;\; F_{u_{T_b}}\,]$ because $\operatorname{Im} F_{n_2} = \operatorname{Im} F_{y_{m_p}}$. The weightings are chosen as $Q_1 = 0$, $Q_2 = I_4$, $\gamma = 10^{-8}$ and $V = I_5$. The unknown input observer gain L is obtained by solving the Riccati equation (4.10) and (4.11). The projector $\hat{H}$ is obtained by using (4.12) where $\mathcal{T}_2 = [\,\mathcal{T}_{y_{m_p}} \;\; \mathcal{T}_{u_{T_b}}\,]$. The Riccati matrix P, unknown input observer gain L and projector $\hat{H}$ are given in Appendix B.3.

The eigenvalues of the unknown input observer are $-5.165\cdot 10^5$, $-1.661\cdot 10^5$, -206.82, $-40.567 \pm 5.974i$, -23.762, $-7.144 \pm 4.308i$ and $-4.958 \pm 7.888i$. Observe that three of these eigenvalues are significantly faster than the rest because γ is very small. However, the unknown input observer does not approximately induce the whole detection space of the nuisance fault because the dimension of the detection space is four. Therefore, the model reduction technique in Section 4.5.1 is used to truncate the three least observable states of the unknown input observer. However, the eigenvalues of the reduced-order observer are not close to the full-order observer. Therefore, the model reduction technique in Section 4.5.2 is used to truncate the three least controllable and observable states of the unknown input observer. However, the eigenvalues of the reduced-order observer are still not close to the full-order observer. The hankel singular values of the unknown input observer are 0.59, 0.33, $7.05 \cdot 10^{-2}$, $2.17 \cdot 10^{-2}$, $3.10 \cdot 10^{-3}$, $9.58 \cdot 10^{-4}$, $5.70 \cdot 10^{-4}$, $3.49 \cdot 10^{-7}$, $3.60 \cdot 10^{-14}$ and $2.22 \cdot 10^{-16}$. By truncating the states associated with the hankel singular values $5.70 \cdot 10^{-4}$,

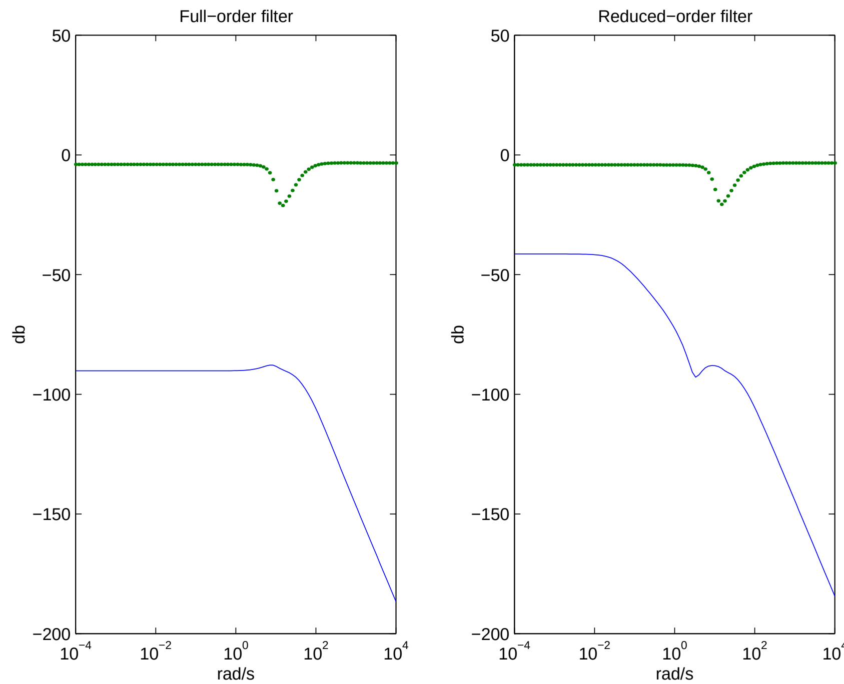

Figure 4.6: Frequency response of the unknown input observer that detects the rear wheel speed sensor fault

$3.60 \cdot 10^{-14}$ and $2.22 \cdot 10^{-16}$, the eigenvalues of the reduced-order observer are $-39.795 \pm 14.048i$, -23.706, $-6.390 \pm 5.634i$, $-4.823 \pm 8.104i$ which are closed to the full-order observer. The reduced-order unknown input observer is given in Appendix B.3. The frequency response from the brake actuator and rear wheel speed sensor faults to the residuals is shown in Figure 4.6. The left figure is the full-order observer and the right figure is the reduced-order observer. The solid line represents the brake actuator fault and the dotted line represents the rear wheel speed sensor fault. Figure 4.6 shows that both observers can detect the rear wheel speed sensor fault and block the brake actuator fault.

Chapter 5

Lateral Fault Detection Filter Design

In this chapter, fault detection filters are designed to detect and identify actuator and sensor faults for the lateral dynamics of the vehicle. From Sections 3.2 and 3.3, there are one actuator and four sensors on the PATH Buick LeSabre that control or measure the lateral dynamics of the vehicle.

Actuators:	u_γ	: Steering actuator.
Sensors:	y_{a_y}	: Lateral accelerometer.
	y_r	: Yaw rate sensor.
	$y_{\tilde{w}_f}$	: Difference of front wheel speed sensors.
	$y_{\tilde{w}_r}$	: Difference of rear wheel speed sensors.

From Section 3.5, the linear lateral vehicle model with one actuator and four sensor faults is

$$\begin{aligned}\dot{x} &= Ax+Bu+F_{u_\gamma}\mu_{u_\gamma}+F_{y_{a_y}}\mu_{y_{a_y}}+F_{y_r}\mu_{y_r}+F_{y_{\tilde{w}_f}}\mu_{y_{\tilde{w}_f}}+F_{y_{\tilde{w}_r}}\mu_{y_{\tilde{w}_r}}\\ y &= Cx+Du\end{aligned}$$

Fault detection filters were designed based on this vehicle model to detect and identify these five faults. Note that using the original lateral model, fault detection filter designed for the lateral accelerometer is not robust when the vehicle operates far from the nominal point. Therefore, the modified lateral model is used to design the lateral accelerometer fault detection filter.

In Section 5.1, the output separability of the faults are checked. In Section 5.2, the five faults to be detected and identified by the fault detection filters are grouped into three sets. In Section 5.3, fault detection filters are designed for each set of faults.

5.1 Output Separability

In this section the output separability of the actuator fault and the four sensor faults are checked. Before checking the output separability, the detection space $\mathcal{T}_i$ is obtained for each fault using (2.6). It is found that the dimension of $C\mathcal{T}_{u_\gamma}$, $C\mathcal{T}_{y_{a_y}}$, $C\mathcal{T}_{y_r}$, $C\mathcal{T}_{y_{\tilde{w}_f}}$ and $C\mathcal{T}_{y_{\tilde{w}_r}}$ is two. The sum of the dimension of each $C\mathcal{T}_i$ is ten. Since it is larger than the dimension of the output space which is four, these five faults are not output separable. Therefore, they are grouped into several sets where the faults in each set are output separable in Section 5.2. Then, fault detection filters are designed for each set of faults in Section 5.3.

Before grouping the faults into several sets, the output separability between each fault is examined, that is,

$$C\mathcal{T}_i \cap C\mathcal{T}_{j\neq i} = 0$$

By examining the singular values of $[\, C\mathcal{T}_i \;\; C\mathcal{T}_{j\neq i} \,]$, every pair of faults is output separable except one pair. The steering actuator fault and lateral accelerometer fault are not output separable. From (2.3), $F_{u_\gamma} = [\, f_{u_\gamma} \;\; \bar{f}_{u_\gamma} \,]$ and $F_{y_{a_y}} = [\, f_{y_{a_y}} \;\; \bar{f}_{y_{a_y}} \,]$ where f_{u_γ}, $f_{y_{a_y}}$ represent the fault rate direction and $\bar{f}_{u_\gamma}$, $\bar{f}_{y_{a_y}}$ represent the fault magnitude direction. These two faults are not output separable because they have the same fault rate direction, $f_{u_\gamma} = f_{y_{a_y}}$. Since $C\mathcal{T}_{u_\gamma} \not\subseteq C\mathcal{T}_{y_{a_y}}$ and $C\mathcal{T}_{y_{a_y}} \not\subseteq C\mathcal{T}_{u\gamma}$, these two faults can be detected and identified by grouping them into different sets.

5.2 Fault Configuration

In this section, the five faults are grouped into three sets respectively. The five faults to be detected and identified by the fault detection filter are steering actuator fault, lateral accelerometer fault, yaw rate sensor fault, front wheel speed sensor fault and rear wheel speed sensor fault. Since the dimension of the detection space of each fault is two and the dimension of the output space is four. Only two faults can be grouped together in each set where the faults are output separable.

Since the steering actuator fault and the lateral accelerometer fault are not output separable, they can not be grouped in the same set. Therefore, the steering actuator fault is grouped with any of the other three sensor fault. The front wheel speed sensor fault is chose to pair with the steering actuator fault with no particular reason. With no particular reason, the yaw rate sensor fault is paired with the rear wheel speed sensor fault and the lateral accelerometer fault is paired with rear wheel speed sensor fault.

In summary, the three fault detection filter sets are

Fault detection filter set no. 4	u_γ : Steering actuator.
	$y_{\tilde{\omega}_f}$: Front wheel speed sensors
Fault detection filter set no. 5	y_r : Yaw rate sensor.
	$y_{\tilde{\omega}_r}$: Rear wheel speed sensors.
Fault detection filter set no. 6	y_{a_y} : Lateral accelerometer.
	$y_{\tilde{\omega}_r}$: Rear wheel speed sensors.

5.3 Lateral Fault Detection Filter Design

In this section, fault detection filters are designed for the three sets of faults determined in Section 5.2 by using the design algorithm in Section 4.4. In Section 5.3.1, two unknown input observers are designed for the fourth set of faults which are the steering actuator and front wheel speed sensors faults. In Section 5.3.2, two unknown input observers are designed for the fifth set of faults which are the yaw rate sensor and rear wheel speed sensors faults. In Section 5.3.3, two unknown input observers are designed for the sixth set of faults which are the lateral accelerometer and rear wheel speed sensors faults.

5.3.1 Fault Detection Filter Set No. 4

In this section, one unknown input observer is designed to detect the steering actuator fault and one unknown input observer is designed to detect the front wheel speed sensors fault. From Sections 3.5 and 4.2.2, the linear lateral vehicle model with steering actuator and front wheel speed sensor is

$$\begin{aligned} \dot{x} &= Ax + Bu + F_{u_\gamma}\mu_{u_\gamma} + F_{y_{\tilde{\omega}_f}}\mu_{y_{\tilde{\omega}_f}} \\ y &= Cx + Du \end{aligned}$$

where A, B, C, D, F_{u_γ} and $F_{y_{\tilde{\omega}_f}}$ are derived when the vehicle is traveling at 20 m/s and given in Appendix A.1.

For the first unknown input observer,

$$\begin{aligned} \dot{\hat{x}} &= A\hat{x} + Bu + L(y - C\hat{x} - Du) \\ r &= \hat{H}(y - C\hat{x} - Du) \end{aligned}$$

The target fault is steering actuator fault $F_1 = F_{u_\gamma}$ and the nuisance fault is the front wheel speed sensor faults $F_2 = F_{y_{\tilde{w}_f}}$. The weighting of the target fault is chosen as $Q_1 = 0I_2$. The weighting of the nuisance fault is chosen as $Q_2 = 100I_2$ and $\gamma = 10^{-6}$. The weighting of the sensor noise V is an diagonal matrix with 0.1, 10^5, 100 and 0.1 on the main diagonal line. The unknown input observer gain L is obtained by solving the Riccati equation (4.10) and (4.11). The projector $\hat{H}$ is obtained by using (4.12) where $\mathcal{T}_2 = \mathcal{T}_{y_{\tilde{w}_f}}$. The Riccati matrix P, unknown input observer gain L and projector $\hat{H}$ are given in Appendix B.1.

The eigenvalues of the unknown input observer are $-3.68 \cdot 10^6$, -530.34, -52.43, -11.77 and $-7.22 \pm 2.90i$. Observe that two of these eigenvalues are significantly faster than the rest because γ is very small and the dimension of the detection space of the nuisance fault is two. The reduced-order unknown input observer is obtained by dropping the two least observable states using dynamic truncation with a steady-state correction (Prakash, 1994). The reduced-order unknown input observer is

$$
\begin{aligned}
\dot{\hat{x}}_r &= A_r \hat{x}_r + B_r \begin{bmatrix} u \\ y \end{bmatrix} \\
r &= C_r \hat{x}_r + D_r \begin{bmatrix} u \\ y \end{bmatrix}
\end{aligned}
$$

where A_r, B_r, C_r, and D_r are given in Appendix B.1. The eigenvalues of the reduced-order observer are -52.89, -11.66, and $-7.27 \pm -2.88i$ which are closed to the full-order observer. The frequency response from the steering actuator and front wheel speed sensor faults to the residuals is shown in Figure 5.1. The left figure is the full-order observer and the right figure is the reduced-order observer. The solid line represents the steering actuator fault and the dotted line represents the front wheel speed sensor fault. Figure 5.1 shows that both observers can detect the steering actuator fault and block the front wheel speed sensor fault.

For the second unknown input observer, the target fault is the front wheel speed sensor fault $F_2 = F_{y_{\tilde{w}_f}}$ and the nuisance fault is steering actuator fault $F_1 = F_{u_\gamma}$. The weighting of the target fault is chosen as $Q_1 = 0I_2$. The weighting of the nuisance fault is chosen as $Q_2 = 100I_2$ and $\gamma = 10^{-6}$. The weighting of the sensor noise is $V = I_4$. The unknown input observer gain L is obtained by solving the Riccati equation (4.10) and (4.11). The projector $\hat{H}$ is obtained by using (4.12) where $\mathcal{T}_2 = F_{u_\gamma}$. The Riccati matrix P, unknown input observer gain L and projector $\hat{H}$ are given in Appendix B.1.

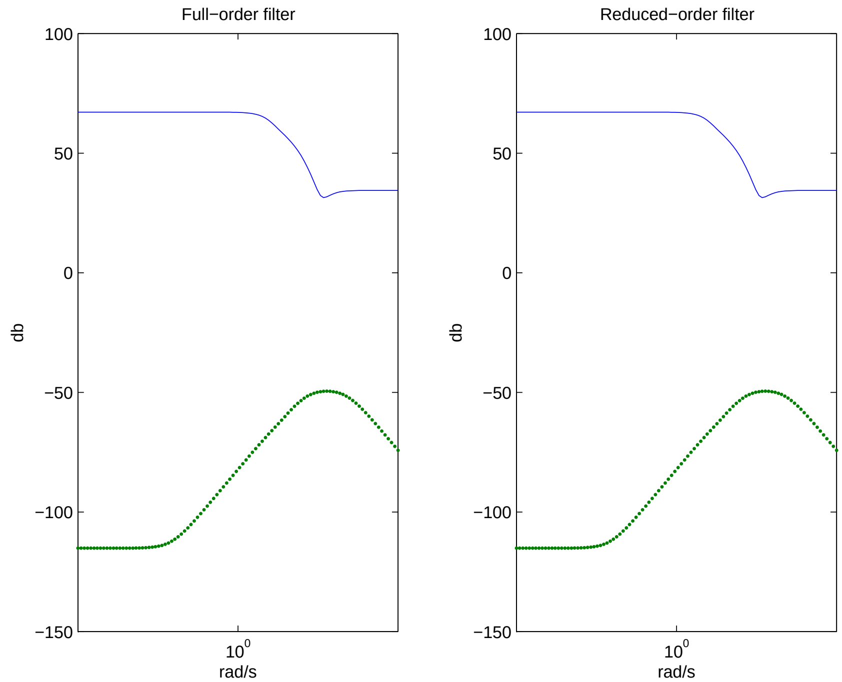

Figure 5.1: Frequency response of the unknown input observer that detects the steering actuator fault

The eigenvalues of the unknown input observer are $-2.92 \cdot 10^7$, $-9.23 \cdot 10^5$, -35.87, $-1.26 \pm 22.96i$ and -7.71. Observe that two of these eigenvalues are significantly faster than the rest because γ is very small and the dimension of the detection space of the nuisance fault is two. The reduced-order unknown input observer is obtained by dropping the two least observable states using dynamic truncation with a steady-state correction (Prakash, 1994). The reduced-order unknown input observer is given in Appendix B.1. The eigenvalues of the reduced-order observer are -35.87, $-1.26 \pm 22.96i$ and -7.71 which are closed to the full-order observer. The frequency response from the front wheel speed sensors and the steering actuator faults to the residuals is shown in Figure 5.2. The left figure is the full-order observer and the right figure is the reduced-order observer. The solid line represents the steering actuator fault and the dotted line represents the front wheel speed sensor fault. Figure 5.2 shows that both observers can detect the front wheel speed sensor fault and block the steering actuator fault.

5.3.2 Fault Detection Filter Set No. 5

In this section, one unknown input observer is designed to detect the yaw rate sensor fault and one unknown input observer is designed to detect the rear wheel speed sensors fault. From Sections 3.5

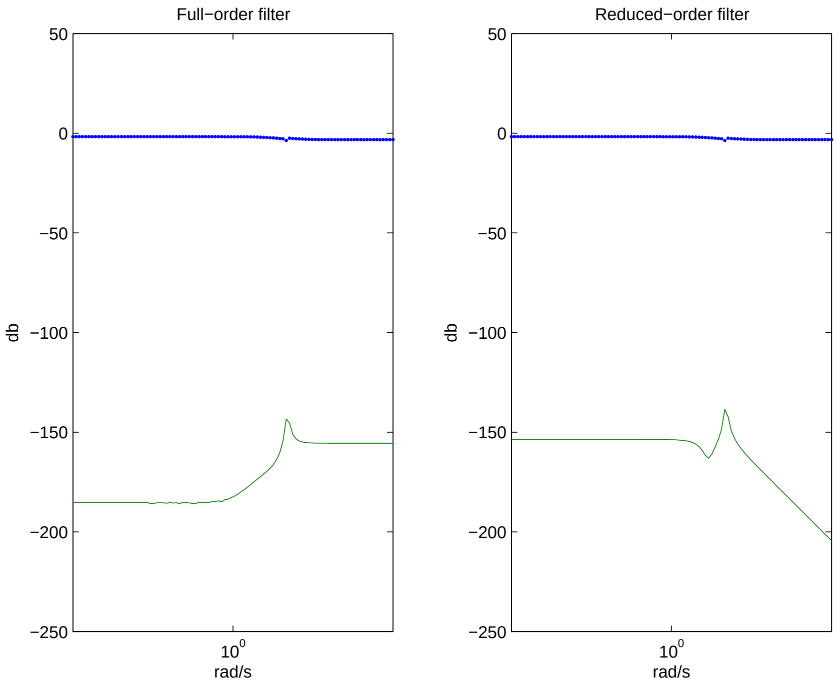

Figure 5.2: Frequency response of the unknown input observer that detects the front wheel speed sensor fault

and 4.2.2, the linear lateral vehicle model with yaw rate sensor and rear wheel speed sensor is

$$\dot{x} = Ax + Bu + F_{y_r}\mu_{y_r} + F_{y_{\tilde{w}_r}}\mu_{y_{\tilde{w}_r}}$$
$$y = Cx + Du$$

where A, B, C, D, F_{y_r} and $F_{y_{\tilde{w}_r}}$ are derived when the vehicle is traveling at 20 m/s and given in Appendix A.1.

For the first unknown input observer,

$$\dot{\hat{x}} = A\hat{x} + Bu + L(y - C\hat{x} - Du)$$
$$r = \hat{H}(y - C\hat{x} - Du)$$

The target fault is yaw rate sensor fault $F_1 = F_{y_r}$ and the nuisance fault is the rear wheel speed sensor faults $F_2 = F_{y_{\tilde{w}_r}}$. The weighting of the target fault is chosen as $Q_1 = 0I_2$. The weighting of the nuisance fault is chosen as $Q_2 = 100I_2$ and $\gamma = 10^{-4}$. The weighting of the sensor noise V is an diagonal matrix with 0.1, 10^5, 10^{-4} and 10^{-4} on the main diagonal line. The unknown input observer gain L is obtained by solving the Riccati equation (4.10) and (4.11). The projector $\hat{H}$ is obtained by using (4.12) where $\mathcal{T}_2 = \mathcal{T}_{y_{\tilde{w}_r}}$. The Riccati matrix P, unknown input observer gain L and projector $\hat{H}$ are given in Appendix B.1.

The eigenvalues of the unknown input observer are $-1.78 \cdot 10^3$, -37.25, -29.30, -9.94, -4.52 and -3.39. Observe that one of these eigenvalues are significantly faster than the rest. The reduced-order unknown input observer is obtained by dropping the least observable states using dynamic truncation with a steady-state correction (Prakash, 1994). The reduced-order unknown input observer is

$$\begin{aligned}\dot{\hat{x}}_r &= A_r\hat{x}_r + B_r\begin{bmatrix} u \\ y \end{bmatrix} \\ r &= C_r\hat{x}_r + D_r\begin{bmatrix} u \\ y \end{bmatrix}\end{aligned}$$

where A_r, B_r, C_r, and D_r are given in Appendix B.1. The eigenvalues of the reduced-order observer are -37.25, -29.31, -9.94, -4.51 and -3.39 which are closed to the full-order observer. The frequency response from the yaw rate sensor and rear wheel speed sensor faults to the residuals is shown in Figure 5.3. The left figure is the full-order observer and the right figure is the reduced-order observer. The solid line represents the yaw rate sensor fault and the dotted line represents the rear wheel speed sensor fault. Figure 5.3 shows that both observers can detect the yaw rate sensor fault and block the rear wheel speed sensor fault.

For the second unknown input observer, the target fault is the rear wheel speed sensor fault $F_1 = F_{y_{\tilde{w}_r}}$ and the nuisance fault is the yaw rate sensor fault $F_2 = F_{y_r}$. The weighting of the target fault is chosen as $Q_1 = 0I_2$. The weighting of the nuisance fault is chosen as $Q_2 = 100I_2$ and $\gamma = 10^{-6}$. The weighting of the sensor noise is $V = I_4$. The unknown input observer gain L is obtained by solving the Riccati equation (4.10) and (4.11). The projector $\hat{H}$ is obtained by using (4.12) where $\mathcal{T}_2 = F_{u_\gamma}$. The Riccati matrix P, unknown input observer gain L and projector $\hat{H}$ are given in Appendix B.1.

The eigenvalues of the unknown input observer are $-3.06 \cdot 10^6$, $-1.00 \cdot 10^4$, -84.57, -35.68, -14.70 and -7.86. Observe that two of these eigenvalues are significantly faster than the rest because γ is very small and the dimension of the detection space of the nuisance fault is two. The reduced-order unknown input observer is obtained by dropping the two least observable states using dynamic truncation with a steady-state correction (Prakash, 1994). The reduced-order unknown input observer is given in Appendix B.1. The eigenvalues of the reduced-order observer are -84.57,

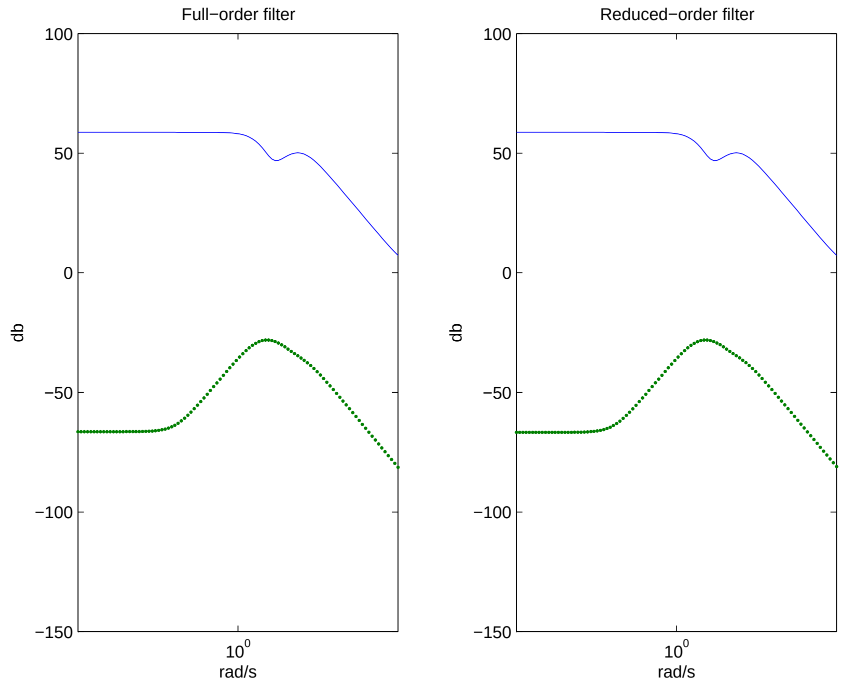

Figure 5.3: Frequency response of the unknown input observer that detects the yaw rate sensor fault

-35.68, -14.70 and -7.86 which are closed to the full-order observer. The frequency response from the rear wheel speed sensors and the yaw rate sensor faults to the residuals is shown in Figure 5.4. The left figure is the full-order observer and the right figure is the reduced-order observer. The solid line represents the yaw rate sensor fault and the dotted line represents the rear wheel speed sensor fault. Figure 5.4 shows that both observers can detect the rear wheel speed sensor fault and block the yaw rate sensor fault.

5.3.3 Fault Detection Filter Set No. 6

In this section, one unknown input observer is designed to detect the lateral accelerometer fault and one unknown input observer is designed to detect the rear wheel speed sensors fault. From Sections 3.5 and 4.2.2, the linear lateral vehicle model with lateral accelerometer and rear wheel speed sensor is

$$
\begin{aligned}
\dot{x} &= Ax + Bu + F_{y_{a_y}} \mu_{y_{a_y}} + F_{y_{\tilde{w}_r}} \mu_{y_{\tilde{w}_r}} \\
y &= Cx + Du
\end{aligned}
$$

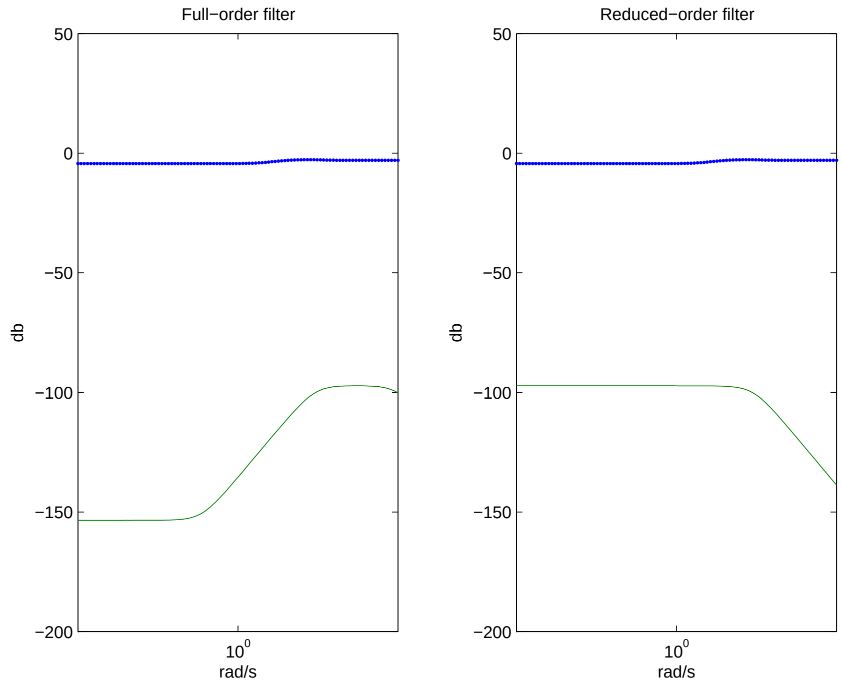

Figure 5.4: Frequency response of the unknown input observer that detects the rear wheel speed sensor fault

When designing the unknown input observer to detect lateral accelerometer fault, A, B, C, D, F_{u_γ} and $F_{y_{\tilde{w}_f}}$ are from the modified model which is obtained form modifying the lateral model derived when the vehicle is traveling at 20 m/s. The modified model is given in Appendix A.1.

For the unknown input observer that detects lateral accelerometer fault,

$$\dot{\hat{x}} = A\hat{x} + Bu + L(y - C\hat{x} - Du)$$
$$r = \hat{H}(y - C\hat{x} - Du)$$

The target fault is lateral accelerometer fault $F_1 = F_{y_{a_y}}$ and the nuisance fault is the rear wheel speed sensor faults $F_2 = F_{y_{\tilde{w}_r}}$. The weighting of the target fault is chosen as $Q_1 = 0I_2$. The weighting of the nuisance fault is chosen as $Q_2 = 100I_2$ and $\gamma = 10^{-6}$. The weighting of the sensor noise V is an diagonal matrix with 100, 10^6, 10^{-4} and 0.01 on the main diagonal line. The unknown input observer gain L is obtained by solving the Riccati equation (4.10) and (4.11). The projector $\hat{H}$ is obtained by using (4.12) where $\mathcal{T}_2 = \mathcal{T}_{y_{\tilde{w}_r}}$. The Riccati matrix P, unknown input observer gain L and projector $\hat{H}$ are given in Appendix B.1.

The eigenvalues of the unknown input observer are $-4.45 \cdot 10^5$, $-9.98 \cdot 10^2$, -39.75, -9.55, -4.98 and -0.29. Observe that two of these eigenvalues are significantly faster than the rest

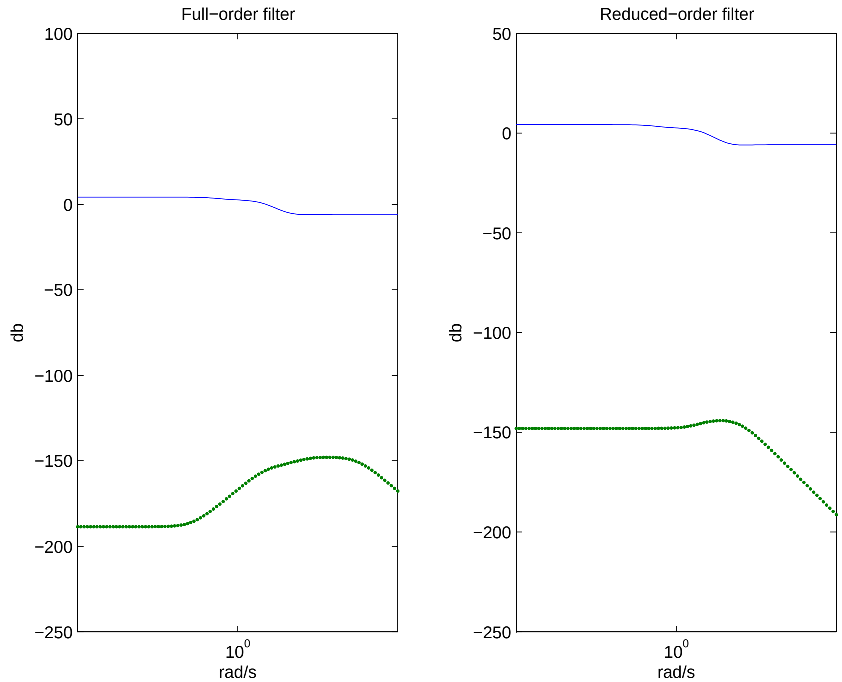

Figure 5.5: Frequency response of the unknown input observer that detects the lateral accelerometer fault

because γ is very small and the dimension of the detection space of the nuisance fault is two. The reduced-order unknown input observer is obtained by dropping the two least observable states using dynamic truncation with a steady-state correction (Prakash, 1994). The reduced-order unknown input observer is

$$\dot{\hat{x}}_r = A_r \hat{x}_r + B_r \begin{bmatrix} u \\ y \end{bmatrix}$$
$$r = C_r \hat{x}_r + D_r \begin{bmatrix} u \\ y \end{bmatrix}$$

where A_r, B_r, C_r, and D_r are given in Appendix B.1. The eigenvalues of the reduced-order observer are -39.75, -9.55, -4.98 and -0.29 which are closed to the full-order observer. The frequency response from the lateral accelerometer and rear wheel speed sensor faults to the residuals is shown in Figure 5.5. The left figure is the full-order observer and the right figure is the reduced-order observer. The solid line represents the lateral accelerometer fault and the dotted line represents the rear wheel speed sensor fault. Figure 5.5 shows that both observers can detect the steering actuator fault and block the front wheel speed sensor fault.

For the unknown input observer that detects the rear wheel speed sensor fault, the original lateral model is used and the target fault is the rear wheel speed sensor fault $F_1 = F_{y_{\tilde{w}_r}}$ and the nuisance fault is lateral accelerometer fault $F_2 = F_{y_{a_y}}$. The weighting of the target fault is chosen as $Q_1 = 0I_2$. The weighting of the nuisance fault is chosen as $Q_2 = 100I_2$ and $\gamma = 10^{-6}$. The weighting of the sensor noise is $V = I_4$. The unknown input observer gain L is obtained by solving the Riccati equation (4.10) and (4.11). The projector $\hat{H}$ is obtained by using (4.12) where $\mathcal{T}_2 = F_{y_{a_y}}$. The Riccati matrix P, unknown input observer gain L and projector $\hat{H}$ are given in Appendix B.1.

The eigenvalues of the unknown input observer are $-1.69 \cdot 10^5$, $-1.36 \cdot 10^2$, -38.95, -32.53, -0.18 and -0.062. Observe that two of these eigenvalues are significantly faster than the rest because γ is very small and the dimension of the detection space of the nuisance fault is two. The reduced-order unknown input observer is obtained by dropping the two least observable states using dynamic truncation with a steady-state correction (Prakash, 1994). The reduced-order unknown input observer is given in Appendix B.1. The eigenvalues of the reduced-order observer are -38.95, -32.54, -0.18 and -0.062 which are closed to the full-order observer. The frequency response from the rear wheel speed sensors and the lateral accelerometer faults to the residuals is shown in Figure 5.6. The left figure is the full-order observer and the right figure is the reduced-order observer. The solid line represents the steering actuator fault and the dotted line represents the front wheel speed sensor fault. Figure 5.6 shows that both observers can detect the rear wheel speed sensor fault and block the lateral accelerometer fault.

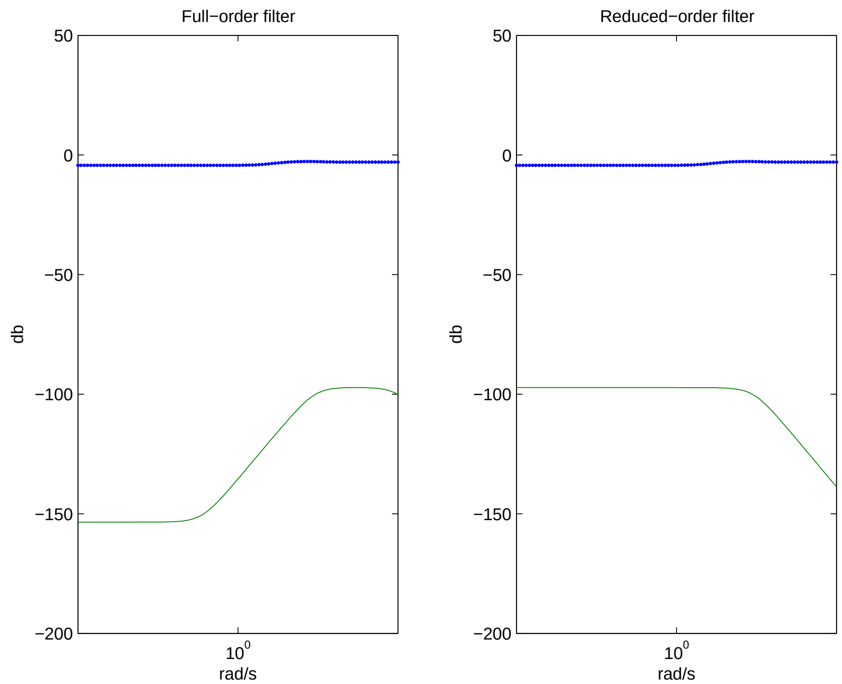

Figure 5.6: Frequency response of the unknown input observer that detects the rear wheel speed sensor fault

Chapter 6

Modified Longitudinal Fault Detection Filter Design

In this chapter, the longitudinal accelerometer fault detection filter from fault detection filter set No.1 is re-designed. Together with the engine speed sensor fault detection filter from the fault detection filter set No.1, a new fault detection filter set N0.1' is formed. Furthermore, the brake actuator fault detection filter from fault detection filter set No.3 is also redesigned. Together with the rear wheel speed sensor fault detection filter from the fault detection filter set No.3, a new fault detection filter set N0.3' is formed. In Sections 6.1 an unknown input observer is designed to detect the lateral accelerometer fault using one dimensional fault modeling technique. In Sections 6.2 an unknown input observer is designed to detect the brake actuator fault after the dynamical equation for brake state is changed.

6.1 Fault Detection Filter Set No. 1'

In this section, the unknown input observer which detects the longitudinal accelerometer fault from the fault detection filter set no.1 is re-designed using the one dimensional fault modeling technique. Then, the re-designed filter is paired with the unknown input observer which detects the engine speed sensor fault from the fault detection filter set no.1 to form the fault detection filter set no.1'. The robustness of the longitudinal accelerometer fault detection filter is enhanced by modeling external disturbances as nonlinearity faults. The new unknown input observer can detect an longitudinal accelerometer fault with smaller magnitude. The one dimensional fault modeling technique is used so that more fault directions can be considered when designing the unknown input observer. From Section 4.2.2 and using the one dimensional fault modeling technique shown in Section 6.1.1 to model the faults, the longitudinal vehicle model with longitudinal accelerometer, engine speed sensor and nonlinearity faults is

$$\begin{bmatrix} \dot{x} \\ \dot{\mu}_1 \\ \dot{\mu}_2 \\ \dot{\mu}_3 \end{bmatrix} = \begin{bmatrix} A & 0 & 0 & 0 \\ 0_{1\times 10} & -1 & 0 & 0 \\ 0_{1\times 10} & 0 & -1 & 0 \\ 0_{1\times 10} & 0 & 0 & -1 \end{bmatrix} \begin{bmatrix} x \\ \mu_1 \\ \mu_2 \\ \mu_3 \end{bmatrix} + \begin{bmatrix} B \\ 0_{3\times 2} \end{bmatrix} u + F_{y_{a_x}} \mu_{y_{a_x}} + F_{y_{\omega_e}} \mu_{y_{\omega_e}} + F_{n_1} \mu_{n_1} + F_{n_2} \mu_{n_2}$$

$$y = \begin{bmatrix} & 0 & 0 & 0 \\ & 0 & 1 & 0 \\ C & 1 & 0 & 1 \\ & 0 & 0 & 0 \\ & 0 & 0 & 0 \end{bmatrix} \begin{bmatrix} x \\ \mu_1 \\ \mu_2 \\ \mu_3 \end{bmatrix}$$

where A, B, and C are derived when the vehicle is traveling at $24m/s$ and given in Appendix A.2. The fault directions $F_{y_{\omega_e}}$, $F_{y_{a_x}}$, F_{n_1} and F_{n_2} are given in Appendix B.7.

For the design of the unknown input observer, target fault is the longitudinal accelerometer fault $F_1 = F_{y_{a_x}}$ and the nuisance fault is the nonlinearity and engine speed sensor faults $F_2 = [\, F_{n_1} \;\; F_{n_2} \;\; F_{y_{a_x}} \,]$. The weighting of the target fault is chosen as $Q_1 = 0$. The weightings of the nuisance fault are chosen as $Q_2 = I_4$ and $\gamma = 10^{-6}$. The weighting of the sensor noise is an diagonal matrix with 1, 10^{-4}, 5, 10^5 and 1 on the main diagonal line. The unknown input observer gain L is obtained by solving the Riccati equation (4.10) and (4.11). The projector $\hat{H}$ is obtained by using (4.12) where $\mathcal{T}_2 = [\, \mathcal{T}_{n_1} \;\; \mathcal{T}_{n_2} \;\; \mathcal{T}_{y_{\omega_e}} \,]$. The Riccati matrix P, unknown input observer gain L and projector $\hat{H}$ are given in Appendix B.7.

The eigenvalues of the unknown input observer are $-1.933 \cdot 10^5$, $-1.442 \cdot 10^5$, $-2.236 \cdot 10^4$, $-1.0001 \cdot 10^2$, $-3.7956 \cdot 10^1$, $-9.9147e \pm 16.707i$, $-3.206e \pm 46.803i$, -3.721, -13.839, -1.250 and -1.000 Observe that four of these eigenvalues are significantly faster than the rest because γ is very small and the dimension of the detection space of the nuisance fault is four. By dropping the four most unobservable states with steady state error correction, the reduced-order unknown input observer is

$$\dot{\hat{x}}_r = A_r \hat{x}_r + B_r \begin{bmatrix} u \\ y \end{bmatrix}$$

$$r = C_r \hat{x}_r + D_r \begin{bmatrix} u \\ y \end{bmatrix}$$

where A_r, B_r, C_r, and D_r are given in Appendix B.7. The eigenvalues of the reduced-order observer are -37.977, -13.837, $-9.9147 \pm 16.707i$, -3.721, $-3.206 \pm 4.680i$, -1.250 and -1.000

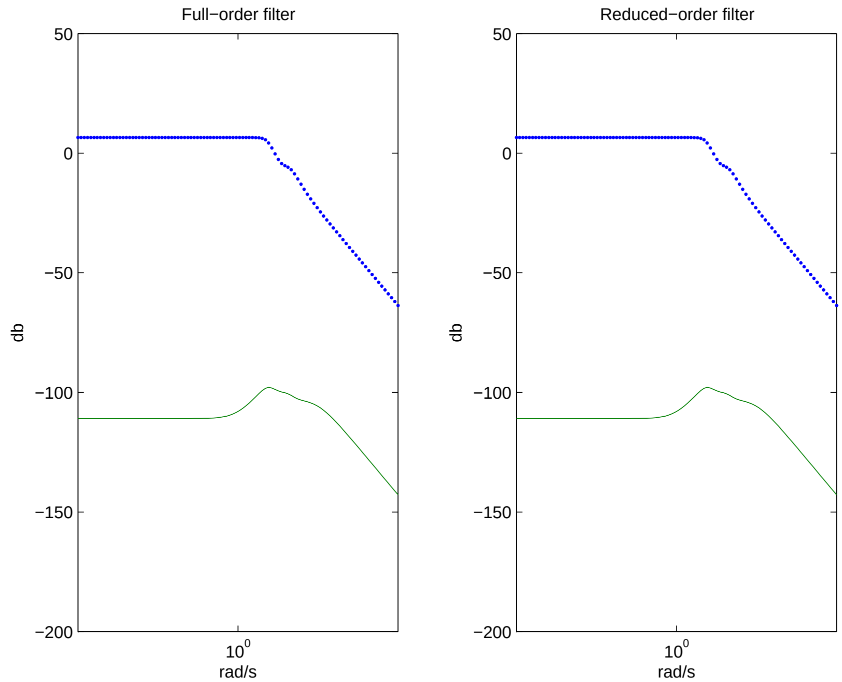

Figure 6.1: Frequency response of the unknown input observer that detects the longitudinal accelerometer fault

which are closed to the full-order observer. The frequency response from the engine speed sensor and longitudinal accelerometer faults to the residuals is shown in Figure 6.1. The left figure is the full-order observer and the right figure is the reduced-order observer. The solid line represents the engine speed sensor fault and the dotted line represents the longitudinal accelerometer fault. Figure 6.1 shows that both observers can detect the longitudinal accelerometer fault and block the engine speed sensor fault.

6.1.1 One Dimensional Fault Modeling

In this section, the one dimensional sensor and actuator fault modeling technique is briefly introduced. Consider a linear system,

$$\begin{aligned} \dot{x} &= Ax + Bu \\ y &= Cx \end{aligned}$$

where u is the control input and y is the measurement. All system variables belong to real vector spaces. System matrices A, B and C can be time varying.

A sensor fault can be modeled as

$$
\begin{aligned}
\dot{x} &= Ax + Bu \\
y &= Cx + E_s\mu_s
\end{aligned}
$$

Where E_s is an one dimensional vector with all elements equal to zero except an element which equals to one at i^{th} row. Assuming that the time-varying sensor fault magnitude μ_s can be represented by the first order differential equation

$$\dot{\mu}_s = -k_s\mu_s + k_s\bar{\mu}_s$$

and appended to the state space equation of the linear model, we obtain

$$
\begin{aligned}
\begin{bmatrix} \dot{x} \\ \dot{\mu}_s \end{bmatrix} &= \begin{bmatrix} A & 0 \\ 0 & -k_s \end{bmatrix} \begin{bmatrix} x \\ \mu_s \end{bmatrix} + \begin{bmatrix} B \\ 0 \end{bmatrix} u + \begin{bmatrix} 0 \\ k_s \end{bmatrix} \bar{\mu}_s \\
y &= \begin{bmatrix} C & E_s \end{bmatrix} \begin{bmatrix} x \\ \mu_s \end{bmatrix}
\end{aligned}
$$

The direction of the sensor fault becomes $\begin{bmatrix} 0 \\ 1 \end{bmatrix}$ which is time invariant.

On the other hand, the actuator fault can be modeled similarly. When the system matrix D is non-zero, the i^{th} actuator fault has the same direction as the i^{th} column of the B and D matrix. An actuator fault can be modeled as an additive term in the state and measurement equations

$$
\begin{aligned}
\dot{x} &= Ax + Bu + b_i\mu_a \\
y &= Cx + Du + d_i\mu_a
\end{aligned}
$$

where b_i is the i^{th} column of the B matrix and d_i is the i^{th} column of the D matrix. Again, by assuming that the time-varying actuator fault magnitude μ_a can be represented by the first order differential equation

$$\dot{\mu}_a = -k_a\mu_a + k_a\bar{\mu}_a$$

and appended to the state space linear model

$$
\begin{aligned}
\begin{bmatrix} \dot{x} \\ \dot{\mu}_a \end{bmatrix} &= \begin{bmatrix} A & b_i \\ 0 & -k_a \end{bmatrix} \begin{bmatrix} x \\ \mu_a \end{bmatrix} + \begin{bmatrix} B \\ 0 \end{bmatrix} u + \begin{bmatrix} 0 \\ k_a \end{bmatrix} \bar{\mu}_a \\
y &= \begin{bmatrix} C & d_i \end{bmatrix} \begin{bmatrix} x \\ \mu_a \end{bmatrix} + Du
\end{aligned}
$$

An time invariant actuator fault direction can be formed as $\begin{bmatrix} 0 \\ 1 \end{bmatrix}$.

6.2 Fault Detection Filter Set No. 3'

In this section, the unknown input observer which detects the brake actuator fault from the fault detection filter set no.3 is re-designed to accelerate the response to the fault by modifying the dynamical equation for the brake state. The new unknown input observer is shown to have a faster response to the brake actuator fault. Then, the re-designed filter is paired with the unknown input observer which detects the rear speed sensors fault from the fault detection filter set no.3 to form the fault detection filter set no.3'.

From the longitudinal vehicle model in Section 3.4, the dynamical equation for the brake state is

$$\dot{x}_{T_b} = -1.25x_{T_b} + 1.25u_{T_b}$$

where x_{T_b} is the brake state and u_{T_b} is the brake command. In order to accelerate the response to the brake actuator fault. The dynamical equation for the brake state is changed to

$$\dot{x}_{T_b} = -10x_{T_b} + 10u_{T_b}$$

and an unknown input observer is redesigned to detect the brake actuator fault using the model with the modified dynamical equation.

From Sections 3.5, 4.2.2 and 4.3, the linear longitudinal vehicle model with brake actuator, rear wheel speed sensor magnitude and nonlinearity faults is

$$\begin{aligned} \dot{x} &= Ax + Bu + F_{u_{T_b}}\mu_{u_{T_b}} + \bar{f}_{y_{\bar{w}_r}}\bar{\mu}_{y_{\bar{w}_r}} + F_{n2}\mu_{n2} \\ y &= Cx \end{aligned}$$

where A, B, C, $F_{u_{T_b}}$ and $\bar{f}_{y_{\bar{w}_r}}$ (the second column of $F_{y_{\bar{w}_r}}$) are derived when the vehicle is traveling at 24 m/s and given in Appendix B.8. F_{n_2} is given by (4.1). When designing the unknown input observer to detect brake actuator fault, the target fault is the brake actuator fault $F_1 = F_{u_{T_b}}$ and the nuisance fault is the nonlinearity and rear wheel speed sensor magnitude faults $F_2 = [\, F_{n_2} \;\; \bar{f}_{y_{\bar{w}_r}} \,]$. For the unknown input observer design, $F_2 = [\, F_{y_{m_p}} \;\; \bar{f}_{y_{\bar{w}_r}} \,]$ is used because $\operatorname{Im} F_{n_2} = \operatorname{Im} F_{y_{m_p}}$. The weightings are chosen as $Q_1 = 1500 I_2$, $\gamma = 10^{-2}$ and

$$Q_2 = \begin{bmatrix} 100 & 0 & 0 \\ 0 & 100 & 0 \\ 0 & 0 & 10000 \end{bmatrix}, \quad V = \begin{bmatrix} 2.5\cdot 10^{-8} & 0 & 0 & 0 & 0 \\ 0 & 2.5\cdot 10^{-5} & 0 & 0 & 0 \\ 0 & 0 & 2.5\cdot 10^{-5} & 0 & 0 \\ 0 & 0 & 0 & 5\cdot 10^{-4} & 0 \\ 0 & 0 & 0 & 0 & 5\cdot 10^{-4} \end{bmatrix}$$

The unknown input observer gain L is obtained by solving the Riccati equation (4.10) and (4.11). The projector $\hat{H}$ is obtained by using (4.12) where $\mathcal{T}_2 = [\, \mathcal{T}_{y_{m_p}} \;\; \bar{f}_{y_{\bar{w}_r}} \,]$. The Riccati matrix P, unknown input observer gain L and projector $\hat{H}$ are given in Appendix B.8.

The eigenvalues of the unknown input observer are $-6.074 \cdot 10^3$, -55.952, -19.111, -16.268, $-13.294 \pm 7.592i$, -10.000, $-5.305 \pm 6.639i$ and -1.097,. Observe that only one of these eigenvalues is significantly faster than the rest because γ is not small enough to approximately induce the whole detection space of the nuisance fault. Note that the dimension of the detection space is three. Therefore, the model reduction technique in Section 4.5.1 is used to truncate the least observable state of the unknown input observer. However, the eigenvalues of the reduced-order observer are not close to the full-order observer. Therefore, the model reduction technique in Section 4.5.2 is used to truncate the least controllable and observable state of the unknown input observer. The reduced-order unknown input observer is given in Appendix B.8. The eigenvalues of the reduced-order observer are -55.951, -19.111, -16.268, $-13.294 \pm 7.592i$, -10.000, $-5.305 \pm 6.639i$, -1.097, which are almost equal to the full-order observer. The frequency response from the brake actuator and rear wheel speed sensor faults to the residuals is shown in Figure 6.2. The left figure is the full-order observer and the right figure is the reduced-order observer. The solid line represents the brake actuator fault and the dotted line represents the rear wheel speed sensor fault. Figure 6.2 shows that the residuals are sensitive to the rear wheel speed sensor fault in the high frequency because only the magnitude direction is used to model the rear wheel speed sensor fault. Therefore, the unknown input observer cannot identify the brake actuator and rear wheel speed sensor faults if the spectral components of the faults are high frequency. However, since the rear wheel speed sensor fault is also detected by another unknown input observer in Section 4.6.2, these two faults can be detected and identified by using the unknown input observers for both sets.

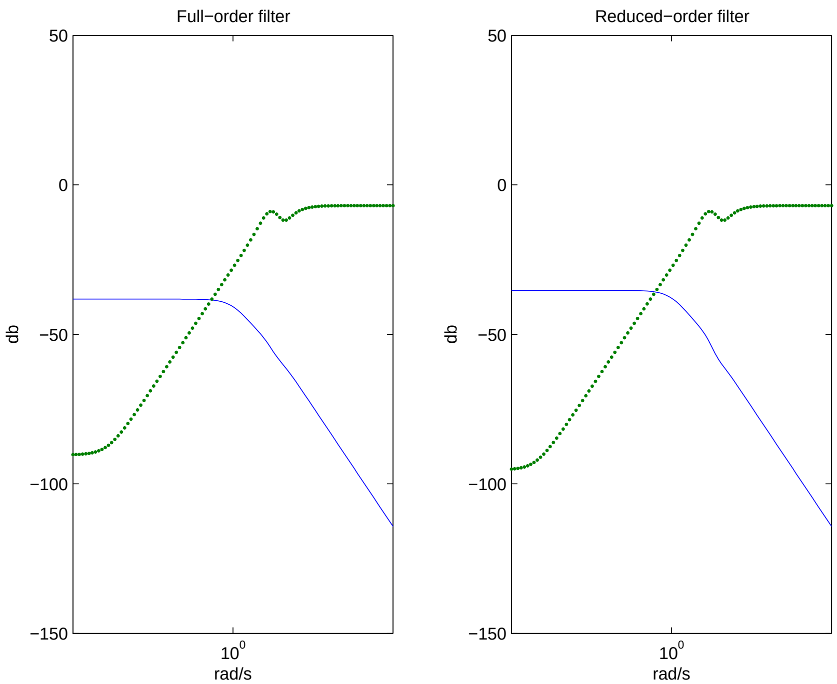

Figure 6.2: Frequency response of the unknown input observer that detects the brake actuator fault

Chapter 7

Parity Equation Design

In this chapter, parity equations are derived to detect the throttle actuator, throttle sensor, brake actuator, brake sensor, manifold pressure sensor and engine speed sensor faults. The parity equation is a static or dynamic function of the control commands and measurements. When the actuators and sensors involved do not have any fault, the residual of the parity equation is zero. When one of the actuators or sensors involved has a fault, the residual of the parity equation becomes nonzero. Therefore, the parity equation can detect the actuator and sensor faults. However, it cannot identify which fault has occurred.

There are three parity equations derived for the PATH Buick LeSabre. The first parity equation is a function of the throttle command and throttle measurement. From the vehicle simulation in Section 3.1,

$$\dot{x}_\alpha = -90x_\alpha + 90u_\alpha \tag{7.1}$$

where x_α is the throttle state and u_α is the throttle command. Since the throttle sensor measures the throttle state, the first parity equation is

$$r = x_\alpha - y_\alpha$$

In order to reduce the effect of the throttle sensor noise, a first-order low pass filter with the pole assigned at -5 is used. Therefore, the first parity equation becomes

$$\dot{r} = -5r + 5(x_\alpha - y_\alpha) \tag{7.2}$$

Since the dynamics of (7.1) are much faster than the dynamics of (7.2), the fast mode can be dropped and the first parity equation becomes

$$\dot{r} = -5r + 5(u_\alpha - y_\alpha)$$

The residual is zero when there is no throttle actuator or throttle sensor fault. The residual becomes nonzero when any of these two faults occurs. Therefore, this parity equation can detect the throttle actuator and throttle sensor faults, but cannot identify these two faults.

The second parity equation is a function of the brake command and brake measurement. From the vehicle simulation in Section 3.1,

$$\dot{x}_{T_b} = -1.25x_{T_b} + 1.25u_{T_b}$$

where x_{T_b} is the brake state and u_{T_b} is the brake command. Since the brake sensor measures the brake state, the second parity equation is

$$r = x_{T_b} - y_{T_b}$$

The residual is zero when there is no brake actuator or brake sensor fault. The residual becomes nonzero when any of these two faults occurs. Therefore, this parity equation can detect the brake actuator and brake sensor faults, but cannot identify these two faults.

The third parity equation is a function of the throttle command, manifold pressure measurement and engine speed measurement. From the vehicle simulation in Section 3.1, the derivative of the manifold air mass state is a nonlinear function of the manifold air mass state, engine speed state and throttle state.

$$\begin{aligned}\dot{x}_{m_a} &= f(x_{m_a}, x_{w_e}, x_\alpha) \\ \dot{x}_\alpha &= -90x_\alpha + 90u_\alpha\end{aligned}$$

Since the engine speed is measured, the manifold air mass state can be estimated by integrating

$$\begin{aligned}\dot{\hat{x}}_{m_a} &= f(\hat{x}_{m_a}, y_{w_e}, x_\alpha) \\ \dot{x}_\alpha &= -90x_\alpha + 90u_\alpha \qquad (7.3)\end{aligned}$$

Since the manifold air mass is linear with the manifold pressure, i.e.,

$$y_{m_p} = 19.3272 \cdot x_{m_a}$$

the third parity equation is

$$r = y_{m_p} - 19.3272 \cdot \hat{x}_{m_a}$$

In order to reduce the effect of the disturbances, a first-order low pass filter with the pole assigned at -5 is used. Therefore, the third parity equation becomes

$$\dot{r} = -5r + 5(y_{m_p} - 19.3272 \cdot \hat{x}_{m_a}) \tag{7.4}$$

Since the dynamics of (7.3) are much faster than the dynamics of (7.4), the fast mode can be dropped and the third parity equation becomes

$$\begin{aligned} \dot{\hat{x}}_{m_a} &= f(\hat{x}_{m_a}, y_{w_e}, u_\alpha) \\ \dot{r} &= -5r + 5(y_{m_p} - 19.3272 \cdot \hat{x}_{m_a}) \end{aligned}$$

The residual is zero when there is no throttle actuator, manifold pressure sensor or engine speed sensor fault. The residual becomes nonzero when any of these three faults occurs. Therefore, this parity equation can detect the throttle actuator, manifold pressure sensor and engine speed sensor faults, but cannot identify these three faults.

Although these three parity equations can detect the faults, none of them can identify a fault by itself. But by combining the parity equations with the unknown input observers in Section 4.6, unique residual patterns are presented allowing each fault to be identified. The patterns are summarized in Figures 7.1 to 7.3. In these figures, each row represents a bias (hard) fault in an actuator or sensor. The columns are the residual responses to the given fault conditions. In Figure 7.1, the first and second rows represent a bias fault in the throttle actuator and throttle sensor, respectively. The first and second columns are responses of the residuals of the first and third parity equations, respectively. Figure 7.1 shows that the throttle actuator and throttle sensor faults can be identified by combining the residuals of the first and third parity equations because the residual pattern is unique in response to each fault. In Figure 7.2, the first and second rows represent a bias fault in the brake actuator and brake sensor, respectively. The first and second columns are responses of the residuals of the second parity equation and the unknown input observer that detects the brake actuator fault in Section 4.6.3, respectively. Figure 7.2 shows that the brake actuator and brake sensor faults can be identified by combining the residuals of the second parity equation and the unknown input observer that detects the brake actuator fault because the residual pattern is unique in response to each fault. In Figure 7.3, the first, second and third rows represent a bias fault in the manifold pressure sensor, engine speed sensor and longitudinal accelerometer,

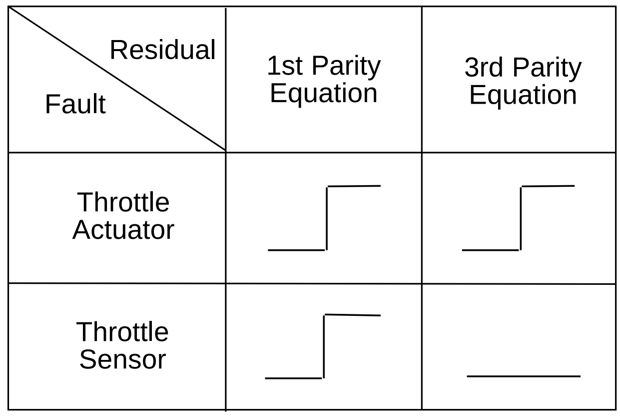

Figure 7.1: Residual patterns

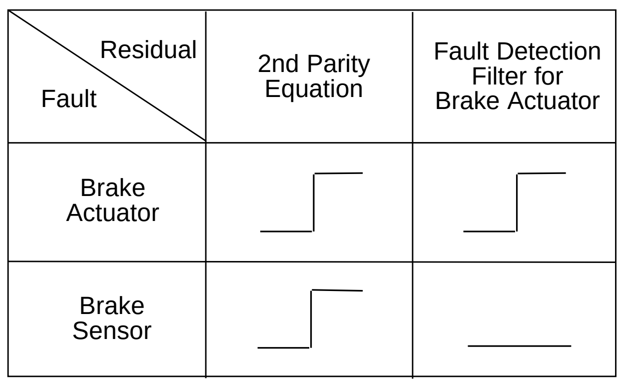

Figure 7.2: Residual patterns

respectively. The first, second and third columns are responses of the residuals of the first parity equation, the unknown input observer that detects the engine speed sensor fault and the unknown input observer that detects the longitudinal accelerometer fault in Section 4.6.1, respectively. This figure shows that the manifold pressure sensor, engine speed sensor and longitudinal accelerometer faults can be identified by combining the residuals of the third parity equation and the unknown input observers that detect the engine speed sensor and longitudinal accelerometer faults because the residual pattern is unique in response to each fault.

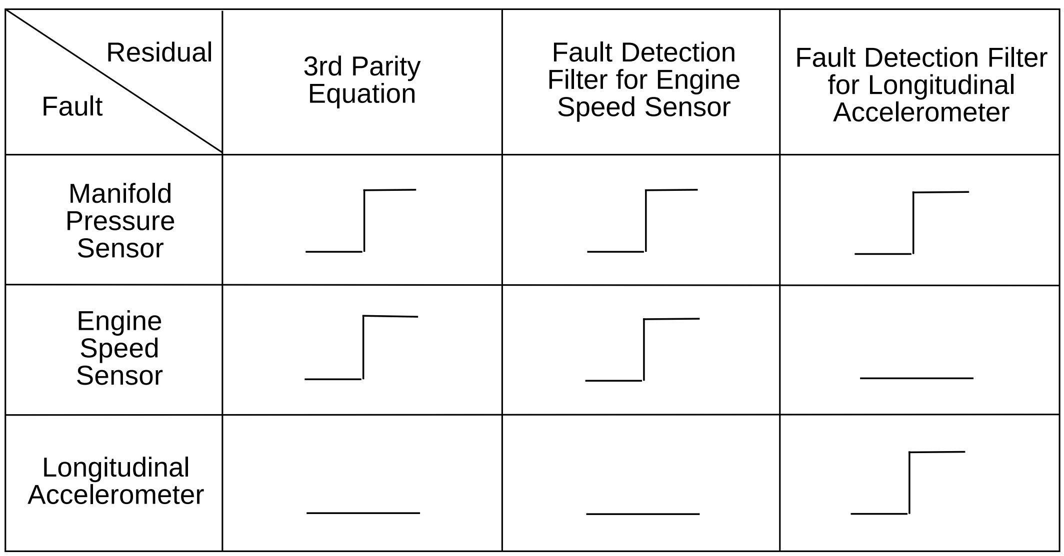

Figure 7.3: Residual patterns

Chapter 8

Residual Processor Design

In this chapter, residual processor is designed to compute probability of fault conditioned hypotheses using the residual pattern constructed by the residual generator. since the longitudinal and lateral vehicles dynamics are decoupled and the residual generator is designed for the longitudinal and lateral mode separately, the design of the residual processor is also spited into two parts respectively. One part processes the residuals generated by the fault detection filters and algebraic parity equations designed for the longitudinal mode. The another part responses to the fault detection filters designed for the lateral mode. Dividing the residual processor into two parts can also reduce the dimension of the input vector and thus, shorten the computation time.

When designing the residual processor for the vehicle longitudinal mode, the residuals of six fault detection filters from fault detection filter set no.1', no.2 and no.3' and two parity equations from parity equation no.1 and no.2 are used. There are five elements from each filter residual and one form each parity equation residual. Therefore, the number of the input elements to the longitudinal residual processor is 32 in total. This leads to intensive computations. To reduce the complexity of the problem and shorten the processing time, the norm of the residual of each filter and parity equation is used instead. Then, the input vector of the longitudinal residual processor has only eight elements. On the other hand, there are six fault detection filters from fault detection filter set no.4, no.5 and no. 6 designed for the vehicle lateral mode. There are four elements from each filter residual and the total number of the input elements to the lateral residual processor is 24. Similarly, the norm of the residual of each filter is used instead. Then, the input vector of the lateral residual processor has only six elements. Another advantage of using just the norm is that only one hypothesis is enough when defining a failure hypothesis. Without the norm operating on the residual, two hypotheses are needed to define one fault. One hypothesis is needed to define the positive fault scenario and the another hypothesis is associated to the negative fault scenario. However, the disadvantage of spiting the design of the residual processor into two parts and using the norm of the residual as the input is that when a fault occurs in the wheel speed sensor, it is not known that whether the fault is in the left wheel or in the right wheel. The problem can be solved by checking the sign of the residual of the wheel speed detection filters after a front wheel speed senor or rear wheel speed sensor fault is announced.

The output of the longitudinal residual processor are the probabilities of no fault, throttle (actuator or sensor) fault, brake actuator fault, brake sensor fault, engine speed sensor fault, longitudinal accelerometer fault, sum of front wheel speed sensor fault and sum of rear wheel speed sensor fault. On the other hand, The probability of no fault, steering actuator fault, lateral accelerometer fault, yaw rate sensor fault, the difference of the front wheel speed sensor fault and the difference of rear wheel speed sensor fault are the outputs of the lateral residual processor. In Section 8.1 the design of the longitudinal residual processor is discussed and in Section 8.2 the design of the lateral residual processor is discussed.

8.1 Longitudinal Residual Processor Design

In the design of the longitudinal residual processor, fifteen hypotheses are defined totally. A no fault hypothesis, also known as null hypothesis in tradition, is defined for the case before any disruption. Two fault hypotheses are defined for each fault direction. Among these two fault hypotheses, the first hypothesis is defined for targeting to smaller magnitude of failures. The second hypothesis is defined for failures with larger magnitude. For each fault, the probability of the fault is just the sum of the probability of these two hypotheses. Although the mean of the residual sequence or correspondingly, the magnitude of the failure is already assumed to have a uniform distribution to encounter the variation of the failure magnitude, two hypotheses corresponding to different size of the fault are still designed. This is to ensure that a small fault can be detected in a shorter time.

The following is the order of the fault detection filter residuals to the input of the longitudinal residual processor and is selected with no particular reason:

1. The residual of front wheel speed sensor fault detection filter from the filter set no. 2.

2. The residual of rear wheel speed sensor fault detection filter from the filter set no. 2.

3. The residual of brake actuator fault detection filter from the filter set no.3'.

4. The residual of rear wheel speed sensor fault detection filter from the filter set no.3'.

5. The residual of engine speed sensor fault detection filter from the filter set no. 1'.

6. The residual of longitudinal accelerometer fault detection filter from the filter set no. 1'.

7. The residual of the first parity equation.

8. The residual of the second parity equation.

Now, we are ready to define the hypothesis conditioned density functions. For the problem at hand, it is assumed that the input vector generated at each time instant is Gaussian distributed. Following the formulation shown in (2.15), a Gaussian distributed random vector $x \in \mathcal{R}^n$ where $x \sim \mathcal{N}(m_i, \Lambda_{x_i})$ with the mean $m_i \in \mathcal{R}^n$ and $m_i \sim Unif[b_i, b_i + 2 \cdot m_i^*] \quad \forall m_i^* \geq 0$ where $b_i \in \mathcal{R}^n$, the probability density function can be written as

$$f_i(x) = \frac{1}{4^n \cdot \Pi_j m_{ij}^*} \cdot [erf\{\frac{1}{\sqrt{2}} \cdot \Lambda_{x_i}^{-1/2} \cdot (x - b_i)\} - erf\{\frac{1}{\sqrt{2}} \cdot \Lambda_{x_i}^{-1/2} \cdot (x - b_i - 2 \cdot m_i^*)\}]$$

Note that Gaussian model may not be the most accurate assumption. Other probability density functions can be chosen to propagate the posterior probability. The analysis in the Shiryayev test still remains the same.

The mean of the conditional probability density under each of the given hypothesis are determined from the simulation. For example, if the magnitude of all the filter residuals are smaller than 0.5 when no fault presents, the mean of the input residual vector can be assumed to be uniformly distributed between 0 and 0.5 when defining the null hypothesis. To define a particular failure hypothesis, the corresponding fault with a variety of magnitude are introduced in the simulation. Then, the corresponding magnitude of the residuals are recorded and the range of the mean can be determined accordingly. The fifteen failure hypotheses have the following distribution: $\mathcal{H}_i$: $x \sim \mathcal{N}(m_i, \Lambda_{x_i})$ with $m_i \sim Unif[b_i, b_i + 2 \cdot m_i^*]$ and $b_i, m_i^* \in \mathcal{R}^n$.

For the null hypothesis, the covariance Λ_{x_i} is a diagonal matrix with 0.01, 0.1, 0.1, 0.001, 0.1, 0.1, 0.1 and 0.1 on the main diagonal line. The range of the mean is defined as $b_i = [\ 0\ \ 0\ \ 0\ \ 0\ \ 0\ \ 0\ \ 0\ \ 0\ ]$ and $m_i^* = [\ 0.25\ \ 0.25\ \ 0.25\ \ 0.25\ \ 0.25\ \ 0.25\ \ 0.25\ \ 0.25\ ]$.

For the small throttle actuator fault hypothesis, the covariance $\Lambda_{x_i} = 0.01 I_8$. The range of the mean is defined as $b_i = [\ 0\ \ 0\ \ 0\ \ 0\ \ 0\ \ 0\ \ 0.5\ \ 0\ ]$ and $m_i^* = [\ 0.25\ \ 0.25\ \ 0.25\ \ 0.25\ \ 0.250.25\ \ 0.5\ \ 0.25\ ]$. For the large throttle actuator fault hypothesis, the covariance $\Lambda_{x_i} = 0.01 I_8$. The range of the mean is defined as $b_i = [\ 0\ \ 0\ \ 0\ \ 0\ \ 0\ \ 0\ \ 1.5\ \ 0\ ]$ and $m_i^* = [\ 0.25\ \ 0.25\ \ 0.25\ \ 0.25\ \ 0.25\ \ 0.25\ \ 1\ \ 0.25\ ]$.

For the small brake actuator fault hypothesis, the covariance Λ_{x_i} is a diagonal matrix with 0.01, 0.001, 0.1, 0.001, 0.01, 0.1, 0.01 and 0.1 on the main diagonal line. The range of the mean is defined as $b_i = [\ 0\ \ 0\ \ 0.5\ \ 0\ \ 0\ \ 0\ \ 0\ \ 0.5\ ]$ and $m_i^* = [\ 0.2507\ \ 0.3004\ \ 0.50000.2500\ \ 0.2804\ \ 0.32\ \ 0.25\ \ 0.5\ ]$. For the large brake actuator fault hypothesis, the covariance Λ_{x_i} is a diagonal matrix with 0.01, 0.001, 0.1, 0.001, 0.01, 0.1, 0.01 and 0.1 on the main diagonal line. The range of the mean is defined as $b_i = [\ 0\ \ 0\ \ 1.5\ \ 0\ \ 0\ \ 0\ \ 0\ \ 1.5\ ]$ and $m_i^* = [\ 0.2520\ \ 0.4012\ \ 1.0000\ \ 0.2500\ \ 0.3413\ \ 0.46\ \ 0.25\ \ 1\ ]$.

For the small brake sensor fault hypothesis, the covariance Λ_{x_i} is a diagonal matrix with 0.1, 0.1, 0.001, 0.1, 0.1, 0.1, 0.1 and 0.1 on the main diagonal line. The range of the mean is defined as $b_i = [0\ \ 0\ \ 0\ \ 0\ \ 0\ \ 0\ \ 0\ \ 0.5\ ]$ and $m_i^* = [\ 0.25\ \ 0.25\ \ 0.25\ \ 0.25\ \ 0.25\ \ 0.25\ \ 0.25\ \ 0.5\ ]$. For the large brake sensor fault hypothesis, the covariance Λ_{x_i} is a diagonal matrix with 0.1, 0.1, 0.001, 0.1, 0.1, 0.1, 0.1 and 0.1 on the main diagonal line. The range of the mean $b_i = [\ 0\ \ 0\ \ 0\ \ 0\ \ 0\ \ 0\ \ 0\ \ 1.5\ ]$ and $m_i^* = [\ 0.25\ \ 0.25\ \ 0.25\ \ 0.25\ \ 0.25\ \ 0.25\ \ 0.25\ \ 1\ ]$.

For the small engine speed sensor fault hypothesis, the covariance Λ_{x_i} is a diagonal matrix with 0.01, 0.01, 0.02, 0.001, 0.01, 0.1, 0.1 and 0.1 on the main diagonal line. The range of the mean is defined as $b_i = [1.2513\ \ 1.1904\ \ 0.9628\ \ 0\ \ 0.5000\ \ 0\ \ 0\ \ 0\ ]$ and $m_i^* = [0.5000\ \ 0.5000\ \ 0.5000\ \ 0.3437\ \ 0.5000\ \ 0.2500\ \ 0.$ For the large engine speed sensor fault hypothesis, the covariance Λ_{x_i} is a diagonal matrix with 0.08, 0.08, 0.08, 0.008, 0.08, 0.8, 1 and 1 on the main diagonal line. The range of the mean is defined as $b_i = [\ 3.0026\ \ 2.8808\ \ 2.4256\ \ 0\ \ 1.5000\ \ 0\ \ 0\ \ 0\ ]$ and $m_i^* = [\ 1.3756\ \ 1.3452\ \ 1.2314\ \ 0.5310\ \ 1.0000\ \ 0.2500\ \ 0.25\ \ 0.$

For the small longitudinal accelerometer fault hypothesis, the covariance Λ_{x_i} is a diagonal matrix with 0.1, 0.001, 0.01, 0.001, 0.1, 0.1, 0.1 and 0.1 on the main diagonal line. The range of the mean is defined as $b_i = [\ 0\ \ 0\ \ 0\ \ 0\ \ 0\ \ 0.5\ \ 0\ \ 0\ ]$ and $m_i^* = [\ 0.2667\ \ 0.2808\ \ 0.3314\ \ 0.2507\ \ 0.2500\ \ 0.5000\ \ 0.25\ \ 0.2$ For the large longitudinal accelerometer fault hypothesis, the covariance Λ_{x_i} is a diagonal matrix with 0.1, 0.001, 0.01, 0.001, 0.1, 0.01, 0.1 and 0.1 on the main diagonal line. The range of the mean is defined as $b_i = [\ 0\ \ 0\ \ 0\ \ 0\ \ 0\ \ 1.5\ \ 0\ \ 0\ ]$ and $m_i^* = [\ 0.3001\ \ 0.3425\ \ 0.49400.2522\ \ 0.2500\ \ 1.0000\ \ 0.25\ \ 0.25\ ]$.

For the small sum of front wheel speed fault hypothesis, the covariance $\Lambda_{x_i}$is a diagonal matrix with 0.1, 0.1, 0.001, 0.1, 0.01, 0.1, 0.1 and 0.1 on the main diagonal line. The range of the mean is defined as $b_i = [\ 0.5000\ \ 0\ \ 0.3968\ \ 0.5718\ \ 0\ \ 0\ \ 0\ \ 0\ ]$ and $m_i^* = [\ 0.5000\ \ 0.2500\ \ 1.5000\ \ 0.5000\ \ 0.4957\ \ 12\ \ 0.25\ \ 0.25$

For the large sum of front wheel speed fault hypothesis, the covariance Λ_{x_i} is a diagonal matrix with 0.5, 0.5, 0.05, 0.5, 0.05, 0.5, 0.1 and 0.1 on the main diagonal line. The range of the mean is defined as $b_i = [\ 1.5000\ \ 0\ \ 1.2937\ \ 1.6436\ \ 0.4828\ \ 0.4160\ \ 0\ \ 0\ ]$ and $m_i^* = [\ 1.0000\ \ 0.2500\ \ 4.5000\ \ 1.0359\ \ 0.7457\ \ 35\ \ 0.25$

For the small sum of rear wheel speed fault hypothesis, the covariance Λ_{x_i} is a diagonal matrix with 0.1, 0.1, 0.3, 0.1, 0.01, 0.1, 0.1 and 0.1 on the main diagonal line. The range of the mean is defined as $b_i = [\ 0\ \ 0.5\ \ 0\ \ 0.5\ \ 0\ \ 0\ \ 0\ \ 0\ ]$ and $m_i^* = [\ 0.2500\ \ 0.5000\ \ 0.25000.5000\ \ 0.4963\ \ 12\ \ 0.25\ \ 0.25\ ]$. For the large sum of rear wheel speed fault hypothesis, the covariance Λ_{x_i} is a diagonal matrix with 0.5, 0.5, 1, 0.5, 0.05, 0.5, 0.1 and 0.1 on the main diagonal line. The range of the mean is defined as $b_i = [0\ \ 1.5000\ \ 0\ \ 1.5000\ \ 0.4853\ \ 0\ \ 0\ \ 0\ ]$ and $m_i^* = [\ 0.2500\ \ 1.0000\ \ 0.2500\ \ 1.0000\ \ 0.7463\ \ 35\ \ 0.25\ \ 0.25\ ]$.

The priori probability of transition $\tilde{p}_i$ is assumed to be 10^{-11} and the a priori probabilities π_i is chosen to be 0.001.

8.2 Lateral Residual Processor Design

The lateral residual processor is designed similarly. A null hypothesis is defined for the case with no fault presented. Two hypotheses are defined for each fault direction except steering actuator fault. Three hypotheses are defined for the steering actuator fault when small, medium and large magnitude of the fault are considered.

The following is the order to the input of the lateral residual processor and is selected with no particular reason:

1. The residual of steering actuator fault detection filter from the filter set no. 1.

2. The residual of front wheel speed sensor fault detection filter from the filter set no. 1.

3. The residual of yaw rate sensor fault detection filter from the filter set no.2.

4. The residual of rear wheel speed sensor fault detection filter from the filter set no.2.

5. The residual of lateral accelerometer fault detection filter from the filter set no. 3.

6. The residual of rear wheel speed sensor fault detection filter from the filter set no. 3.

The twelve hypothesis have the following distribution: $\mathcal{H}_i : x \sim \mathcal{N}(m_i, \Lambda_{x_i})$ with $m_i \sim Unif[b_i, b_i + 2 \cdot m_i^*]$ and $b_i, m_i^* \in \mathcal{R}^n$.

For the null hypothesis, the covariance Λ_{x_i} is a diagonal matrix with 0.1, 1, 0.001, 0.01, 0.1 and 1 on the main diagonal line. The range of the mean is defined as $b_i = [\ 0\ \ 0\ \ 0\ \ 0\ \ 0\ \ 0\ ]$ and $m_i^* = [\ 0.25\ \ 0.25\ \ 0.25\ \ 0.25\ \ 0.25\ \ 0.25\ ]$.

For the small steering actuator fault hypothesis, the covariance Λ_{x_i} is a diagonal matrix with 0.1, 0.01, 1, 0.01, 0.2 and 0.01 on the main diagonal line. The range of the mean is defined as $b_i = [\ 0.5000\ \ 0\ \ 0.6833\ \ 0\ \ 0.3931\ \ 0\ ]$ and $m_i^* = [\ 0.5000\ \ 0.2500\ \ 0.5000\ \ 0.2870\ \ 0.5000\ \ 0.2638\ ]$. For the medium steering actuator fault hypothesis, the covariance Λ_{x_i} is a diagonal matrix with 0.01, 0.01, 0.01, 0.01, 0.1 and 0.01 on the main diagonal line. The range of the mean is defined as $b_i = [\ 1.5000\ \ 0\ \ 1.8666\ \ 0\ \ 1.2862\ \ 0\ ]$ and $m_i^* = [\ 1.00000.2500\ \ 1.0917\ \ 0.3610\ \ 0.9466\ \ 0.2915\ ]$. For the large steering actuator fault hypothesis, the covariance Λ_{x_i} is a diagonal matrix with 0.1, 0.01, 0.1, 0.1, 0.1 and 0.01 on the main diagonal line. The range of the mean is defined as $b_i = [\ 3.5000\ \ 0\ \ 4.2332\ \ 0\ \ 3.0724\ \ 0\ ]$ and $m_i^* = [\ 1.5000\ \ 0.2500\ \ 1.6833\ \ 0.4720\ \ 1.3931\ \ 0.3331\ ]$.

For the small lateral accelerometer fault hypothesis, the covariance Λ_{x_i} is a diagonal matrix with 0.1, 0.01, 1, 0.01, 0.01 and 0.01 on the main diagonal line. The range of the mean is defined as $b_i = [\ 0\ \ 0\ \ 0\ \ 0\ \ 0.5000\ \ 0\ ]$ and $m_i^* = [\ 0.2803\ \ 0.2552\ \ 0.3117\ \ 0.3607\ \ 0.5000\ \ 0.2500\ ]$. For the large lateral accelerometer fault hypothesis, the covariance Λ_{x_i} is a diagonal matrix with 0.01, 0.01, 0.001, 0.01, 0.01 and 0.01 on the main diagonal line. The range of the mean is defined as $b_i = [\ 0\ \ 0\ \ 0\ \ 0\ \ 1.5000\ \ 0\ ]$ and $m_i^* = [\ 0.3410\ \ 0.2656\ \ 0.4353\ \ 0.5820\ \ 1.0000\ \ 0.2500\ ]$.

For the small yaw rate sensor fault hypothesis, the covariance Λ_{x_i} is a diagonal matrix with 0.1, 0.01, 0.001, 0.01, 10 and 0.01 on the main diagonal line. The range of the mean is defined as $b_i = [\ 0.3123\ \ 0\ \ 0.5000\ \ 0\ \ 0\ \ 0\ ]$ and $m_i^* = [\ 0.5000\ \ 0.2529\ \ 0.5000\ \ 0.2500\ \ 0.2996\ \ 0.2540\ ]$. For the large yaw rate sensor fault hypothesis, the covariance Λ_{x_i} is a diagonal matrix with 0.1, 0.01, 0.1, 0.01, 0.3 and 0.01 on the main diagonal line. The range of the mean is defined as $b_i = [\ 1.1246\ \ 0\ \ 1.5000\ \ 0\ \ 0\ \ 0\ ]$ and $m_i^* = [\ 0.9062\ \ 0.2586\ \ 1.0000\ \ 0.2500\ \ 0.3988\ \ 0.2620\ ]$.

For the small difference of front wheel speed fault hypothesis, the covariance Λ_{x_i} is a diagonal matrix with 0.1, 0.01, 0.01, 0.01, 0.1 and 0.01 on the main diagonal line. The range of the mean is defined as $b_i = [\ 00.5000\ \ 0\ \ 0.8950\ \ 3.4900\ \ 1.0660\ ]$ and $m_i^* = [\ 0.2500\ \ 0.5000\ \ 0.3594\ \ 0.5000\ \ 0.5000\ \ 0.5000\ ]$. For the large difference of front wheel speed fault hypothesis, the covariance Λ_{x_i} is a diagonal matrix with 0.1, 0.01, 0.01, 0.01, 0.1 and 0.01 on the main diagonal line. The range of the mean is defined as $b_i = [\ 0\ \ 1.5000\ \ 0\ \ 2.2790\ \ 7.4800\ \ 2.6320\ ]$ and $m_i^* = [\ 0.2500\ \ 1.0000\ \ 0.5784\ \ 1.1943\ \ 2.4950\ \ 1.2830\ ]$.

For the small difference of rear wheel speed fault hypothesis, the covariance Λ_{x_i} is a diagonal matrix with 0.1, 0.01, 0.01, 0.01, 0.01 and 0.01 on the main diagonal line. The range of the mean is defined as $b_i = [\ 0\ \ 0.2042\ \ 0\ \ 0.5000\ \ 0\ \ 0.5000\ ]$ and $m_i^* = [\ 0.2918\ \ 0.5000\ \ 0.2500\ \ 0.5000\ \ 0.2500\ \ 0.5000\ ]$. For the large difference of rear wheel speed fault hypothesis, the covariance Λ_{x_i} is a diagonal matrix with 0.1, 0.01, 0.01, 0.01, 0.01 and 0.01 on the main diagonal line. The range of the mean is defined as $b_i = [\ 0\ \ 0.9084\ \ 0\ \ 1.5000\ \ 0\ \ 1.5000\ ]$ and $m_i^* = [\ 0.3752\ \ 0.8521\ \ 0.2500\ \ 1.0000\ \ 0.2500\ \ 1.0000\ ]$.

This time, the priori probability of transition $\tilde{p}_i$ is assumed to be 10^{-9} and the a priori probabilities π_i is chosen to be 0.001.

Chapter 9

Fault Detection Filter Set No.1, No.2 and No.3 Evaluation

In this chapter, fault detection filter set no.1, no.2 and no.3 are first evaluated using simulated data generated by the vehicle simulation. Then, the three fault detection filter sets are evaluated using empirical data recorded when driving a PATH Buick LeSabre at Crow's Landing. Finally, a real-time testing environment is developed using Linux operating system and C language. This allows the fault detection filters to be evaluated in real-time on a PATH Buick LeSabre. The real-time evaluation at Crow's Landing demonstrates that the fault detection filters can detect and identify actuator and sensor faults as expected even under various disturbances and uncertainties including sensor noise, road noise, system parameter variations, unmodeled dynamics and nonlinearities.

In Section 9.1, the norms of the residuals generated by the fault detection filters are scaled to one when their associated faults of certain magnitudes occur. In Section 9.2, fault detection filters are evaluated using vehicle simulation. In Section 9.3, fault detection filters are evaluated using empirical data. In Section 9.4, the experiment setup (i.e., the real-time testing environment) is discussed. From Sections 9.5 to 9.9, fault detection filters are evaluated in real-time on a PATH Buick LeSabre under different scenarios. In Section 9.10, two issues regarding the fault detection filters are discussed and recommendations are made for future improvement.

9.1 Residual Scaling

Before evaluating the fault detection filters, it is needed to decide how to examine the performance of the fault detection filters. Since the residuals are zero vectors when there is no fault and nonzero vectors when their associated faults occur, the performance of the fault detection filters is examined by checking the norms of the residuals. If the norms of the residuals are zero, there is no fault. If the norm of one of the residuals is nonzero, the fault associated with the nonzero residual occurs.

When evaluating the fault detection filters, the norms of the residuals are scaled to one when their associated faults of certain magnitudes occur. Therefore, the norm of each residual rises to one when evaluated using the same linear model used for fault detection filter design with its associated fault being a step with the magnitude given below.

Engine speed sensor fault: 20 rad/s

Longitudinal accelerometer fault: 1 m/s^2

Front wheel speed sensor fault: 7.5 rad/s

Rear wheel speed sensor fault: 7.5 rad/s

Brake actuator fault: 200 $Nt \cdot m$

The scaling factors by which the norms of the residuals are divided are

Fault detection filter set no. 1	Engine speed sensor residual: 13.401
	Longitudinal accelerometer residual: 665.560
Fault detection filter set no. 2	Front wheel speed sensor residual: 11.942
	Rear wheel speed sensor residual: 6.767
Fault detection filter set no. 3	Brake actuator residual: 8.009
	Rear wheel speed sensor residual: 4.662

If the magnitudes of the faults occurred are twice the magnitudes given above, the norms of the residuals will rise to two. If the magnitudes of the faults occurred are half of the magnitudes given above, the norms of the residuals will rise to one-half. The purpose of the scaling is to present the performance of the fault detection filters in a clearer fashion, i.e., zero residuals represent no fault and residuals of magnitude one represent the occurrence of their associated faults. Note that the residuals can be scaled with respect to any other fault magnitudes if that were desired.

9.2 Evaluation Using Vehicle Simulation

Fault detection filters are first evaluated using simulated data generated by the vehicle simulation. The block diagram is shown in Figure 9.1. Since the fault detection filters are designed based on the linearized vehicle dynamics derived from the nonlinear vehicle dynamics at certain nominal operating point, the nominal values of the control commands and measurements have to be subtracted from the simulated data generated by the vehicle simulation before the fault detection filters can use these data to generate the residuals. From Section 4.6, fault detection filter set no. 1 and 3 are designed based on the linear vehicle model derived at 24 m/s and fault detection filter set no. 2 is designed based on the linear vehicle model derived at 20 m/s. The nominal values of the control commands and measurements at 24 m/s are

Throttle command: 10.2261 deg

Brake command: 0 $Nt \cdot m$

Manifold pressure measurement: 35.8241 psi

Engine speed measurement: 254.2849 rad/s

Longitudinal acceleration measurement: 0 m/s^2

Sum of front wheel speed measurements: 162.3495 rad/s

Sum of rear wheel speed measurements: 156.7578 rad/s

The nominal values of the control commands and measurements at 20 m/s are

Throttle command: 8.6805 deg

Brake command: 0 $Nt \cdot m$

Manifold pressure measurement: 35.2509 psi

Engine speed measurement: 212.7200 rad/s

Longitudinal acceleration measurement: 0 m/s^2

Sum of front wheel speed measurements: 135.2920 rad/s

Sum of rear wheel speed measurements: 130.6160 rad/s

Now fault detection filters can be evaluated using simulated data generated by the vehicle simulation as shown in Figure 9.1. The evaluation shows that the fault detection filters can detect and identify actuator and sensor faults as expected. However, the evaluation is not shown here because the fault detection filters are evaluated in real-time on a PATH Buick LeSabre in later sections which present a more interesting and practical evaluation.

9.3 Evaluation Using Empirical Data

Next, fault detection filters are evaluated using empirical data recorded when driving a PATH Buick LeSabre at Crow's Landing. The block diagram is shown in Figure 9.2. Before evaluating the fault detection filters, a comparison is made between the vehicle simulation and empirical data. Since the simulation does not match the empirical data on some control commands and measurements, a transformation is derived to approximately match the simulation and empirical data when the vehicle is travelling at different constant speeds. Then, the transformation is applied to the control commands and measurements of the empirical data before the fault detection filters use these data to generate the residuals. The transformation is derived as followed.

First, the manifold pressure measurements are obtained from the empirical data when the vehicle is travelling at constant speeds of 20, 22, 24, 26 and 28 m/s, respectively. This is plotted as the 'circle'-line in Figure 9.3. The manifold pressure measurement at each vehicle speed is the average of four manifold pressure measurements obtained from two experiments at Crow's Landing when the vehicle was travelling in both directions. Then, the manifold pressures are obtained from the simulation when the vehicle is travelling at constant speeds of 20, 21, 22, 23, 24, 25, 26, 27 and 28 m/s, respectively. This is plotted as the 'square'-line in Figure 9.3. It is clear that the simulation does not match the empirical data. This might be caused by engine modeling error, which causes the simulation deviates from real vehicle, or sensor error, which causes the empirical data deviates from real vehicle. Therefore, a transformation is obtained to match the simulation and empirical data approximately.

$$\bar{y}_{m_p} = \frac{y_{m_p} + 47}{2.5}$$

where y_{m_p} is from the empirical data and $\bar{y}_{m_p}$ is the transformed manifold pressure measurement which is plotted as the 'triangle'-line in Figure 9.3. Figure 9.3 shows that the transformed manifold pressure measurement matches the simulation and therefore can be used by the fault detection filters to generate residuals. Note that the fault detection filters consider the 'circle'-line in Figure 9.3 to be the nominal (fault-free) measurements and any further deviations are considered as faults.

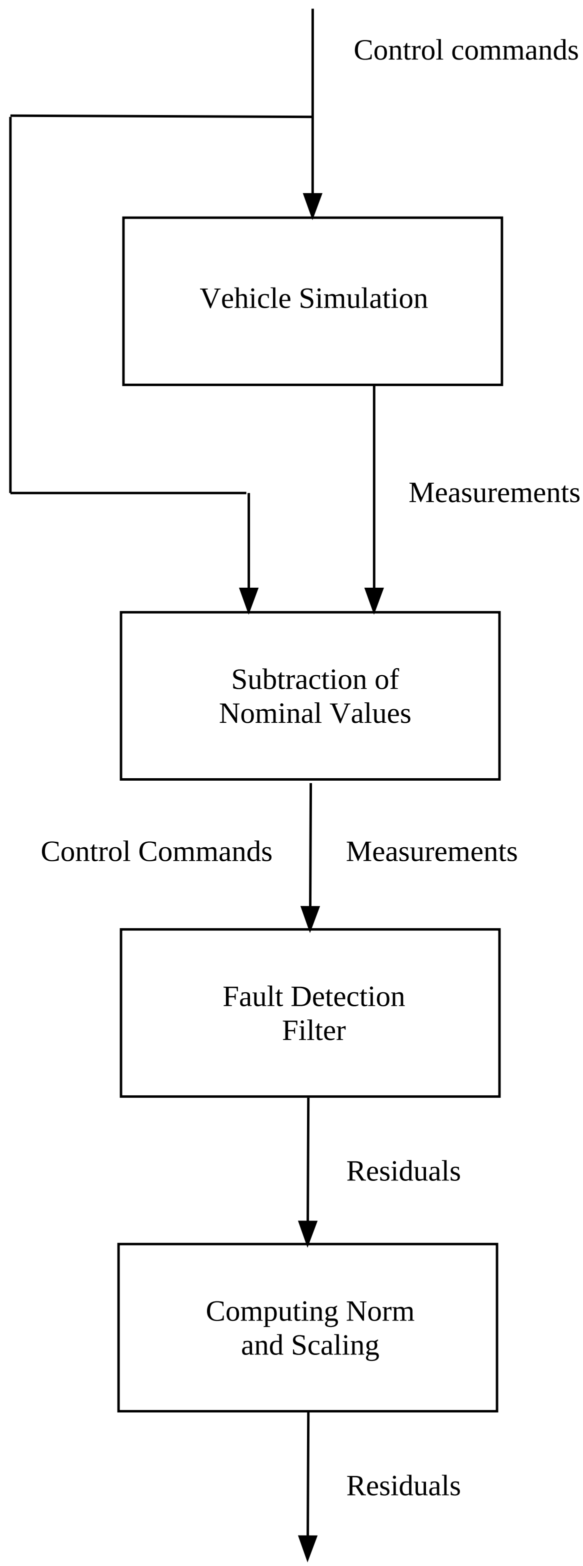

Figure 9.1: Fault detection filter evaluation using vehicle simulation

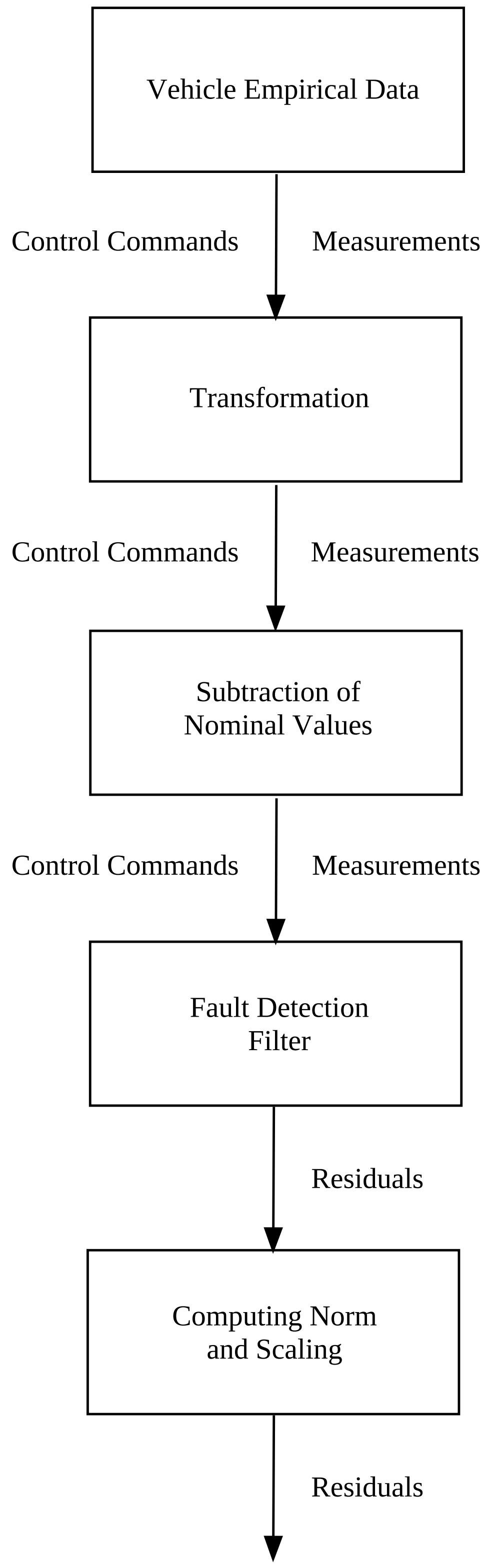

Figure 9.2: Fault detection filter evaluation using empirical data

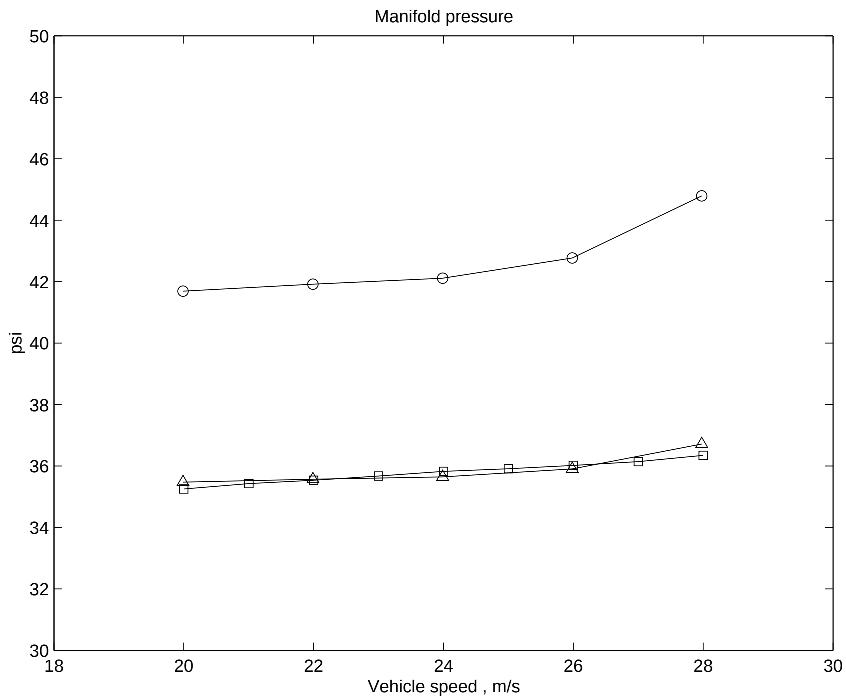

Figure 9.3: Manifold pressure from the simulation and empirical data

For the engine speed measurement, the transformation is derived similarly as shown in Figure 9.4. The 'circle'-line represents the engine speed measurement from the empirical data. The 'square'-line represents the engine speed from the simulation. A transformation is obtained to match the simulation and empirical data approximately.

$$\bar{y}_{w_e} = 1.0913 \left(y_{w_e} \frac{2\pi}{60} \right) + 4.4468$$

where y_{w_e} is from the empirical data and $\bar{y}_{w_e}$ is the transformed engine speed which is plotted as the 'triangle'-line. In the transformation, $\frac{2\pi}{60}$ is used because the units of the engine speed in the simulation and empirical data are rad/s and rpm, respectively. Note that the fault detection filters consider the 'circle'-line in Figure 9.4 to be the nominal (fault-free) measurements and any further deviations are considered as faults.

For the longitudinal acceleration measurement, there is a noisy bias in the longitudinal accelerometer as shown in Figure 9.5. In the top figure, the vehicle reaches constant speed after 40th second. However, the longitudinal acceleration in the bottom figure has a mean of 0.5623 m/s^2 between 40th and 120th seconds. Therefore, a transformation is used to subtract this bias.

$$\bar{y}_{a_x} = y_{a_x} - 0.5623$$

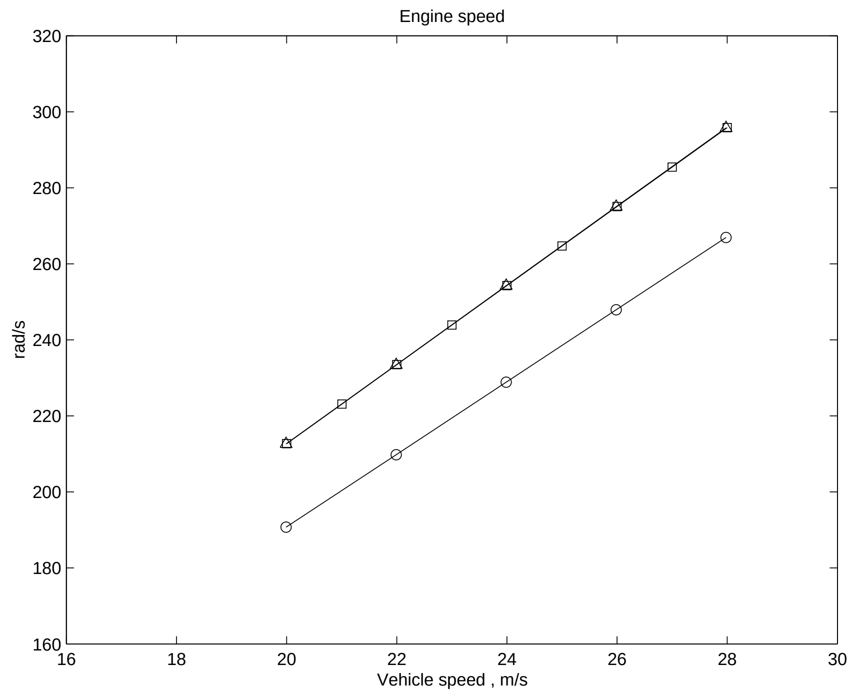

Figure 9.4: Engine speed from the simulation and empirical data

where y_{a_x} is from the empirical data and $\bar{y}_{a_x}$ is the transformed longitudinal acceleration. Note that the fault detection filters consider the longitudinal acceleration with this bias to be the nominal (fault-free) measurement and any further deviations are considered as faults. If a more accurate accelerometer is installed in the future, this transformation will not be needed or a smaller bias will be subtracted in the transformation.

For the front and rear wheel speed measurements, the simulation matches the empirical data. However, the units of the wheel speed in the simulation and empirical data are rad/s and m/s, respectively. Therefore, a transformation is used to transform the wheel speeds in m/s to rad/s.

$$\bar{y}_{\bar{w}_f} = \frac{y_{w_{fl}} + y_{w_{fr}}}{0.2957}$$
$$\bar{y}_{\bar{w}_r} = \frac{y_{w_{rl}} + y_{w_{rr}}}{0.3066}$$

where $y_{w_{fl}}$, $y_{w_{fr}}$, $y_{w_{rl}}$ and $y_{w_{rr}}$ are the four wheel speed measurements from the empirical data, and $\bar{y}_{\bar{w}_f}$ and $\bar{y}_{\bar{w}_f}$ are the transformed wheel speeds. Note that 0.2957 and 0.3066 are the approximate radius of the front and rear tires in the simulation, respectively.

For the throttle command, the transformation is derived similarly to the manifold pressure measurement as shown in Figure 9.6. The 'circle'-line represents the throttle command from

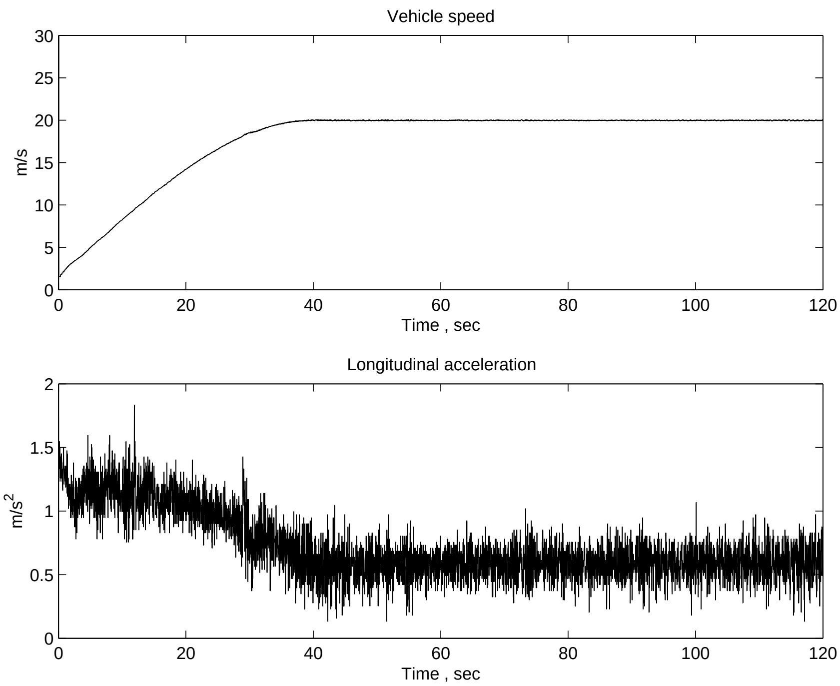

Figure 9.5: Vehicle speed and longitudinal acceleration from the empirical data

the empirical data. The 'square'-line represents the throttle command from the simulation. A transformation is obtained to match the simulation and empirical data approximately.

$$\bar{u}_\alpha = \frac{u_\alpha + 7.25}{2.5}$$

where u_α is from the empirical data and $\bar{u}_\alpha$ is the transformed throttle command which is plotted as the 'triangle'-line.

For the brake command, a different approach has to be used because the brake command is zero when the vehicle is travelling at constant speed. Since the brake command in the empirical data is the brake pressure in the master cylinder and the brake command in the simulation is the brake torque applied to the four wheels, a transformation is needed to transformed the brake pressure into the brake torque. This is done by using the fault detection filter that detects the brake actuator fault. First, a 50 *psi* brake command as shown in the top figure of Figure 9.7 was applied to the vehicle, and the control commands and measurements were recorded. Then, the fault detection filter that detects the brake actuator fault uses these measurements and throttle command with zero brake command to generate the residual shown in the middle figure of Figure 9.7. The residual increases from 0.05 to 0.2 because the brake commands to the vehicle and fault detection filter are different and this difference represents a brake actuator fault. Since this 50 *psi* brake actuator

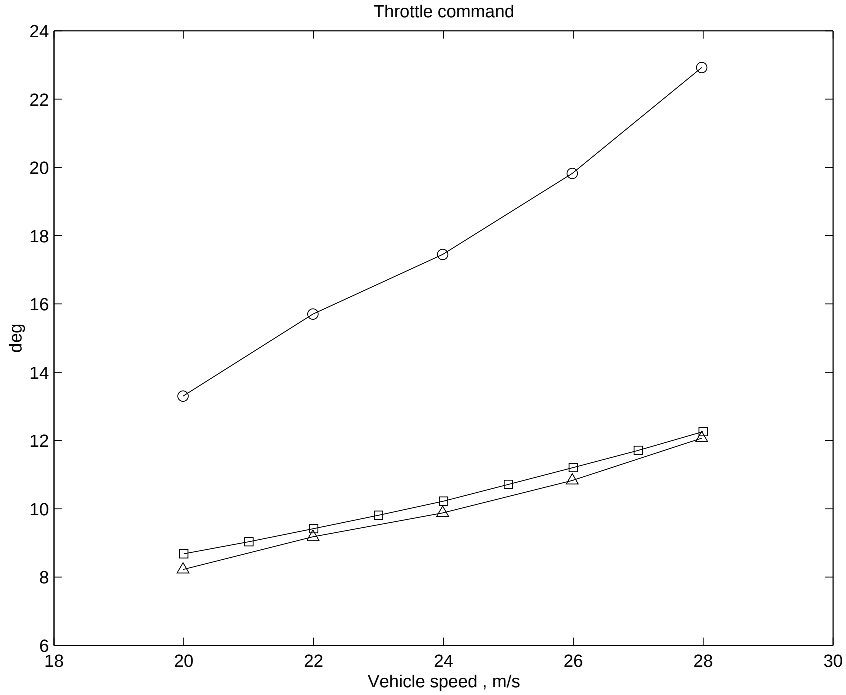

Figure 9.6: Throttle command from the simulation and empirical data

fault causes 0.15 or 0.25 increase in the residual depending on the signs of 0.05 and 0.2, and 200 $Nt \cdot m$ brake actuator fault would cause the residual to increase by one, 50 psi brake pressure is equivalent to 30 or 50 $Nt \cdot m$ brake torque. Therefore, the transformation could be $\bar{u}_{T_b} = 0.6u_{T_b}$ or $\bar{u}_{T_b} = u_{T_b}$ where u_{T_b} is the brake pressure from the empirical data and $\bar{u}_{T_b}$ is the equivalent brake torque. In order to determine which transformation is correct, the fault detection filter uses the control commands and measurements recorded to generate the residual which should remain small if the correct transformation is used. The residual generated by using $\bar{u}_{T_b} = u_{T_b}$ is shown in the bottom figure of Figure 9.7. A 70 psi brake command was also applied to the vehicle to evaluate both transformations. It turns out the transformation should be

$$\bar{u}_{T_b} = u_{T_b}$$

Now the fault detection filters can be evaluated using empirical data recorded when driving a PATH Buick LeSabre at Crow's Landing as shown in Figure 9.2. The evaluation shows that the fault detection filters can detect and identify actuator and sensor faults as expected. However, the evaluation is not shown here because the fault detection filters are evaluated in real-time on a PATH Buick LeSabre in later sections which present a more interesting and practical evaluation.

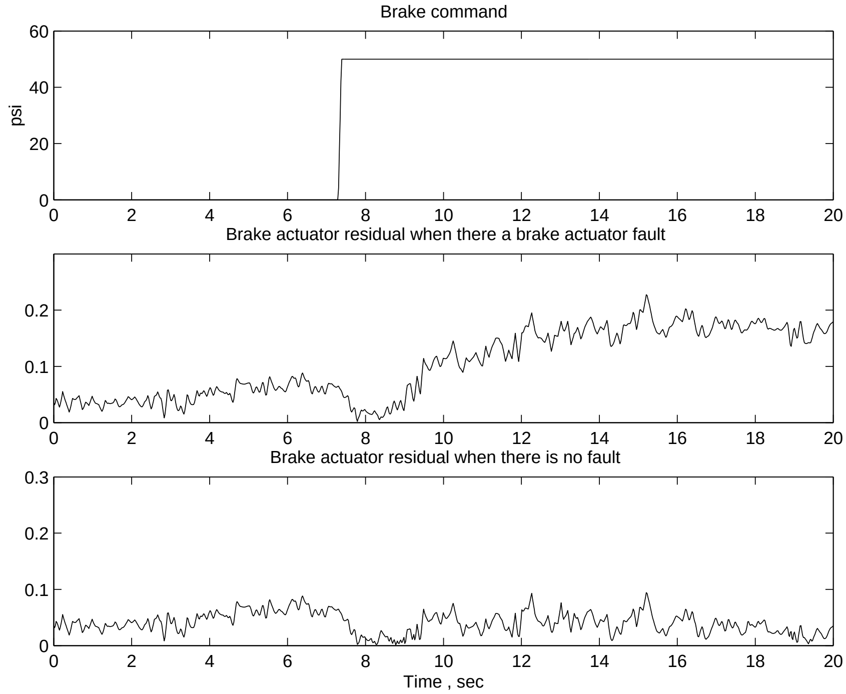

Figure 9.7: Brake command and brake actuator residuals

9.4 Experiment Setup

In this section, a real-time testing environment is developed using Linux operating system and C language to evaluate the fault detection filters in real-time on a PATH Buick LeSabre as shown in Figure 9.8. The fault detection filters are written in C code and executed on a laptop running Linux operating system. The laptop is connected to the computer in the trunk of the PATH Buick LeSabre through a serial port. An input/output interface is developed to allow the data, control commands and sensor measurements, be transmitted from the PATH computer to the UCLA laptop every twenty-one millisecond. The UCLA laptop checks its serial port buffer and downloads the data if the complete set of data is in the buffer. Then, the fault detection filter code is executed to generated the residuals. This process requires much less than twenty-one millisecond. After the residuals are generated, the UCLA laptop proceeds to check the serial port buffer and waits for the next set of data.

From Sections 9.5 to 9.9, fault detection filters are evaluated in real-time on a PATH Buick LeSabre at Crow's Landing under different scenarios. Before evaluating the fault detection filters, it is needed to decide how to generate the actuator and sensor faults. Since it is not practical to really break the actuators or sensors, most faults are simulated by the computer. For the sensor

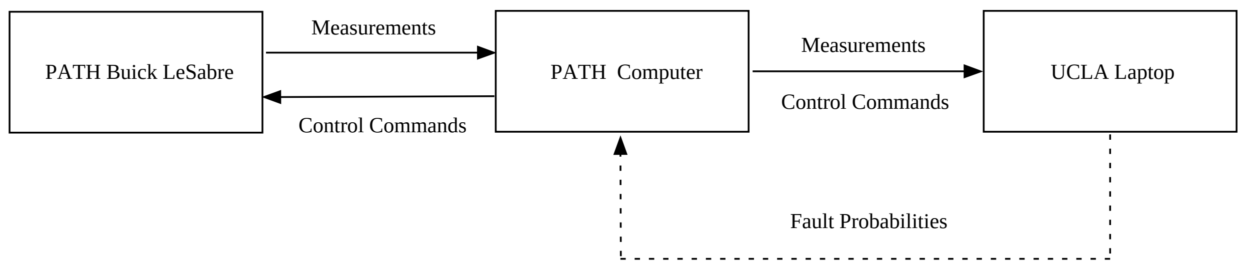

Figure 9.8: Experiment setup

fault, it is simulated by superimposing the fault onto the measurement, i.e., the faulty measurement is the sum of the correct measurement and the sensor fault. For fault detection filter evaluation, this is as real as an actual sensor fault because the faulty measurement that the fault detection filters use is the same whether the fault is generated by the actual sensor or simulated by the PATH computer or UCLA laptop. However, it is important that the sensor fault simulated is realistic in the sense that it represents how the sensor fails.

For the actuator fault, it is simulated by giving the fault detection filters a different control command than the control command applied to the vehicle. The difference between these two control commands will be the actuator fault because it can be viewed that the fault detection filters receive the correct control command, but the vehicle receives a different control command due to an actuator fault. For example, if an actuator has a bias, the control command applied to the fault detection filters will be the control command applied to the vehicle subtracted by the bias. If an actuator is stuck, the control command to the vehicle will be a constant and the control command to the fault detection filters would be any control command decided by the designer.

From Sections 9.5 to 9.8, fault detection filters are evaluated in real-time on a PATH Buick LeSabre at Crow's Landing with actuator and sensor faults simulated by the UCLA laptop. The faults are simulated as bias with magnitudes given below.

Engine speed sensor fault: 175 rpm

Longitudinal accelerometer fault: 1 m/s^2

Front wheel speed sensor fault: 2.218 m/s

Rear wheel speed sensor fault: 2.299 m/s

Brake actuator fault: 200 psi

After applying the transformation in Section 9.3, these fault magnitudes are equivalent to the fault magnitudes in the vehicle simulation that are used to scale the residuals in Section 9.1. In Section 9.9, fault detection filters are evaluated in real-time on a PATH Buick LeSabre at Crow's Landing with a brake actuator fault generated by stepping on the brake pedal. Since this additional brake is only applied to the vehicle, but not to the fault detection filters, this creates a real brake actuator fault for fault detection filter evaluation.

9.5 Evaluation Scenario No. 1: Constant Vehicle Speed

In this section, fault detection filters are evaluated in real-time on a PATH Buick LeSabre at Crow's Landing when the vehicle is travelling at a constant speed of 22 m/s (49.5 mph). Figure 9.9 shows the vehicle speed and throttle command generated by the controller designed by Dr. Xiao-Yun Lu at Richmond Field Station. The figure is plotted along the data point instead of time and each data point represents twenty-one milliseconds. For example, one thousand data points in the figure represents a time interval of twenty-one seconds.

Figure 9.10 shows the performance of the fault detection filter set no. 1. The first row is the engine speed sensor residual and the second row is the longitudinal accelerometer residual. The first column shows both residuals when there is no fault. The second column shows both residuals when an engine speed sensor fault occurs after 4000th data point. The engine speed sensor fault is a bias with magnitude of 175 rpm. The third column shows both residuals when a longitudinal accelerometer fault occurs after 4000th data point. The longitudinal accelerometer fault is a bias with magnitude of 1 m/s^2. Figure 9.10 shows that when each fault occurs, only the associated residual rises to one while the other residual remains very small. Therefore, fault detection filter set no. 1 can detect and identify the engine speed sensor and longitudinal accelerometer faults.

Figure 9.11 shows the performance of the fault detection filter set no. 2. The first row is the front wheel speed sensor residual and the second row is the rear wheel speed sensor residual. The first column shows both residuals when there is no fault. The second column shows both residuals when a front wheel speed sensor fault occurs after 4000th data point. The front wheel speed sensor fault is a bias with magnitude of 2.218 m/s. The third column shows both residuals when a rear wheel speed sensor fault occurs after 4000th data point. The rear wheel speed sensor fault is a bias with magnitude of 2.299 m/s. Figure 9.11 shows that when each fault occurs, only the associated

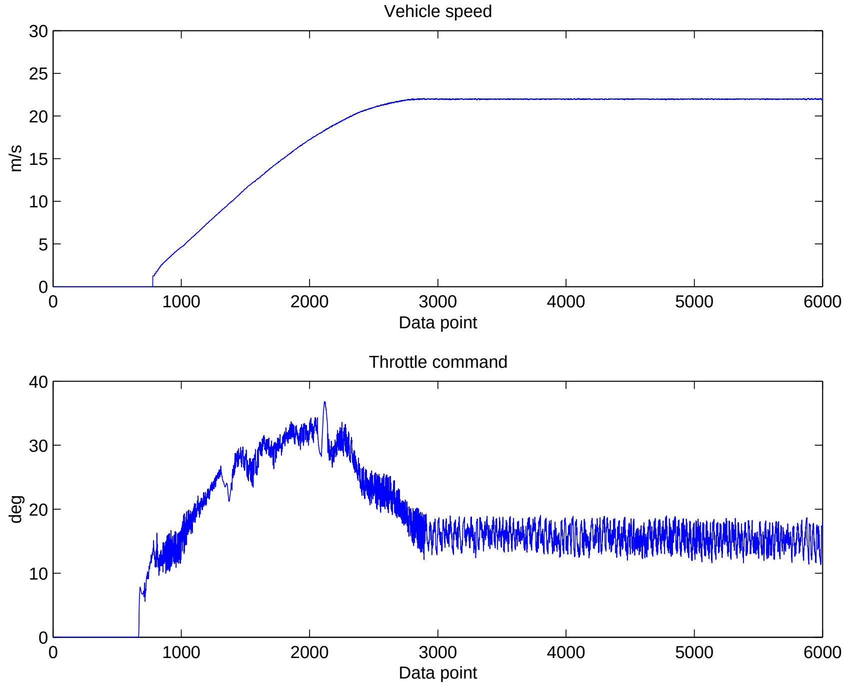

Figure 9.9: Vehicle speed and throttle command

residual rises to one while the other residual remains very small. Therefore, fault detection filter set no. 2 can detect and identify the front and rear wheel speed sensor faults.

Figure 9.12 shows the performance of the fault detection filter set no. 3. The first row is the brake actuator residual and the second row is the rear wheel speed sensor residual. The first column shows both residuals when there is no fault. The second column shows both residuals when a brake actuator fault occurs after 4000th data point. The brake actuator fault is a bias of magnitude 200 psi. The third column shows both residuals when a rear wheel speed sensor fault occurs after 4000th data point. The rear wheel speed sensor fault is a bias of magnitude 2.299 m/s. Figure 9.12 shows that when each fault occurs, only the associated residual rises to one while the other residual remains very small. Therefore, fault detection filter set no. 3 can detect and identify the brake actuator and rear wheel speed sensor faults. Note that the brake actuator residual rises approximately to 0.2 very briefly when the rear wheel speed sensor fault occurs because only the fault magnitude direction is used to model the rear wheel speed sensor fault direction in Section 4.6.3.

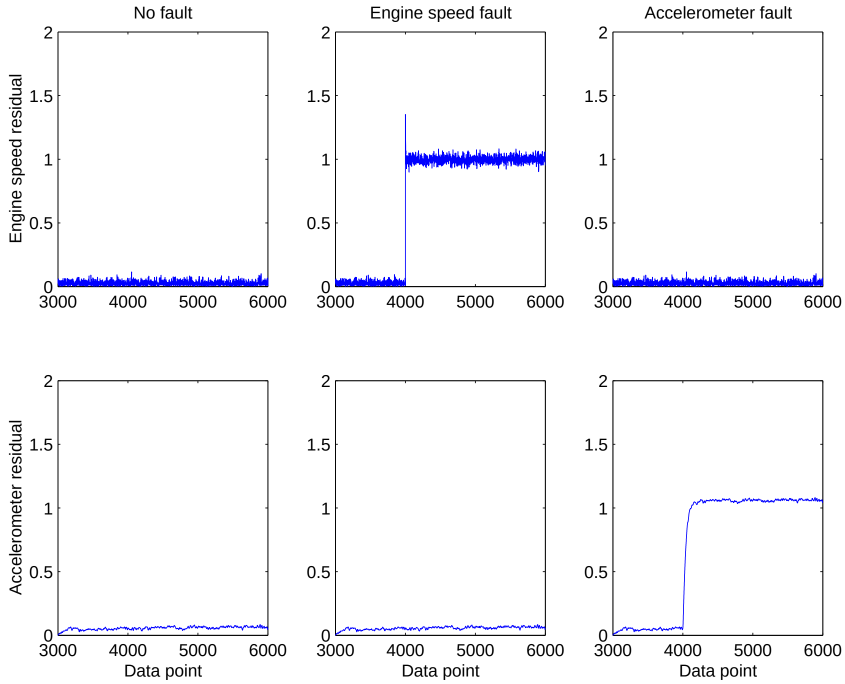

Figure 9.10: Residuals of the fault detection filter set no. 1

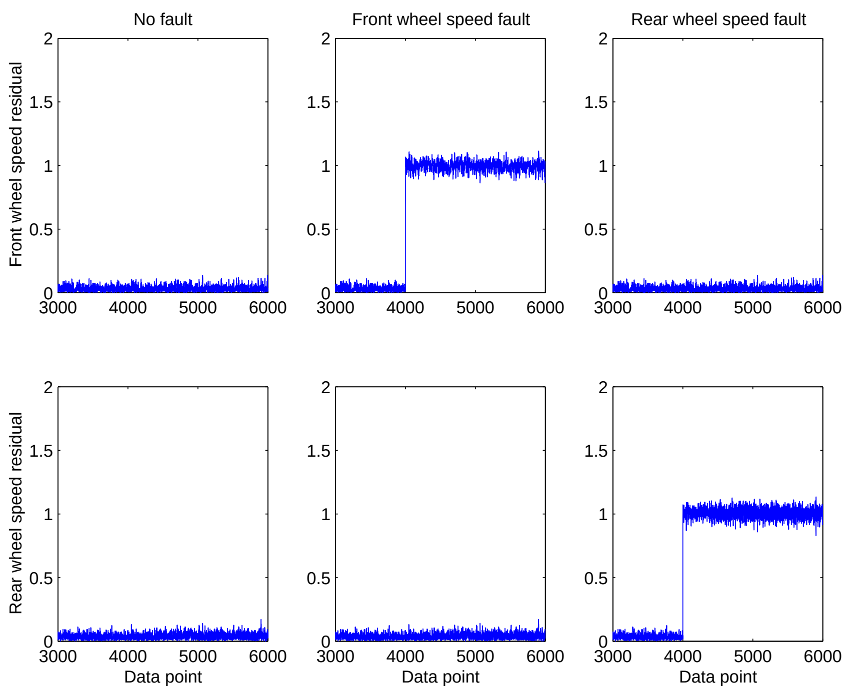

Figure 9.11: Residuals of the fault detection filter set no. 2

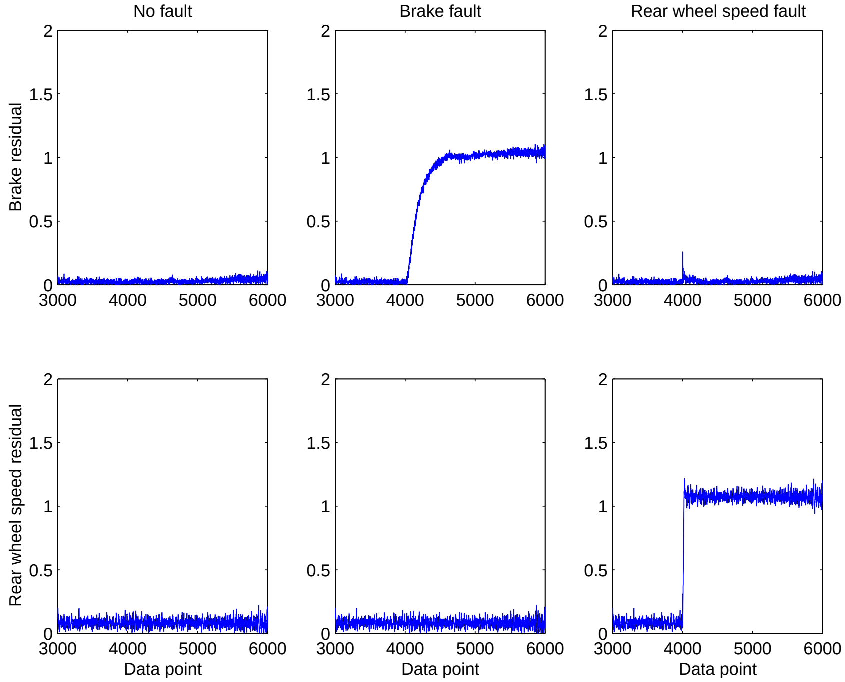

Figure 9.12: Residuals of the fault detection filter set no. 3

9.6 Evaluation Scenario No. 2: Increasing Vehicle Speed

In this section, fault detection filters are evaluated in real-time on a PATH Buick LeSabre at Crow's Landing when the vehicle speed increases from 20 to 28 m/s (45 to 63 mph). The vehicle first reaches a constant speed of 20 m/s. Then, the vehicle increases speed to 28 m/s by increasing the throttle angle. Figure 9.13 shows the vehicle speed and throttle command. The figure is plotted along the data point instead of time and each data point represents twenty-one milliseconds. For example, one thousand data points in the figure represents a time interval of twenty-one seconds.

Figure 9.14 shows the performance of the fault detection filter set no. 1. The first row is the engine speed sensor residual and the second row is the longitudinal accelerometer residual. The first column shows both residuals when there is no fault. The second column shows both residuals when an engine speed sensor fault occurs after 4000th data point. The engine speed sensor fault is a bias with magnitude of 175 rpm. The third column shows both residuals when a longitudinal accelerometer fault occurs after 4000th data point. The longitudinal accelerometer fault is a bias with magnitude of 1 m/s^2. Figure 9.14 shows that when each fault occurs, only the associated residual rises to one while the other residual remains very small. Therefore, fault detection filter set no. 1 can detect and identify the engine speed sensor and longitudinal accelerometer faults.

Note that the residuals increase a little around 3300th data point due to the nonlinearity when increasing the throttle angle.

Figure 9.15 shows the performance of the fault detection filter set no. 2. The first row is the front wheel speed sensor residual and the second row is the rear wheel speed sensor residual. The first column shows both residuals when there is no fault. The second column shows both residuals when a front wheel speed sensor fault occurs after 4000th data point. The front wheel speed sensor fault is a bias with magnitude of 2.218 m/s. The third column shows both residuals when a rear wheel speed sensor fault occurs after 4000th data point. The rear wheel speed sensor fault is a bias with magnitude of 2.299 m/s. Figure 9.15 shows that when each fault occurs, only the associated residual rises to one while the other residual remains very small. Therefore, fault detection filter set no. 2 can detect and identify the front and rear wheel speed sensor faults. Note that the residuals increase to 0.45 around 3300th data point due to the nonlinearity when increasing the throttle angle.

Figure 9.16 shows the performance of the fault detection filter set no. 3. The first row is the brake actuator residual and the second row is the rear wheel speed sensor residual. The first column shows both residuals when there is no fault. The second column shows both residuals when a brake actuator fault occurs after 4000th data point. The brake actuator fault is a bias of magnitude 200 psi. The third column shows both residuals when a rear wheel speed sensor fault occurs after 4000th data point. The rear wheel speed sensor fault is a bias of magnitude 2.299 m/s. Figure 9.16 shows that when each fault occurs, only the associated residual becomes large while the other residual remains very small. Therefore, fault detection filter set no. 3 can detect and identify the brake actuator and rear wheel speed sensor faults. Note that the brake actuator residual increases a little around 3300th data point due to the nonlinearity when increasing the throttle angle. Also note that the brake actuator residual rises approximately to 0.5 very briefly when the rear wheel speed sensor fault occurs because only the fault magnitude direction is used to model the rear wheel speed sensor fault direction in Section 4.6.3.

9.7 Evaluation Scenario No. 3: Decreasing Vehicle Speed

In this section, fault detection filters are evaluated in real-time on a PATH Buick LeSabre at Crow's Landing when the vehicle speed decreases from 24 to 18 m/s (54 to 40.5 mph). The vehicle first

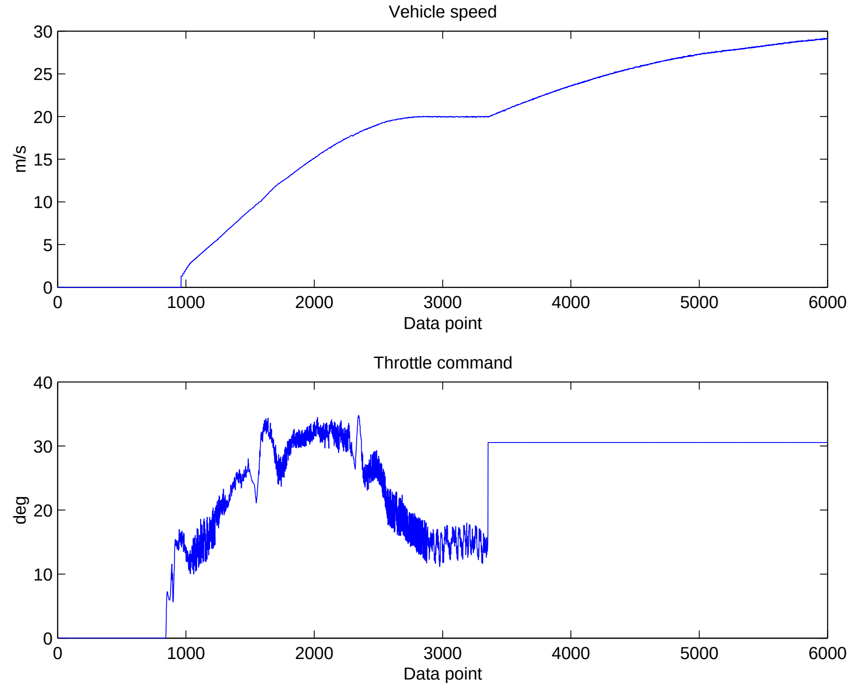

Figure 9.13: Vehicle speed and throttle command

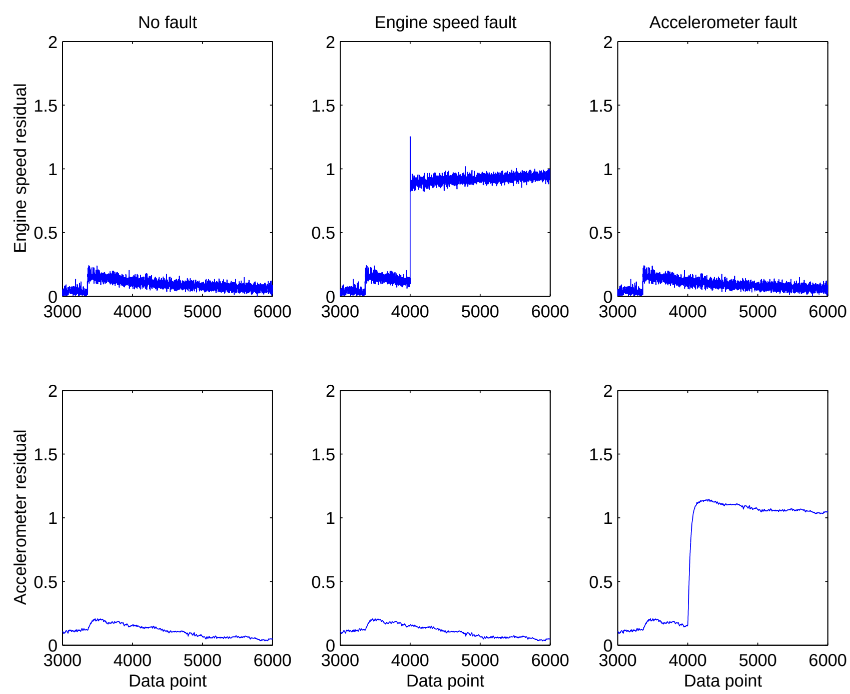

Figure 9.14: Residuals of the fault detection filter set no. 1

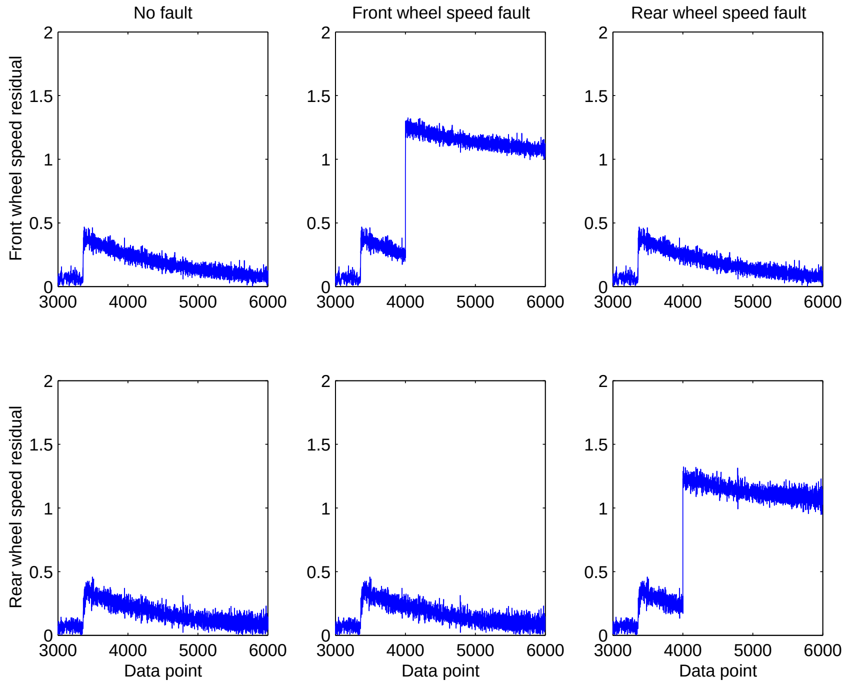

Figure 9.15: Residuals of the fault detection filter set no. 2

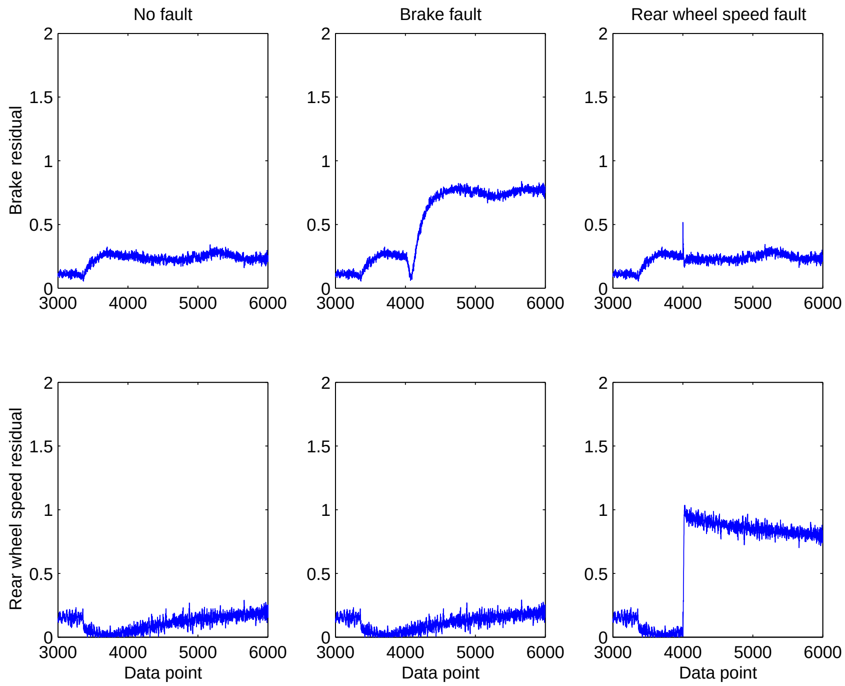

Figure 9.16: Residuals of the fault detection filter set no. 3

reaches a constant speed of 24 m/s. Then, the vehicle decreases speed to 18 m/s by decreasing the throttle angle. Figure 9.17 shows the vehicle speed and throttle command. The figure is plotted along the data point instead of time and each data point represents twenty-one milliseconds. For example, one thousand data points in the figure represents a time interval of twenty-one seconds.

Figure 9.18 shows the performance of the fault detection filter set no. 1. The first row is the engine speed sensor residual and the second row is the longitudinal accelerometer residual. The first column shows both residuals when there is no fault. The second column shows both residuals when an engine speed sensor fault occurs after 4000th data point. The engine speed sensor fault is a bias with magnitude of 175 rpm. The third column shows both residuals when a longitudinal accelerometer fault occurs after 4000th data point. The longitudinal accelerometer fault is a bias with magnitude of 1 m/s^2. Figure 9.18 shows that when each fault occurs, only the associated residual rises to one while the other residual remains very small. Therefore, fault detection filter set no. 1 can detect and identify the engine speed sensor and longitudinal accelerometer faults. Note that the residuals increase a little around 3600th data point due to the nonlinearity when decreasing the throttle angle.

Figure 9.19 shows the performance of the fault detection filter set no. 2. The first row is the front wheel speed sensor residual and the second row is the rear wheel speed sensor residual. The first column shows both residuals when there is no fault. The second column shows both residuals when a front wheel speed sensor fault occurs after 4000th data point. The front wheel speed sensor fault is a bias with magnitude of 2.218 m/s. The third column shows both residuals when a rear wheel speed sensor fault occurs after 4000th data point. The rear wheel speed sensor fault is a bias with magnitude of 2.299 m/s. Figure 9.19 shows that when each fault occurs, only the associated residual rises to one while the other residual remains very small. Therefore, fault detection filter set no. 2 can detect and identify the front and rear wheel speed sensor faults. Note that the residuals increase a little around 3600th data point due to the nonlinearity when decreasing the throttle angle.

Figure 9.20 shows the performance of the fault detection filter set no. 3. The first row is the brake actuator residual and the second row is the rear wheel speed sensor residual. The first column shows both residuals when there is no fault. The second column shows both residuals when a brake actuator fault occurs after 4000th data point. The brake actuator fault is a bias of

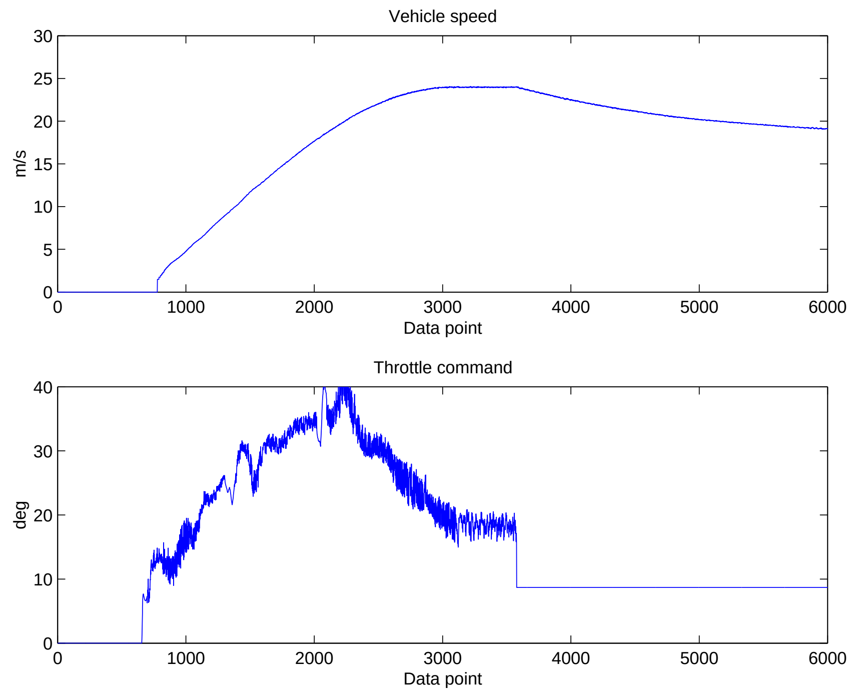

Figure 9.17: Vehicle speed and throttle command

magnitude 200 *psi*. The third column shows both residuals when a rear wheel speed sensor fault occurs after 4000th data point. The rear wheel speed sensor fault is a bias of magnitude 2.299 m/s. Figure 9.20 shows that when each fault occurs, only the associated residual rises to one while the other residual remains very small. Therefore, fault detection filter set no. 3 can detect and identify the brake actuator and rear wheel speed sensor faults. Note that the residuals increase a little around 3600th data point due to the nonlinearity when decreasing the throttle angle.

9.8 Evaluation Scenario No. 4: Increasing and Decreasing Vehicle Speed

In this section, fault detection filters are evaluated in real-time on a PATH Buick LeSabre at Crow's Landing when the vehicle speed increases from 24 to 28 m/s (54 to 63 *mph*) then decreases to 24 m/s. The vehicle first reaches a constant speed of 24 m/s. Then, the vehicle increases speed to 28 m/s by increasing the throttle angle. Finally, the vehicle decreases speed to 24 m/s by decreasing the throttle angle. Figure 9.21 shows the vehicle speed and throttle command. The figure is plotted along the data point instead of time and each data point represents twenty-one milliseconds. For example, one thousand data points in the figure represents a time interval of twenty-one seconds.

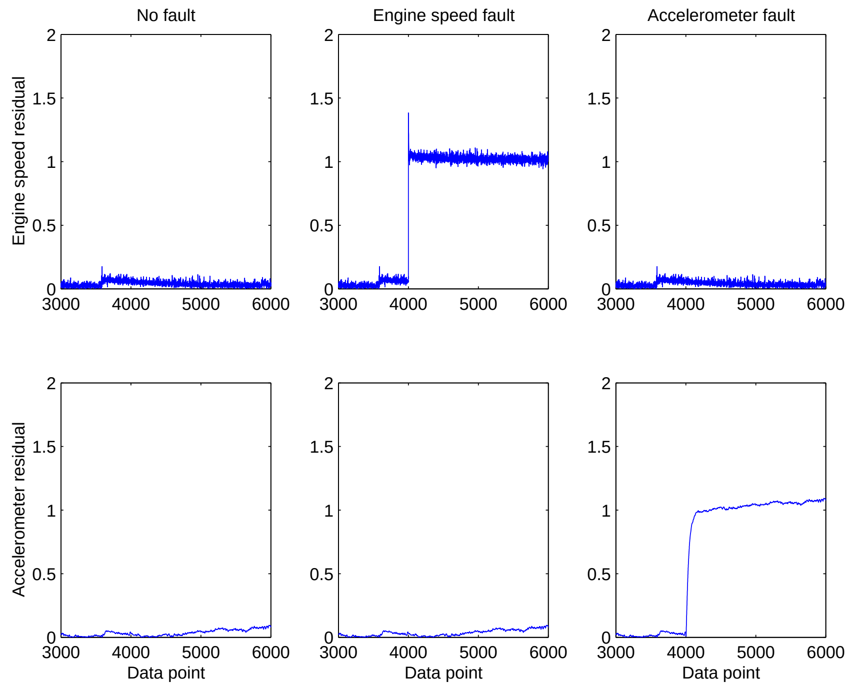

Figure 9.18: Residuals of the fault detection filter set no. 1

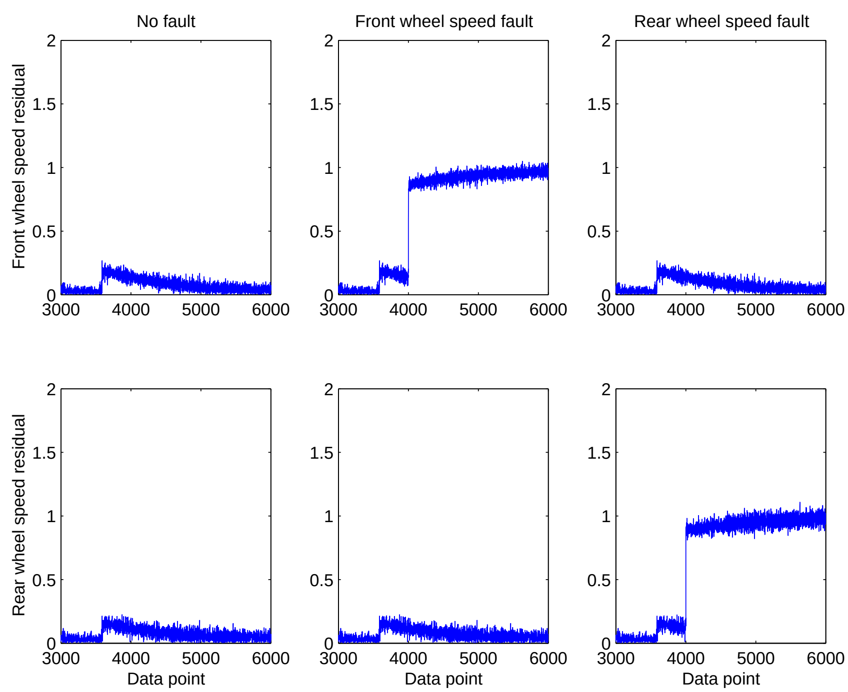

Figure 9.19: Residuals of the fault detection filter set no. 2

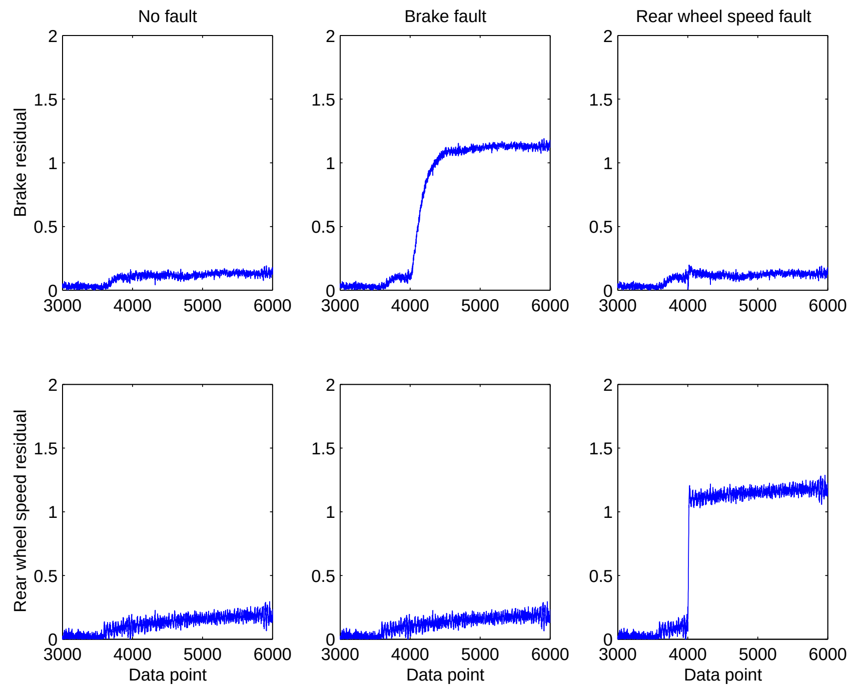

Figure 9.20: Residuals of the fault detection filter set no. 3

Figure 9.22 shows the performance of the fault detection filter set no. 1. The first row is the engine speed sensor residual and the second row is the longitudinal accelerometer residual. The first column shows both residuals when there is no fault. The second column shows both residuals when an engine speed sensor fault occurs after 4000th data point. The engine speed sensor fault is a bias with magnitude of 175 rpm. The third column shows both residuals when a longitudinal accelerometer fault occurs after 4000th data point. The longitudinal accelerometer fault is a bias with magnitude of 1 m/s^2. Figure 9.22 shows that when each fault occurs, only the associated residual rises to one while the other residual remains very small. Therefore, fault detection filter set no. 1 can detect and identify the engine speed sensor and longitudinal accelerometer faults.

Figure 9.23 shows the performance of the fault detection filter set no. 2. The first row is the front wheel speed sensor residual and the second row is the rear wheel speed sensor residual. The first column shows both residuals when there is no fault. The second column shows both residuals when a front wheel speed sensor fault occurs after 4000th data point. The front wheel speed sensor fault is a bias with magnitude of 2.218 m/s. The third column shows both residuals when a rear wheel speed sensor fault occurs after 4000th data point. The rear wheel speed sensor fault is a bias with magnitude of 2.299 m/s. Figure 9.23 shows that when each fault occurs, only the associated

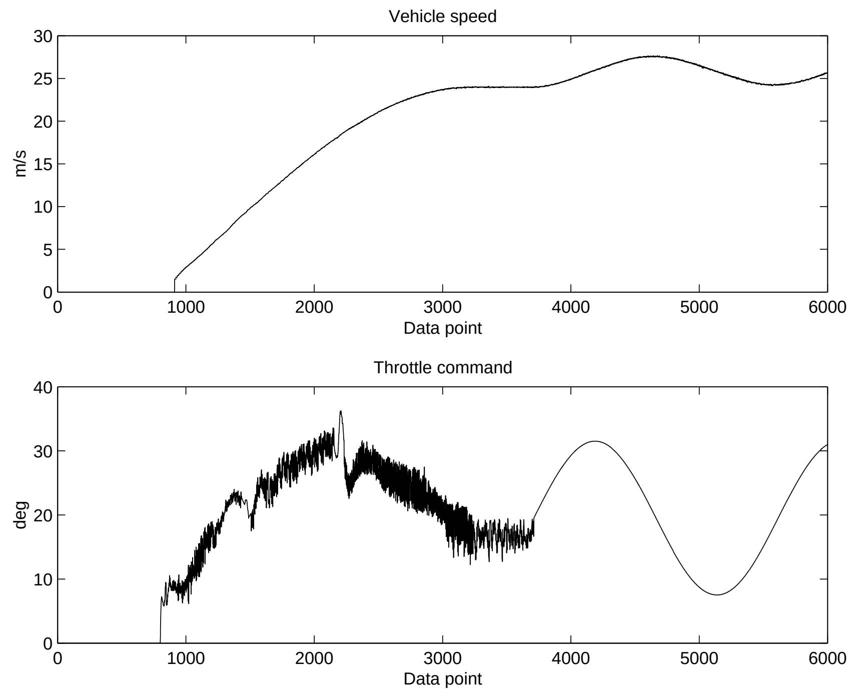

Figure 9.21: Vehicle speed and throttle command

residual rises to one while the other residual remains very small. Therefore, fault detection filter set no. 2 can detect and identify the front and rear wheel speed sensor faults.

Figure 9.24 shows the performance of the fault detection filter set no. 3. The first row is the brake actuator residual and the second row is the rear wheel speed sensor residual. The first column shows both residuals when there is no fault. The second column shows both residuals when a brake actuator fault occurs after 4000th data point. The brake actuator fault is a bias of magnitude 200 psi. The third column shows both residuals when a rear wheel speed sensor fault occurs after 4000th data point. The rear wheel speed sensor fault is a bias of magnitude 2.299 m/s. Figure 9.24 shows that when each fault occurs, only the associated residual becomes large while the other residual remains very small. Therefore, fault detection filter set no. 3 can detect and identify the brake actuator and rear wheel speed sensor faults. Note that the brake actuator residual rises approximately to 0.2 very briefly when the rear wheel speed sensor fault occurs because only the fault magnitude direction is used to model the rear wheel speed sensor fault direction in Section 4.6.3.

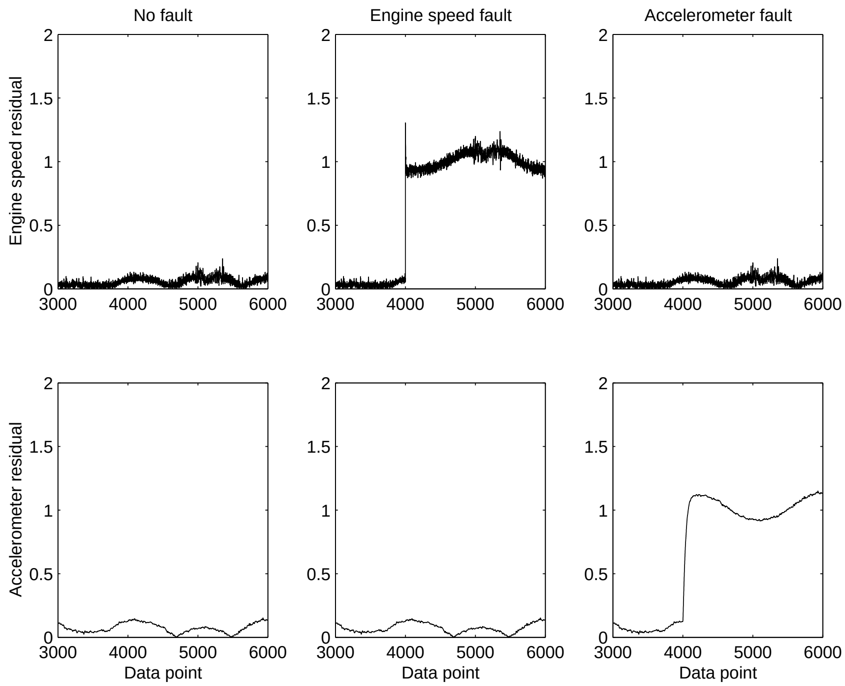

Figure 9.22: Residuals of the fault detection filter set no. 1

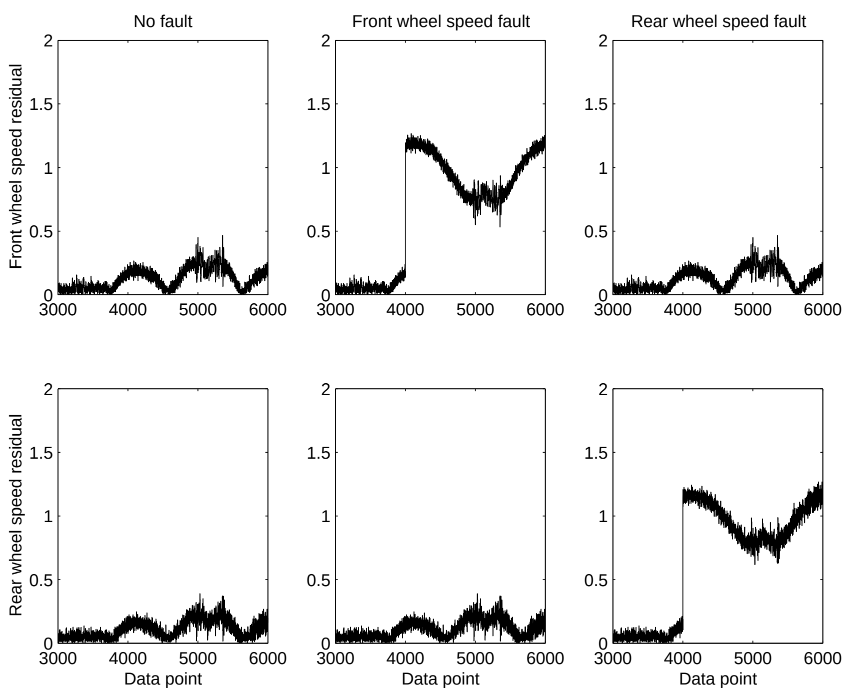

Figure 9.23: Residuals of the fault detection filter set no. 2

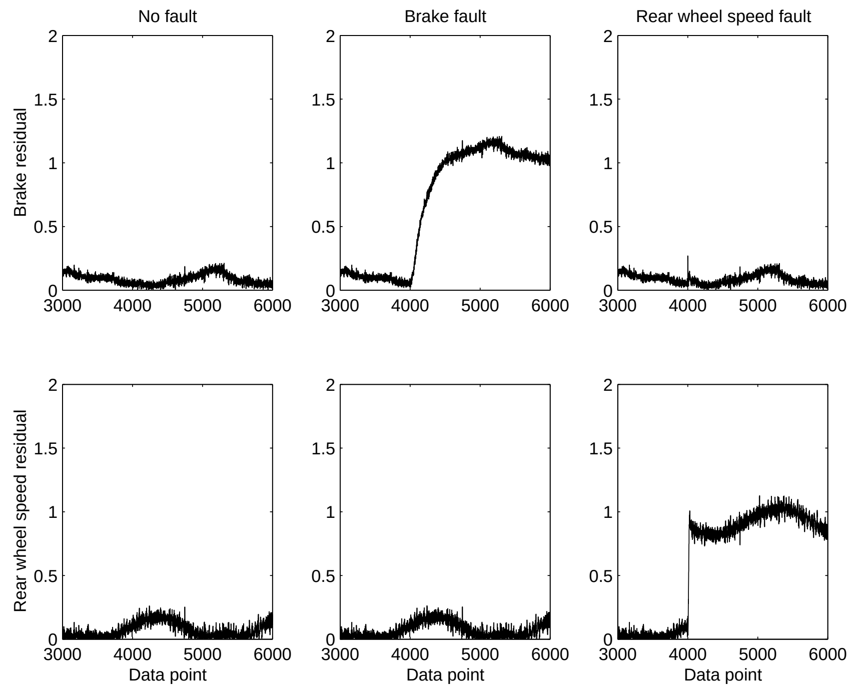

Figure 9.24: Residuals of the fault detection filter set no. 3

9.9 Evaluation Scenario No. 5: Real Brake Actuator Fault

In this section, fault detection filters are evaluated in real-time on a PATH Buick LeSabre at Crow's Landing with a real brake actuator fault. Figure 9.25 shows the vehicle speed. The vehicle first reaches a constant speed of 24 m/s (54 mph). Then, a real brake actuator fault is generated by stepping on the brake pedal around 3400th data point which causes the vehicle speed decreases to 18 m/s (40.5 mph). The figure is plotted along the data point instead of time and each data point represents twenty-one milliseconds. For example, one thousand data points in the figure represents a time interval of twenty-one seconds.

Figure 9.26 shows the performance of the fault detection filter set no. 3. The top figure is the brake actuator residual and the bottom figure is the rear wheel speed sensor residual. It is clear that the brake actuator residual becomes large when the real brake actuator fault occurs while the rear wheel speed sensor residual remains small. Therefore, fault detection filter set no. 3 can detect the brake actuator fault. Note that the brake actuator residual becomes small again after releasing the brake pedal.

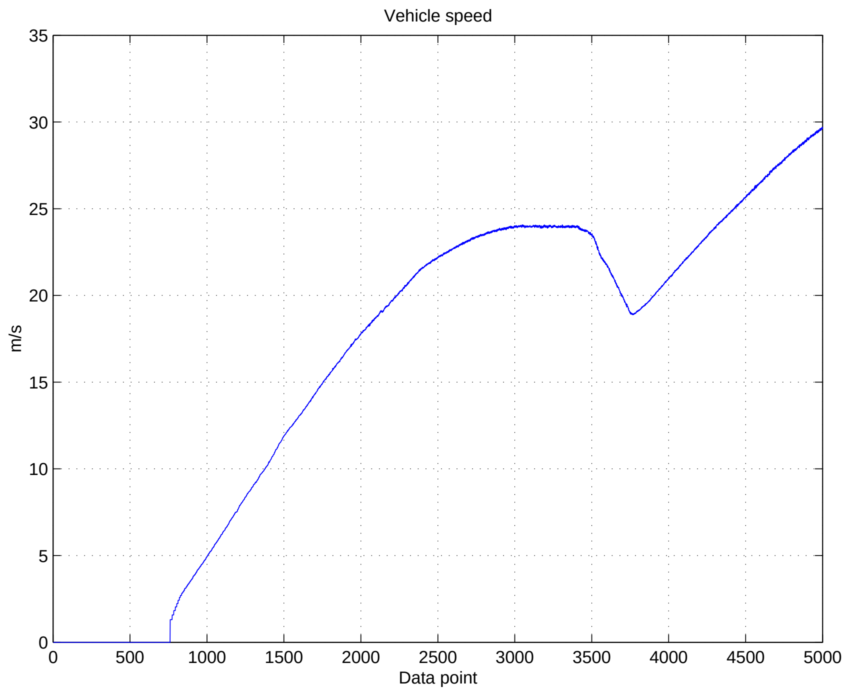

Figure 9.25: Vehicle speed

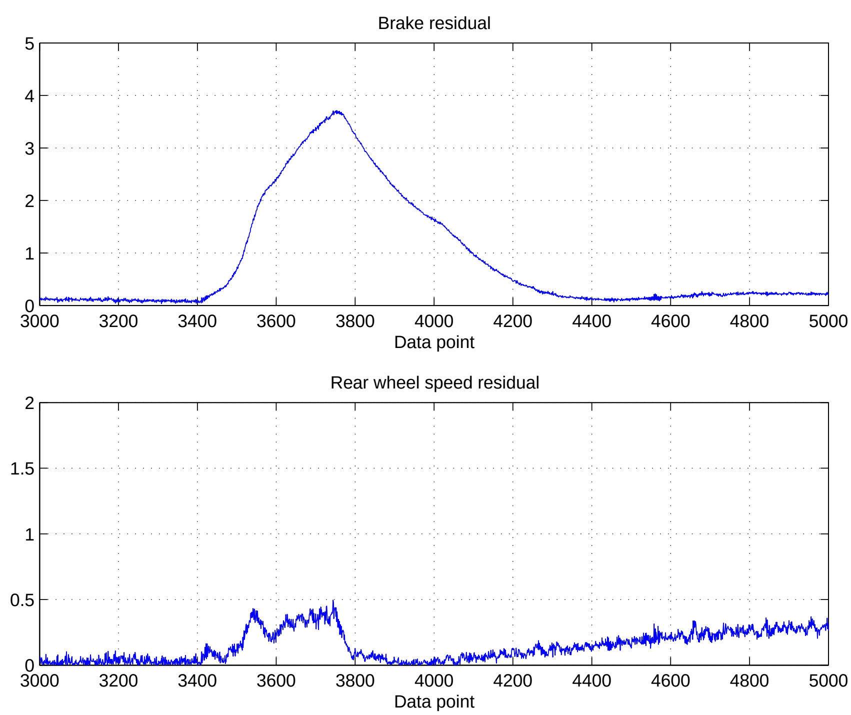

Figure 9.26: Residuals of the fault detection filter set no. 3

9.10 Issues and Recommendation

In this section, two issues regarding fault detection filters are discussed and recommendations are made for future improvement. The first issue is that the fault detection filters developed in Section 4.6 only work when the vehicle is in the third gear. Therefore, fault detection filters have to be developed for each gear and when the vehicle switches gears, the fault detection filters also have to switch.

The second issue is that some fault detection filters do not perform well when the throttle angle is very small. Figure 9.27 shows the vehicle speed and throttle command. Figures 9.28 to 9.30 show the performance of the fault detection filters examined in the same way as previous sections. When the throttle command is near 5 degrees just before 6000th data point, three of the six fault detection filters have small spikes around the same region. This is due to the inconsistency of the engine speed between the vehicle simulation and empirical data. This is shown in Figure 9.31 where the dashed line is the engine speed from the vehicle simulation using the throttle angle in Figure 9.27 and the solid line is the engine speed from the empirical data after applying the transformation in Section 9.3. Figure 9.31 shows that when the throttle angle is small, just before 6000th data point, the engine has some irregular behaviors which are not captured by the vehicle simulation. When the throttle angle becomes even smaller as in Figure 9.32, the performance of these three fault detection filters become worse as in Figures 9.33 to 9.35. Also, the inconsistency of the engine speed between the vehicle simulation and empirical data becomes larger as in Figure 9.36. Since fault detection filters are designed based on the linear models derived from the nonlinear vehicle simulation, a more accurate engine model in the vehicle simulation will be needed in order to improve the performance of these three fault detection filters regarding this issue.

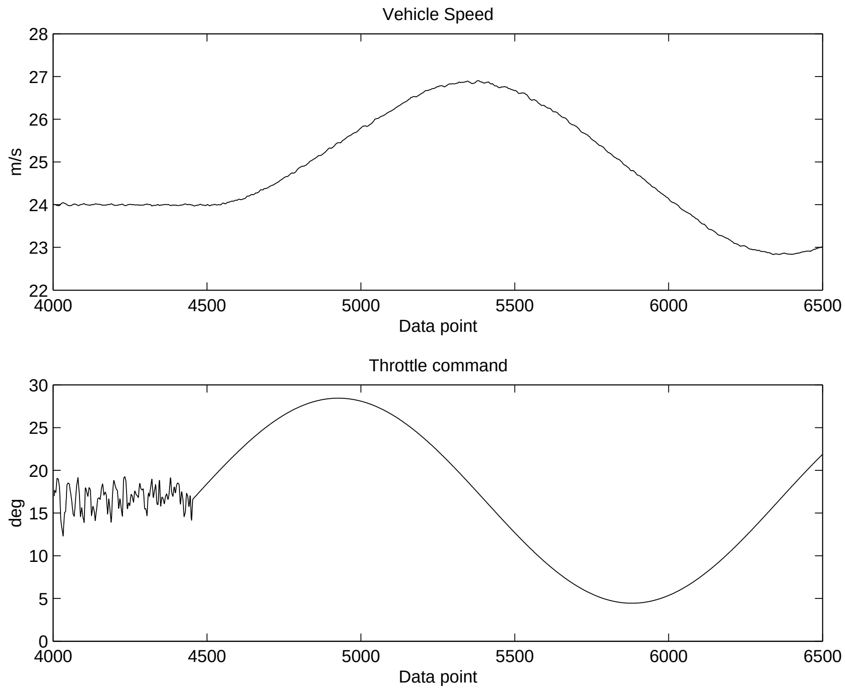

Figure 9.27: Vehicle speed and throttle command

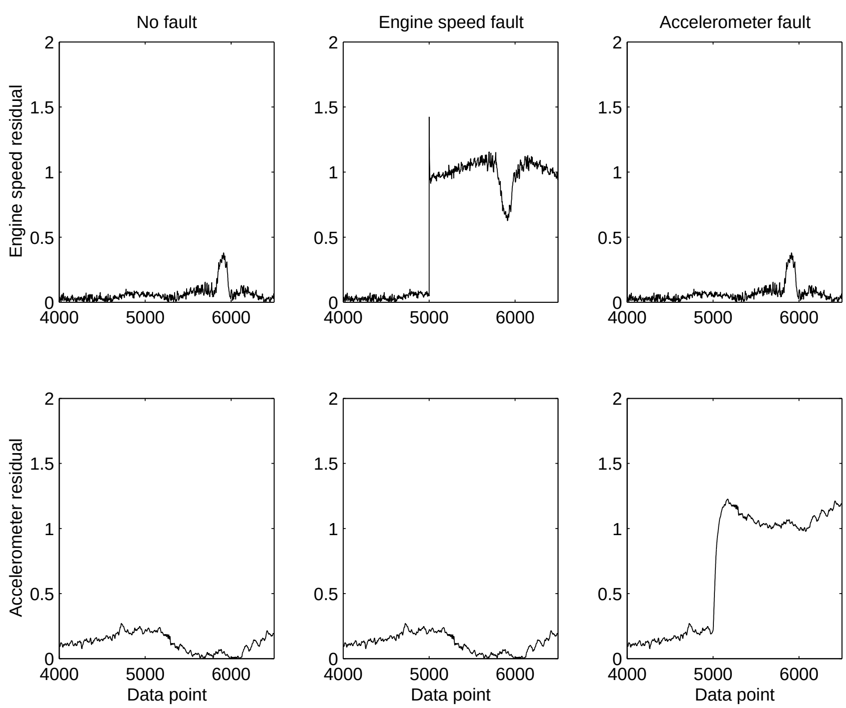

Figure 9.28: Residuals of the fault detection filter set no. 1

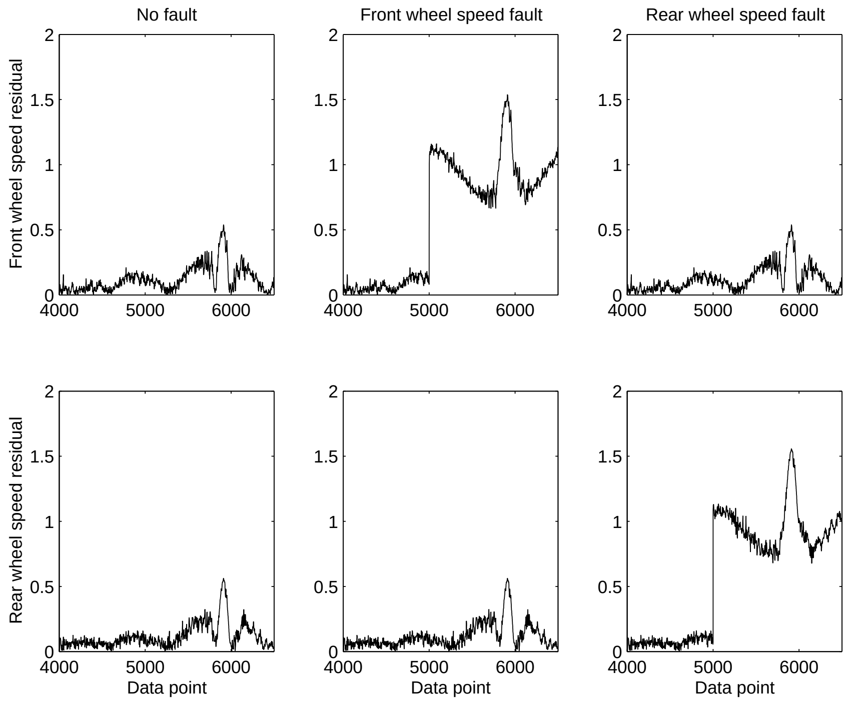

Figure 9.29: Residuals of the fault detection filter set no. 2

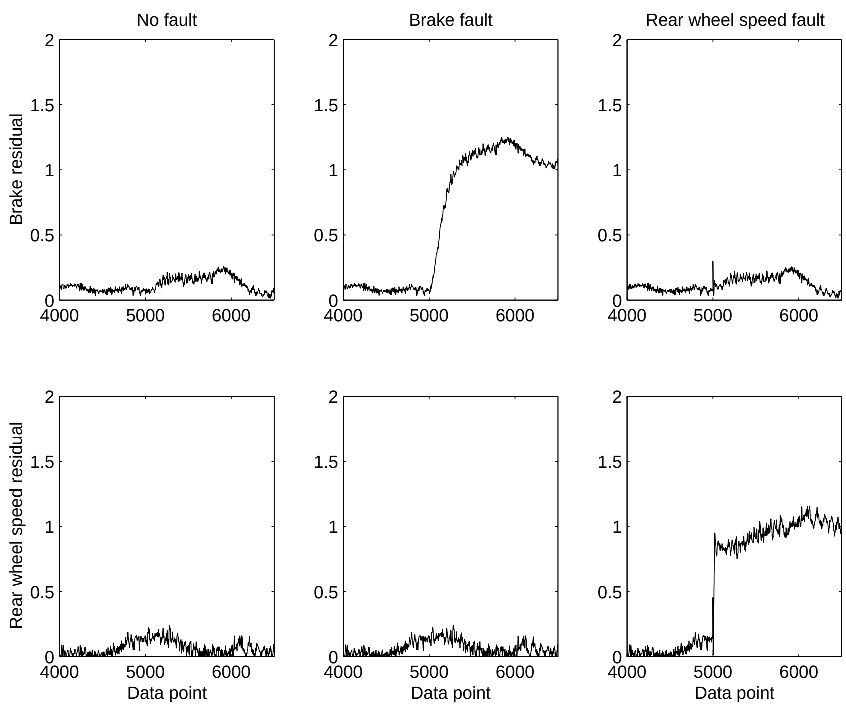

Figure 9.30: Residuals of the fault detection filter set no. 3

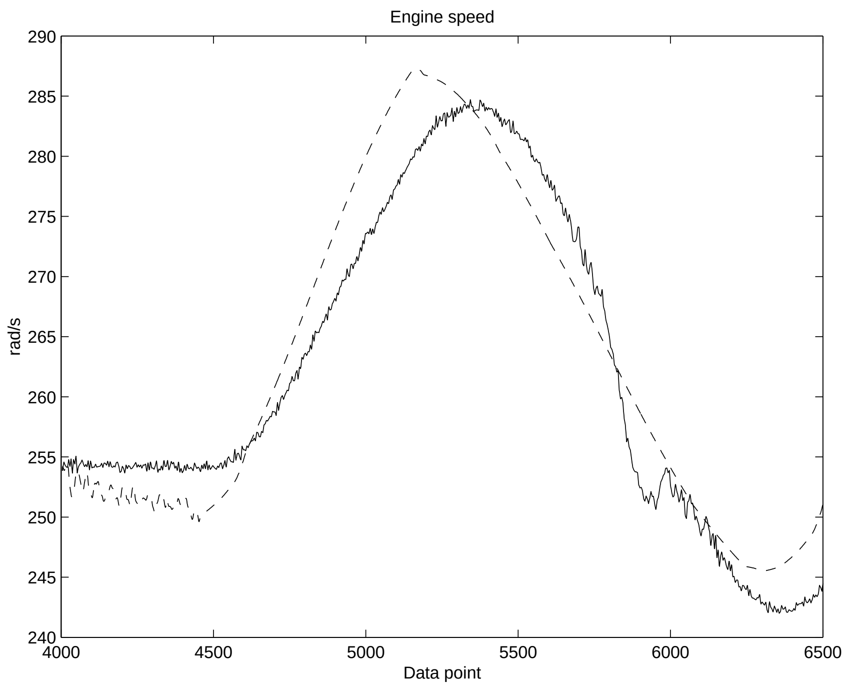

Figure 9.31: Engine speed

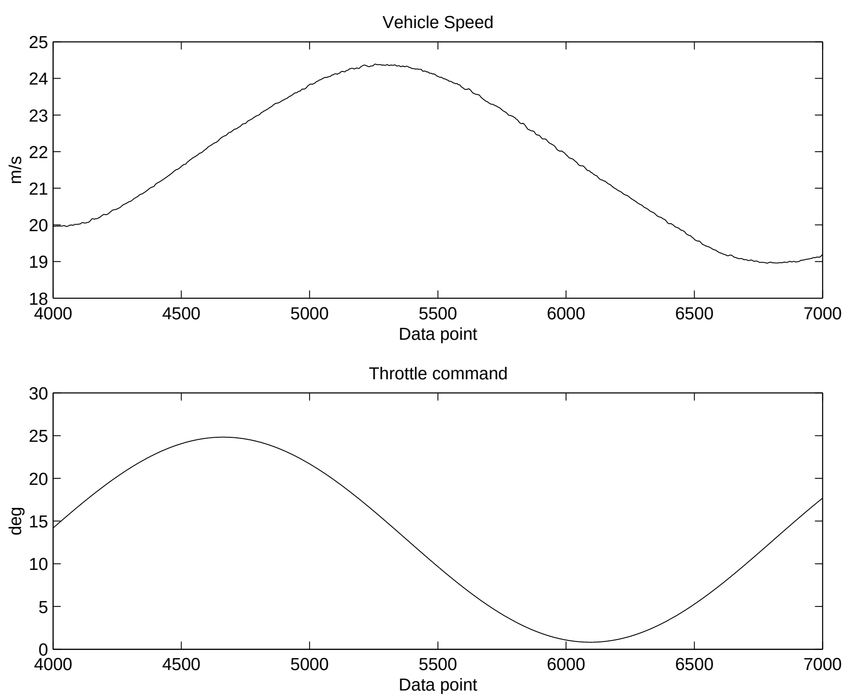

Figure 9.32: Vehicle speed and throttle command

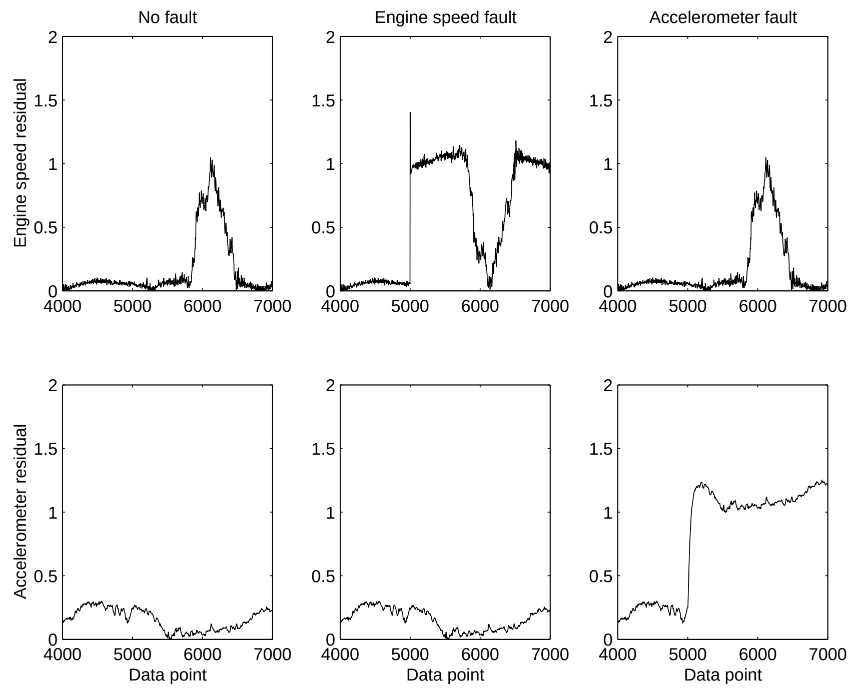

Figure 9.33: Residuals of the fault detection filter set no. 1

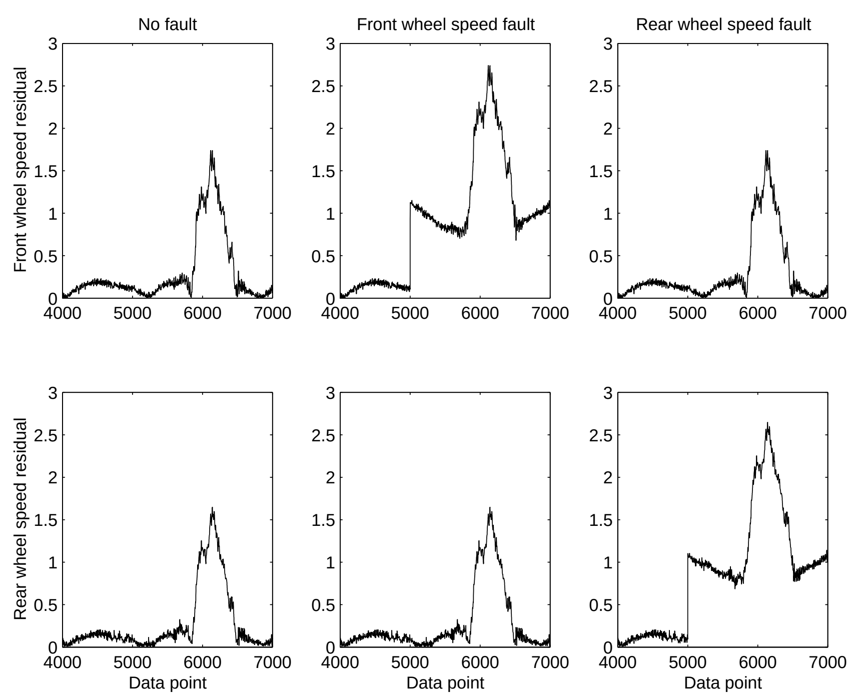

Figure 9.34: Residuals of the fault detection filter set no. 2

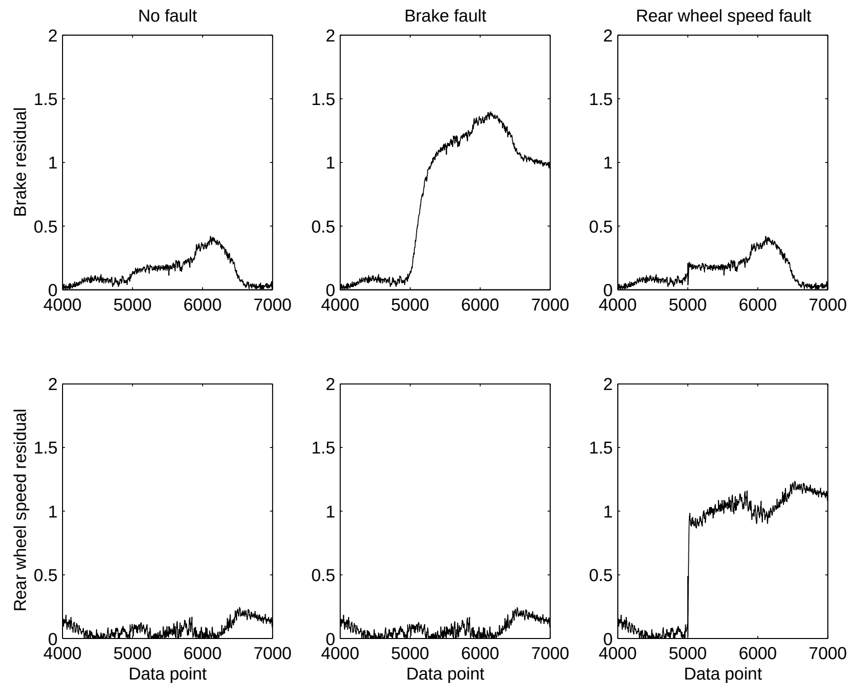

Figure 9.35: Residuals of the fault detection filter set no. 3

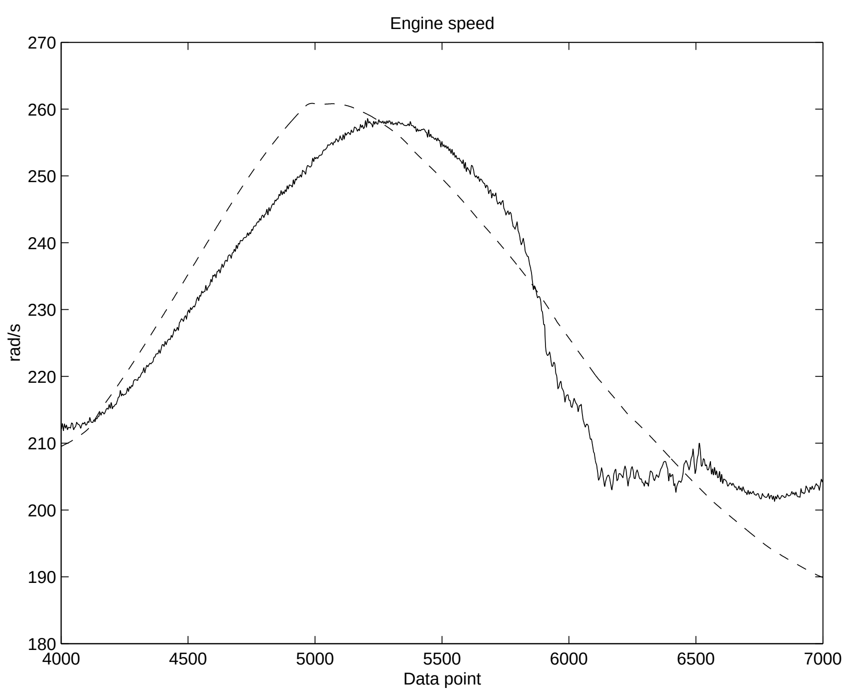

Figure 9.36: Engine speed

Chapter 10

Parity Equation Evaluation

In this chapter, parity equations are evaluated using empirical data recorded when driving a PATH Buick LeSabre at Crow's Landing. In Section 10.1, the first parity equation is evaluated. In Section 10.2, the second parity equation is evaluated. In Section 10.3, the third parity equation is evaluated.

10.1 Parity Equation No. 1

In this section, the first parity equation is evaluated using empirical data. Before evaluating the parity equation, the throttle command and throttle measurement are compared in Figure 10.1. The top left figure is when the vehicle speed is constant at 22 m/s as in Section 9.5. The top right figure is when the vehicle speed increases from 20 to 28 m/s as in Section 9.6. The bottom left figure is when the vehicle speed decreases from 24 to 18 m/s as in Section 9.7. The bottom right figure is when the vehicle speed increases from 24 to 28 m/s then decreases to 24 m/s as in Section 9.8. Figure 10.1 shows that there is always an error in throttle actuator or throttle sensor. Furthermore, this error is not a constant, but is ranged from almost zero to four degrees. Therefore, the first parity equation in Chapter 7 is modified as

$$\dot{r} = -5r + 5(u_\alpha - y_\alpha + 2)$$

where 2 is used to partially offset the error.

The first parity equation is evaluated under four scenarios. The first scenario is when the vehicle speed is constant at 22 m/s which is the top left figure of Figure 10.1. Figure 10.2 shows the absolute value of the residual when there is no fault, a throttle actuator fault and a throttle sensor fault, respectively. Both faults are bias with magnitude of 5 degrees and occur after 4000th

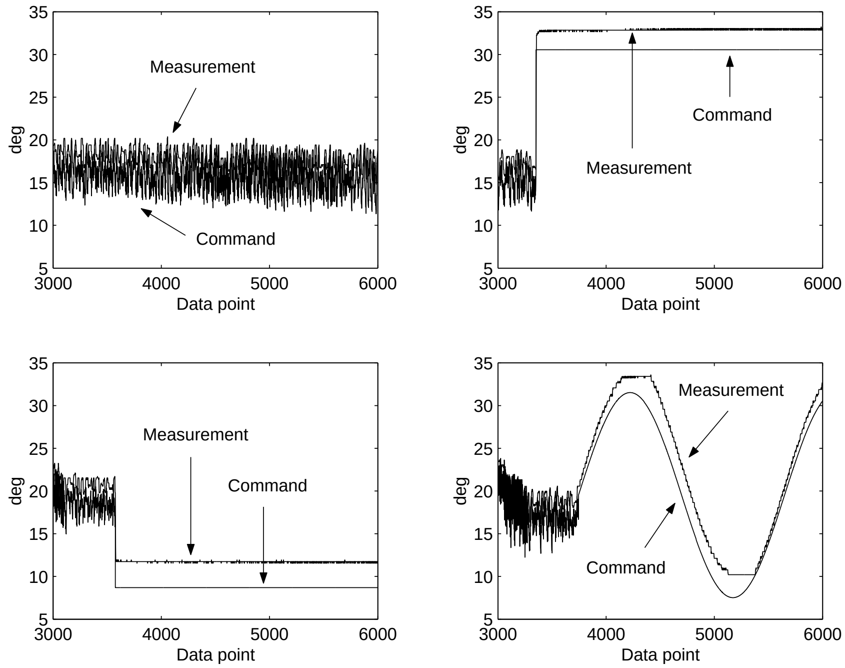

Figure 10.1: Throttle command and throttle measurement

data point. Note that the residual of the first parity equation is not scaled and represents the magnitude of the fault. The second scenario is when the vehicle speed increases from 20 to 28 m/s which is the top right figure of Figure 10.1. Figure 10.3 shows the absolute value of the residual when there is no fault, a throttle actuator fault and a throttle sensor fault, respectively. The third scenario is when the vehicle speed decreases from 24 to 18 m/s which is the bottom left figure of Figure 10.1. Figure 10.4 shows the absolute value of the residual when there is no fault, a throttle actuator fault and a throttle sensor fault, respectively. The fourth scenario is when the vehicle speed increases from 24 to 28 m/s then decreases to 24 m/s which is the bottom right figure of Figure 10.1. Figure 10.5 shows the absolute value of the residual when there is no fault, a throttle actuator fault and a throttle sensor fault, respectively. Figures 10.2 to 10.5 show that the first parity equation can detect the throttle actuator and throttle sensor faults. Note that the residuals in the left figures of Figures 10.2 to 10.5 are nonzero when there is no fault because there is an error in throttle actuator or throttle sensor.

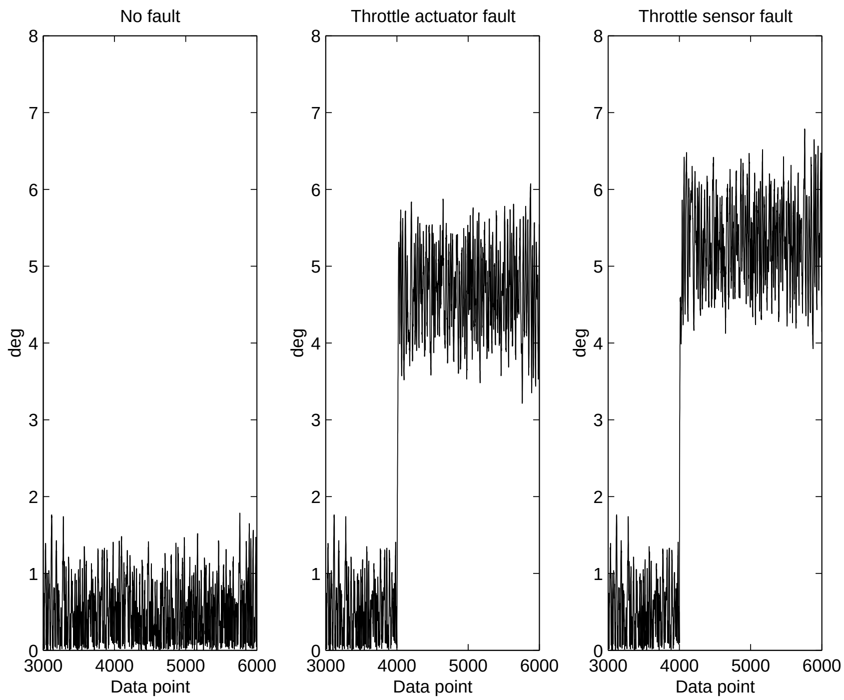

Figure 10.2: Parity equation no. 1: constant vehicle speed

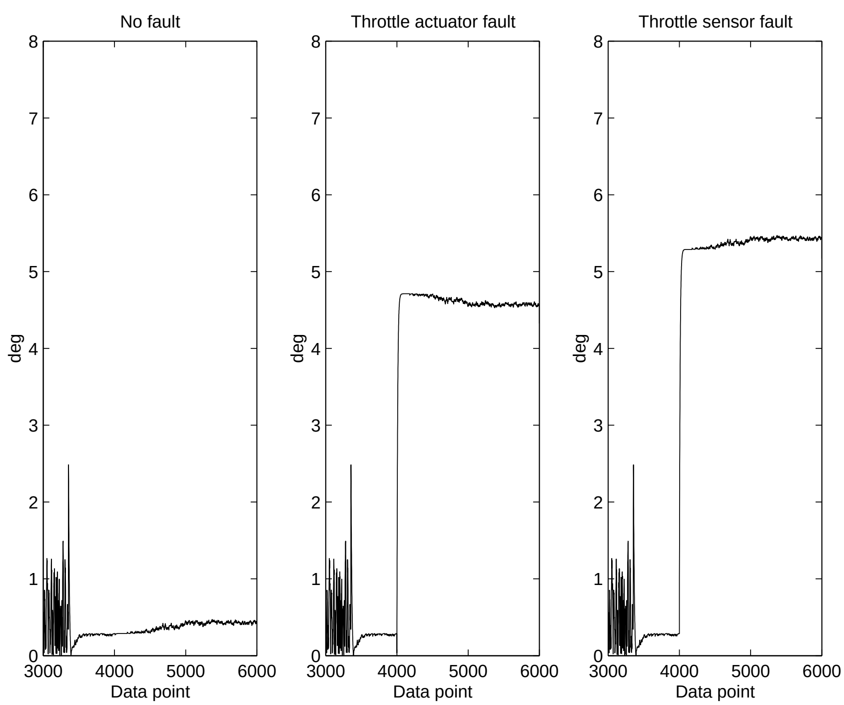

Figure 10.3: Parity equation no. 1: increasing vehicle speed

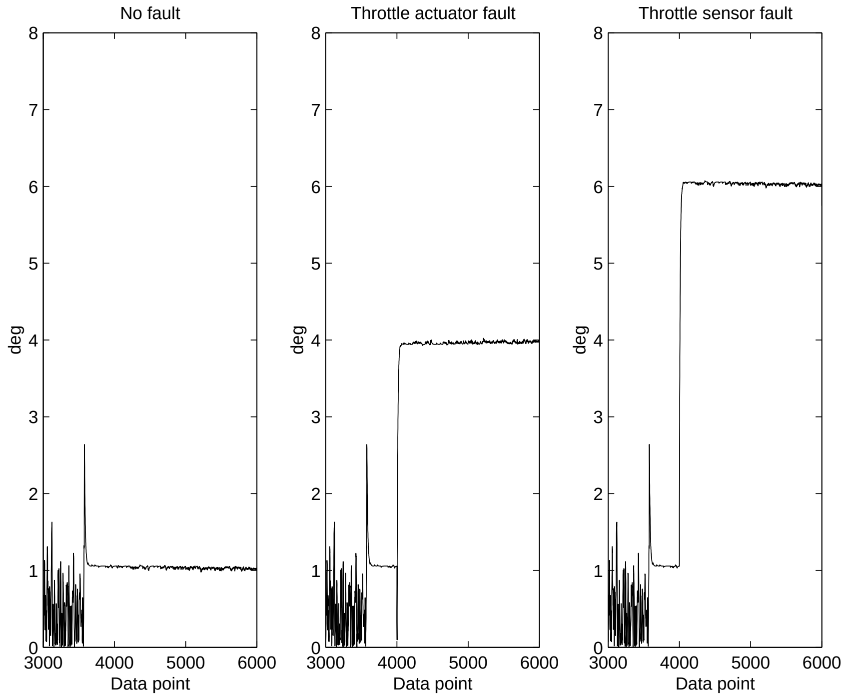

Figure 10.4: Parity equation no. 1: decreasing vehicle speed

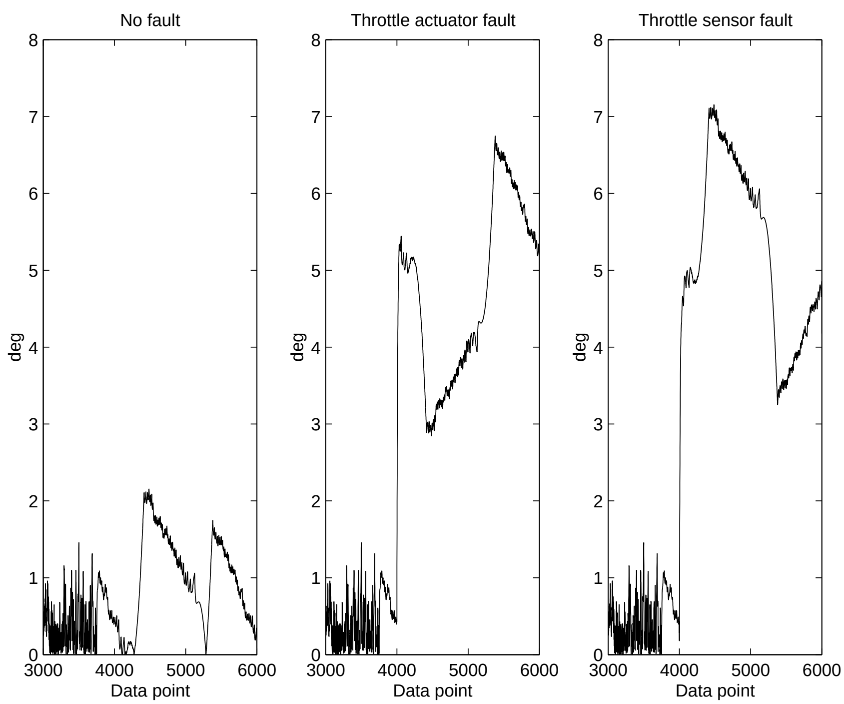

Figure 10.5: Parity equation no. 1: increasing and decreasing vehicle speed

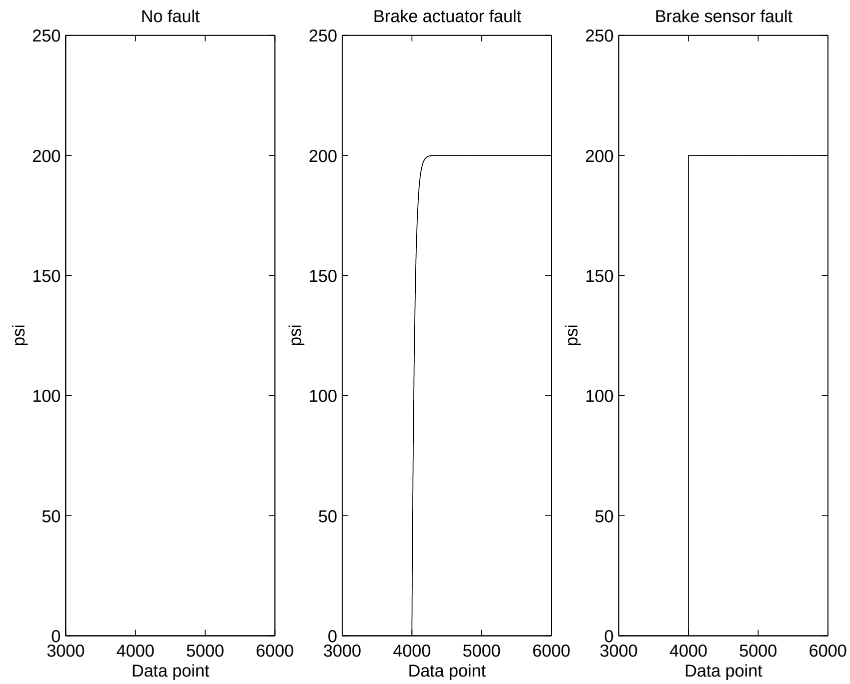

Figure 10.6: Parity equation no. 2: constant vehicle speed

10.2 Parity Equation No. 2

In this section, the second parity equation is evaluated using empirical data under the same four scenarios used in Section 10.1. The first scenario is when the vehicle speed is constant at 22 m/s. Figure 10.6 shows the absolute value of the residual when there is no fault, a brake actuator fault and a brake sensor fault, respectively. Both faults are bias with magnitude of 200 psi and occur after 4000th data point. Note that the residual of the second parity equation is not scaled and represents the magnitude of the fault. The second scenario is when the vehicle speed increases from 20 to 28 m/s. Figure 10.7 shows the absolute value of the residual when there is no fault, a brake actuator fault and a brake sensor fault, respectively. The third scenario is when the vehicle speed decreases from 24 to 18 m/s. Figure 10.8 shows the absolute value of the residual when there is no fault, a brake actuator fault and a brake sensor fault, respectively. The fourth scenario is when the vehicle speed increases from 24 to 28 m/s then decreases to 24 m/s. Figure 10.9 shows the absolute value of the residual when there is no fault, a brake actuator fault and a brake sensor fault, respectively. Figures 10.6 to 10.9 show that the second parity equation can detect the brake actuator and brake sensor faults.

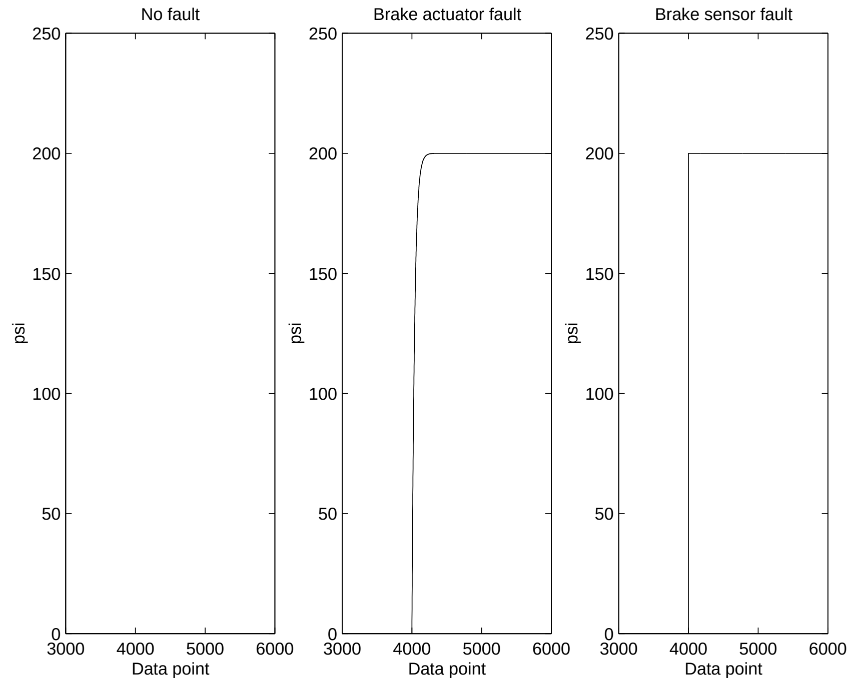

Figure 10.7: Parity equation no. 2: increasing vehicle speed

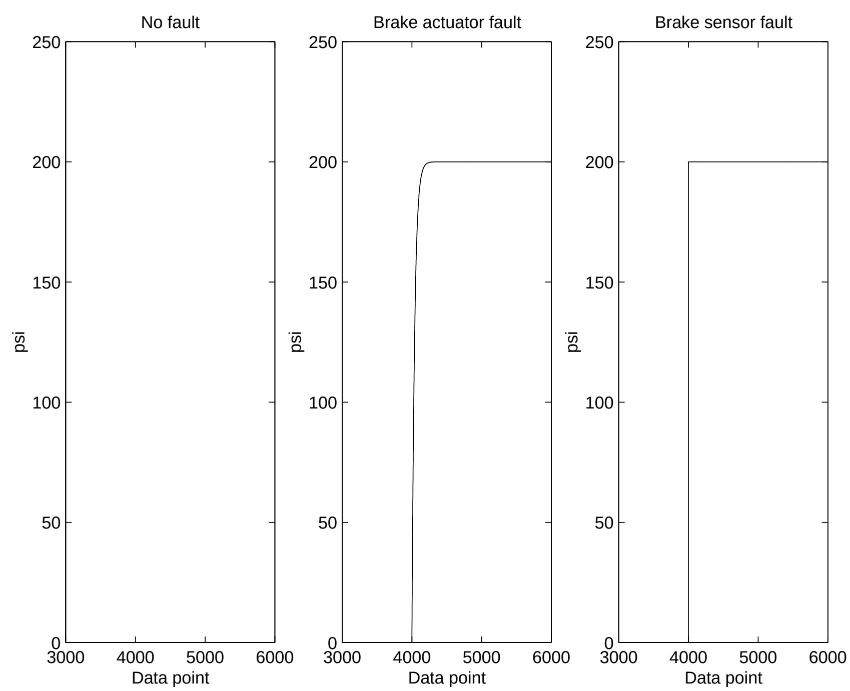

Figure 10.8: Parity equation no. 2: decreasing vehicle speed

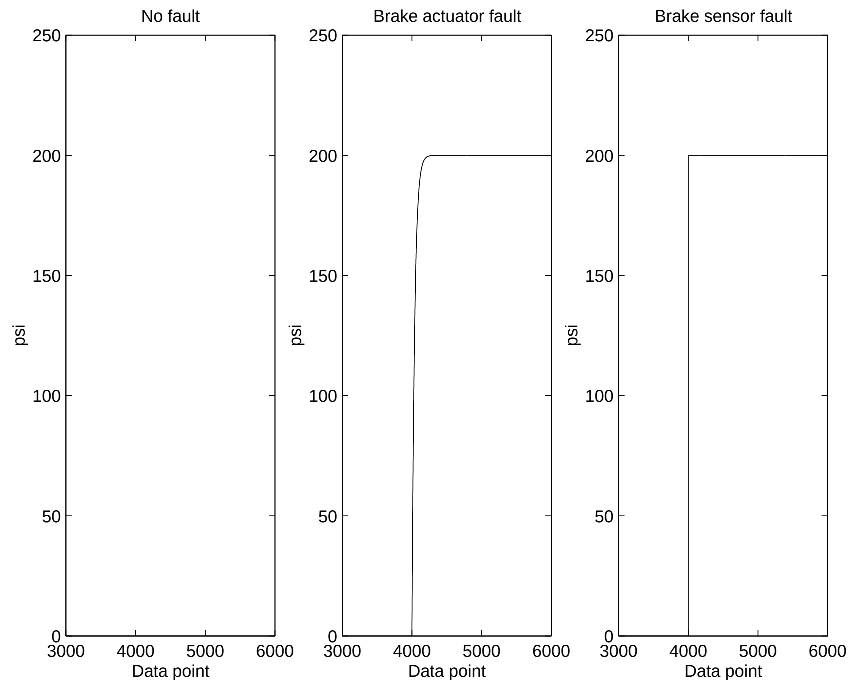

Figure 10.9: Parity equation no. 2: increasing and decreasing vehicle speed

10.3 Parity Equation No. 3

In this section, the third parity equation is evaluated using empirical data. Since the third parity equation is derived from the engine model of the vehicle simulation, the transformation in Section 9.3 is applied to the throttle command, manifold pressure measurement and engine speed measurement of the empirical data before the third equation uses these data to generate the residual. However, the nominal values of the throttle command, manifold pressure measurement and engine speed measurement do not need to be subtracted from these data because the third parity equation is derived from the nonlinear vehicle model, not the linear vehicle models.

The third parity equation is evaluated under the same first two scenarios used in Section 10.1. The first scenario is when the vehicle speed is constant at 22 m/s. Figure 10.10 shows the absolute value of the residual when there is no fault, a throttle actuator fault, a manifold pressure sensor fault and an engine speed sensor fault, respectively. All three faults are bias with magnitudes of 5 degrees, 7.5 psi and 175 rpm, respectively, and occur after 4000th data point. Note that the residual of the third parity equation is not scaled. The second scenario is when the vehicle speed increases from 20 to 28 m/s. Figure 10.11 shows the absolute value of the residual when there is no fault, a throttle actuator fault, a manifold pressure sensor fault and an engine speed sensor fault,

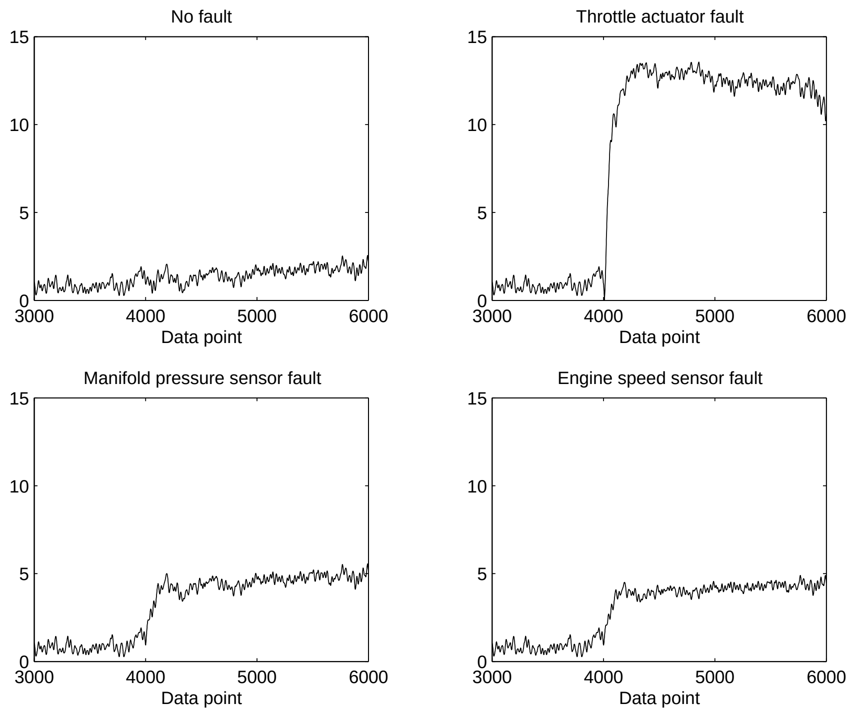

Figure 10.10: Parity equation no. 3: constant vehicle speed

respectively. Figure 10.10 shows that the third parity equation can detect the throttle actuator, manifold pressure sensor and engine speed sensor faults when the vehicle speed is a constant. However, Figure 10.11 shows that the third parity equation cannot detect these three faults when the vehicle speed increases. Therefore, the third parity equation cannot detect these three faults. This indicates that the engine model in the vehicle simulation is not accurate enough because the third parity equation is derived from this engine model and there is no design parameter involved. A more accurate engine model is needed in order to improve the performance of the third parity equation.

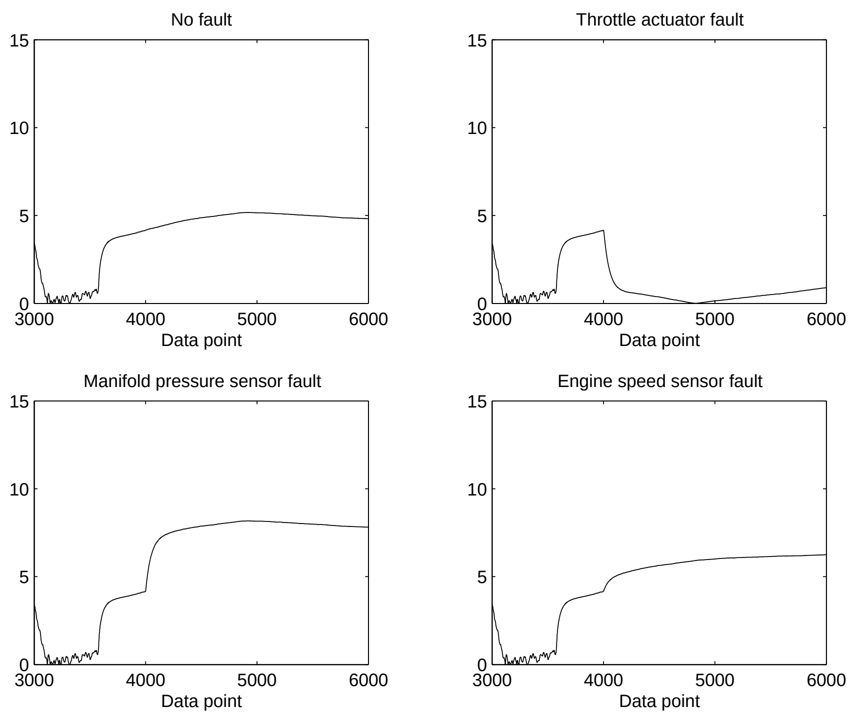

Figure 10.11: Parity equation no. 3: increasing vehicle speed

Chapter 11

Vehicle Health Monitoring System Evaluation

In this chapter, the performance of the vehicle health monitoring system composed of residual generator and residual processor is first evaluated using simulated data generated by the vehicle simulation and empirical data recorded at Crow's landing. Second, the health monitoring system is evaluated in real-time on a PATH Buick LeSabre when the actuator and sensor faults are simulated and imposed by UCLA laptop. Then, the health monitoring system is evaluated in real-time on a PATH Buick LeSabre when the actuator and sensor faults are directly injected by the PATH vehicle computer. Finally, real steering actuator and real brake actuator faults are created by the driver and the performance of the health monitoring system is evaluated. The real-time evaluation at Crow's Landing demonstrates that the vehicle health monitoring system can detect and identify actuator and sensor fault under various disturbances and uncertainties.

In Section 11.1, the norms of the residuals generated by the fault detection filters are scaled to one when their associated faults of certain magnitudes occur. In Section 11.2, the health monitoring system is evaluated using vehicle simulation. In Section 11.3, fault detection filters are evaluated using empirical data. In Section 11.4, the experiment setup (i.e., the real-time testing environment) is discussed. From Sections 11.5 to 11.7, the health monitoring system is evaluated in real-time on a PATH Buick LeSabre under different scenarios.

11.1 Residual Scaling

In this section, the norms of the residuals of fault detection filter set no.1', no.2, no.3', no.4, no.5 and no.6 are scaled to one when their associated faults of certain magnitudes occur. Therefore, the norm of each residual rises to one when evaluated using the same linear model used for fault detection filter design with its associated fault being a step with the magnitude given below.

Engine speed sensor fault: 20 rad/s

Longitudinal accelerometer fault: 0.4 m/s^2

Front wheel speed sensor fault: 7.5 rad/s

Rear wheel speed sensor fault: 7.5 rad/s

Brake actuator fault: 200 $Nt \cdot m$

Lateral accelerometer fault: 1 m/s^2

Yaw rate sensor fault: 0.035 rad/s

Steering actuator fault: 0.015rad

The scaling factors by which the norms of the residuals are divided are

Fault detection filter set no. 1'	Engine speed sensor residual: 13.401
	Longitudinal accelerometer residual: 0.8592
Fault detection filter set no. 2	Front wheel speed sensor residual: 11.942
	Rear wheel speed sensor residual: 6.767
Fault detection filter set no. 3'	Brake actuator residual: 2.4540
	Rear wheel speed sensor residual: 4.662
Fault detection filter set no. 4	Steering actuator residual: 14.7020
	Front wheel speed sensor residual: 6.1252
Fault detection filter set no. 5	Yaw rate sensor residual: 30.1302
	Rear wheel speed sensor residual: 4.5394
Fault detection filter set no. 6	Lateral accelerometer residual: 1.6235
	Rear wheel speed sensor residual: 3.9230

If the magnitudes of the faults occurred are twice the magnitudes given above, the norms of the residuals will rise to two. If the magnitudes of the faults occurred are half of the magnitudes given above, the norms of the residuals will rise to one-half. The purpose of the scaling is to present the performance of the fault detection filters in a clearer fashion, i.e., zero residuals represent no fault and residuals of magnitude one represent the occurrence of their associated faults. Note that the residuals can be scaled with respect to any other fault magnitudes if that were desired.

11.2 Evaluation Using Vehicle Simulation

Before evaluating the vehicle health monitoring system using simulated data generated by the vehicle simulation. Similar to the fault detection filters designed for the longitudinal vehicle dynamics, the lateral fault detection filters are designed based on the linearized vehicle dynamics derived from the nonlinear vehicle dynamics at certain nominal operating point, the nominal values of the control commands and measurements have to be subtracted from the simulated data generated by the vehicle simulation before the fault detection filters can use these data to generate the residuals. From Section 5.3, fault detection filter set no. 4, 5 and 6 are designed based on the linear vehicle model derived at 20 m/s. Since the model is derived when the vehicle is traveling straight ahead. The nominal values of the control commands and measurements corresponded to the vehicle lateral dynamics are all zeros.

Now the vehicle health monitoring system can be evaluated using vehicle simulation. The evaluation shows that heath monitoring system detect and identify actuator and sensor faults with probability as expected. However, the evaluation is not shown here because the health monitoring system is evaluated in real-time on a PATH Buick LeSabre in later sections which present a more interesting and practical evaluation.

11.3 Evaluation Using Empirical Data

Before evaluating the fault detection filters using empirical data recorded when driving a PATH Buick LeSabre at Crow's Landing, a comparison is made between the vehicle simulation and empirical data. Since the simulation does not match the empirical data on some control commands and measurements, a transformation is derived to approximately match the simulation and empirical data. Then, the transformation is applied to the control commands and measurements of the empirical data before the fault detection filters use these data to generate the residuals. The transformation is derived as followed.

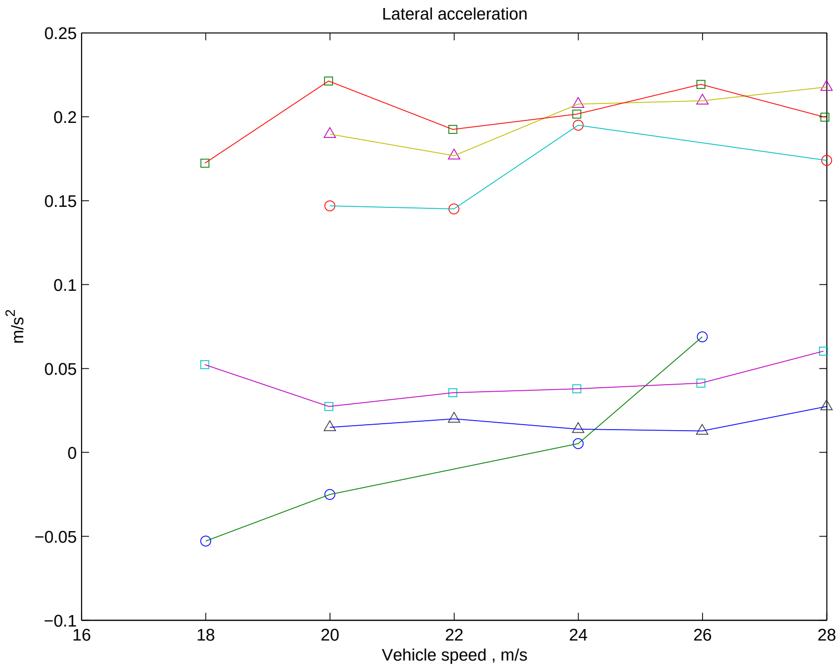

Figure 11.1: Lateral accelerometer from empirical data

First, the lateral accelerometer measurements are obtained from the empirical data when the vehicle is traveling straight ahead at constant speeds of 20, 22, 24, 26 and 28 m/s, respectively. This is represented by the six lines plotted in Figure 11.1. Each pair of the 'circle'-line, 'square'-line and 'triangle'-line represent the data obtained from the same set of experiment. The lateral accelerometer measurement at each vehicle speed is the average of the lateral accelerometer measurements in each run obtained from three experiments at Crow's Landing when the vehicle was traveling straight ahead in both directions. Since the vehicle is traveling straight ahead, the lateral accelerometer measurement is expected to be zero. Figure 11.1 shows that there is a bias in the lateral accelerometer and range between 0 m/s^2 and 0.2 m/s^2 approximately. Therefore, a transformation is used to subtract this bias,

$$\bar{y}_{a_y} = y_{a_y} - 0.1$$

where y_{a_y} is from the empirical data and $\bar{y}_{a_y}$ is the transformed lateral acceleration.

Second, the yaw rate sensor measurements are obtained from the empirical data when the vehicle is traveling straight ahead at constant speeds of 20, 22, 24, 26 and 28 m/s, respectively. Similarly, this is plotted in Figure 11.2. The yaw rate sensor measurement at each vehicle speed is the average of the yaw rate measurements in each run recorded at Crow's Landing when the vehicle

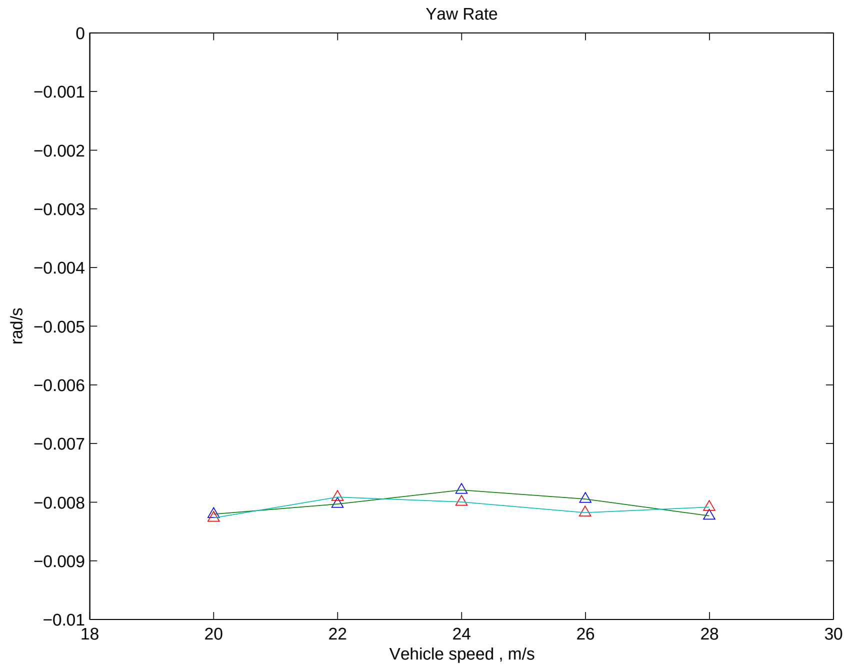

Figure 11.2: Yaw rate sensor from empirical data

was traveling straight ahead in both directions. Since the vehicle is traveling straight ahead, the yaw rate sensor measurement is also expected to be zero. Figure 11.2 shows that there is a bias with magnitude of -0.008 rad/s in the yaw rate sensor approximately. Therefore, a transformation is used to subtract this bias.

$$\bar{y}_r = y_r + 0.008$$

where y_r is from the empirical data and $\bar{y}_{a_y}$ is the transformed yaw rate sensor.

Next, the empirical data generated when the vehicle is traveling on the magnetic curve track at constant speed of 20 m/s is obtained. Then, the steering command from the empirical data is used in the simulation to generate longitudinal accelerometer, yaw rate, front wheel speed and rear wheel speed measurements. In Figure 11.3, the lateral accelerometer measurements from the empirical data after subtracting the bias is plotted by the solid line and is compared to the simulation which is plotted by the dotted line on the first row of the figure. Similarly, on the first row of the Figure 11.4, Figure 11.5 and Figure 11.6, the empirical data which is plotted by solid line is compared to the simulation which is plotted by the dotted line respectively. Note that the yaw rate sensor measurements form the empirical data is plotted after the bias is subtracted. It is clear that the simulation does not match the empirical data. Here, the empirical data of each individual

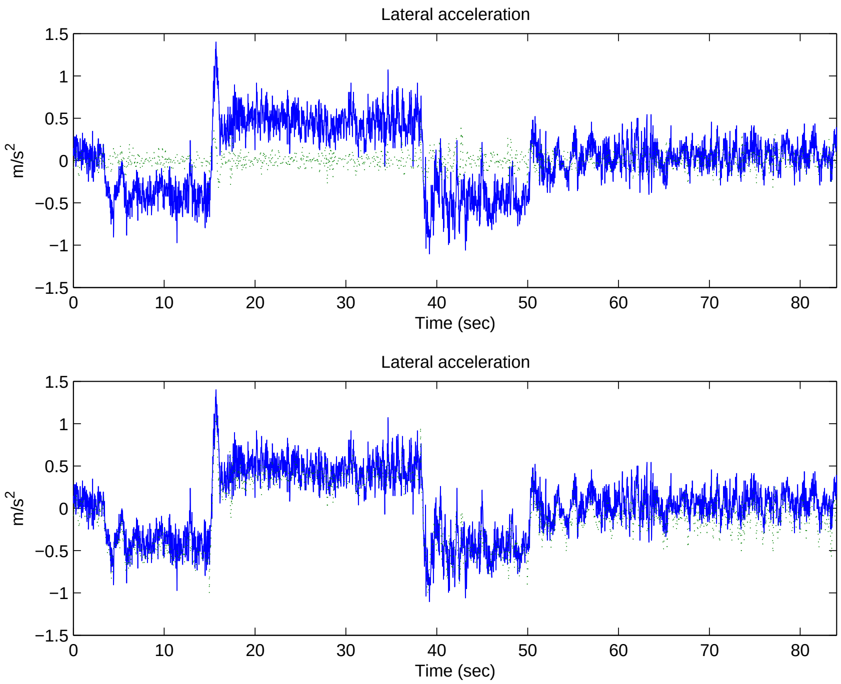

Figure 11.3: Lateral accelerometer from the simulation and empirical data

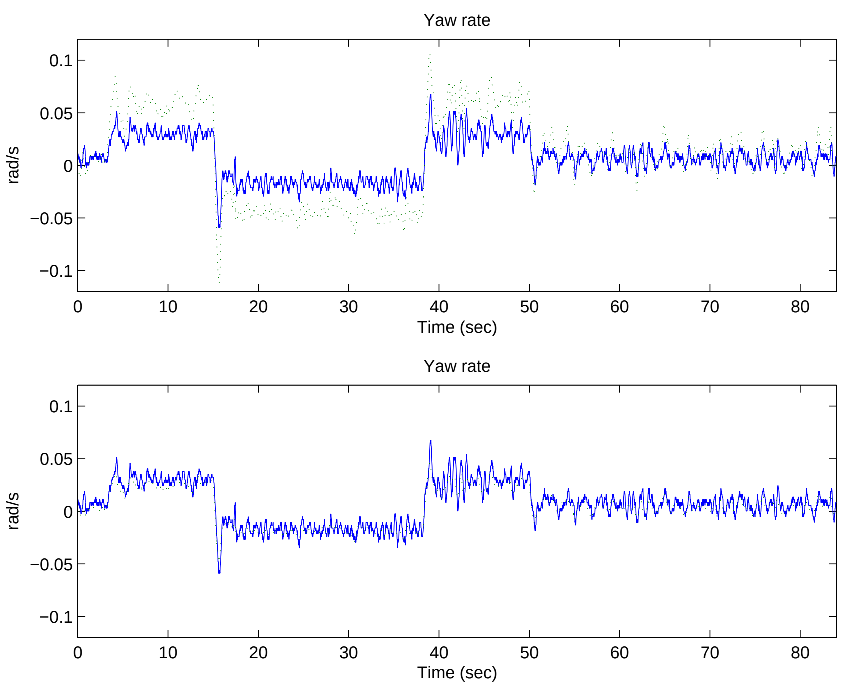

Figure 11.4: Yaw rate from the simulation and empirical data

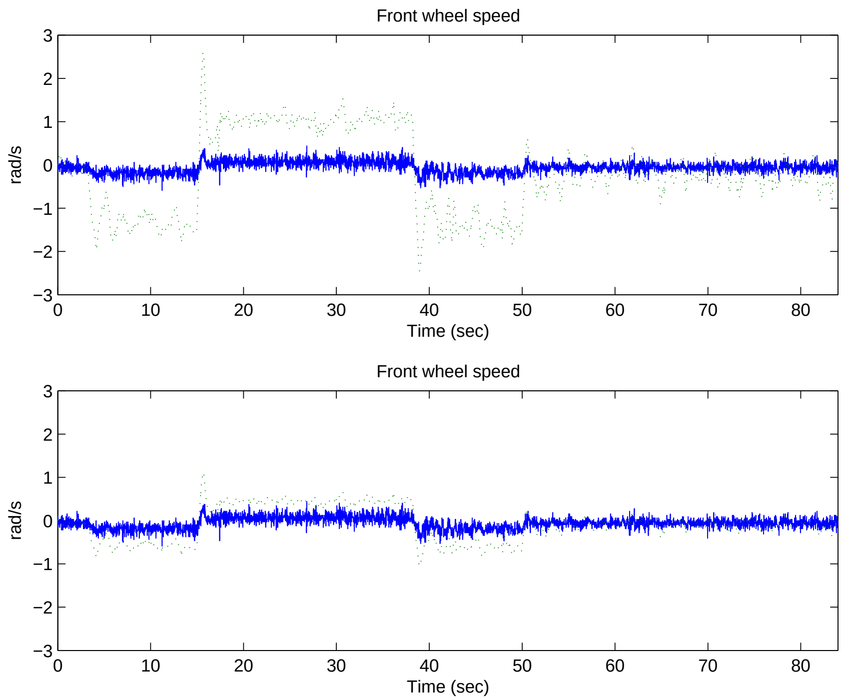

Figure 11.5: Front wheel speed from the simulation and empirical data

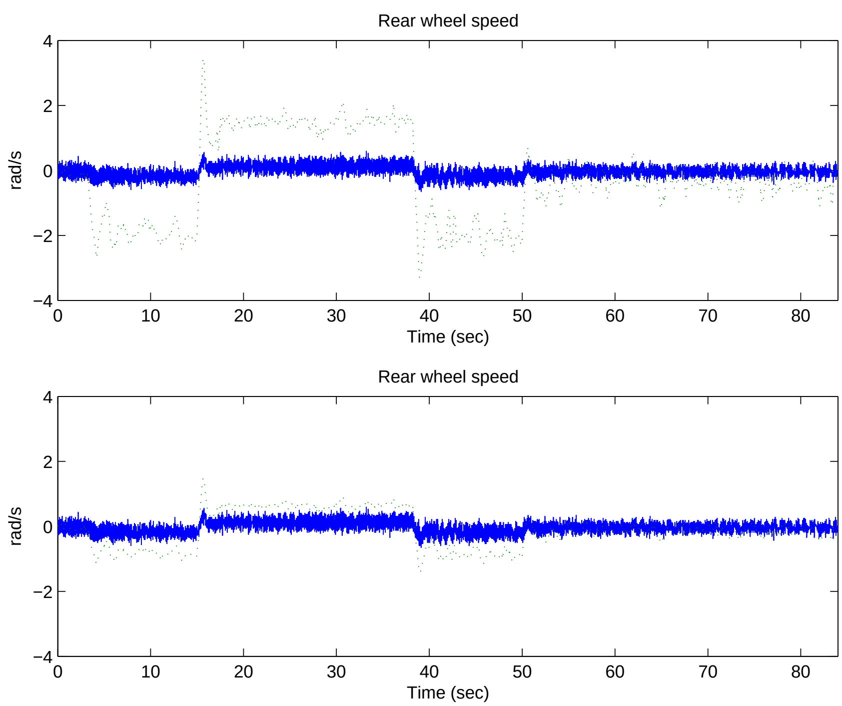

Figure 11.6: Rear wheel speed from the simulation and empirical data

sensor measurements can be directly translated to match the simulation respectively or the steering command from the empirical data can be translated to generate simulated measurements that match the empirical data if possible. The later approach is chosen because only one translation is needed. It is found that the following transformation can be used to translate the steering command which generates simulated yaw rate, front wheel speed and rear wheel speed measurements that match the empirical data.

$$\bar{u}_\gamma = -0.43 \left(u_\gamma \frac{\pi}{180 \cdot 17} \right) \tag{11.1}$$

where u_γ is from the empirical data and $\bar{u}_\gamma$ is the transformed steering command. In the above transformation, the negative sign is used such that the definition of the sign associated to the turning direction of the vehicle is consistent in both simulation and the real vehicle. Since the steering command from the empirical data measures the turning angle of the hand wheel in degree. It is first divided by 17 to obtain the steering angle of the front wheels and then transform from deg to rad/s which is the unit used in the simulation.

For the front and rear wheel speed measurements, the units of the wheel speed in the simulation and empirical data are rad/s and m/s, respectively. Therefore, a transformation is used to transform the wheel speeds in m/s to rad/s.

$$\bar{y}_{\tilde{\omega}_f} = \frac{y_{w_{fl}} - y_{w_{fr}}}{0.2957} \tag{11.2}$$

$$\bar{y}_{\tilde{\omega}_r} = \frac{y_{w_{rl}} - y_{w_{rr}}}{0.3066} \tag{11.3}$$

where $y_{w_{fl}}$, $y_{w_{fr}}$, $y_{w_{rl}}$ and $y_{w_{rr}}$ are the four wheel speed measurements from the empirical data, and $\bar{y}_{\tilde{\omega}_f}$ and $\bar{y}_{\tilde{\omega}_f}$ are the transformed difference of wheel speeds. Note that 0.2957 and 0.3066 are the approximate radius of the front and rear tires in the simulation, respectively.

After using transformations (11.1), (11.2) and (11.3), the second row of Figure 11.4, Figure 11.5 and Figure 11.6 show that the empirical data match the simulation approximately in this three measurements. The fault detection filters from the fault detection filter set no.4, no.5 and the fault detection filter that detects the rear wheel speed sensor fault from filter set no.6 will use empirical data after above transformations to generate residuals.

Although not showing here, the measurements of the lateral accelerometer from the empirical data does not match the simulation using the above transformation. Therefore, instead of transforming the empirical data to match the simulation, a modified linear model is used such that the simulated data will match the empirical data. In addition, the following transformation is used in the lateral accelerometer measurement so that the definition of the vehicle turning direction is consistent.

$$\bar{y}_{a_y} = -(y_{a_y} - 0.1) \tag{11.4}$$

The second row of Figure 11.3 shows that the lateral accelerometer measurements form the empirical data match the simulation from the modified linear model. Note that lateral accelerometer fault detection filter from filter set no.6 is designed using the modified linear model and the residual is generated using the empirical data after the transformations in the lateral accelerometer, front wheel speed and rear wheel speed measurements (11.4), (11.2) and (11.3).

Now the vehicle health monitoring system can be evaluated using vehicle simulation. The evaluation shows that heath monitoring system detect and identify actuator and sensor faults with probability as expected. However, the evaluation is not shown here because the health monitoring system is evaluated in real-time on a PATH Buick LeSabre in later sections which present a more interesting and practical evaluation

11.4 Experiment Setup

In this section, a real-time testing environment is developed using Linux operating system and C language to evaluate the vehicle health monitoring system in real-time on a PATH Buick LeSabre. The health monitoring system is written in C code and executed on a laptop running Linux operating system. The laptop is connected to the computer in the trunk of the PATH Buick LeSabre through a serial port. An input/output interface is developed to allow the data, control commands and sensor measurements, be transmitted from the PATH computer to the UCLA laptop every twenty-one millisecond. The UCLA laptop checks its serial port buffer and downloads the data if the complete set of data is in the buffer. Then, the health monitoring system code is executed to generated the fault detection filter residuals and probability of each possible failure. This process requires much less than twenty-one millisecond. After the residuals and failure probabilities are generated, the UCLA laptop proceeds to check the serial port buffer and waits for the next set of data.

From Sections 11.5 to 11.7, vehicle health monitoring system is evaluated in real-time on a PATH Buick LeSabre at Crow's Landing under different scenarios. For the first part of the evaluation, actuator faults and sensors are imposed by the UCLA laptop after the correct control commands and sensor measurements are transmitted from the PATH vehicle computer to the laptop. In this case, the control commands and the sensor measurements used by the controller are free of disruption and the fault is "opened-loop" since it is not circulated in the control loop. For the second part of the evaluation, the sensor faults are imposed by the PATH vehicle computer. In this case, the fault is "closed-loop" because the vehicle controller use the corrupted sensor measurements to generate control commands of the vehicle and the vehicle health monitoring system use these control commands and sensor measurements to generate filter residuals and failure probabilities. In the last part of the evaluation, real steering actuator fault and real brake actuator fault are created manually by turning the steering wheel and stepping on the brake pedal while the vehicle is traveling on the magnetic curve track under automatic control.

In Sections 11.5 the vehicle health monitoring system is evaluated in real-time on a PATH Buick LeSabre at Crow's Landing with actuator and sensor faults simulated by the UCLA laptop. The faults are simulated as bias with magnitudes given below.

Engine speed sensor fault: 175 rpm

Longitudinal accelerometer fault: 0.4 m/s^2

Front wheel speed sensor fault: 2.218 m/s

Rear wheel speed sensor fault: 2.299 m/s

Brake actuator fault: 200 psi

Throttle actuator fault: 4 deg

Steering actuator fault: 14.610 deg

Lateral accelerometer fault: 1 m/s^2

Yaw rate sensor fault: 0.035 rad/s

Throttle sensor fault: 4 deg

Brake sensor fault: 200 psi

After applying the transformation in Section 11.3, these fault magnitudes are equivalent to the fault magnitudes in the vehicle simulation that are used to scale the residuals in Section 11.1.

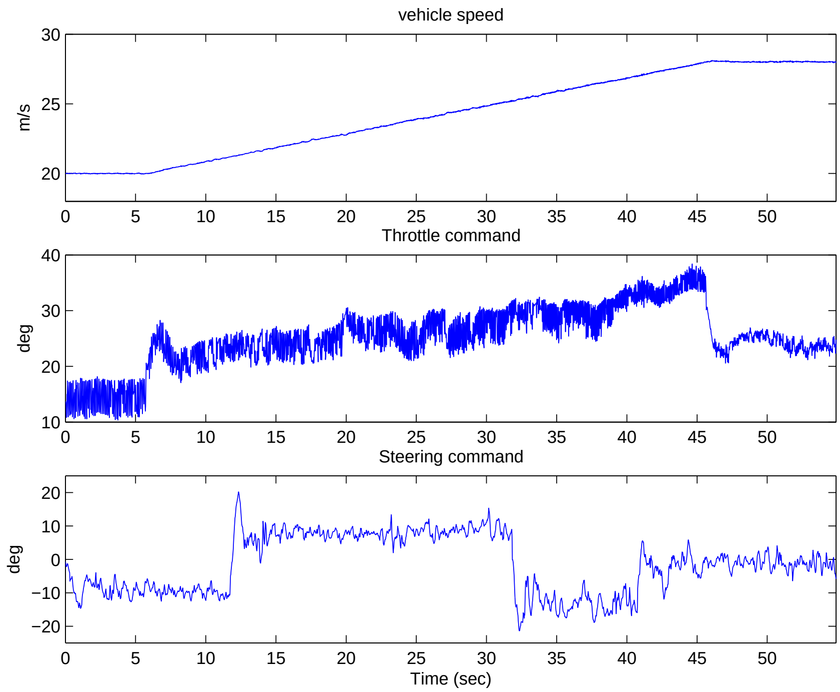

Figure 11.7: Vehicle speed, throttle and steering commands

In Section 11.6, health monitoring system is evaluated in real time when the sensor faults are injected by the vehicle computer. The magnitude of failure is different to that shown above in some sensors and will be specified in each evaluation. In Section 11.7, health monitoring system is evaluated in real-time on a PATH Buick LeSabre at Crow's Landing with a brake actuator fault generated by stepping on the brake pedal and a steering actuator fault generated by manually turning the steering wheel by the driver. The magnitude of the two actuator faults are not known in this case because the additional brake and steering are not measured. Since this additional brake or steering is only applied to the vehicle, but not to the control commands used by the health monitoring system, this creates a real steering actuator fault and brake actuator fault for vehicle health monitoring system evaluation.

11.5 Evaluation Scenario No. 1: Opened Loop Fault

In this section, the vehicle health monitoring system is evaluated in real-time on a PATH Buick LeSabre at Crow's Landing. All of the simulated actuator faults and sensor faults are imposed by the UCLA laptop after the measurements are received from the PATH vehicle computer. The vehicle measurements are created when the vehicle is traveling on the magnetic curve track with

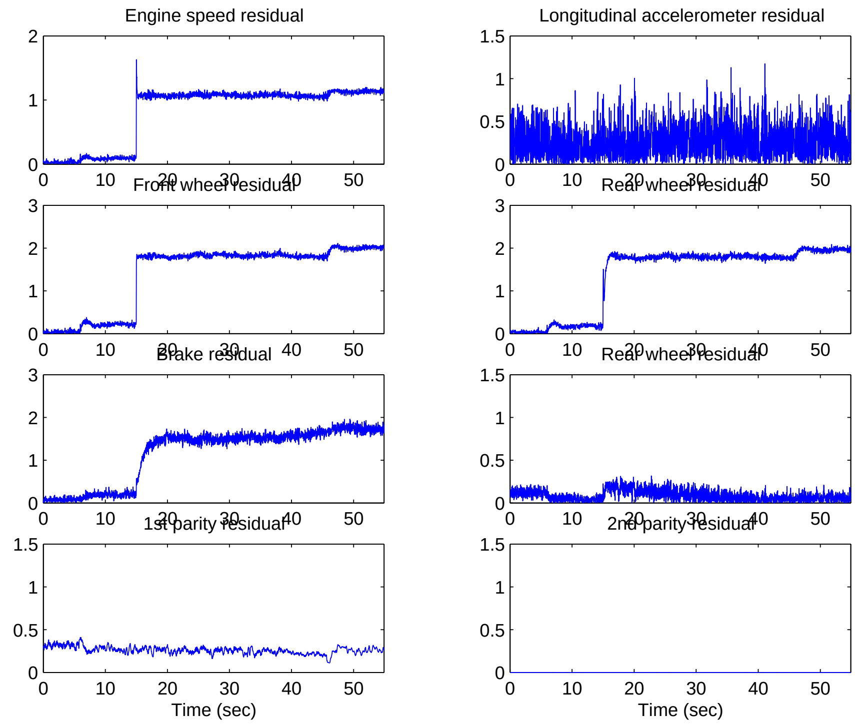

Figure 11.8: Engine speed sensor fault occurs

speed from 20 to 28 m/s (45 to 63 mph). The vehicle first reaches a constant speed of 20 m/s (45 mph). Then, the vehicle increases speed to 28 m/s (63 mph) by increasing the throttle angle. Figure 11.7 shows the vehicle speed, throttle and steering command.

Figure 11.8 shows the performance of the residual generator designed for the vehicle longitudinal dynamics when an engine speed sensor fault occurs after 15th second. The engine speed sensor fault is a bias with magnitude of 175 rpm. The first row is the residuals of fault detection filter set no. 1', the second row is the residuals of fault detection filter set no. 2, the third row is the residuals of fault detection filter set no. 3' and the fourth row shows the residuals from 1st and 2nd parity equation. The longitudinal residual processor process this residual pattern and generate the probability of each defined hypothesis. Figure 11.9 shows that the probability of engine speed sensor fault goes from zero to one immediately after the fault occured. Therefore, the engine speed sensor fault can be detected and identified with probability by the health monitoring system. The residual generator and processor designed for the vehicle lateral dynamics are not shown here because they will not respond to this fault.

Figure 11.10 shows the performance of the residual generator designed for the vehicle longitudinal dynamics when an longitudinal accelerometer fault occurs after 15th second. The longitudinal

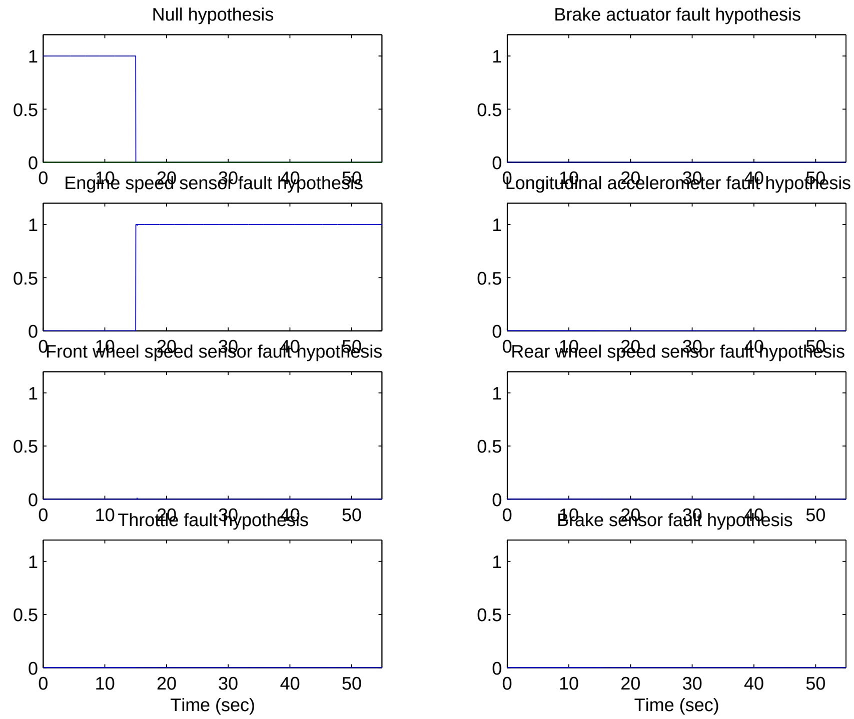

Figure 11.9: Engine speed sensor fault occurs

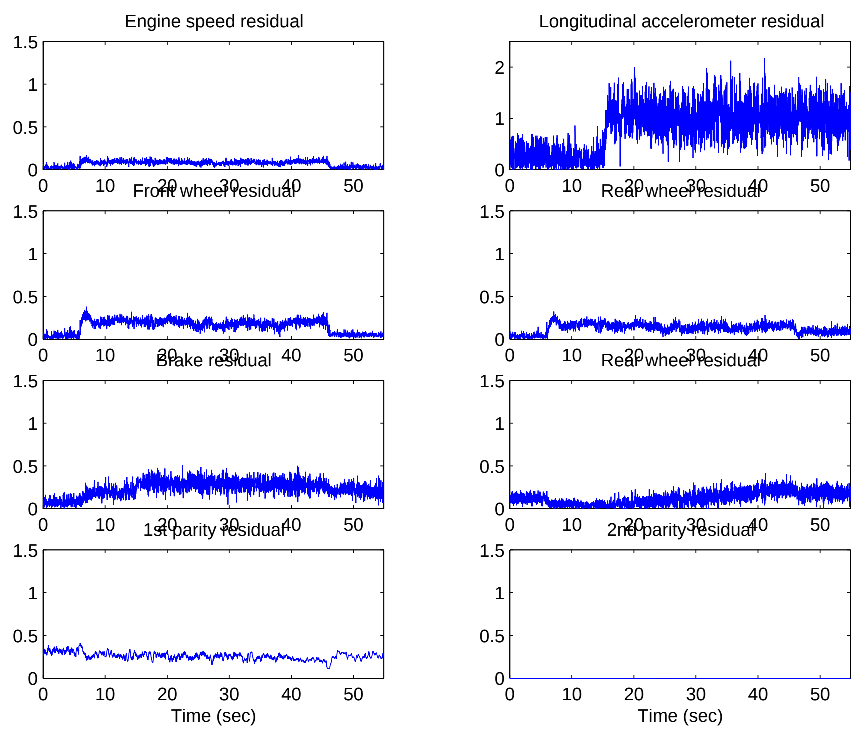

Figure 11.10: Longitudinal accelerometer fault occurs

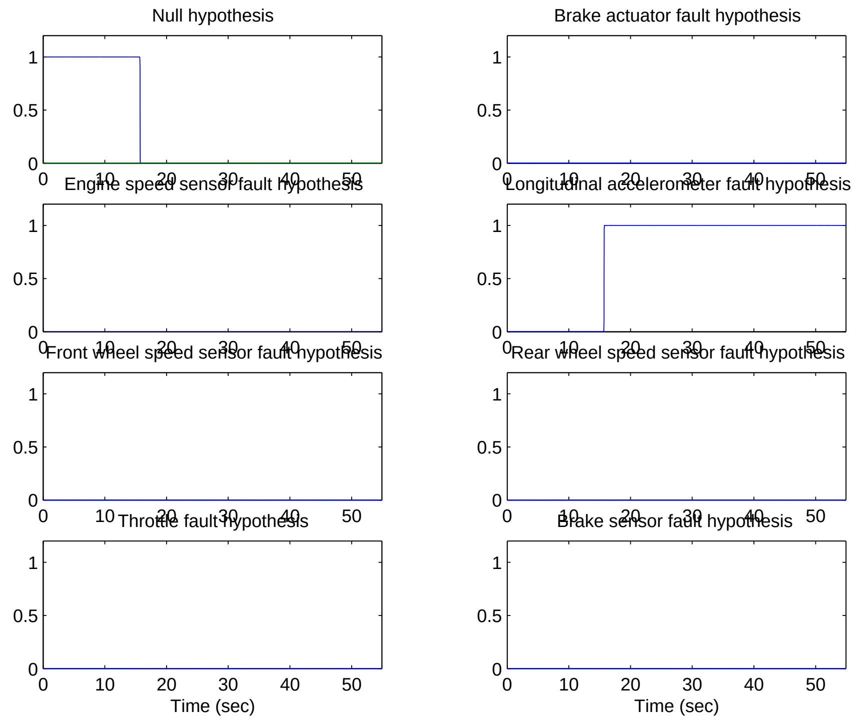

Figure 11.11: Longitudinal accelerometer fault occurs

accelerometer fault is a bias with magnitude of $0.4m/s^2$. Figure 11.11 shows that the probability of longitudinal accelerometer fault goes from zero to one quickly. Therefore, the longitudinal accelerometer fault can be detected and identified with probability by the health monitoring system. The residual generator and processor designed for the vehicle lateral dynamics are not shown here because they will not respond to this fault.

Figure 11.12 and Figure 11.14 show the performance of the residual generator designed for the vehicle longitudinal dynamics and the vehicle lateral dynamics respectively when a fault occurs in front left wheel speed sensor after 15th second. The front wheel speed fault is a bias with magnitude of 2.218 m/s. In Figure 11.14, the first row is the residuals of fault detection filter set no. 4, the second row is the residuals of fault detection filter set no. 5 and the third row is the residuals of fault detection filter set no. 6. Figure 11.13 and Figure 11.15 show that the probability of front wheel speed sensor fault goes from zero to one immediately after the fault occured. Therefore, the front wheel speed sensor fault can be detected and identified with probability by the health monitoring system. Note that the residual generator and processor designed for both longitudinal and lateral vehicle dynamics respond to the front wheel speed sensor fault but the system can not identify whether the fault occurs in the front left wheel or front right wheel. This identification

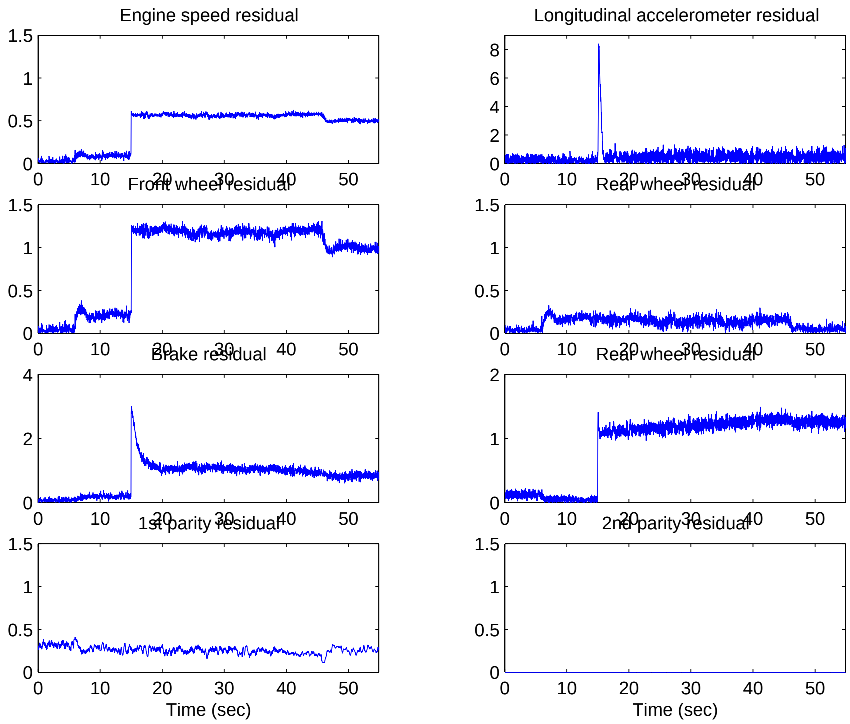

Figure 11.12: Front wheel speed sensor fault occurs

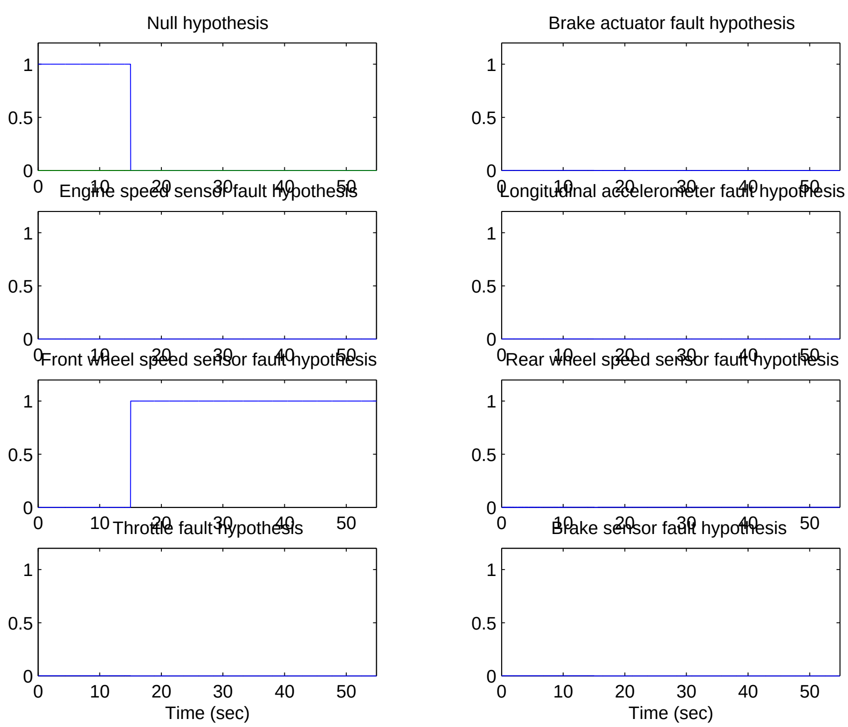

Figure 11.13: Front wheel speed sensor fault occurs

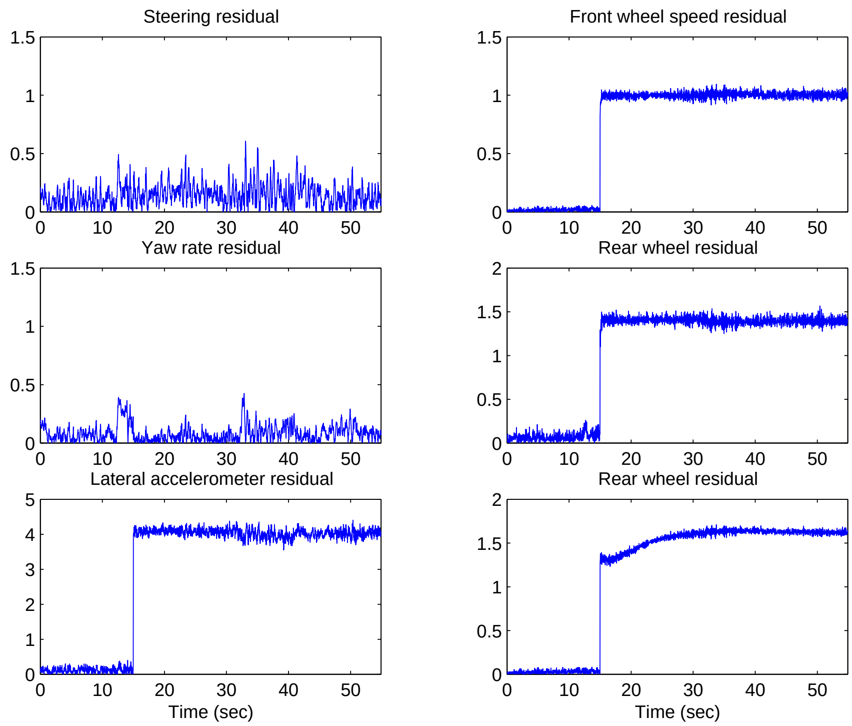

Figure 11.14: Front wheel speed sensor fault occurs

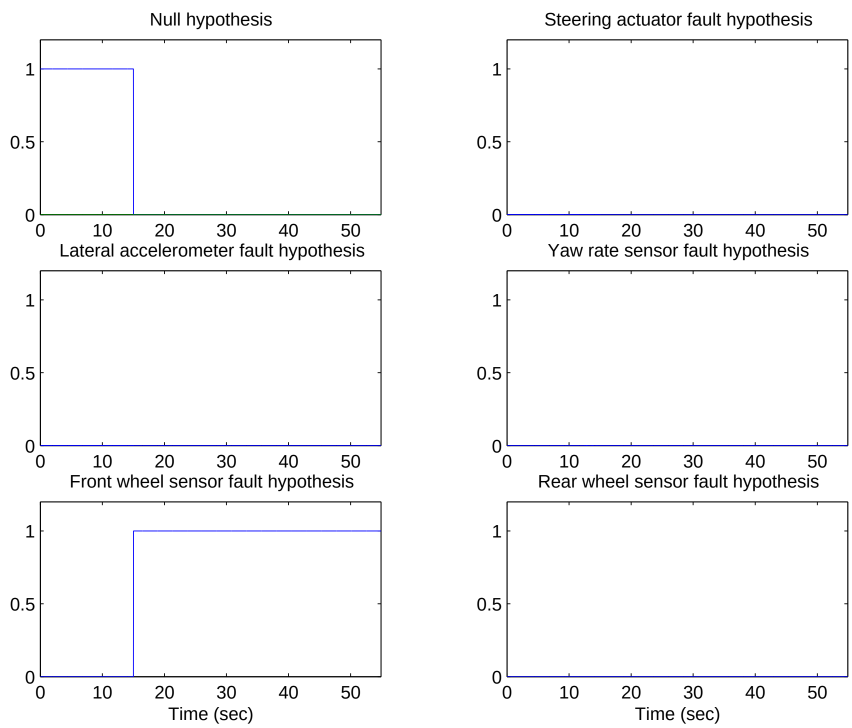

Figure 11.15: Front wheel speed sensor fault occurs

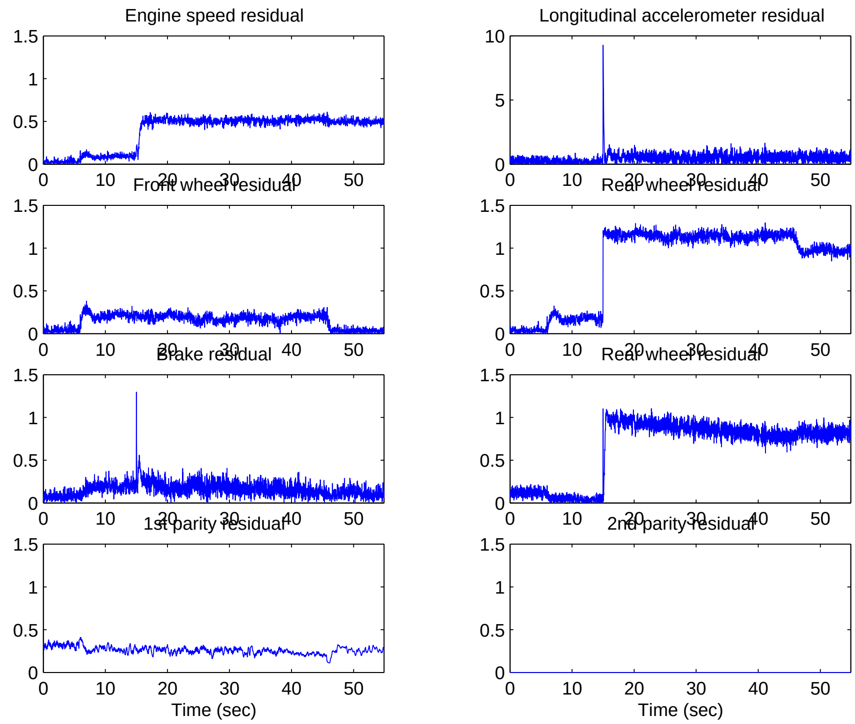

Figure 11.16: Rear wheel speed sensor fault occurs

task can be easily accomplished by checking the sign of the fault detection filter residuals and is not discussed here.

Figure 11.16 and Figure 11.18 show the performance of the residual generator designed for the vehicle longitudinal dynamics and the vehicle lateral dynamics respectively when an fault occurs in rear left wheel speed sensor after 15th second. The rear wheel speed fault is a bias with magnitude of 2.299 m/s. Figure 11.17 and Figure 11.19 show that the probability of rear wheel speed sensor fault goes from zero to one immediately after the fault occured. Therefore, the rear wheel speed sensor fault can be detected and identified with probability by the health monitoring system. Note that the residual generator and processor designed for both longitudinal and lateral vehicle dynamics respond to the rear wheel speed sensor fault but the system can not identify whether the fault occurs in the rear left wheel or rear right wheel. This identification task can be accomplished by checking the sign of the fault detection filter residuals and is not discussed here.

Figure 11.20 shows the performance of the residual generator designed for the vehicle longitudinal dynamics when a brake actuator fault occurs after 15th second. The brake actuator fault is a bias with magnitude of 200 psi. Figure 11.21 shows that the probability of Brake actuator fault goes from zero to one quickly. Therefore, the brake actuator fault can be detected and identified

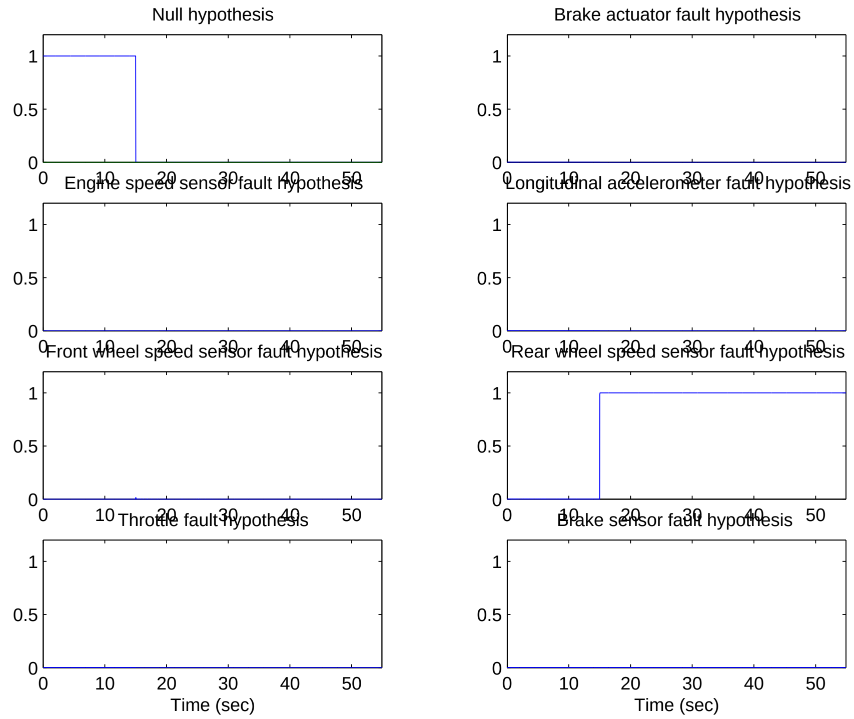

Figure 11.17: Rear wheel speed sensor fault occurs

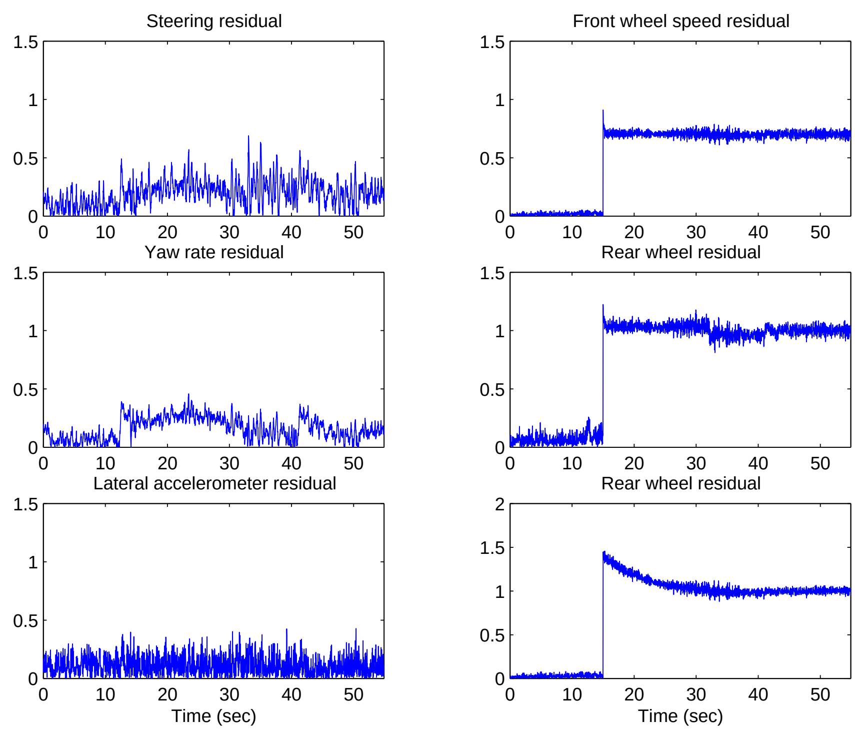

Figure 11.18: Rear wheel speed sensor fault occurs

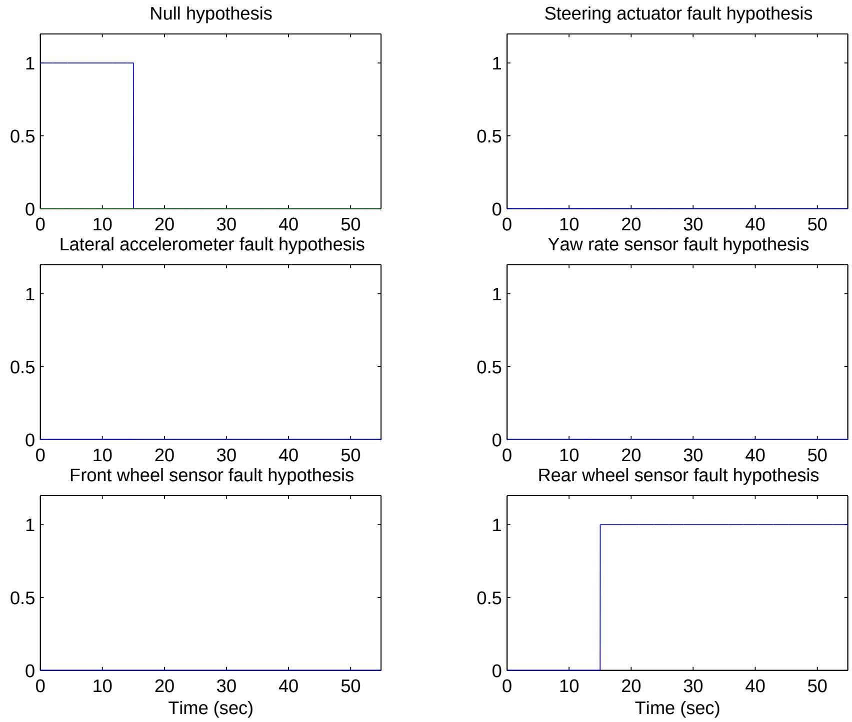

Figure 11.19: Rear wheel speed sensor fault occurs

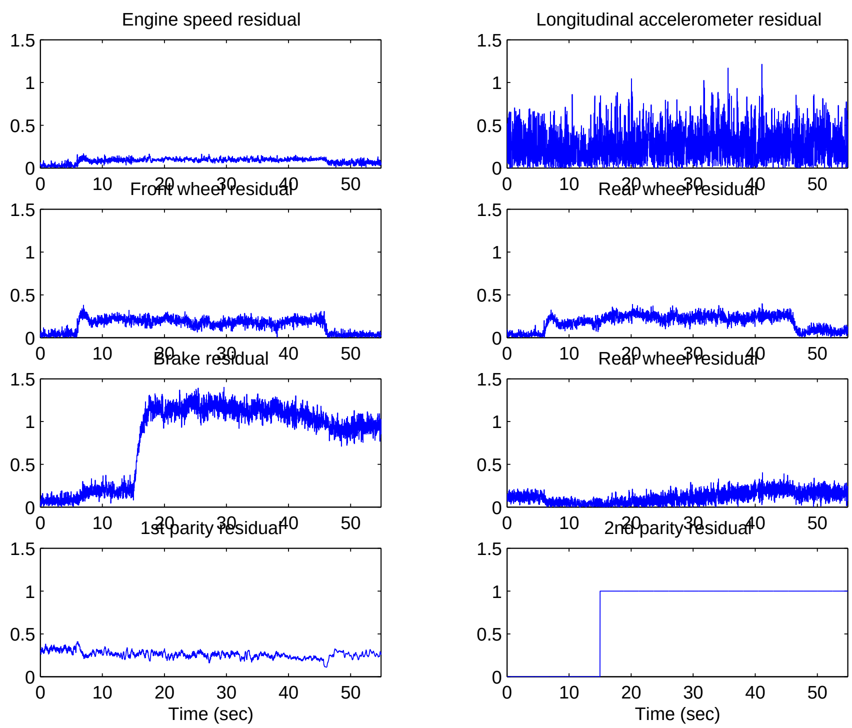

Figure 11.20: Brake actuator fault occurs

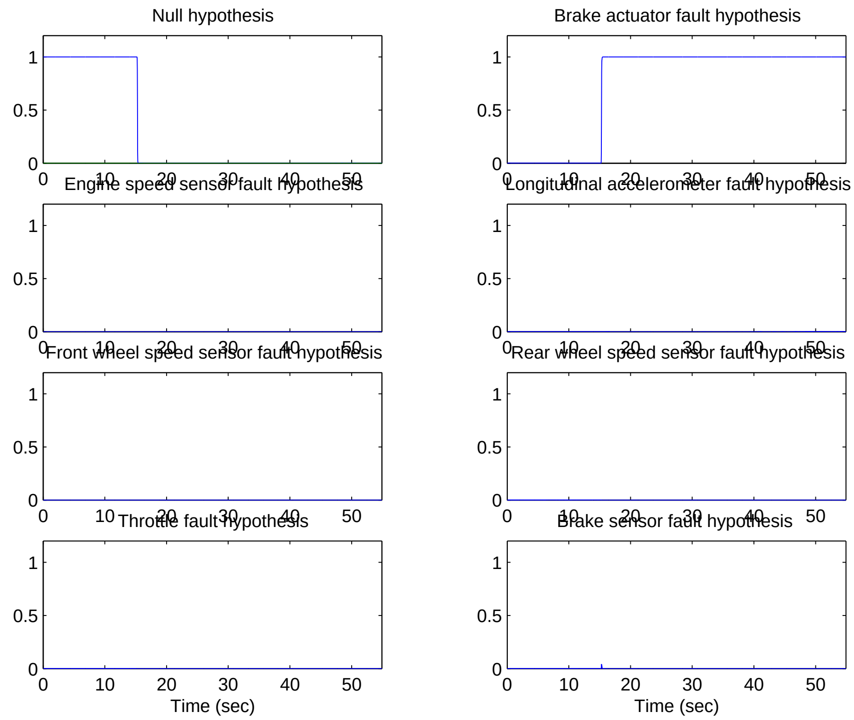

Figure 11.21: Brake actuator fault occurs

with probability by the health monitoring system. The residual generator and processor designed for the vehicle lateral dynamics are not shown here because they will not respond to this fault.

Figure 11.22 shows the performance of the residual generator designed for the vehicle longitudinal dynamics when a throttle actuator fault occurs after 15th second. The throttle actuator fault is a bias with magnitude of 2 *deg*. Figure 11.23 shows that the probability of Throttle fault goes from zero to one quickly. Therefore, the health monitoring system can detect a fault occurs in either throttle actuator or throttle sensor but can not identified whether the fault is in actuator or sensor. The residual generator and processor designed for the vehicle lateral dynamics are not shown here because they will not respond to this fault.

Figure 11.24 shows the performance of the residual generator designed for the vehicle lateral dynamics when a steering actuator fault occurs after 15th second. The steering actuator fault is a bias with magnitude of 14.61. *deg*. In Figure 11.24, the first row is the residuals of fault detection filter set no. 4, the second row is the residuals of fault detection filter set no. 5 and the third row is the residuals of fault detection filter set no. 6. Figure 11.25 shows that the probability of steering actuator fault goes from zero to one quickly. Therefore, the steering actuator fault can be detected and identified with probability by the health monitoring system. Note that the residual generator

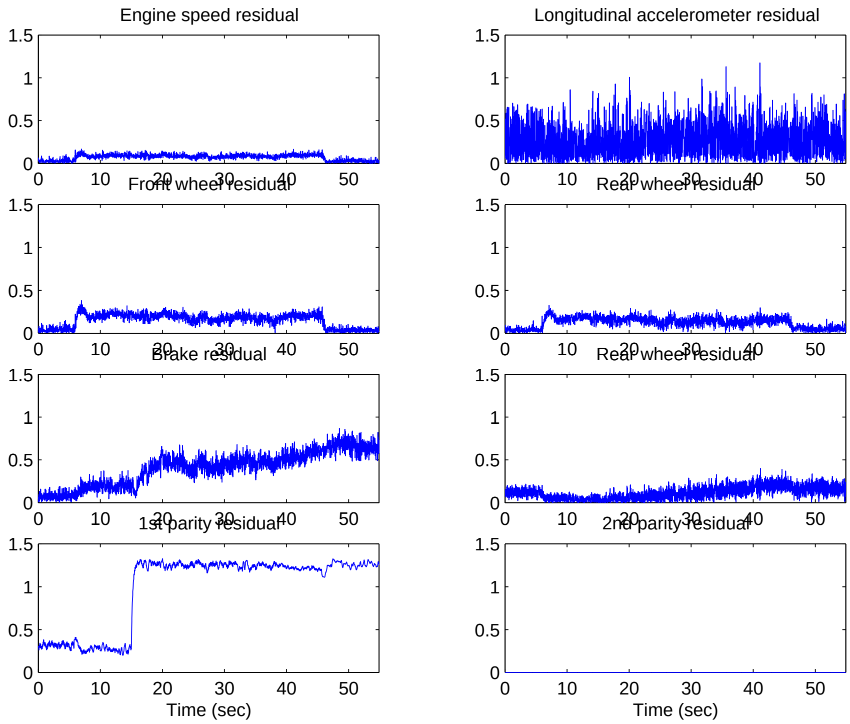

Figure 11.22: Throttle actuator fault occurs

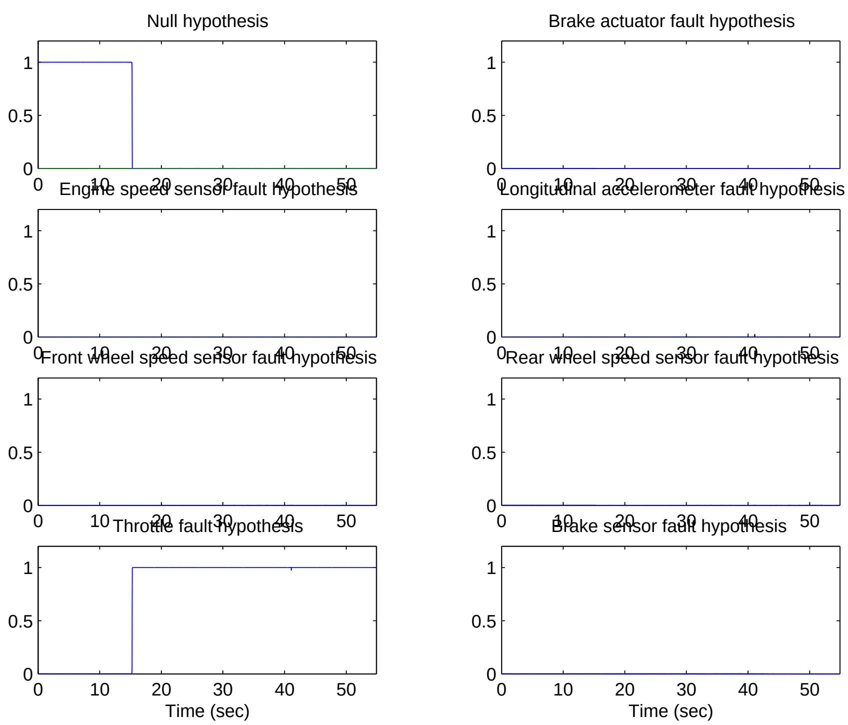

Figure 11.23: Throttle actuator fault occurs

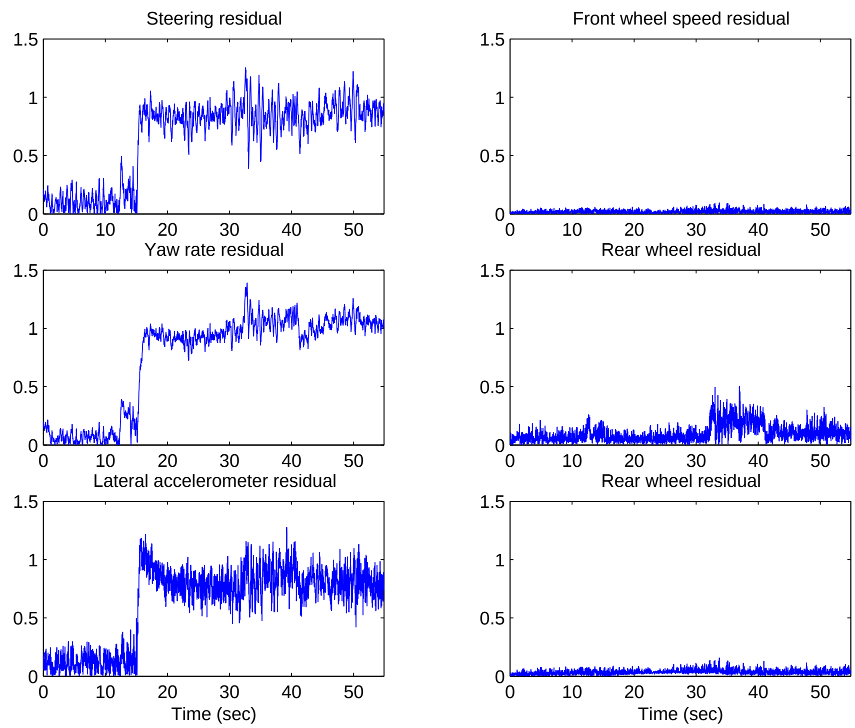

Figure 11.24: Steering actuator fault occurs

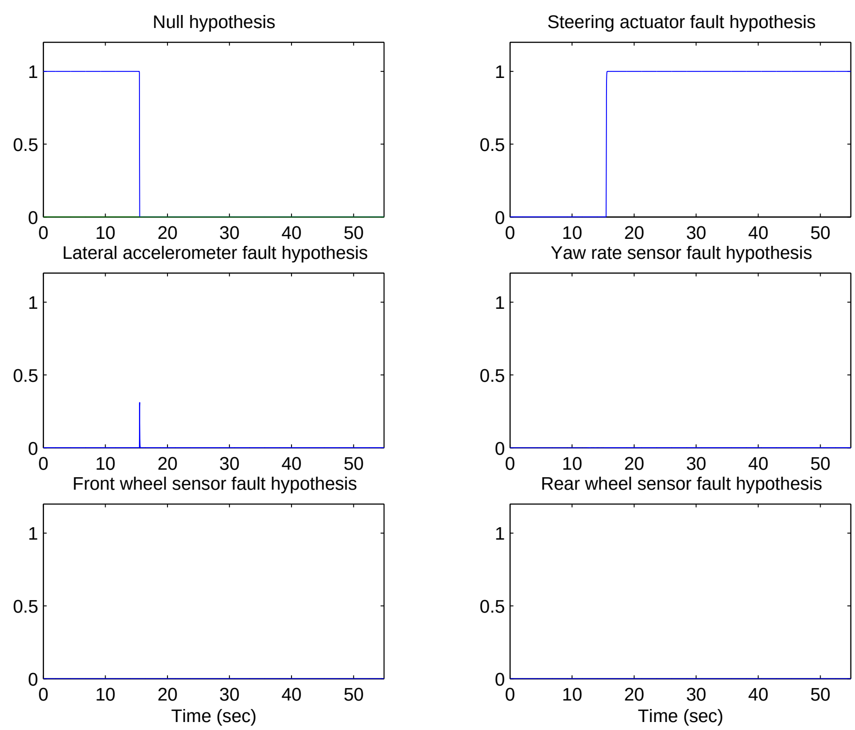

Figure 11.25: Steering actuator fault occurs

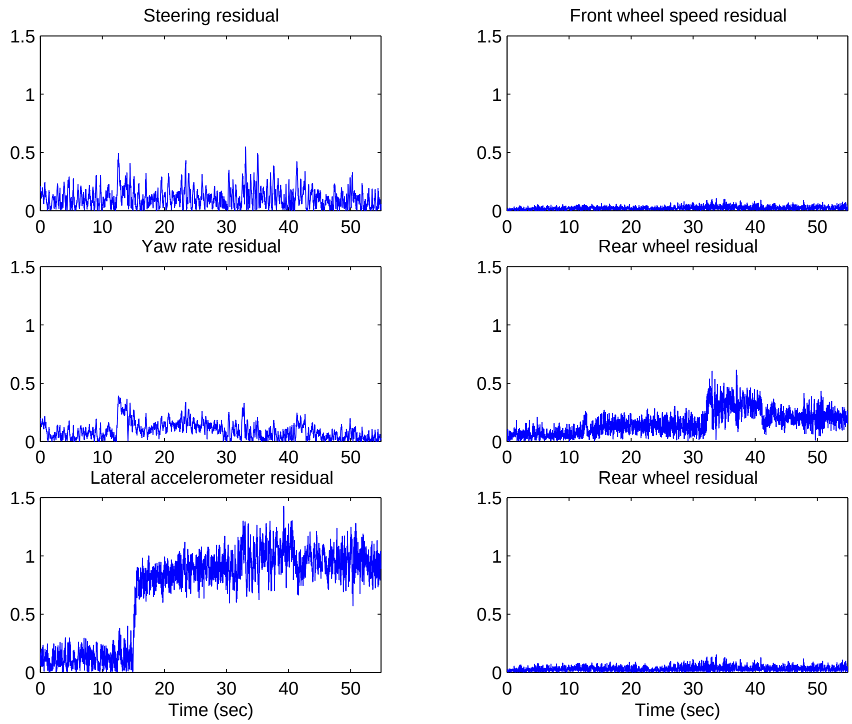

Figure 11.26: Lateral accelerometer fault occurs

and processor designed for vehicle longitudinal dynamics are not shown here because they will not respond to this fault.

Figure 11.26 shows the performance of the residual generator designed for the vehicle lateral dynamics when a lateral accelerometer fault occurs after 15th second. The lateral accelerometer is a bias with magnitude of 1 m/s^2. Figure 11.27 shows that the probability of lateral accelerometer fault goes from zero to one immediately. Therefore, the lateral accelerometer fault can be detected and identified with probability by the health monitoring system. Note that the residual generator and processor designed for vehicle longitudinal dynamics are not shown here because they will not respond to this fault.

Figure 11.28 shows the performance of the residual generator designed for the vehicle lateral dynamics when a yaw rate sensor fault occurs after 15th second. The yaw rate sensor fault is a bias with magnitude of 0.035 rad/s. Figure 11.29 shows that the probability of yaw rate sensor fault goes from zero to one immediately. Therefore, the yaw rate sensor fault can be detected and identified with probability by the health monitoring system. Note that the residual generator and processor designed for vehicle longitudinal dynamics are not shown here because they will not respond to this fault.

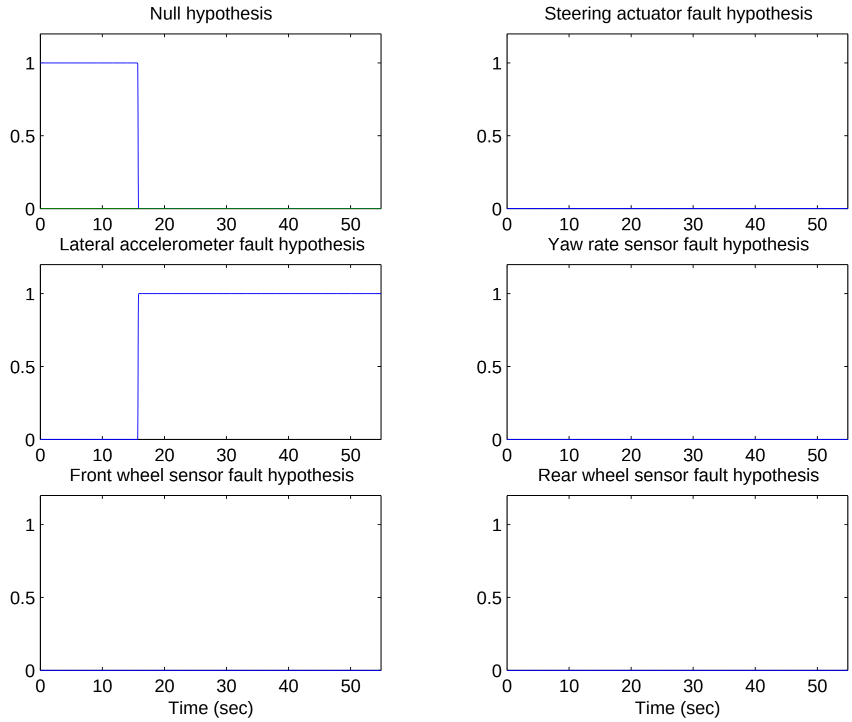

Figure 11.27: Lateral accelerometer fault occurs

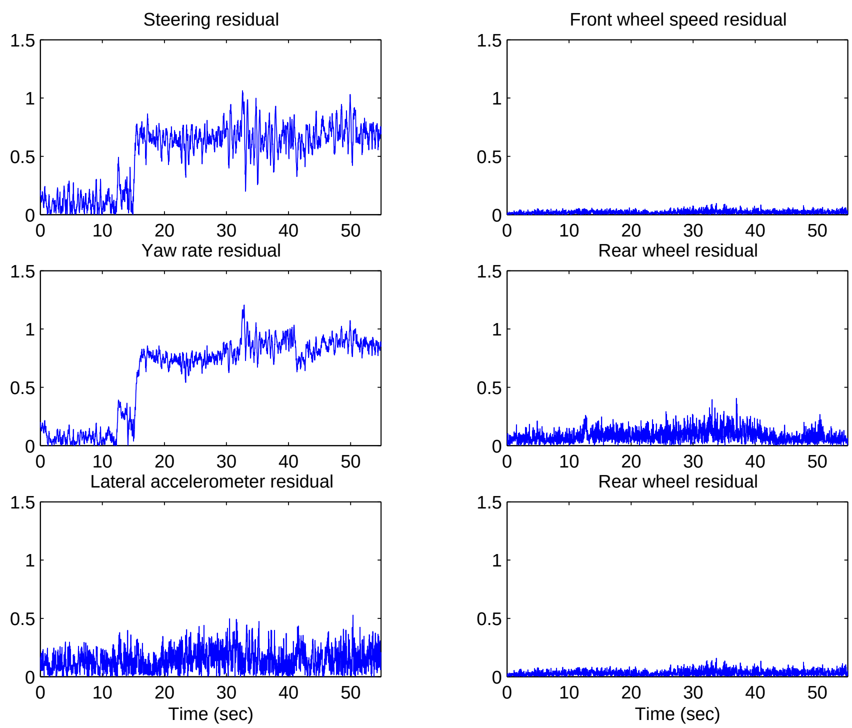

Figure 11.28: Yaw rate sensor fault occurs

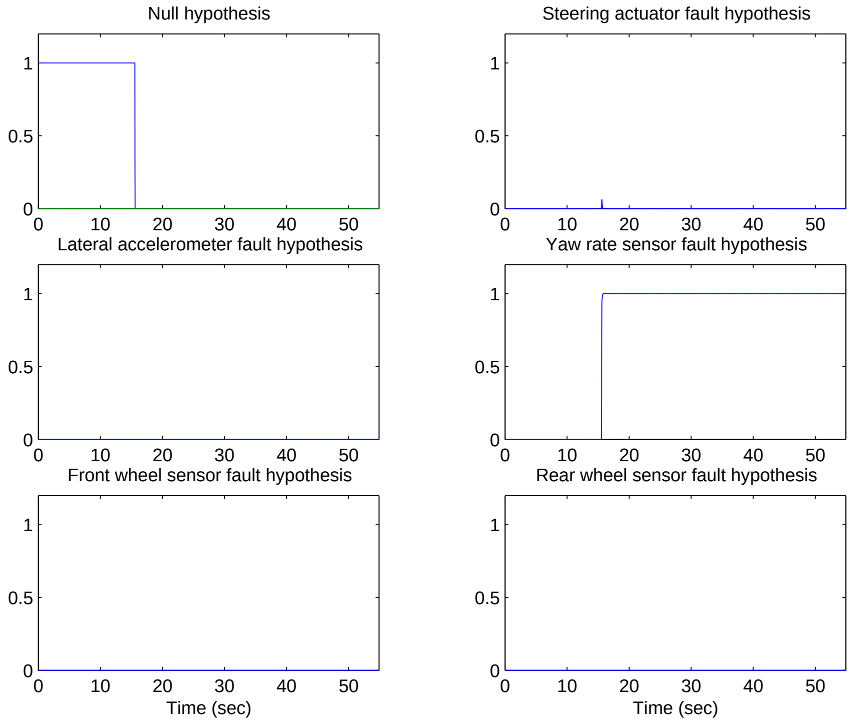

Figure 11.29: Yaw rate sensor fault occurs

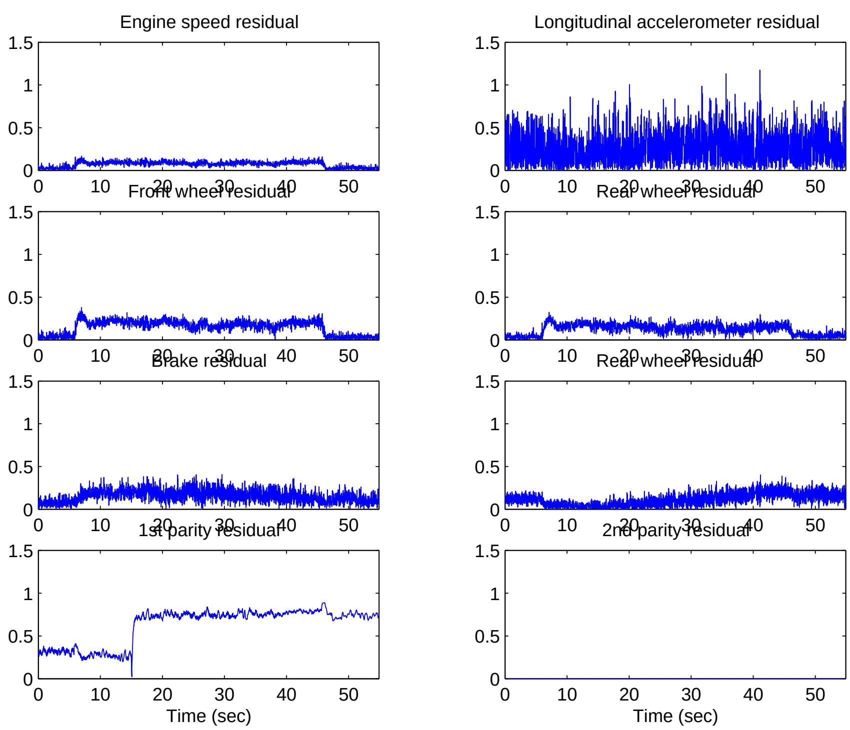

Figure 11.30: Throttle sensor fault occurs

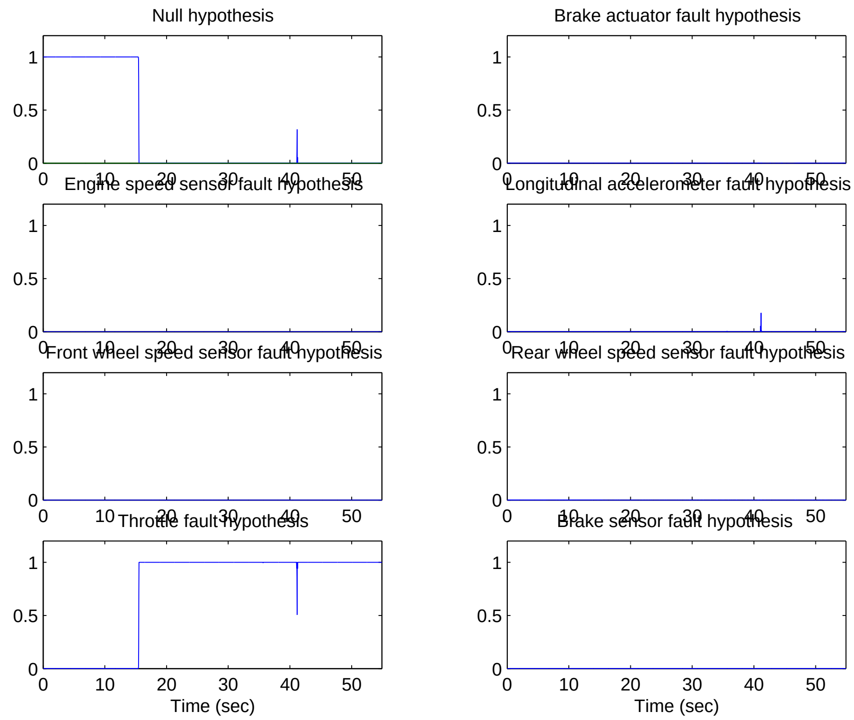

Figure 11.31: Throttle sensor fault occurs

Figure 11.30 shows the performance of the residual generator designed for the vehicle longitudinal dynamics when a throttle sensor fault occurs after 15th second. The throttle sensor fault is a bias with magnitude of 4 deg. Figure 11.31 shows that the probability of Throttle fault goes from zero to one quickly. Therefore, the health monitoring system can detect a fault occurs in either throttle actuator or throttle sensor but can not identified whether the fault is in actuator or sensor. The residual generator and processor designed for the vehicle lateral dynamics are not shown here because they will not respond to this fault.

Figure 11.32 shows the performance of the residual generator designed for the vehicle longitudinal dynamics when a brake sensor fault occurs after 15th second. The brake sensor fault is a bias with magnitude of 200 psi. Figure 11.21 shows that the probability of Brake sensor fault goes from zero to one quickly. Therefore, the brake sensor fault can be detected and identified with probability by the health monitoring system. The residual generator and processor designed for the vehicle lateral dynamics are not shown here because they will not respond to this fault.

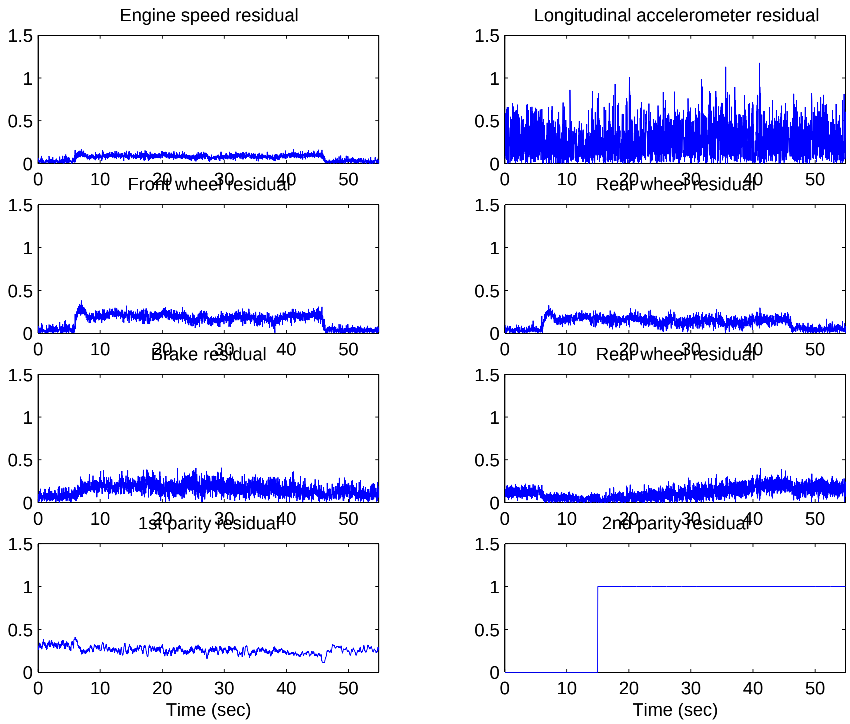

Figure 11.32: Brake sensor fault occurs

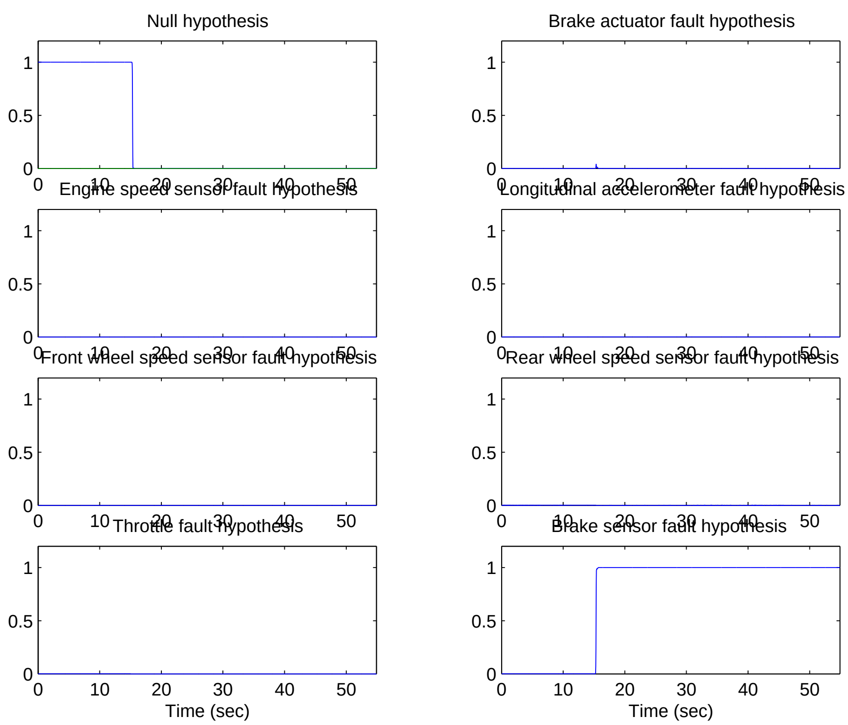

Figure 11.33: Brake sensor fault occurs

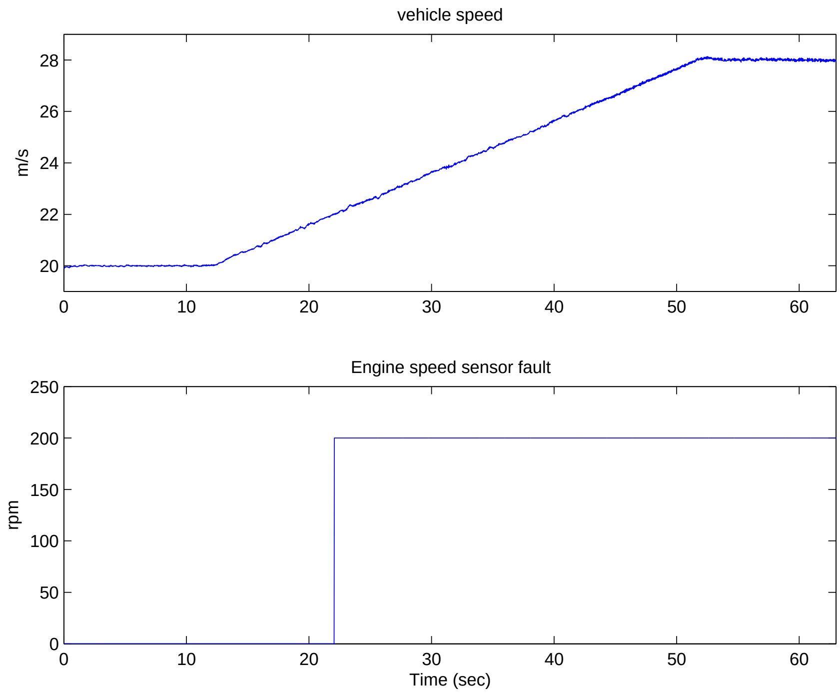

Figure 11.34: Vehicle speed and fault magnitude

11.6 Evaluation Scenario No. 2: Closed Loop Fault

In this section, the vehicle health monitoring system is evaluated in real-time on a PATH Buick LeSabre at Crow's Landing when the vehicle is traveling on the magnetic curve track. A simulated bias fault is imposed in engine speed sensor, longitudinal accelerometer, vehicle speed sensor, throttle actuator, throttle sensor and brake sensor by the PATH computer respectively. Note that, since the vehicle controller command is generated without using lateral accelerometer sensor measurement and yaw rate sensor measurement. For this two sensor, no difference will be made between imposing the fault by the PATH vehicle computer or imposing the fault by the UCLA laptop. Therefore, these two sensor faults are not simulated by the PATH vehicle computer in this section. As for the brake actuator fault and steering actuator fault, they will be created manually and the corresponding performance of the vehicle health monitoring system will be evaluated in next section.

Figure 11.34 shows the vehicle speed and the imposed engine speed sensor fault. The vehicle increases speed from 20 m/s (45 mph) to 28 m/s (63 mph) when traveling on the magnetic curve track. Figure 11.35 shows the performance of the residual generator designed for the vehicle longitudinal dynamics when an engine speed sensor fault occurs around 22nd second. The engine

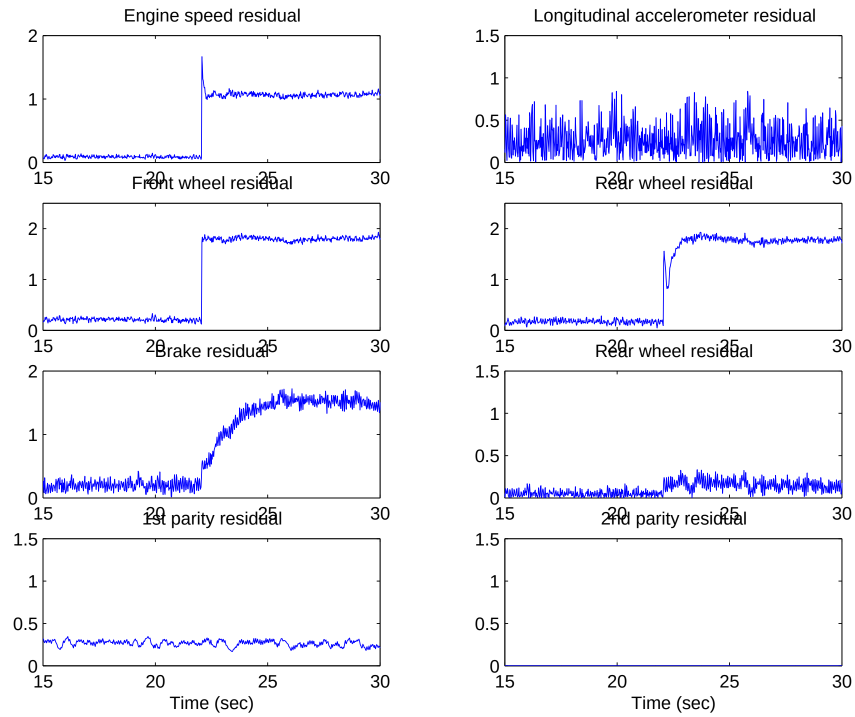

Figure 11.35: Engine speed sensor fault occurs

speed sensor fault is a bias with magnitude of 200 rpm. The first row is the residuals of fault detection filter set no. 1', the second row is the residuals of fault detection filter set no. 2, the third row is the residuals of fault detection filter set no. 3' and the fourth row shows the residuals from 1st and 2nd parity equation. Note that the engine speed sensor residual goes above one because the magnitude of the fault is bigger than 175 rpm where the residual is scaled to one. Figure 11.36 shows that the probability of engine speed sensor fault goes from zero to one immediately after the fault is imposed. Therefore, the engine speed sensor fault can be detected and identified with probability by the health monitoring system. The residual generator and processor designed for the vehicle lateral dynamics are not shown here because they will not respond to this fault.

Figure 11.37 shows the vehicle speed and the imposed longitudinal accelerometer fault. The vehicle increases speed from 20 m/s (45 mph) to 28 m/s (63 mph) when traveling on the magnetic curve track. Figure 11.38 shows the performance of the residual generator designed for the vehicle longitudinal dynamics when an longitudinal accelerometer fault occurs around 17th second. The longitudinal accelerometer fault is a bias with magnitude of 0.4 m/s^2. The first row is the residuals of fault detection filter set no. 1', the second row is the residuals of fault detection filter set no. 2, the third row is the residuals of fault detection filter set no. 3' and the fourth row shows the

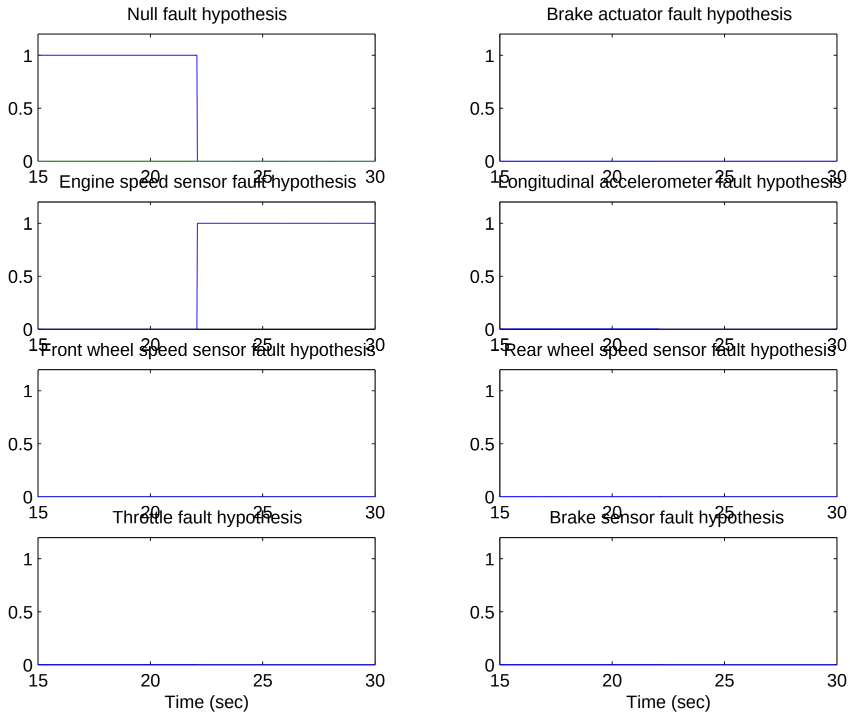

Figure 11.36: Engine speed sensor fault occurs

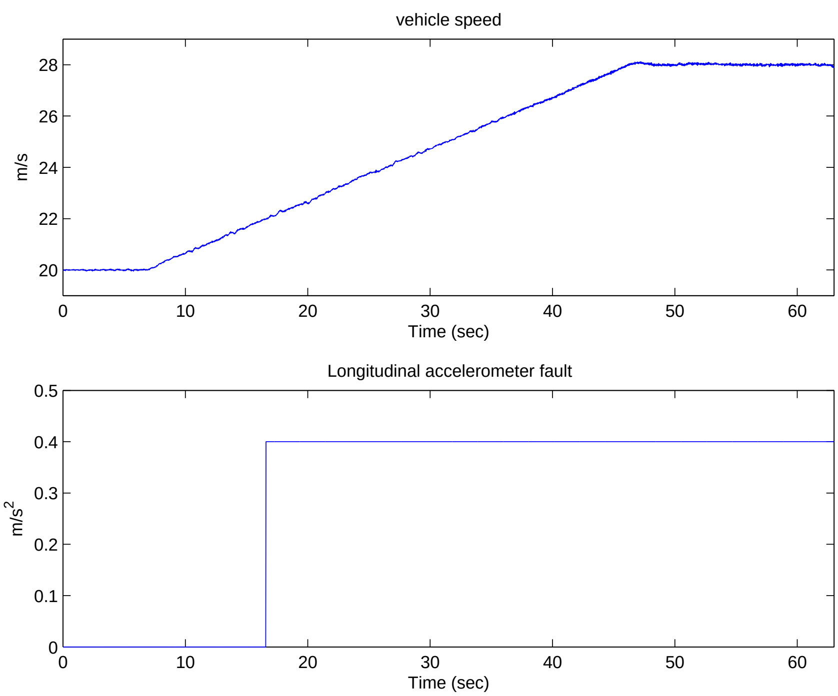

Figure 11.37: Vehicle speed and fault magnitude

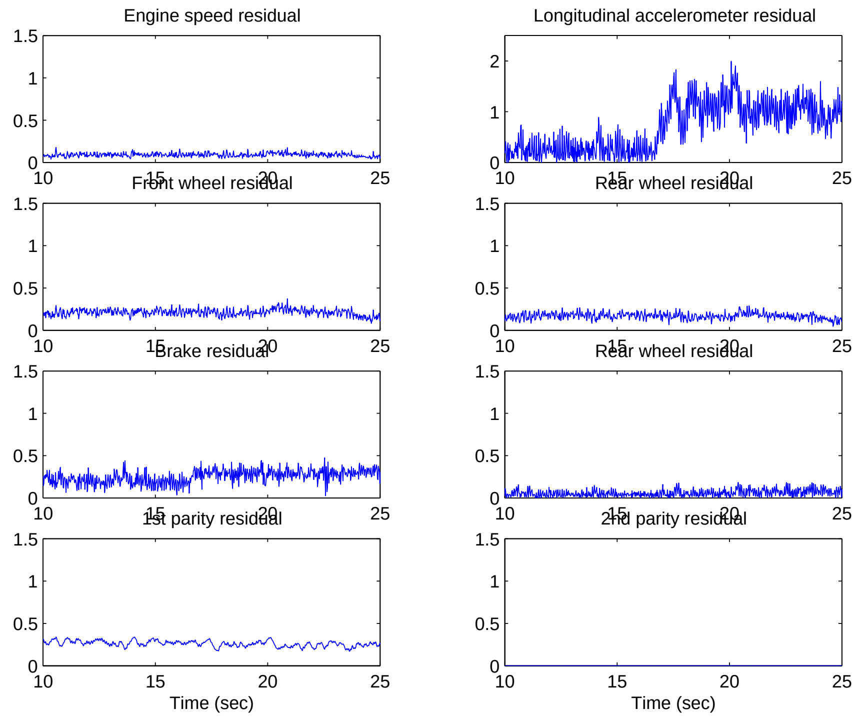

Figure 11.38: Longitudinal accelerometer fault occurs

residuals from 1st and 2nd parity equation. Figure 11.39 shows that the probability of longitudinal accelerometer fault goes from zero to one shortly after the fault is imposed. Therefore, longitudinal accelerometer fault can be detected and identified with probability by the health monitoring system. The residual generator and processor designed for the vehicle lateral dynamics are not shown here because they will not respond to this fault.

Figure 11.40 shows the vehicle speed and the imposed wheel speed fault. Note that the vehicle speed increased from 20 m/s to 27.5 m/s instead of from 20 m/s to the expected 28 m/s due to the presence of a 2 m/s wheel speed sensor fault. The vehicle controller used the average of the speed from the four wheels to track the vehicle speed. Since a bias of 2 m/s fault is imposed in one of the four wheel the actual vehicle speed is reduce by 0.5 m/s. Figure 11.41 and Figure 11.43 show the performance of the residual generator designed for the vehicle longitudinal dynamics and the vehicle lateral dynamics respectively when an front wheel speed sensor fault occurs around 22nd second. In Figure 11.43, the first row is the residuals of fault detection filter set no. 4, the second row is the residuals of fault detection filter set no. 5 and the third row is the residuals of fault detection filter set no. 6. Figure 11.42 and Figure 11.44 show that the probability of front wheel speed sensor fault goes from zero to one immediately. Therefore, the front wheel speed sensor fault

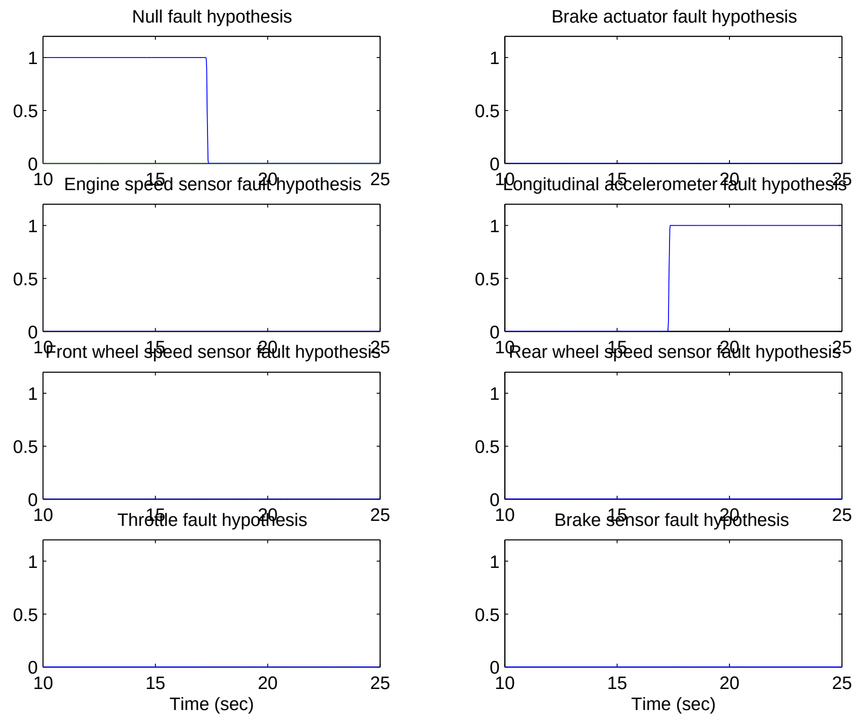

Figure 11.39: Longitudinal accelerometer fault occurs

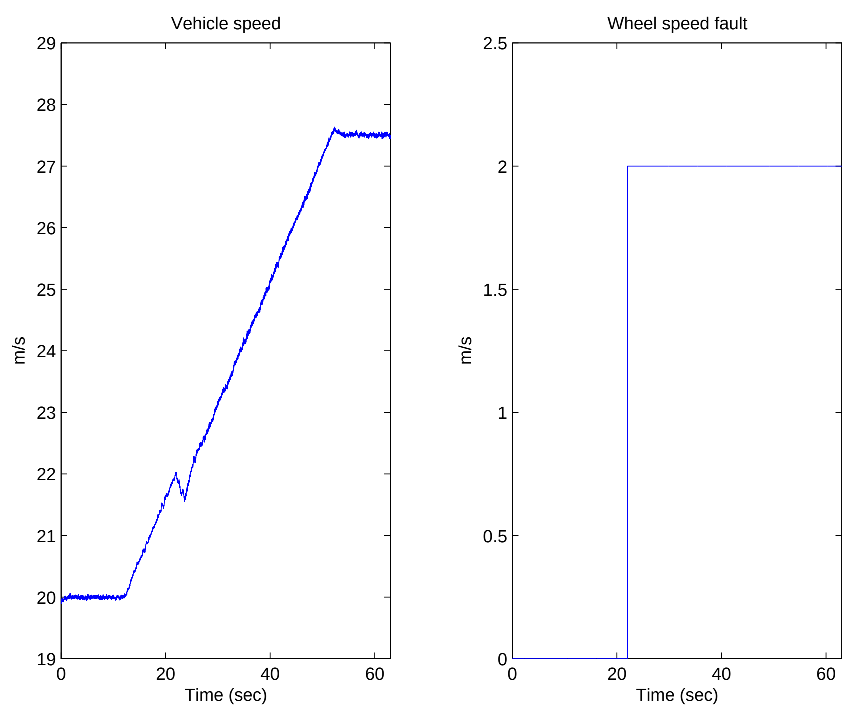

Figure 11.40: Vehicle speed and fault magnitude

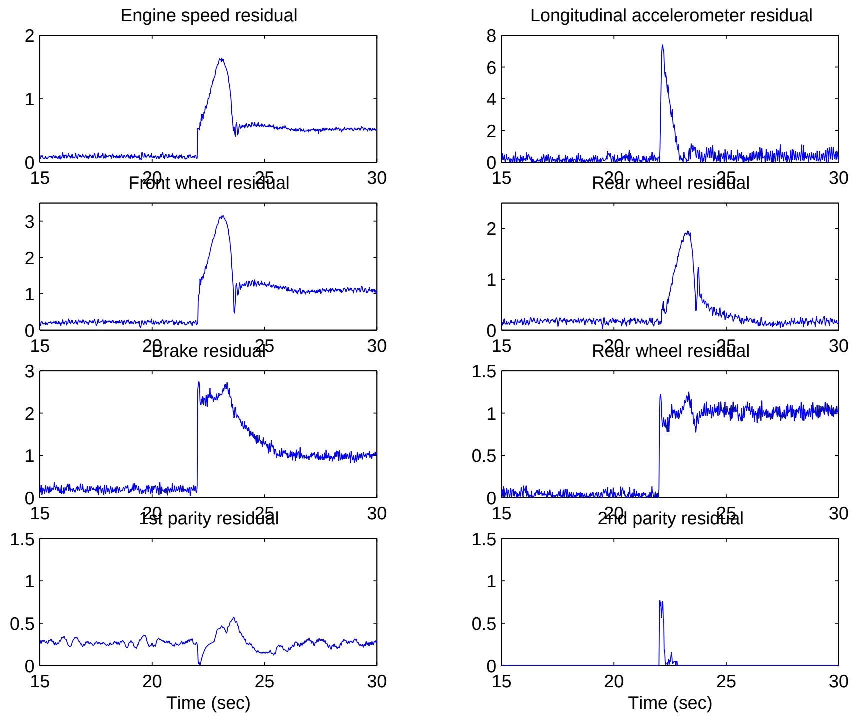

Figure 11.41: Front wheel speed sensor fault occurs

can be detected and identified with probability by the health monitoring system.

Figure 11.45 and Figure 11.47 show the performance of the residual generator designed for the vehicle longitudinal dynamics and the vehicle lateral dynamics respectively when an rear wheel speed sensor fault occurs around 22nd second. Figure 11.46 and Figure 11.48 show that the probability of rear wheel speed sensor fault goes from zero to one immediately. Therefore, the rear wheel speed sensor fault can be detected and identified with high probability by the health monitoring system.

Figure 11.49 shows the vehicle speed and the imposed throttle actuator fault. The vehicle increases speed from 20 m/s (45 mph) to 28 m/s (63 mph) when traveling on the magnetic curve track. Figure 11.50 shows the performance of the residual generator designed for the vehicle longitudinal dynamics when an throttle actuator fault occurs around 4th second. The throttle actuator fault is a bias with magnitude of 4 deg. Figure 11.51 shows that the probability of throttle actuator fault goes from zero to one in about a second after the fault is imposed. This shows that, the health monitoring system can detect a fault occurs in either throttle actuator or throttle sensor although it can not identified whether the fault is in actuator or sensor. The residual generator and processor designed for the vehicle lateral dynamics are not shown here because they

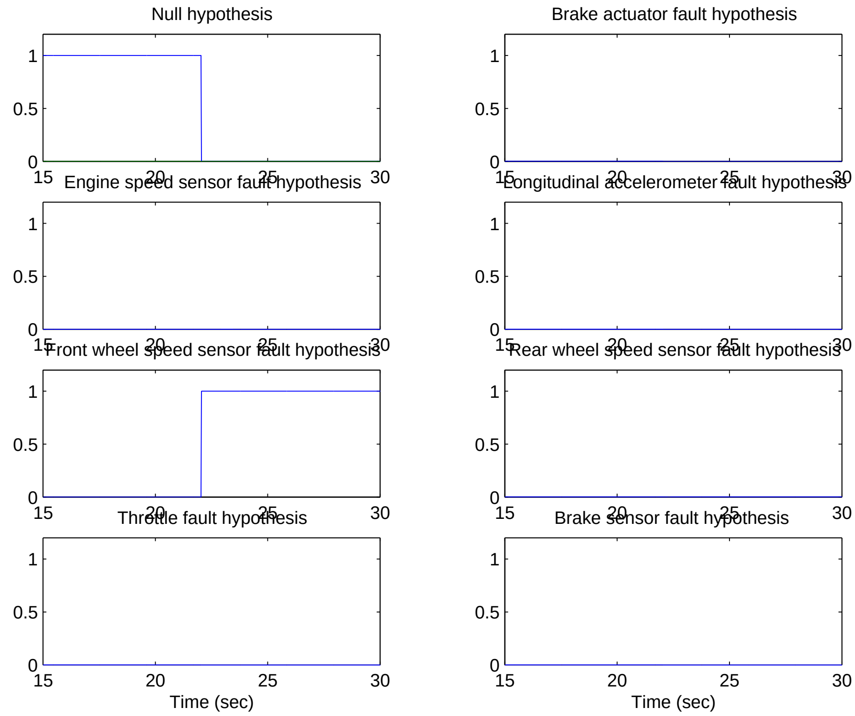

Figure 11.42: Front wheel speed sensor fault occurs

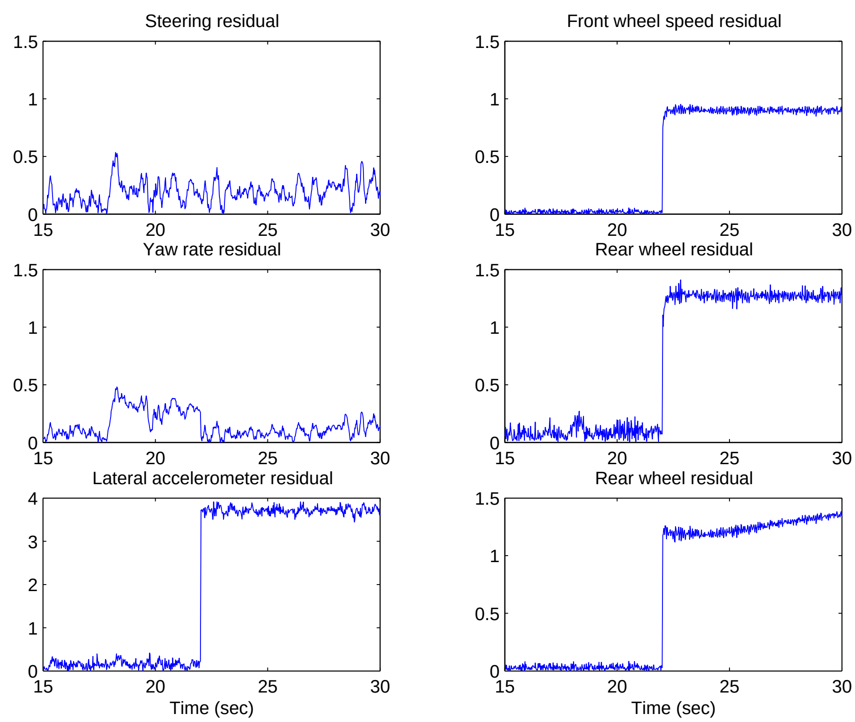

Figure 11.43: Front wheel speed sensor fault occurs

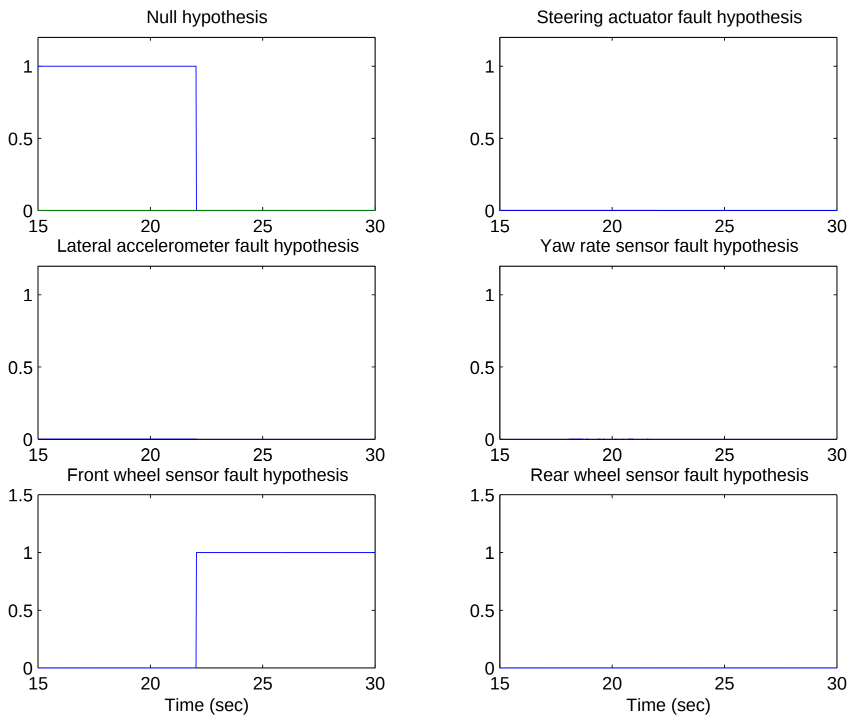

Figure 11.44: Front wheel speed sensor fault occurs

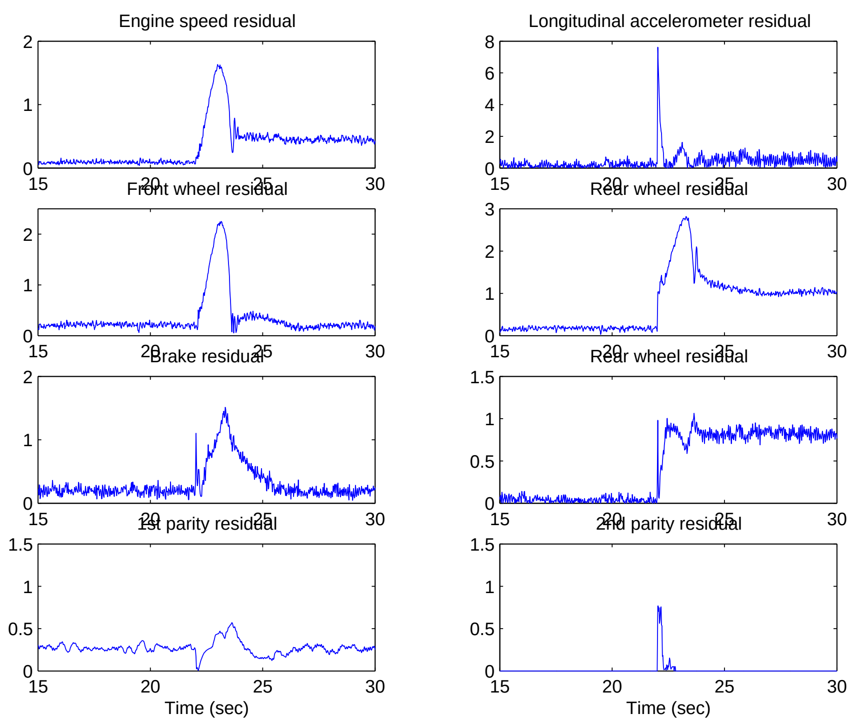

Figure 11.45: Rear wheel speed sensor fault occurs

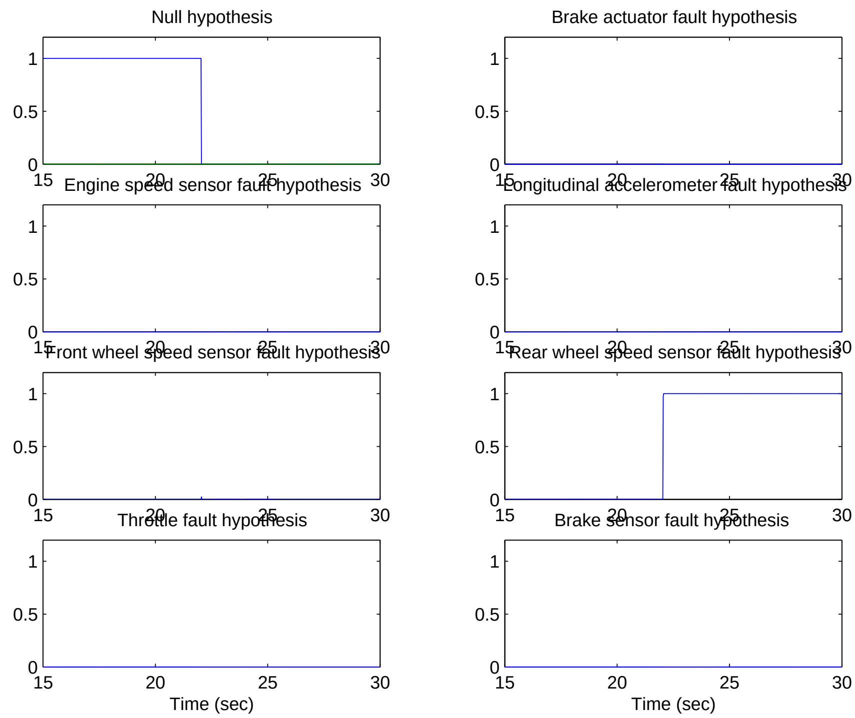

Figure 11.46: Rear wheel speed sensor fault occurs

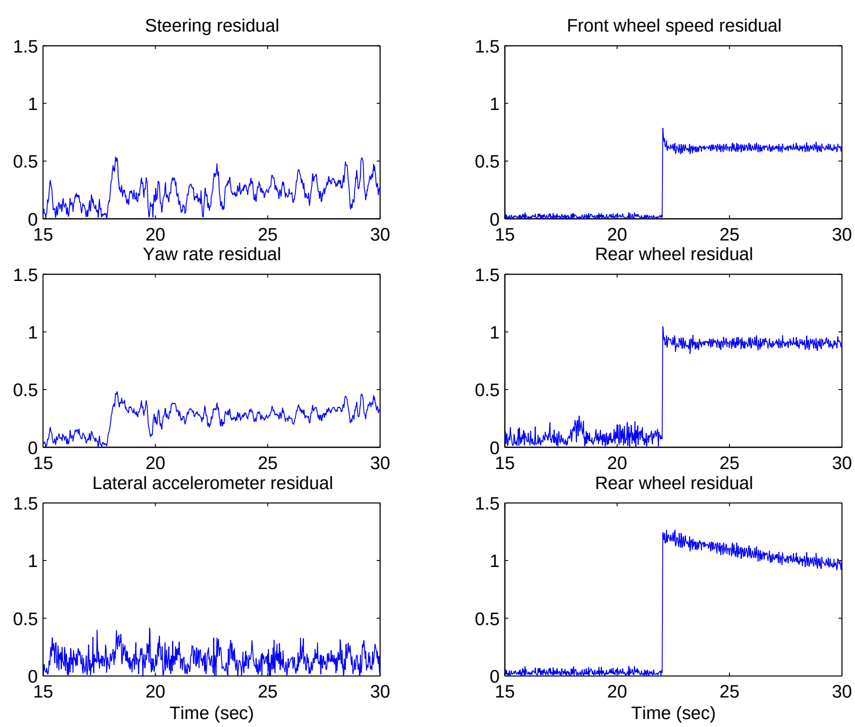

Figure 11.47: Rear wheel speed sensor fault occurs

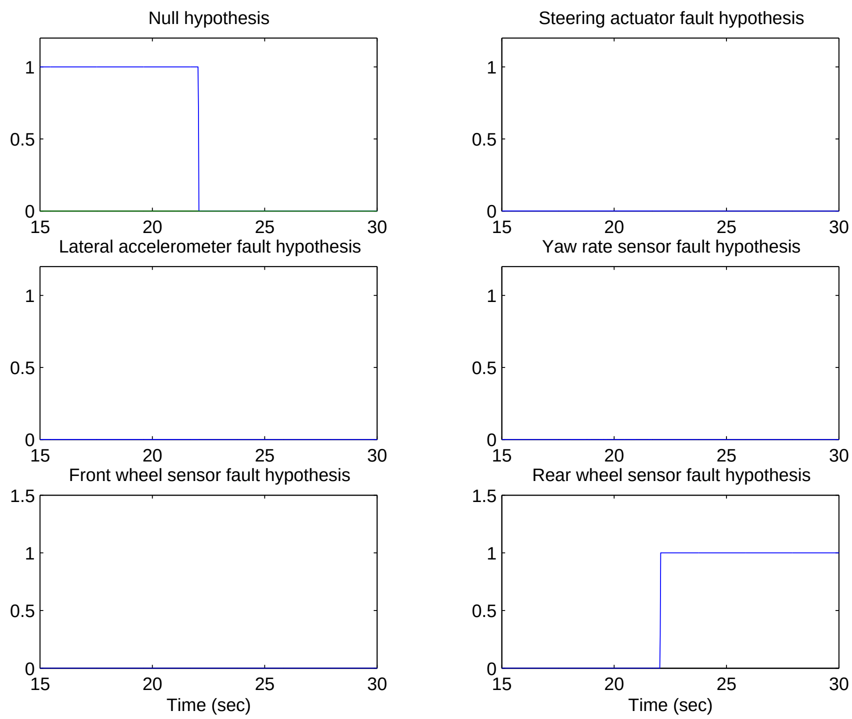

Figure 11.48: Rear wheel speed sensor fault occurs

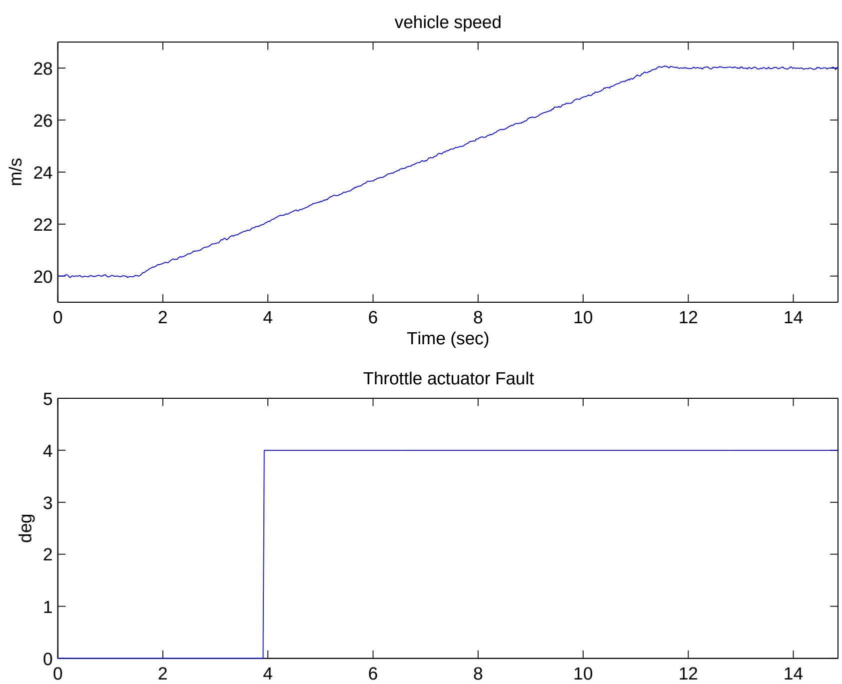

Figure 11.49: Vehicle speed and fault magnitude

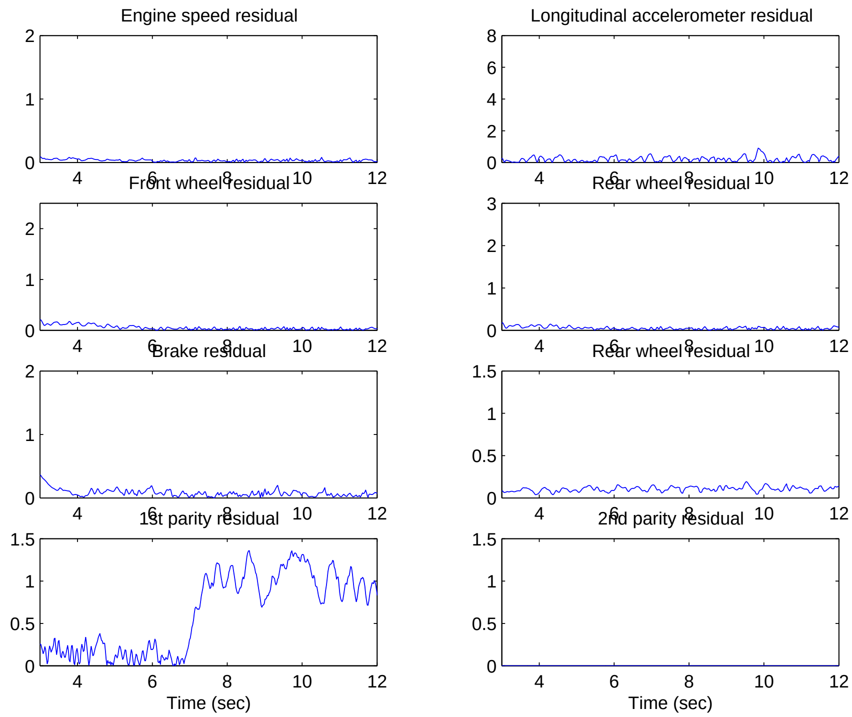

Figure 11.50: Throttle actuator fault occurs

will not respond to this fault.

Figure 11.52 shows the vehicle speed and the imposed throttle sensor fault. The vehicle increases speed from 20 m/s (45 mph) to 28 m/s (63 mph) when traveling on the magnetic curve track. Figure 11.53 shows the performance of the residual generator designed for the vehicle longitudinal dynamics when an throttle sensor fault occurs around 4th second. The throttle actuator fault is a bias with magnitude of 4 deg. Figure 11.54 shows that the probability of throttle sensor fault goes from zero to one in about a second after the fault is imposed. This shows that, the health monitoring system can detect a fault occurs in either throttle actuator or throttle sensor although it can not identified whether the fault is in actuator or sensor. The residual generator and processor designed for the vehicle lateral dynamics are not shown here because they will not respond to this fault.

Figure 11.55 shows the vehicle speed and the imposed brake sensor fault. In this case, the vehicle speed stay constant at 20 m/s (45 mph) when traveling on the magnetic curve track. Figure 11.56 shows the performance of the residual generator designed for the vehicle longitudinal dynamics when the brake sensor fault occurs around 1st second. The brake sensor fault is a bias with magnitude of 200 psi. Figure 11.57 shows that the probability of brake sensor fault goes from

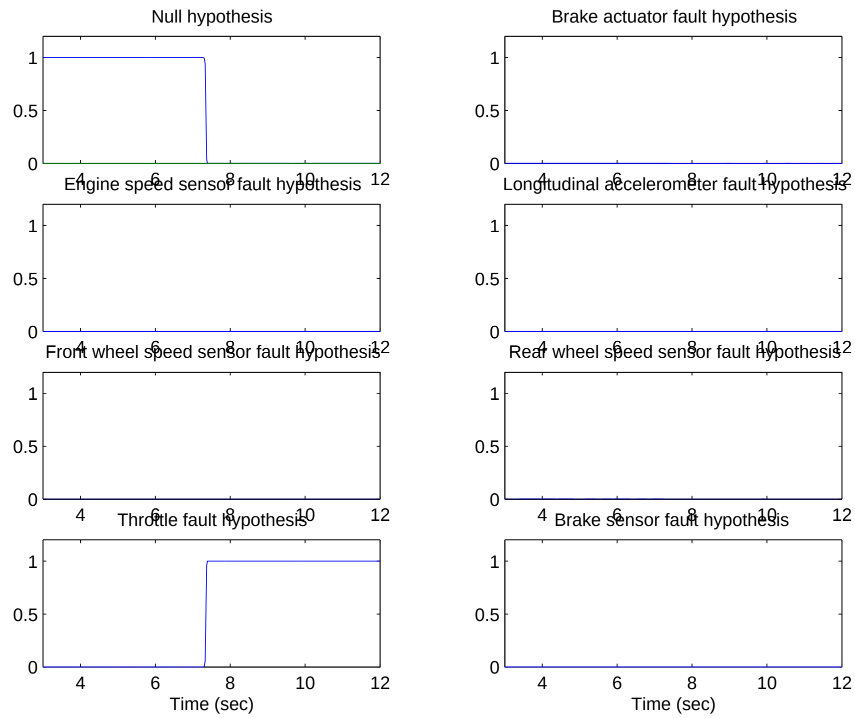

Figure 11.51: Throttle actuator fault occurs

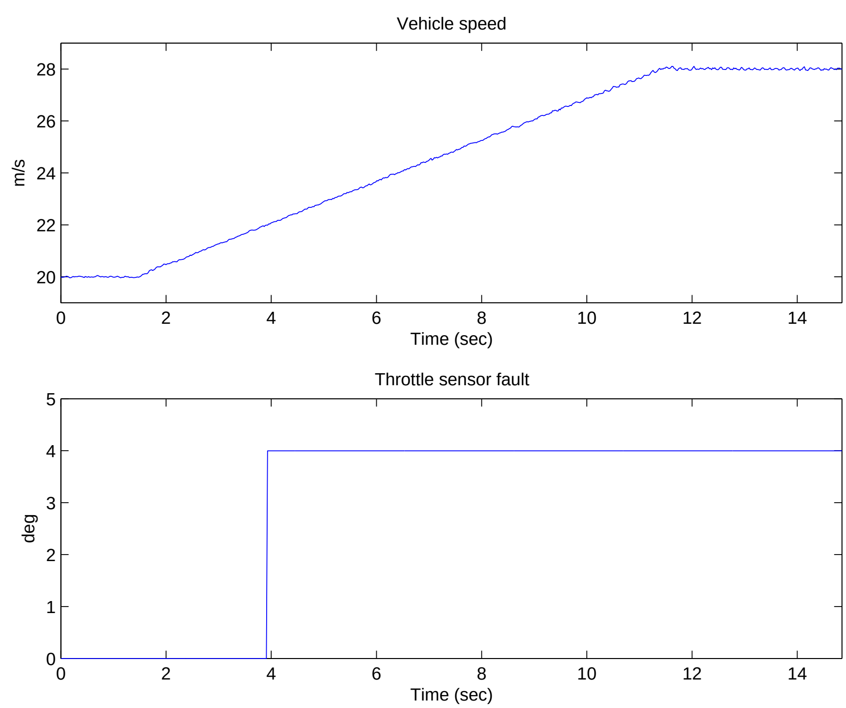

Figure 11.52: Vehicle speed and fault magnitude

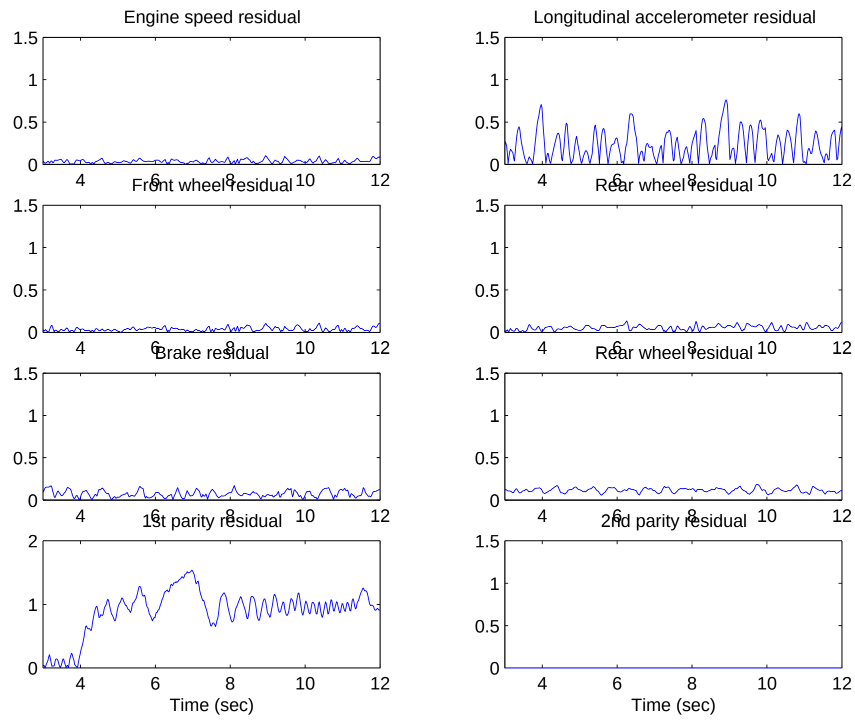

Figure 11.53: Throttle sensor fault occurs

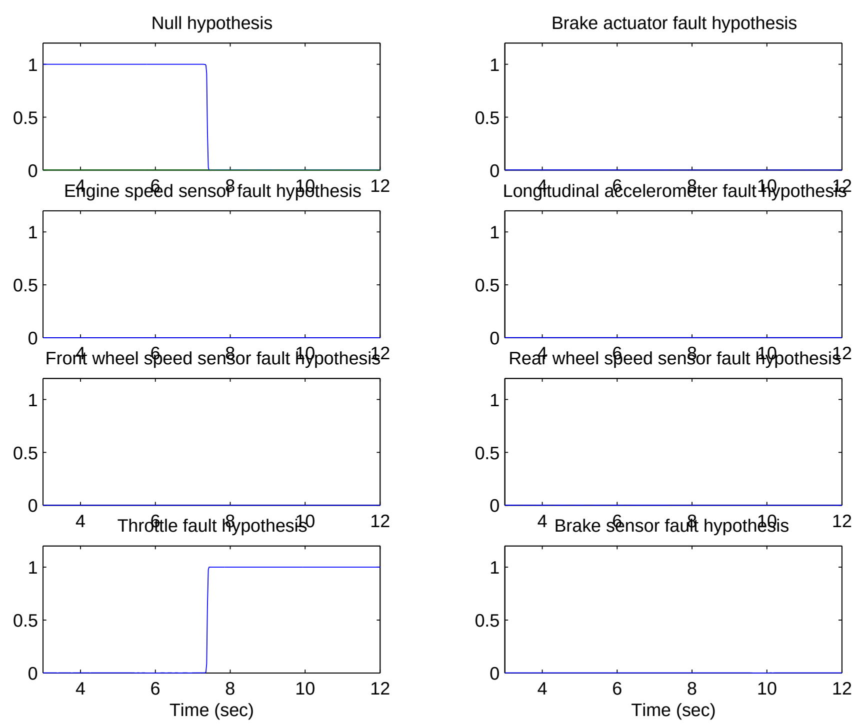

Figure 11.54: Throttle sensor fault occurs

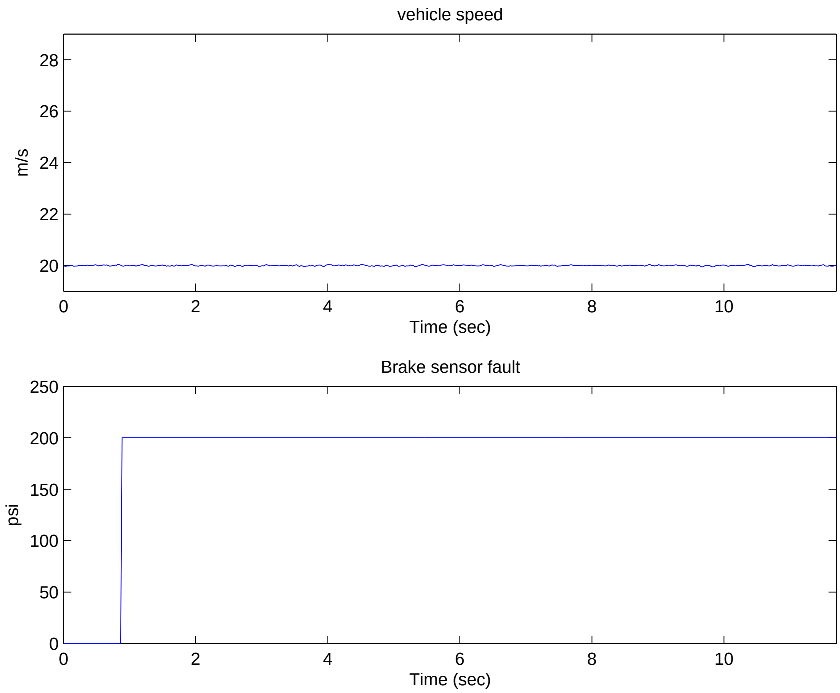

Figure 11.55: Vehicle speed and fault magnitude

zero to one in about one second after the fault is imposed. Therefore, brake sensor fault can be detected and identified with probability by the health monitoring system. The residual generator and processor designed for the vehicle lateral dynamics are not shown here because they will not respond to this fault.

We experienced a real fault in the wheel speed sensor that was not artificially introduced into real data. The performance of the fault detection filter and residual processor is given in Figure 11.58. The left figure shows the measurement of the wheel speed sensor on the front left wheel. Around the 64th second, there was a drop in the measurement indicating that a real fault occurred and went away in a very short period of time. The middle figure shows the residual associated with the front left wheel speed sensor fault. When there was no fault, this residual was very small. When a front left wheel speed sensor fault occurred, this residual became very large. This shows that the fault detection filter performed well. The right figure shows the probability of the front left wheel speed sensor fault. When the front left wheel speed sensor fault occurred, its probability went from 0 to 1 showing that the faulty sensor was correctly picked by the residual processor.

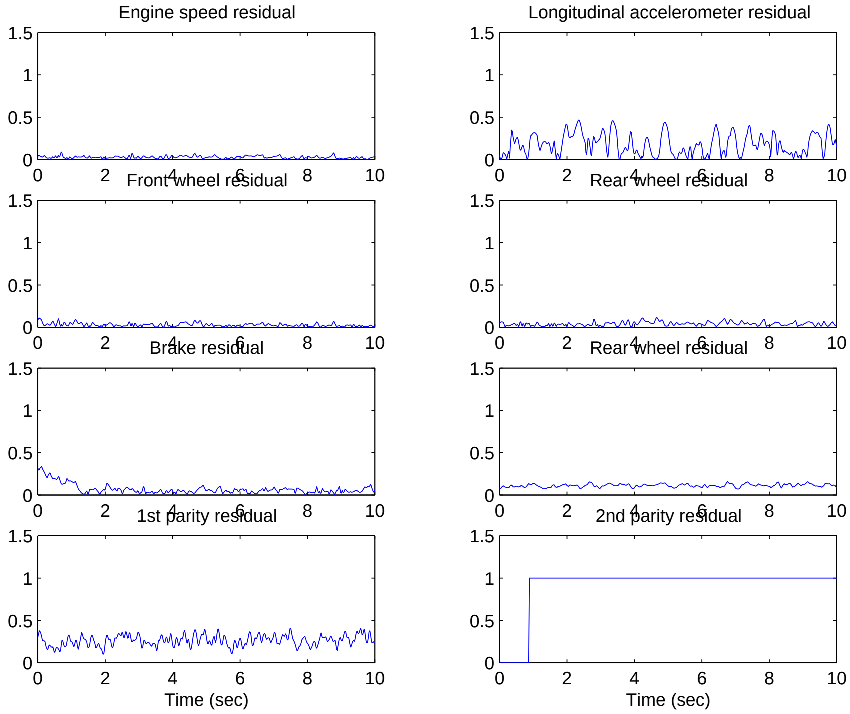

Figure 11.56: Brake sensor fault occurs

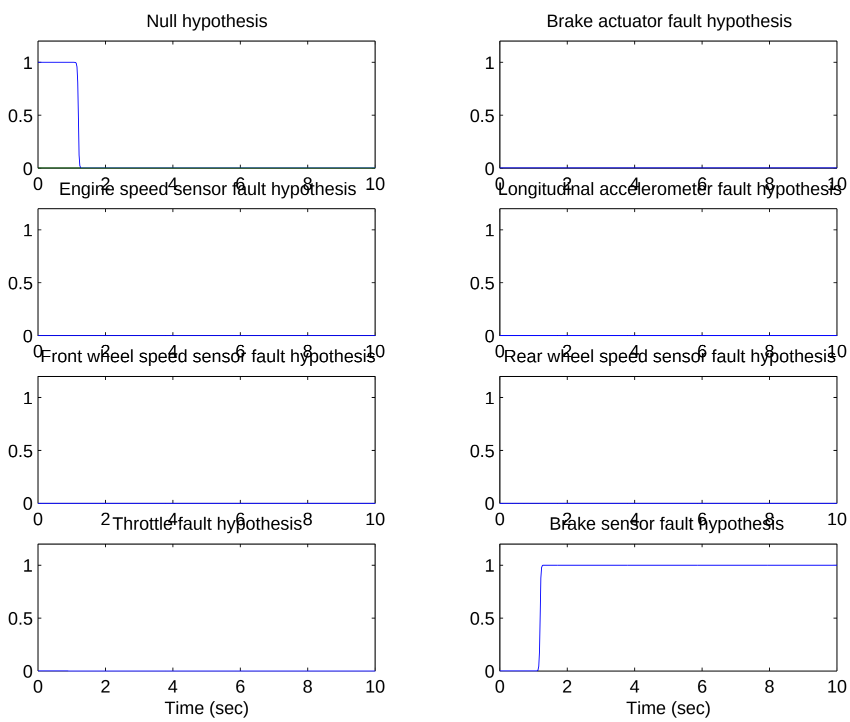

Figure 11.57: Brake sensor fault occurs

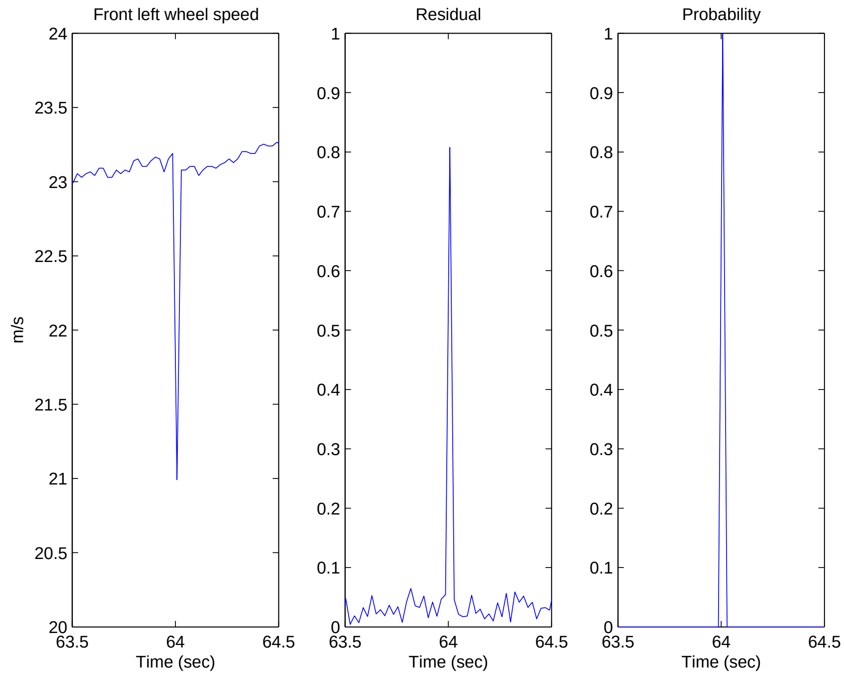

Figure 11.58: Residual generator and processor: wheel speed sensor

11.7 Evaluation Scenario No. 3: Real Actuator Fault

In this section, the vehicle health monitoring system is evaluated in real-time on a PATH Buick LeSabre at Crow's Landing when the vehicle is traveling on the magnetic curve track at constant speed. A real steering actuator fault is created by manually turning the steering wheel by the driver when the vehicle is under automatic control. Similarly, a real brake actuator fault is created by stepping on the brake padel by the driver when the vehicle is under automatic control.

Figure 11.59 shows the vehicle speed and the steering angle. The vehicle is first driven to 20 m/s on the magnetic curve track then the driver created the steering actuator fault by turning the steering wheel manually when the vehicle is still under automatic control. The vehicle is deviated from the original maneuver by this interruption and the experiment is terminated shortly after this action for safety concern. Figure 11.60 shows the performance of the residual generator designed for the vehicle lateral dynamics when the steering actuator fault is created between the 3rd and the fourth second. The first row is the residuals of fault detection filter set no. 4, the second row is the residuals of fault detection filter set no. 5, the third row is the residuals of fault detection filter set no. 6. Figure 11.61 shows that the probability of steering actuator fault goes from zero to one almost immediately after the fault is created. This experiment demonstrates that steering

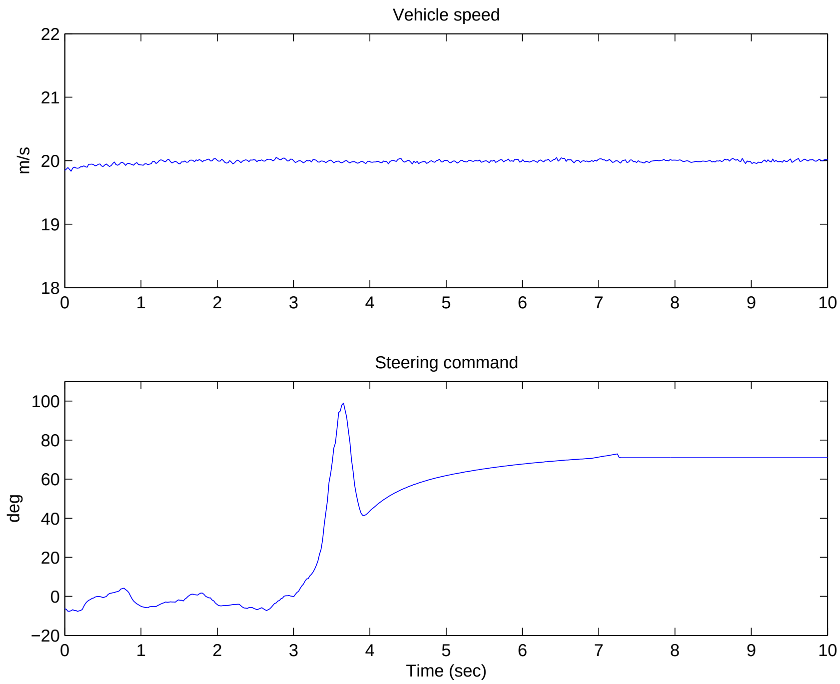

Figure 11.59: Vehicle speed and steering angle

actuator fault can be detected and identified with probability by the health monitoring system. The residual generator and processor designed for the vehicle lateral dynamics are not shown here because they will not respond to this fault.

Figure 11.62 shows the vehicle speed and the throttle command. The vehicle is first driven to 24 m/s on the magnetic curve track then the driver created the brake actuator fault by stepping on the brake padel manually when the vehicle is still under automatic control. From the second row of Figure 11.62, it is shown that the vehicle controller tried to compensate this fault by increasing the throttle angle in order to keep the desired vehicle speed. Figure 11.63 shows the performance of the residual generator designed for the vehicle longitudinal dynamics when the brake actuator fault is created around 23rd second. The first row is the residuals of fault detection filter set no. 1', the second row is the residuals of fault detection filter set no. 2, the third row is the residuals of fault detection filter set no. 3'. Figure 11.64 shows that the probability of brake actuator fault goes from zero to one almost immediately after the fault is created. This experiment demonstrates that brake actuator fault can be detected and identified with probability by the health monitoring system. The residual generator and processor designed for the vehicle lateral dynamics are not shown here because they will not respond to this fault.

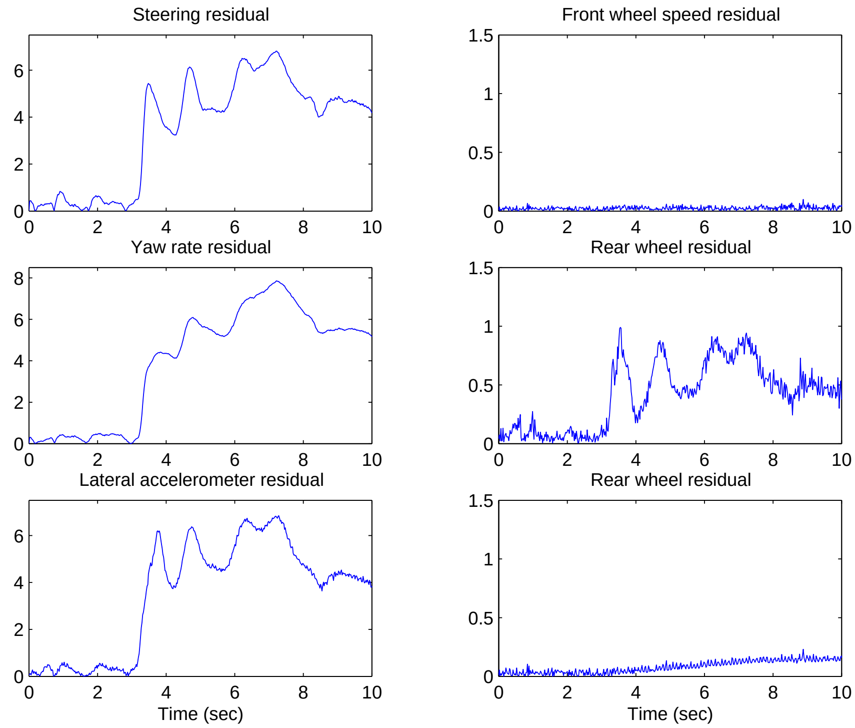

Figure 11.60: Steering actuator fault occurs

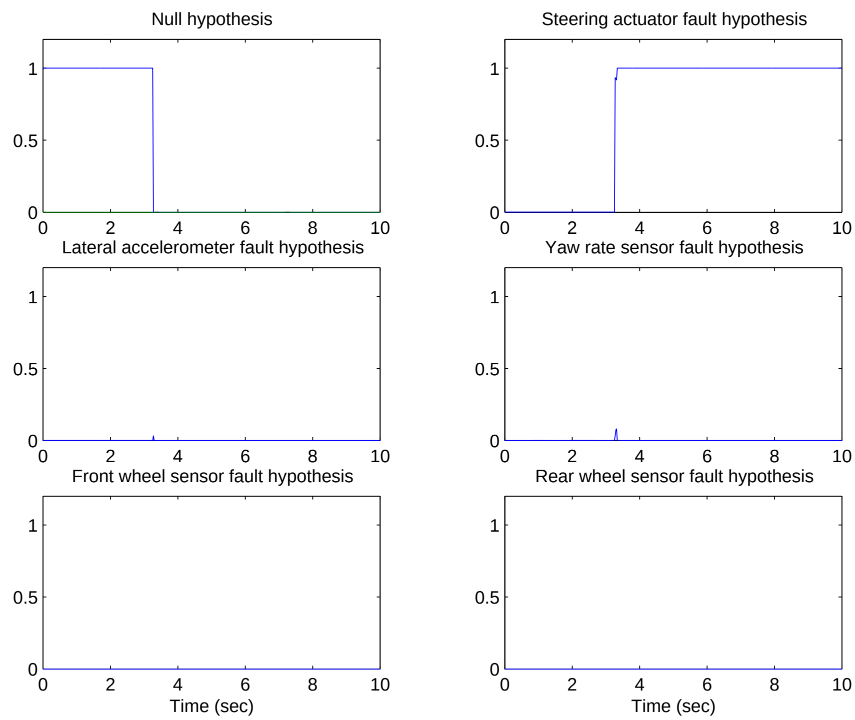

Figure 11.61: Steering actuator fault occurs

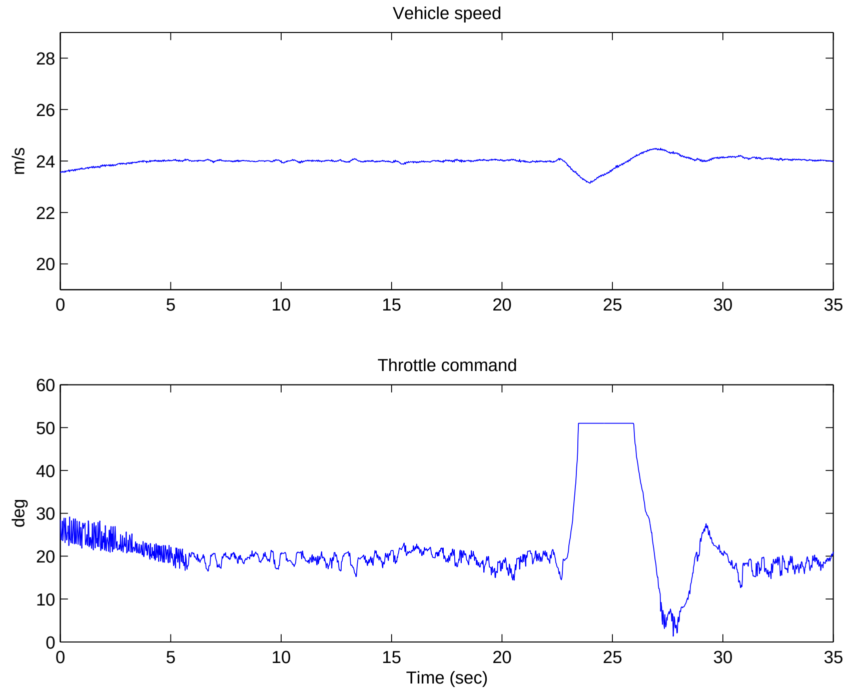

Figure 11.62: Vehicle speed and throttle commands

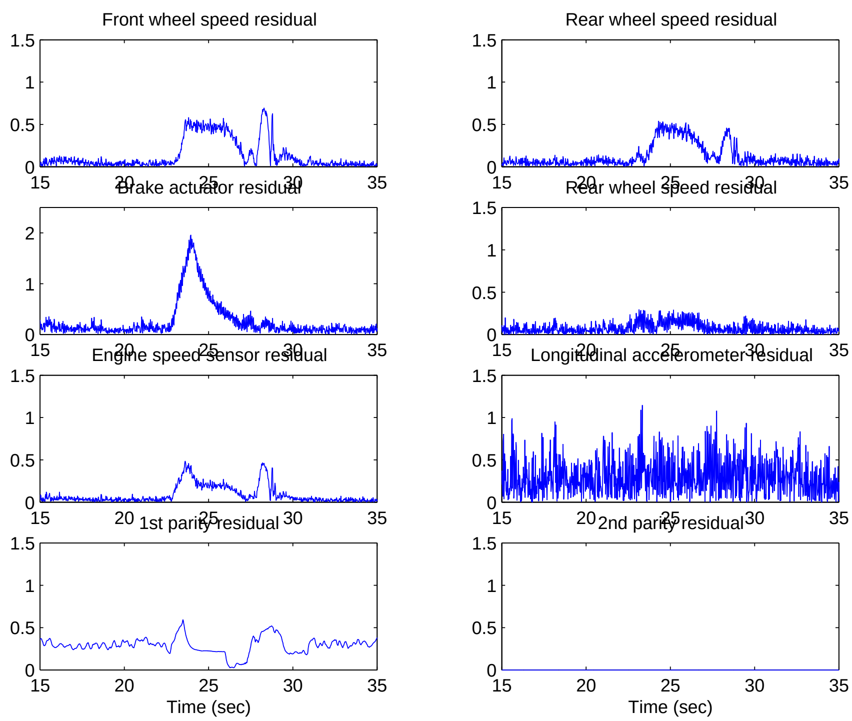

Figure 11.63: Brake actuator fault occurs

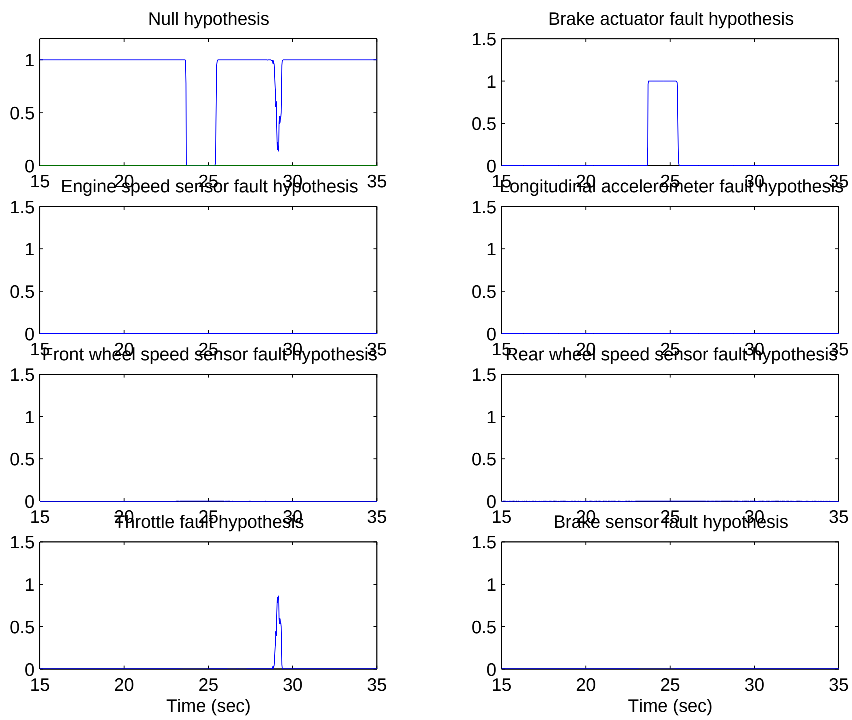

Figure 11.64: Brake actuator fault occurs

Chapter 12

Optimal Stochastic Fault Detection Filter

N THIS CHAPTER, a design algorithm, called optimal stochastic fault detection filter, is determined for the unknown input observer. The objective of the filter is to monitor a single fault, called the target fault, and block other faults, called the nuisance faults, in the presence of the process and sensor noises. The filter is derived by maximizing the transmission from the target fault while minimizing the transmission from the nuisance faults. The transmission is defined on the projected output error by using a matrix projector to be derived from solving the optimization problem. Therefore, the residual is affected primarily by the target fault and minimally by the nuisance faults. The transmission from the process and sensor noises is also minimized so that the filter is robust with respect to these disturbances. Since certain types of model uncertainties can be modeled as additive noises (Patton and Chen, 1992; Douglas *et al.*, 2004), the filter can also be made robust to these model uncertainties. A related approach can be found in (Lee, 1994; Brinsmead *et al.*, 1997).

In the limit where the weighting on the nuisance fault transmission goes to infinity, the filter blocks the nuisance faults completely. It is shown that the filter places the nuisance faults into a minimal (C, A)-unobservability subspace for time-invariant systems and a similar invariant subspace for time-varying systems. A minimal (C, A)-unobservability subspace implies that there is a projector $\tilde{H}$ induced from the nuisance fault directions such that $(\tilde{H}C, A - LC)$ has an unobservable subspace where L is the filter gain (Massoumnia, 1986; Massoumnia *et al.*, 1989). Therefore, the filter recovers the geometric structure of the unknown input observer in the limit and extends the unknown input observer to the time-varying case. These limiting results are important in ensuring that both fault detection and identification can occur. For time-invariant systems, the nuisance fault directions are generalized to prevent the invariant zeros of the nuisance faults or their mirror images from becoming part of the eigenvalues of the filter.

The limiting behavior of the filter can also be determined by using a perturbation method. Further, the perturbation method captures the asymptotic behavior of the filter near the limit. In (Chung and Speyer, 1998; Chen and Speyer, 2000), the Goh transformation in singular optimal control theory (Bell and Jacobson, 1975; Moylan and Moore, 1971) is used to determine the filter in the limit. However, the Goh transformation cannot determine the asymptotic behavior of the filter. Although the Goh transformation leads to an elegant general form, the perturbation method is more direct and insightful. The asymptotic result also provides a more robust numerical algorithm to solve the Riccati equation near the limit which is ill-conditioned because of the large parameters.

In Section 12.1, the system model and three essential assumptions about the system are given. The problem is formulated in Section 12.2 and its solution is derived in Section 12.3. In Section 12.4, the limiting properties of the filter are determined. In Section 12.5, the asymptotic behavior of the filter is determined. In Section 12.6, numerical examples are given.

12.1 System Model and Assumptions

In this section, the system model and three assumptions about the system that are needed in order to have a well-conditioned unknown input observer are given. Consider a linear system,

$$\dot{x} = Ax + B_u u \tag{12.1a}$$

$$y = Cx \tag{12.1b}$$

where u is the control input and y is the measurement. All system variables belong to real vector spaces, $x \in \mathcal{X}$, $u \in \mathcal{U}$ and $y \in \mathcal{Y}$. System matrices A, B_u and C can be time-varying. To design any linear observer, Assumption 12.1 is required (Kwakernaak and Sivan, 1972a).

Assumption 12.1. For time-varying systems, (C, A) is uniformly observable. For time-invariant systems, (C, A) is detectable.

Following the development in (Beard, 1971; White and Speyer, 1987; Chung and Speyer, 1998), any plant, actuator and sensor fault can be modeled as an additive term in the state equation

(12.1a). Therefore, a linear system with q failure modes can be modeled by

$$\dot{x} = Ax + B_u u + \sum_{i=1}^{q} \bar{F}_i \bar{\mu}_i \tag{12.2a}$$

$$y = Cx \tag{12.2b}$$

where $\bar{\mu}_i$ belong to real vector spaces and $\bar{F}_i$ can be time-varying. The failure modes $\bar{\mu}_i$ are unknown and arbitrary functions of time that are zero when there is no failure. The failure signatures $\bar{F}_i$ are maps that are known. A failure mode $\bar{\mu}_i$ models the time-varying amplitude of a failure while a failure signature $\bar{F}_i$ models the directional characteristics of a failure. Assume the $\bar{F}_i$ are monic so that $\bar{\mu}_i \neq 0$ imply $\bar{F}_i \bar{\mu}_i \neq 0$. Since the unknown input observer is designed to detect only one fault and block other faults, let $\mu_1 = \bar{\mu}_i$ be the target fault and $\mu_2 = [\, \bar{\mu}_1^T \; \cdots \; \bar{\mu}_{i-1}^T \;\; \bar{\mu}_{i+1}^T \; \cdots \; \bar{\mu}_q^T \,]^T$ be the nuisance fault. Then, (12.2) can be rewritten as (Massoumnia *et al.*, 1989)

$$\dot{x} = Ax + B_u u + F_1 \mu_1 + F_2 \mu_2 \tag{12.3a}$$

$$y = Cx \tag{12.3b}$$

where $F_1 = \bar{F}_i$ and $F_2 = [\, \bar{F}_1 \; \cdots \; \bar{F}_{i-1} \;\; \bar{F}_{i+1} \; \cdots \; \bar{F}_q \,]$. There are two assumptions about the system (12.3) that are needed in order to have a well-conditioned unknown input observer.

Assumption 12.2. F_1 and F_2 are output separable.

Assumption 12.2 ensures that the unknown input observer can isolate the target fault from the nuisance fault (Massoumnia *et al.*, 1989; Chung and Speyer, 1998). The definition of the output separability is $C\mathcal{T}_1 \cap C\mathcal{T}_2 = \emptyset$ where $\mathcal{T}_1$ and $\mathcal{T}_2$ are the invariant subspaces in which the target fault and nuisance fault are placed, respectively. More details about these invariant subspaces are given in Section 12.4.1. In Remark 6 of Section 12.4.3, the output separability assumption is relaxed by imposing a less restrictive condition since the optimal stochastic fault detection filter only creates an invariant subspace for the nuisance fault, but not the target fault.

Assumption 12.3. For time-invariant systems, (C, A, F_1) does not have invariant zeros at origin.

Assumption 12.3 ensures that, for time-invariant systems, the residual is nonzero in steady state when the target fault occurs. Consider a linear observer with dynamics and residual,

$$\dot{\hat{x}} = A\hat{x} + B_u u + L(y - C\hat{x})$$

$$r = y - C\hat{x}$$

When the target fault occurs, the dynamic equation of the error, $e = x - \hat{x}$, and the residual can be written as

$$\dot{e} = (A - LC)e + F_1\mu_1$$
$$r = Ce$$

For a bias target fault, the steady-state residual will be zero if $(C, A - LC, F_1)$ has an invariant zero at origin (Chen, 1984). Since the filter gain L does not change the invariant zero, $(C, A - LC, F_1)$ has an invariant zero at origin if and only if (C, A, F_1) has an invariant zero at origin. Therefore, to ensure a nonzero residual in steady state when the target fault occurs, (C, A, F_1) cannot have invariant zeros at origin.

12.2 Problem Formulation

In this section, the optimal stochastic fault detection filter problem is formulated. Consider a linear system similar to (12.3),

$$\dot{x} = Ax + B_u u + B_w w + F_1\mu_1 + F_2\mu_2 \tag{12.4a}$$
$$y = Cx + v \tag{12.4b}$$

where w is the process noise, v is the sensor noise, and B_w can be time-varying. Assume that the unknown and arbitrary failure amplitudes μ_1, μ_2, and the disturbances w, v are zero mean, white Gaussian noises with variances

$$\mathrm{E}\left[\mu_1(t)\mu_1(\tau)^T\right] = Q_1\delta(t - \tau) \tag{12.5a}$$
$$\mathrm{E}\left[\mu_2(t)\mu_2(\tau)^T\right] = Q_2\delta(t - \tau) \tag{12.5b}$$
$$\mathrm{E}\left[w(t)w(\tau)^T\right] = Q_w\delta(t - \tau) \tag{12.5c}$$
$$\mathrm{E}\left[v(t)v(\tau)^T\right] = V\delta(t - \tau) \tag{12.5d}$$

and the initial state is a random vector with variance

$$\mathrm{E}\left[x(t_0)x(t_0)^T\right] = P_0 \tag{12.5e}$$

where E[•] is the expectation operator. μ_1, μ_2, w and v are assumed to be uncorrelated with each other and with $x(t_0)$.

The objective of the optimal stochastic fault detection filter problem is to find a filter gain L for the linear observer,

$$\dot{\hat{x}} = A\hat{x} + B_u u + L(y - C\hat{x}) \quad , \quad \hat{x}(t_0) = \mathrm{E}[x(t_0)] \tag{12.6}$$

and a projector $\hat{H}$ for the residual,

$$r = \hat{H}(y - C\hat{x}) \tag{12.7}$$

such that the residual is affected primarily by the target fault μ_1 and minimally by the nuisance fault μ_2, process noise w, sensor noise v and initial condition error $x(t_0) - \hat{x}(t_0)$. By using (12.4) and (12.6), the dynamic equation of the error, $e = x - \hat{x}$, is

$$\dot{e} = (A - LC)e + F_1\mu_1 + F_2\mu_2 + B_w w - Lv$$

Then, the error can be written as

$$e(t) = \Phi(t, t_0)e(t_0) + \int_{t_0}^{t} \Phi(t, \tau)(F_1\mu_1 + F_2\mu_2 + B_w w - Lv)d\tau \tag{12.8}$$

subject to

$$\frac{d}{dt}\Phi(t, t_0) = (A - LC)\Phi(t, t_0) \quad , \quad \Phi(t_0, t_0) = I \tag{12.9}$$

Note that $e(t_0)$ is a zero mean random vector with variance P_0. The residual (12.7) can be written as

$$r = \hat{H}(Ce + v)$$

Now a cost criterion is needed for deriving L and $\hat{H}$. If the cost criterion is associated with the residual, it is unusable from the statistical viewpoint since the variance of the residual generates a δ-function due to the sensor noise. Therefore, the cost criterion will be associated with the projected output error $\hat{H}Ce$. In order to determine the cost criterion, define

$$h_1(t) \triangleq \hat{H}C \int_{t_0}^{t} \Phi(t, \tau)F_1\mu_1 d\tau \tag{12.10a}$$

$$h_2(t) \triangleq \hat{H}C \int_{t_0}^{t} \Phi(t, \tau)F_2\mu_2 d\tau \tag{12.10b}$$

$$h_v(t) \triangleq \hat{H}C \left[\Phi(t, t_0)e(t_0) + \int_{t_0}^{t} \Phi(t, \tau)(B_w w - Lv)d\tau\right] \tag{12.10c}$$

From (12.8), h_1 represents the transmission from μ_1 to $\hat{H}Ce$. h_2 represents the transmission from μ_2 to $\hat{H}Ce$. h_v represents the transmission from w, v and $e(t_0)$ to $\hat{H}Ce$. The objective of the optimal stochastic fault detection filter problem is to make $\hat{H}Ce$ sensitive to μ_1, but insensitive to μ_2, w, v and $e(t_0)$. Thus, h_2 and h_v are to be minimized while h_1 is to be maximized.

Therefore, the optimal stochastic fault detection filter problem is to find the filter gain L and the projector $\hat{H}$ which minimize the cost criterion,

$$J = \mathrm{tr}\left\{\frac{1}{\gamma}\mathrm{E}[h_2(t)h_2(t)^T] + \mathrm{E}[h_v(t)h_v(t)^T] - \mathrm{E}[h_1(t)h_1(t)^T]\right\} \tag{12.11}$$

where t is the current time and γ is a positive scalar. Making γ small places a large weighting on reducing the nuisance fault transmission. The trace operator forms a scalar cost criterion of the matrix output error variance. Note that the power spectral densities Q_1 and Q_2 can be considered as design parameters. Since no assumption is made on the failure amplitudes, its white noise representation is a convenience. However, the power spectral densities Q_w and V and the variance P_0 can have physical values. Q_1 and Q_w are non-negative definite. Q_2, V and P_0 are positive definite. When Q_1 increases, the transmission from the target fault increases. When Q_2 increases, the transmission from the nuisance fault reduces. When Q_w, V and P_0 increase, the transmission from the process noise, sensor noise and initial condition error reduces, respectively.

Since the effect of the process and sensor noises on the residual is explicitly minimized, the filter is robust with respect to these disturbances. Certain types of model uncertainties can also be modeled as additive noises (Patton and Chen, 1992; Douglas *et al.*, 2004). Therefore, the filter can be made robust to these model uncertainties. In Section 12.4, it is shown that the filter recovers the geometric structure of the unknown input observer in the limit as $\gamma \to 0$ and the nuisance fault is completely blocked. When it is not in the limit, the filter is an approximate unknown input observer and the nuisance fault is partially blocked. Since the filter does not need to block the nuisance fault completely, the filter structure is less constrained which leads to a potentially more robust unknown input observer.

12.3 Solution

In this section, the minimization problem given by (12.11) is solved. By using (12.5) and (12.10), the cost criterion, rewritten as

$$\begin{aligned} J = \mathrm{tr}\Big[&\hat{H}C\int_{t_0}^{t}\Phi(t,\tau)\left(LVL^T + \frac{1}{\gamma}F_2Q_2F_2^T - F_1Q_1F_1^T + B_wQ_wB_w^T\right)\Phi(t,\tau)^T d\tau\, C^T\hat{H} \\ &+\hat{H}C\Phi(t,t_0)P_0\Phi(t,t_0)^T C^T\hat{H}\Big] \end{aligned}$$

is to be minimized with respect to L and $\hat{H}$ subject to (12.9) and that $\hat{H}$ is a projector. To put the minimization problem in a more transparent context, J is manipulated in the following. By adding the zero term

$$\begin{aligned}\operatorname{tr}\Big\{&\hat{H}C\Phi(t,t)P(t)\Phi(t,t)^TC^T\hat{H} - \hat{H}C\Phi(t,t_0)P(t_0)\Phi(t,t_0)^TC^T\hat{H}\\ &-\hat{H}C\int_{t_0}^{t}\frac{d}{d\tau}\left[\Phi(t,\tau)P(\tau)\Phi(t,\tau)\right]d\tau\, C^T\hat{H}\Big\}\end{aligned}$$

to J and using (12.9),

$$\begin{aligned}J = \operatorname{tr}\Big\{&\hat{H}C\int_{t_0}^{t}\Phi(t,\tau)\Big[(L-PC^TV^{-1})V(L-PC^TV^{-1})^T - \dot{P} + AP + PA^T - PC^TV^{-1}CP\\ &+\frac{1}{\gamma}F_2Q_2F_2^T - F_1Q_1F_1^T + B_wQ_wB_w^T\Big]\Phi(t,\tau)^Td\tau\, C^T\hat{H}\\ &+\hat{H}C\Phi(t,t_0)[P_0 - P(t_0)]\Phi(t,t_0)^TC^T\hat{H} + \hat{H}CP(t)C^T\hat{H}\Big\}\end{aligned}$$

Then, the minimization problem can be rewritten as

$$\min_{L,\hat{H}}\operatorname{tr}\left[\hat{H}C\int_{t_0}^{t}\Phi(t,\tau)(L-PC^TV^{-1})V(L-PC^TV^{-1})^T\Phi(t,\tau)^Td\tau\, C^T\hat{H} + \hat{H}CP(t)C^T\hat{H}\right] \tag{12.12}$$

subject to (12.9) and that $\hat{H}$ is a projector where

$$\dot{P} = AP + PA^T - PC^TV^{-1}CP + \frac{1}{\gamma}F_2Q_2F_2^T - F_1Q_1F_1^T + B_wQ_wB_w^T\ ,\quad P(t_0) = P_0 \tag{12.13}$$

By inspection, the optimal filter gain is

$$L^* = PC^TV^{-1} \tag{12.14}$$

By applying (12.14) to (12.12), the minimization problem reduces to

$$\min_{\hat{H}}\operatorname{tr}[\hat{H}CP(t)C^T\hat{H}]$$

subject to that $\hat{H}$ is a projector. This is an eigenvalue problem. The solution for the optimal $\hat{H}$ depends on the rank of $\hat{H}$. If the rank is chosen as one, the optimal projector is

$$\hat{H}^* = \rho_m\rho_m^T \tag{12.15}$$

where ρ_m is the eigenvector of $CP(t)C^T$ associated with the smallest eigenvalue λ_m and $m = \dim\mathcal{Y}$. The minimal cost associated with (12.15) is λ_m. Alternately, (12.15) can be written as

$$\hat{H}^* : \mathcal{Y}\to\mathcal{Y},\ \operatorname{Ker}\hat{H}^* = \operatorname{Im}\begin{bmatrix}\rho_1 & \cdots & \rho_{m-1}\end{bmatrix},\ \hat{H}^* = I - \begin{bmatrix}\rho_1 & \cdots & \rho_{m-1}\end{bmatrix}\begin{bmatrix}\rho_1 & \cdots & \rho_{m-1}\end{bmatrix}^T \tag{12.16}$$

where ρ_i, $i = 1 \cdots m-1$, are the eigenvectors of $CP(t)C^T$ and their associated eigenvalues $\lambda_1 \geq \lambda_2 \geq \cdots \geq \lambda_{m-1}$.

In Sections 12.4 and 12.5, it is shown that $CP(t)C^T$ has p_2 infinite eigenvalues in the limit as $\gamma \to 0$ and p_2 large eigenvalues near the limit when γ is small where $p_2 = \dim F_2$. Since the remaining $m - p_2$ eigenvalues are very small compared to the p_2 large eigenvalues, the rank of $\hat{H}$ can be chosen as $m - p_2$ and the optimal projector is

$$\hat{H}^* = \begin{bmatrix} \rho_m & \rho_{m-1} & \cdots & \rho_{p_2+1} \end{bmatrix} \begin{bmatrix} \rho_m & \rho_{m-1} & \cdots & \rho_{p_2+1} \end{bmatrix}^T \tag{12.17}$$

The minimal cost associated with (12.17) is $\sum_{i=p_2+1}^{m} \lambda_i$. Alternately, (12.17) can be written as

$$\hat{H}^* : \mathcal{Y} \to \mathcal{Y},\ \operatorname{Ker} \hat{H}^* = \operatorname{Im} \begin{bmatrix} \rho_1 & \cdots & \rho_{p_2} \end{bmatrix},\ \hat{H}^* = I - \begin{bmatrix} \rho_1 & \cdots & \rho_{p_2} \end{bmatrix} \begin{bmatrix} \rho_1 & \cdots & \rho_{p_2} \end{bmatrix}^T \tag{12.18}$$

Note that both (12.16) and (12.18) are optimal projectors depending on the rank chosen. In Sections 12.4 and 12.5, it is shown that $\operatorname{Im}[\,\rho_1 \cdots \rho_{p_2}\,]$ contains the nuisance fault completely in the limit and partially near the limit. Thus, $\operatorname{Ker} \hat{H}^*$ only needs to contain $\operatorname{Im}[\,\rho_1 \cdots \rho_{p_2}\,]$ in order to block the nuisance fault. Furthermore, (12.18) allows more or equal target fault transmission than (12.16) because $\operatorname{Im}[\,\rho_1 \cdots \rho_{p_2}\,] \subseteq \operatorname{Im}[\,\rho_1 \cdots \rho_{m-1}\,]$. Therefore, (12.18) is a better choice than (12.16). In Section 12.4, it is shown that (12.18) becomes equivalent to the projector used by the unknown input observer in the limit.

Remark 1. For implementation of the optimal stochastic fault detection filter, the filter gain (12.14) and the projector (12.18) have to be constructed continuously with respect to time because in the cost criterion, t is the current time.

Remark 2. The properties of the Riccati equation (12.13) are best established within the linear quadratic regulator problem (Speyer, 1986) which can be viewed as a dual problem of the optimal stochastic fault detection filter problem. Consider the following linear quadratic regulator problem,

$$\min_u J = \min_u \frac{1}{2} \int_{-t}^{-t_0} \Big(\| x(s) \|^2_{\frac{1}{\gamma} F_2(-s) Q_2(-s) F_2(-s)^T - F_1(-s) Q_1(-s) F_1(-s)^T + B_w(-s) Q_w(-s) B_w(-s)^T} + \| u(s) \|^2_{V(-s)} \Big) ds + \frac{1}{2} \| x(-t_0) \|^2_{P_0}$$

subject to

$$\dot{x}(s) = A(-s)^T x(s) + C(-s)^T u(s)$$

The solution is

$$u(s)^* = -V(-s)^{-1}C(-s)\bar{P}(s)x(s)$$

where

$$-\dot{\bar{P}}(s) = A(-s)\bar{P}(s)+\bar{P}(s)A(-s)^T - \bar{P}(s)C(-s)^T V(-s)^{-1}C(-s)\bar{P}(s)+\frac{1}{\gamma}F_2(-s)Q_2(-s)F_2(-s)^T$$
$$- F_1(-s)Q_1(-s)F_1(-s)^T + B_w(-s)Q_w(-s)B_w(-s)^T \tag{12.19}$$

and $\bar{P}(-t_0) = P_0$. The minimal cost is

$$J^* = \frac{1}{2} \parallel x(-t) \parallel^2_{\bar{P}(-t)}$$

Since (A^T, C^T) is controllable, $\bar{P}(-t)$ is bounded from above. Therefore, if $\bar{P}(-t)$ has a finite escape time, $\bar{P}(-t)$ goes to $-\infty$ when Q_1 is too large.

Let $\tau = -s$, (12.19) becomes

$$\dot{\bar{P}}(-\tau) = A(\tau)\bar{P}(-\tau) + \bar{P}(-\tau)A(\tau)^T - \bar{P}(-\tau)C(\tau)^T V(\tau)^{-1}C(\tau)\bar{P}(-\tau)$$
$$+ \frac{1}{\gamma}F_2(\tau)Q_2(\tau)F_2(\tau)^T - F_1(\tau)Q_1(\tau)F_1(\tau)^T \tag{12.20}$$

By comparing (12.13) and (12.20),

$$P(\tau) = \bar{P}(-\tau)$$

Then, $P(t) = \bar{P}(-t)$ has a finite escape time and goes to $-\infty$ when Q_1 is too large. This can be interpreted as an attempt to make the residual sensitive to the target fault. If Q_1 is too large, the target fault could destabilize the filter. Therefore, Q_1 has to be chosen small enough to avoid the finite escape time. Note that $P(t)$ does not have a finite escape time when $Q_1 = 0$. This will be illustrated by the numerical example in Section 12.6.4. ◀

12.4 Limiting Case

In this section, the limiting properties of the optimal stochastic fault detection filter are determined when $\gamma \to 0$. It is shown that the nuisance fault is placed in an invariant subspace in the limit. For time-invariant systems, this invariant subspace is equivalent to the minimal (C, A)-unobservability subspace of F_2. Therefore, the filter becomes equivalent to the unknown input observer in the limit. For time-varying systems, there exists a similar invariant subspace. Therefore, the filter extends the unknown input observer to the time-varying case. In Section 12.4.1, the geometric structure of the unknown input observer is given (Massoumnia *et al.*, 1989). In Section 12.4.2, the limiting properties of the filter are determined. In Section 12.4.3, the nuisance fault directions are generalized for time-invariant systems to prevent the invariant zeros of the nuisance fault or their mirror images from becoming part of the eigenvalues of the filter.

12.4.1 Geometric Structure of Unknown Input Observer

The unknown input observer places the nuisance fault into an invariant subspace which is unobservable to the residual (Massoumnia *et al.*, 1989). This invariant subspace, denoted $\mathcal{T}_2$, is the minimal (C, A)-unobservability subspace of F_2 which can be obtained by (Wonham, 1985)

$$\mathcal{T}_2 = \mathcal{W}_2 \oplus \mathcal{V}_2 \tag{12.21}$$

$\mathcal{W}_2$ is the minimal (C, A)-invariant subspace of F_2 given by (Chung and Speyer, 1998)

$$\mathcal{W}_2 = \left[\begin{array}{ccccccccccccc} f_1 & Af_1 & \cdots & A^{\delta_1} f_1 & f_2 & Af_2 & \cdots & A^{\delta_2} f_2 & \cdots & f_{p_2} & Af_{p_2} & \cdots & A^{\delta_{p2}} f_{p_2} \end{array}\right] \tag{12.22}$$

where f_i is the i-th column of F_2 and δ_i is the smallest non-negative integer such that $CA^{\delta_i} f_i \neq 0$. $\mathcal{V}_2$ is the subspace spanned by the invariant zero directions of (C, A, F_2). Note that $\mathcal{T}_2$ is the unobservable subspace of $(\tilde{H}C, A - LC)$ (Massoumnia, 1986; Massoumnia *et al.*, 1989) where L is the filter gain and

$$\tilde{H} : \mathcal{Y} \to \mathcal{Y} \ , \ \ \operatorname{Ker} \tilde{H} = \operatorname{Im} \left[\begin{array}{cccc} CA^{\delta_1} f_1 & CA^{\delta_2} f_2 & \cdots & CA^{\delta_{p2}} f_{p_2} \end{array}\right] \tag{12.23}$$

Therefore, the nuisance fault is unobservable to the residual using $\tilde{H}$ as the projector. To ensure that the target fault can be detected from the residual, F_1 and F_2 are required to be output separable (Massoumnia *et al.*, 1989) which is defined by

$$C\mathcal{T}_1 \cap C\mathcal{T}_2 = \emptyset \Leftrightarrow C\mathcal{W}_1 \cap C\mathcal{W}_2 = \emptyset$$

where $\mathcal{T}_1$ is the minimal (C, A)-unobservability subspace of F_1 and $\mathcal{W}_1$ is the minimal (C, A)-invariant subspace of F_1. Note that the output separability condition is a sufficient condition since the unknown input observer does not need to place the target fault into an invariant subspace. In Remark 6 of Section 12.4.3, the output separability condition is relaxed by imposing a less restrictive condition.

For time-varying systems, the minimal (C, A)-invariant subspace of F_2 is (Chung and Speyer, 1998)

$$\mathcal{W}_2 = \left[\begin{array}{cccccccccccccc} b_{1,0} & b_{1,1} & \cdots & b_{1,\delta_1} & b_{2,0} & b_{2,1} & \cdots & b_{2,\delta_2} & \cdots & b_{p_2,0} & b_{p_2,1} & \cdots & b_{p_2,\delta_{p_2}} \end{array} \right] \tag{12.24}$$

The vectors $b_{i,j}$, $j = 0 \cdots \delta_i$, are obtained from the iteration defined by the Goh transformation (Bell and Jacobson, 1975; Moylan and Moore, 1971),

$$\begin{aligned} b_{i,0} &= f_i \\ b_{i,j} &= Ab_{i,j-1} - \dot{b}_{i,j-1} \end{aligned}$$

where f_i is the i-th column of F_2. δ_i is the smallest non-negative integer such that $Cb_{i,\delta_i} \neq 0$ for $t \in [t_0, t_1]$. For time-varying systems, the minimal (C, A)-unobservability subspace cannot be obtained by (12.21) because the concept of invariant zero is for time-invariant systems only. The time-varying extension of (12.23) is (Chung and Speyer, 1998)

$$\tilde{H} : \mathcal{Y} \rightarrow \mathcal{Y} \ , \ \ \text{Ker}\, \tilde{H} = \text{Im} \left[\begin{array}{cccc} Cb_{1,\delta_1} & Cb_{2,\delta_2} & \cdots & Cb_{p_2,\delta_{p_2}} \end{array} \right] \tag{12.25}$$

For time-varying systems, the output separability condition can be checked by (Chung and Speyer, 1998; Chen and Speyer, 2000)

$$C\mathcal{W}_1 \cap C\mathcal{W}_2 = \emptyset$$

Remark 3. (12.22) and (12.24) are based on the assumption that

$$\text{Rank}\,(C\mathcal{W}_2) = p_2 \tag{12.26}$$

where $p_2 = \dim F_2$. If Rank $(C\mathcal{W}_2) < p_2$, a new basis for F_2 with a lower or equal dimension can be formed such that (12.26) is satisfied (Chen, 2000). Then, the new basis of F_2 can be used in (12.22) or (12.24) and consequently in (12.23) or (12.25).

12.4.2 Limiting Property

In this section, it is assumed that the Riccati matrix P is positive definite. From Remark 2 in Section 12.3, there always exists positive definite P for some Q_1. Then, P can be written as

$$P = \sum_{i=1}^{n} \frac{1}{\bar{\lambda}_i} \bar{\rho}_i \bar{\rho}_i^T$$

where $\bar{\lambda}_i^{-1}$ is the i-th eigenvalue of P and $\bar{\rho}_i$ is the associated eigenvector. In the limit as $\gamma \to 0$, P goes to infinity because of the term $\frac{1}{\gamma}F_2Q_2F_2^T$ in (12.13). This implies that some $\bar{\lambda}_i$'s go to zero in the limit. Define

$$\Pi \stackrel{\triangle}{=} P^{-1} = \sum_{i=1}^{n} \bar{\lambda}_i \bar{\rho}_i \bar{\rho}_i^T$$

Then, P goes to infinity in the limit along the null space of Π. By using (12.13),

$$\begin{aligned}-\frac{d}{d\tau}(P^{-1}) &= P^{-1}\dot{P}P^{-1} \\ &= P^{-1}A + A^T P^{-1} - C^T V^{-1} C + P^{-1}\left(\frac{1}{\gamma}F_2Q_2F_2^T - F_1Q_1F_1^T + B_wQ_wB_w^T\right)P^{-1}\end{aligned}$$

Then,

$$-\dot{\Pi} = \Pi A + A^T\Pi + \Pi\left(\frac{1}{\gamma}F_2Q_2F_2^T - F_1Q_1F_1^T + B_wQ_wB_w^T\right)\Pi - C^T V^{-1} C \tag{12.27}$$

with initial condition $\Pi(t_0) = P_0^{-1}$. Define

$$\bar{\Pi} \stackrel{\triangle}{=} \lim_{\gamma \to 0} \Pi$$

In the limit, in order for (12.27) to have a solution,

$$\bar{\Pi} F_2 = 0 \tag{12.28}$$

This indicates that $\bar{\Pi}$ has a null space which contains F_2. It turns out that $\operatorname{Ker}\bar{\Pi}$ is the key to block the nuisance fault. Theorem 12.1 shows that $\operatorname{Ker}\bar{\Pi}$ is a (C, A)-invariant subspace. Therefore, the optimal stochastic fault detection filter places the nuisance fault into an invariant subspace in the limit.

Theorem 12.1. $\operatorname{Ker}\bar{\Pi}$ is a (C, A)-invariant subspace.

Proof. The filter can be written as

$$\Pi\dot{\hat{x}} = \Pi A\hat{x} + \Pi B u + C^T V^{-1}(y - C\hat{x})$$

When the nuisance fault occurs, the dynamic equation of the error can be written as

$$\Pi\dot{e} = (\Pi A - C^T V^{-1} C)e + \Pi F_2 \mu_2$$

By adding $\dot{\Pi}e$ to both sides and using (12.27),

$$\frac{d}{d\tau}(\Pi e) = -\left[A^T + \Pi\left(\frac{1}{\gamma}F_2Q_2F_2^T - F_1Q_1F_1^T + B_wQ_wB_w^T\right)\right]\Pi e + \Pi F_2\mu_2 \tag{12.29}$$

In the limit, if the error initially lies in $\operatorname{Ker}\bar{\Pi}$, (12.29) implies that the error will never leave $\operatorname{Ker}\bar{\Pi}$ because of (12.28). Therefore, $\operatorname{Ker}\bar{\Pi}$ is a (C, A)-invariant subspace.

Other directions in $\operatorname{Ker}\bar{\Pi}$ are obtained now. For time-invariant systems, $\operatorname{Ker}\bar{\Pi}$ is related to the minimal (C, A)-unobservability subspace of F_2. For time-varying systems, $\operatorname{Ker}\bar{\Pi}$ is related to the unobservable subspace of $(\tilde{H}C, A - LC)$ where L is (12.14) and $\tilde{H}$ is (12.25). Theorem 12.2 shows that $\operatorname{Ker}\bar{\Pi}$ contains the minimal (C, A)-invariant subspace of F_2.

Theorem 12.2. $\bar{\Pi}\mathcal{W}_2 = 0$ where $\mathcal{W}_2$ is (12.22) for time-invariant systems and (12.24) for time-varying systems.

Proof. Consider the time-varying case first. From (12.28), $\bar{\Pi}b_{1,0} = 0$ and

$$\frac{d}{d\tau}(\bar{\Pi}b_{1,0}) = \dot{\bar{\Pi}}b_{1,0} + \bar{\Pi}\dot{b}_{1,0} = 0 \tag{12.30}$$

In the limit, by multiplying (12.27) by $b_{1,0}^T$ from the left and $b_{1,0}$ from the right and using (12.28),

$$\frac{1}{\sqrt{\gamma}}F_2^T\bar{\Pi}b_{1,0} = 0 \tag{12.31}$$

By using (12.30), (12.27), (12.28) and (12.31),

$$\bar{\Pi}b_{1,1} = \bar{\Pi}(Ab_{1,0} - \dot{b}_{1,0}) = C^TV^{-1}Cb_{1,0} = 0$$

Similarly, it can be shown that

$$\frac{d}{d\tau}(\bar{\Pi}b_{1,1}) = 0 \Rightarrow \bar{\Pi}b_{1,2} = 0$$

By iterating this procedure, $\bar{\Pi}[\,b_{1,0}\;\; b_{1,1}\;\cdots\; b_{1,\delta_1}\,] = 0$. Similarly, it can be shown that $\bar{\Pi}[\,b_{i,0}\;\; b_{i,1}\;\cdots\; b_{i,\delta_i}\,] = 0$ for $i = 2\cdots p_2$. Therefore, $\bar{\Pi}\mathcal{W}_2 = 0$. For the time-invariant case, it can be shown similarly.

For time-invariant systems, whether $\operatorname{Ker}\bar{\Pi}$ contains the invariant zero directions of (C, A, F_2) is discussed now. By using the result in (Massoumnia, 1986; Massoumnia *et al.*, 1989), if $\operatorname{Ker}\bar{\Pi}$ does not contain the invariant zero directions, the invariant zeros will become part of the filter eigenvalues (i.e., the eigenvalues of $A - LC$). By using the result in (Kwakernaak, 1976), if there exist left-half plane invariant zeros, part of the filter eigenvalues will be at the invariant zeros in the limit. If there exist right-half plane invariant zeros, part of the filter eigenvalues will be at the mirror images of the invariant zeros in the limit. This implies that $\operatorname{Ker} \bar{\Pi}$ contains the invariant zero directions associated with the right-half plane invariant zeros, but not the invariant zero directions associated with the left-half plane invariant zeros. In Section 12.4.3, the nuisance fault directions are generalized so that $\operatorname{Ker} \bar{\Pi}$ contains all the invariant zero directions. Furthermore, this generalization prevents the invariant zeros or their mirror images from becoming part of the filter eigenvalues. This is important because the invariant zeros or their mirror images might be ill-conditioned even though stable.

For time-invariant systems, $\operatorname{Ker} \bar{\Pi} \supseteq \mathcal{W}_2$ from Theorem 12.2 and $\operatorname{Ker} \bar{\Pi} \supseteq \mathcal{V}_2$ from the generalization of the nuisance fault directions in Section 12.4.3. Then, $\operatorname{Ker} \bar{\Pi} \supseteq \mathcal{T}_2$. By using the result in (Chung and Speyer, 1998; Chen and Speyer, 2000), it can be shown that $\operatorname{Ker} \bar{\Pi} \subseteq \mathcal{T}_2$. Therefore, $\operatorname{Ker} \bar{\Pi}$ is equivalent to the minimal (C, A)-unobservability subspace of F_2 and the optimal stochastic fault detection filter becomes equivalent to the unknown input observer in the limit. For time-varying systems, $\operatorname{Ker} \bar{\Pi} \supseteq \mathcal{W}_2$ from Theorem 12.2. By using the result in (Chung and Speyer, 1998; Chen and Speyer, 2000), $\operatorname{Ker} \bar{\Pi}$ is contained in the unobservable subspace of $(\tilde{H}C, A - LC)$ where L is (12.14) and $\tilde{H}$ is (12.25). Therefore, the optimal stochastic fault detection filter places the nuisance fault into a similar invariant subspace in the limit and extends the unknown input observer to the time-varying case.

Remark 4. Since P goes to infinity in the limit along $\operatorname{Ker} \bar{\Pi}$, CPC^T goes to infinity along $C \operatorname{Ker} \bar{\Pi}$. For time-invariant systems,

$$C \operatorname{Ker} \bar{\Pi} = \operatorname{Im} \begin{bmatrix} CA^{\delta_1} f_1 & CA^{\delta_2} f_2 & \cdots & CA^{\delta_{p_2}} f_{p_2} \end{bmatrix}$$

because $\operatorname{Ker} \bar{\Pi} = \mathcal{T}_2$. For time-varying systems,

$$C \operatorname{Ker} \bar{\Pi} = \operatorname{Im} \begin{bmatrix} Cb_{1,\delta_1} & Cb_{2,\delta_2} & \cdots & Cb_{p_2,\delta_{p_2}} \end{bmatrix}$$

because $\operatorname{Ker} \bar{\Pi} \supseteq \mathcal{W}_2$ and $\operatorname{Ker} \bar{\Pi}$ is contained in the unobservable subspace of $(\tilde{H}C, A - LC)$ where L is (12.14) and $\tilde{H}$ is (12.25). Therefore, CPC^T has p_2 infinite eigenvalues in the limit because $\dim(C \operatorname{Ker} \bar{\Pi}) = p_2$. Further, the p_2 associated eigenvectors span $C \operatorname{Ker} \bar{\Pi}$. Therefore, the optimal projector (12.18) becomes equivalent to $\tilde{H}$ (12.23), used by the unknown input observer, in the limit for time-invariant systems. For time-varying systems, (12.18) becomes equivalent to $\tilde{H}$ (12.25). Note that the nuisance fault is contained in $C \operatorname{Ker} \bar{\Pi}$ in the output space $\mathcal{Y}$ in the limit because the nuisance fault is contained in $\operatorname{Ker} \bar{\Pi}$ in the state space $\mathcal{X}$.

Remark 5. By using the optimal filter gain (12.14) and the optimal projector (12.18), the minimization problem (12.11) can be written as

$$\frac{1}{\gamma} \operatorname{tr}\{\mathrm{E}[h_2(t)h_2(t)^T]\} + \operatorname{tr}\{\mathrm{E}[h_v(t)h_v(t)^T]\} - \operatorname{tr}\{\mathrm{E}[h_1(t)h_1(t)^T]\} = \sum_{i=p_2+1}^{m} \lambda_i$$

Then,

$$\frac{\operatorname{tr}\{\mathrm{E}[h_2(t)h_2(t)^T]\} + \gamma \operatorname{tr}\{\mathrm{E}[h_v(t)h_v(t)^T]\}}{\operatorname{tr}\{\mathrm{E}[h_1(t)h_1(t)^T]\}} = \gamma \left\{ 1 + \frac{\sum_{i=k_2+1}^{n} \lambda_i}{\operatorname{tr}\{\mathrm{E}[h_1(t)h_1(t)^T]\}} \right\}$$

In the limit as $\gamma \to 0$,

$$\frac{\operatorname{tr}\{\mathrm{E}[h_2(t)h_2(t)^T]\}}{\operatorname{tr}\{\mathrm{E}[h_1(t)h_1(t)^T]\}} \to 0$$

This implies that the nuisance fault transmission is zero in the limit.

12.4.3 Nuisance Fault Direction Generalization

The invariant zero of (C, A, F_2) is defined as z at which

$$\begin{bmatrix} zI - A & F_2 \\ C & 0 \end{bmatrix}$$

loses rank. The invariant zero direction ν is formed from a partitioning of the null space as

$$\begin{bmatrix} zI - A & F_2 \\ C & 0 \end{bmatrix} \begin{bmatrix} \nu \\ \bar{\nu} \end{bmatrix} = 0 \tag{12.32}$$

When f_i, a column vector of F_2, has a left-half plane invariant zero z_i and the invariant zero direction is called ν_i, $\operatorname{Ker} \bar{\Pi}$ contains $\operatorname{Im} [\, f_i \;\; Af_i \;\cdots\; A^{\delta_i} f_i \,]$, but not $\operatorname{Im} \nu_i$. Also, z_i becomes one of the filter eigenvalues in the limit. If the nuisance fault direction f_i is replaced by ν_i, z_i will not become one of the filter eigenvalues. Furthermore, since $\operatorname{Ker} \bar{\Pi}$ contains $\operatorname{Im} [\, \nu_i \;\; A\nu_i \;\cdots\; A^{\delta_i+1}\nu_i \,]$ which is equivalent to $\operatorname{Im}[\, f_i \;\; Af_i \;\cdots\; A^{\delta_i} f_i \;\; \nu_i \,]$ by (12.32), this generalization will still block the nuisance fault. Note that $\operatorname{Ker} \bar{\Pi}$ contains the invariant zero direction now. If the invariant zero is in the right-half plane, this generalization prevents the mirror image of the invariant zero from becoming one of the filter eigenvalues in the limit. If (C, A, ν_i) has invariant zeros, the same procedure can be repeated until there is no invariant zero. If the invariant zero is associated with not just one, but several column vectors of F_2, only one of these vectors needs to be replaced by the invariant zero direction. This will be demonstrated by the numerical example in Section 12.6.3.

Remark 6. In order to be able to detect the target fault, F_1 cannot intersect $\operatorname{Ker}\bar{\Pi}$ which is unobservable to the residual, i.e., $F_1 \cap \operatorname{Ker}\bar{\Pi} = \emptyset$. If it does, the target fault will be difficult or impossible to detect because it is blocked from the residual along with the nuisance fault even though the filter can still be derived by solving the minimization problem. This condition is less restrictive than the output separability condition, $C\mathcal{W}_1 \cap C\mathcal{W}_2 = \emptyset$, required by the unknown input observer (Massoumnia *et al.*, 1989; Chung and Speyer, 1998). For example, when $F_1 \cap \operatorname{Ker}\bar{\Pi} = \emptyset$, but $C\mathcal{W}_1 \cap C\mathcal{W}_2 \neq \emptyset$, the optimal stochastic fault detection filter may still be able to detect the target fault and block the nuisance fault since the filter only creates an invariant subspace for the nuisance fault, but not the target fault. ◀

12.5 Perturbation Analysis

In Section 12.4, the limiting properties of the Riccati matrices Π and P are determined. However, what Π and P are in the limit and how they behave near the limit are still unknown. In (Chung and Speyer, 1998; Chen and Speyer, 2000), the Goh transformation in singular optimal control theory (Bell and Jacobson, 1975; Moylan and Moore, 1971) is used to determine Π in the limit. However, the Goh transformation cannot determine Π near the limit. In this section, what Π and P are in the limit and near the limit is determined by using a perturbation method. The asymptotic expansions of Π and P are derived in which Π and P are explicitly expressed as functions of γ. This gives an understanding of the properties of Π and P when γ is small, but not zero which is the region where the filter design takes place. Although the Goh transformation leads to an elegant general form, the perturbation method is more direct and insightful. The asymptotic results also provide a more robust numerical algorithm to solve the Riccati equations near the limit which are ill-conditioned because of the large parameters. In Section 12.5.1, Π is expanded around $\gamma = 0$. This shows explicitly the characteristics of Π near and in the limit. In the limit, the result is consistent with the one in (Chung and Speyer, 1998; Chen and Speyer, 2000) derived by using the Goh transformation. In Section 12.5.2, the inverse of Π is derived. This shows explicitly the characteristics of P near and in the limit.

12.5.1 Expansion

In this section, Π is expanded around $\gamma = 0$ as

$$\Pi = \sum_{i=0}^{\infty} \gamma^{\frac{i}{4}} \Pi_i \tag{12.33}$$

By substituting (12.33) into (12.27) and collecting terms of common power, the equations used for solving (12.33) are obtained in Lemma 12.3.

Lemma 12.3.

$$\Pi = \left[\begin{array}{cc} u_1 & u_2 \end{array}\right] \left(\begin{bmatrix} 0 & 0 \\ 0 & \Pi_{022} \end{bmatrix} + \gamma^{\frac{1}{4}} \begin{bmatrix} 0 & 0 \\ 0 & \Pi_{122} \end{bmatrix} + \gamma^{\frac{1}{2}} \begin{bmatrix} \Pi_{211} & \Pi_{212} \\ \Pi_{212}^T & \Pi_{222} \end{bmatrix} + \gamma^{\frac{3}{4}} \begin{bmatrix} \Pi_{311} & \Pi_{312} \\ \Pi_{312}^T & \Pi_{322} \end{bmatrix} + \cdots \right) \begin{bmatrix} u_1^T \\ u_2^T \end{bmatrix}$$

where

$$F_2 Q_2 F_2^T = \left[\begin{array}{cc} u_1 & u_2 \end{array}\right] \begin{bmatrix} \sigma & 0 \\ 0 & 0 \end{bmatrix} \begin{bmatrix} u_1^T \\ u_2^T \end{bmatrix} = u_1 \sigma u_1^T$$

$\sigma > 0$ and $[\, u_1 \;\; u_2 \,]$ is unitary. Note that $\operatorname{Im} u_1 = \operatorname{Im} F_2$. Π_{022}, Π_{211} and Π_{212} require the solution to

$$0 = \Pi_{211} \sigma \Pi_{211} - R_{11} \tag{12.34a}$$

$$0 = \Pi_{211} \sigma \Pi_{212} + A_{21}^T \Pi_{022} - R_{12} \tag{12.34b}$$

$$-\dot{\Pi}_{022} = \Pi_{022} A_{22} + A_{22}^T \Pi_{022} - \Pi_{022} Q_{22} \Pi_{022} - R_{22} + \Pi_{212}^T \sigma \Pi_{212} \tag{12.34c}$$

Π_{122}, Π_{311} and Π_{312} require the solution to

$$0 = \Pi_{311} \sigma \Pi_{211} + \Pi_{211} \sigma \Pi_{311} \tag{12.35a}$$

$$0 = \Pi_{211} \sigma \Pi_{312} + A_{21}^T \Pi_{122} + \Pi_{311} \sigma \Pi_{212} \tag{12.35b}$$

$$-\dot{\Pi}_{122} = \Pi_{122}(A_{22} - Q_{22}\Pi_{022}) + (A_{22} - Q_{22}\Pi_{022})^T \Pi_{122} + \Pi_{212}^T \sigma \Pi_{312} + \Pi_{312}^T \sigma \Pi_{212} \tag{12.35c}$$

where

$$\begin{bmatrix} A_{11} & A_{12} \\ A_{21} & A_{22} \end{bmatrix} \triangleq \begin{bmatrix} u_1^T \\ u_2^T \end{bmatrix} A \left[\begin{array}{cc} u_1 & u_2 \end{array}\right] + \begin{bmatrix} \dot{u}_1^T u_1 & \dot{u}_1^T u_2 \\ \dot{u}_2^T u_1 & \dot{u}_2^T u_2 \end{bmatrix}$$

$$\begin{bmatrix} Q_{11} & Q_{12} \\ Q_{12}^T & Q_{22} \end{bmatrix} \triangleq \begin{bmatrix} u_1^T \\ u_2^T \end{bmatrix} (F_1 Q_1 F_1^T - B_w Q_w B_w^T) \left[\begin{array}{cc} u_1 & u_2 \end{array}\right]$$

$$\begin{bmatrix} R_{11} & R_{12} \\ R_{12}^T & R_{22} \end{bmatrix} \triangleq \begin{bmatrix} u_1^T \\ u_2^T \end{bmatrix} C^T V^{-1} C \left[\begin{array}{cc} u_1 & u_2 \end{array}\right]$$

The equations for the higher-order terms can be found in Appendix 12.7.1.

Proof. See Appendix 12.7.1.

In Lemma 12.4, the solution of (12.34) and (12.35) is discussed when $CF_2 \neq 0$. In Lemma 12.5, the solution is discussed when $CF_2 = 0$ and $C(AF_2 - \dot{F}_2) \neq 0$. The higher-order cases, such as $CF_2 = C(AF_2 - \dot{F}_2) = 0$ and $C[A(AF_2 - \dot{F}_2) - \frac{d}{d\tau}(AF_2 - \dot{F}_2)] \neq 0$, can be considered similarly.

Lemma 12.4. When $CF_2 \neq 0$,

$$\Pi = \begin{bmatrix} u_1 & u_2 \end{bmatrix} \left(\begin{bmatrix} 0 & 0 \\ 0 & \Pi_{022} \end{bmatrix} + \gamma^{\frac{1}{2}} \begin{bmatrix} \Pi_{211} & \Pi_{212} \\ \Pi_{212}^T & \Pi_{212}^T \Pi_{211}^{-1} \Pi_{212} + \bar{\Pi}_{222} \end{bmatrix} + \gamma \cdots \right) \begin{bmatrix} u_1^T \\ u_2^T \end{bmatrix} \tag{12.36}$$

where

$$\begin{aligned}
-\dot{\Pi}_{022} &= \Pi_{022}(A_{22} - A_{21}R_{11}^{-1}R_{12}) + (A_{22} - A_{21}R_{11}^{-1}R_{12})^T \Pi_{022} + \Pi_{022}(A_{21}R_{11}^{-1}A_{21}^T - Q_{22})\Pi_{022} \\
&\quad - (R_{22} - R_{12}^T R_{11}^{-1} R_{12}) \\
\Pi_{211} &= R_{11}^{1/2}(R_{11}^{1/2} \sigma R_{11}^{1/2})^{-1/2} R_{11}^{1/2} \\
\Pi_{212} &= \sigma^{-1} \Pi_{211}^{-1}(R_{12} - A_{21}^T \Pi_{022}) \\
\dot{\bar{\Pi}}_{222} &= \bar{\Pi}_{222}(-A_{22} + Q_{22}\Pi_{022} + A_{21}\Pi_{211}^{-1}\Pi_{212}) + (-A_{22} + Q_{22}\Pi_{022} + A_{21}\Pi_{211}^{-1}\Pi_{212})^T \bar{\Pi}_{222}
\end{aligned}$$

Proof. See Appendix 12.7.2.

In the limit, when $CF_2 \neq 0$,

$$\Pi = \begin{bmatrix} u_1 & u_2 \end{bmatrix} \begin{bmatrix} 0 & 0 \\ 0 & \Pi_{022} \end{bmatrix} \begin{bmatrix} u_1^T \\ u_2^T \end{bmatrix} \tag{12.37}$$

Therefore, $\operatorname{Ker} \Pi \supseteq \operatorname{Im} F_2$ in the limit because $\operatorname{Im} u_1 = \operatorname{Im} F_2$. This is consistent with Theorem 12.2 and the result in (Chung and Speyer, 1998; Chen and Speyer, 2000) derived by using the Goh transformation. For time-invariant systems, the result in Section 12.4 implies that Π_{022} is positive definite when (C, A, F_2) does not have any invariant zero. If (C, A, F_2) has invariant zeros, the associated nuisance fault direction will be replaced by the invariant zero direction ν. Since $C\nu = 0$ (12.32), the case where $C\nu = 0$ and $CA\nu \neq 0$ is included in Lemma 12.5. Therefore, $\operatorname{Ker} \Pi = \operatorname{Im} F_2$ and Π_{022} is positive definite.

Lemma 12.5. When $CF_2 = 0$ and $C(AF_2 - \dot{F}_2) \neq 0$,

$$\Pi = \begin{bmatrix} u_1 & u_2v_1 & u_2v_2 \end{bmatrix} \begin{bmatrix} \gamma^{\frac{3}{4}}\Pi_{311} & \gamma^{\frac{1}{2}}\Pi_{2121} & \gamma^{\frac{1}{2}}\Pi_{2122} \\ \gamma^{\frac{1}{2}}\Pi_{2121}^T & \gamma^{\frac{1}{4}}\Pi_{12211} & \gamma^{\frac{1}{4}}\Pi_{12212} \\ \gamma^{\frac{1}{2}}\Pi_{2122}^T & \gamma^{\frac{1}{4}}\Pi_{12212}^T & \Pi_{02222} \end{bmatrix} \begin{bmatrix} u_1^T \\ v_1^T u_2^T \\ v_2^T u_2^T \end{bmatrix} + \cdots$$

where $[\, v_1 \;\; v_2 \,]$ is unitary and $\operatorname{Im} v_1 = \operatorname{Im} A_{21}$. Only the lowest-order term of each element is kept for simplicity. The equation for each element can be found in Appendix 12.7.3.

Proof. See Appendix 12.7.3.

In the limit, when $CF_2 = 0$ and $C(AF_2 - \dot{F}_2) \neq 0$,

$$\Pi = \begin{bmatrix} u_1 & u_2v_1 & u_2v_2 \end{bmatrix} \begin{bmatrix} 0 & 0 & 0 \\ 0 & 0 & 0 \\ 0 & 0 & \Pi_{02222} \end{bmatrix} \begin{bmatrix} u_1^T \\ v_1^T u_2^T \\ v_2^T u_2^T \end{bmatrix} \tag{12.38}$$

Since $\operatorname{Im} v_1 = \operatorname{Im} A_{21}$, $\dot{u}_2^T u_1 = -u_2^T \dot{u}_1$ from $u_2^T u_1 = 0$, $[\, u_1 \;\; u_2 \,]$ is unitary and $\operatorname{Im} u_1 = \operatorname{Im} F_2$,

$$\begin{aligned} \operatorname{Im}[\, u_1 \;\; u_2v_1 \,] &= \operatorname{Im}[\, u_1 \;\; u_2(u_2^T A u_1 + \dot{u}_2^T u_1) \,] = \operatorname{Im}[\, u_1 \;\; u_2u_2^T(Au_1 - \dot{u}_1) \,] \\ &= \operatorname{Im}[\, u_1 \;\; (I - u_1u_1^T)(Au_1 - \dot{u}_1) \,] = \operatorname{Im}[\, u_1 \;\; Au_1 - \dot{u}_1 \,] = \operatorname{Im}[\, F_2 \;\; AF_2 - \dot{F}_2 \,] \end{aligned}$$

Therefore, $\operatorname{Ker}\Pi \supseteq \operatorname{Im}[\, F_2 \;\; AF_2 - \dot{F}_2 \,]$ in the limit. This is consistent with Theorem 12.2 and the result in (Chung and Speyer, 1998; Chen and Speyer, 2000) derived by using the Goh transformation. For time-invariant systems, the result in Section 12.4 implies that Π_{02222} is positive definite when (C, A, F_2) does not have any invariant zero. If (C, A, F_2) has invariant zeros, the associated nuisance fault direction will be replaced by the invariant zero direction ν. Since $C\nu = CA\nu = 0$ (12.32), the case where $C\nu = CA\nu = 0$ and $CA^2\nu \neq 0$ is included in the case where $CF_2 = C(AF_2 - \dot{F}_2) = 0$ and $C[A(AF_2 - \dot{F}_2) - \frac{d}{d\tau}(AF_2 - \dot{F}_2)] \neq 0$ which can be considered similarly. Therefore, $\operatorname{Ker}\Pi = \operatorname{Im}[\, F_2 \;\; AF_2 - \dot{F}_2 \,]$ and Π_{02222} is positive definite.

12.5.2 Analysis

In this section, the inverse of Π is derived. This shows explicitly the characteristics of P near and in the limit. The discussion is limited to the time-invariant case because Π_{022} in (12.37) and Π_{02222} in (12.38) may not be invertible for the time-varying case. In Lemma 12.6, P is discussed when $CF_2 \neq 0$. In Lemma 12.7, P is discussed when $CF_2 = 0$ and $CAF_2 \neq 0$. The higher-order case, such as $CF_2 = CAF_2 = 0$ and $CA^2F_2 \neq 0$, can be considered similarly.

Lemma 12.6. When $CF_2 \neq 0$,

$$P = \begin{bmatrix} u_1 & u_2 \end{bmatrix} \left(\gamma^{\frac{-1}{2}} \begin{bmatrix} \Pi_{211}^{-1} & 0 \\ 0 & 0 \end{bmatrix} + \begin{bmatrix} \Pi_{211}^{-1}(\Pi_{212}\Pi_{022}^{-1}\Pi_{212}^T - \Pi_{411})\Pi_{211}^{-1} & -\Pi_{211}^{-1}\Pi_{212}\Pi_{022}^{-1} \\ -\Pi_{022}^{-1}\Pi_{212}^T\Pi_{211}^{-1} & \Pi_{022}^{-1} \end{bmatrix} + \cdots \right) \begin{bmatrix} u_1^T \\ u_2^T \end{bmatrix} \tag{12.39}$$

Proof. By using Lemma 12.4 and matrix inversion lemma, P in the above form is obtained.

Lemma 12.7. When $CF_2 = 0$ and $CAF_2 \neq 0$,

$$P = \begin{bmatrix} \begin{bmatrix} u_1 & u_2 v_1 \end{bmatrix} & u_2 v_2 \end{bmatrix} \begin{bmatrix} \bar{\Pi}_{11} & \bar{\Pi}_{12} \\ \bar{\Pi}_{12}^T & \Pi_{02222}^{-1} \end{bmatrix} \begin{bmatrix} \begin{bmatrix} u_1^T \\ v_1^T u_2^T \end{bmatrix} \\ v_2^T u_2^T \end{bmatrix} + \cdots \tag{12.40}$$

where

$$\bar{\Pi}_{11} = \begin{bmatrix} \gamma^{-3/4}(\Pi_{311} - \Pi_{2121}\Pi_{12211}^{-1}\Pi_{2121}^T)^{-1} & -\gamma^{-1/2}\Pi_{311}^{-1}\Pi_{2121}(\Pi_{12211} - \Pi_{2121}^T\Pi_{311}^{-1}\Pi_{2121})^{-1} \\ -\gamma^{-1/2}(\Pi_{12211} - \Pi_{2121}^T\Pi_{311}^{-1}\Pi_{2121})^{-1}\Pi_{2121}^T\Pi_{311}^{-1} & \gamma^{-1/4}(\Pi_{12211} - \Pi_{2121}^T\Pi_{311}^{-1}\Pi_{2121})^{-1} \end{bmatrix}$$

$$\bar{\Pi}_{12} = \begin{bmatrix} 0 \\ (\Pi_{12211} - \Pi_{2121}^T\Pi_{311}^{-1}\Pi_{2121})^{-1}(\Pi_{2121}^T\Pi_{311}^{-1}\Pi_{2122} - \Pi_{12212}) \end{bmatrix}$$

Only the lowest-order term of each element is kept for simplicity.

Proof. See Appendix 12.7.4.

In the limit, when $CF_2 \neq 0$, Lemma 12.6 shows that P goes to infinity in the direction of $\operatorname{Im} F_2$. When $CF_2 = 0$ and $CAF_2 \neq 0$, Lemma 12.7 shows that P goes to infinity in the direction of $\operatorname{Im} [\, F_2 \;\; AF_2 \,]$.

Remark 7. By using the result in (Kwakernaak and Sivan, 1972b), for the time-invariant and infinite-time case, under the assumption that (C, A, F_2) does not have right-half plane invariant zeros,

$$\gamma P \to 0 \tag{12.41a}$$

$$L \to \frac{1}{\gamma^{1/2}} F_2 Q_2^{1/2} U^T V^{-1/2} \tag{12.41b}$$

as $\gamma \to 0$ where U is an arbitrary m by p_2 matrix such that $U^T U = I$.

By multiplying (12.39) and (12.40) by γ, (12.41a) is satisfied. By substituting (12.39) into (12.14),

$$L \to \frac{1}{\gamma^{1/2}} u_1 \Pi_{211}^{-1} u_1^T C^T V^{-1}$$

as $\gamma \to 0$. Then, L goes to infinity along the direction of $\frac{1}{\gamma^{1/2}}\,\mathrm{Im}\,F_2$ which is consistent with (12.41b). By substituting (12.40) into (12.14),

$$
\begin{aligned}
L \to & \frac{1}{\gamma^{1/2}} u_1 \Pi_{311}^{-1} \Pi_{2121} (\Pi_{12211} - \Pi_{2121}^T \Pi_{311}^{-1} \Pi_{2121})^{-1} v_1^T u_2^T C^T \\
& + \frac{1}{\gamma^{1/4}} u_2 v_1 (\Pi_{12211} - \Pi_{2121}^T \Pi_{311}^{-1} \Pi_{2121})^{-1} v_1^T u_2^T C^T
\end{aligned}
$$

as $\gamma \to 0$. Then, L goes to infinity essentially along the direction of $\frac{1}{\gamma^{1/2}}\,\mathrm{Im}\,F_2$ which is consistent with (12.41b). Note that L also goes to infinity along the direction of $\frac{1}{\gamma^{1/4}}\,\mathrm{Im}\,[\,AF_2\;\;F_2\,]$. Therefore, the perturbation method is consistent with (Kwakernaak and Sivan, 1972b), but provides more information about L and P than (Kwakernaak and Sivan, 1972b). The perturbation method can also be applied to the singular optimal control problem to obtain a more precise interpretation of the behavior of the Riccati equation near the singular surface.

12.6 Example

In this section, four numerical examples are used to demonstrate the performance and properties of the optimal stochastic fault detection filter. In Section 12.6.1, the filter is applied to a time-invariant system. In Section 12.6.2, the filter is applied to a time-varying system. In Section 12.6.3, the null space of the Riccati matrix Π in the limit is discussed. In Section 12.6.4, the effect of the target fault's power spectral density Q_1 on the Riccati matrix P and the filter is discussed.

12.6.1 Example 1

In this section, three cases are presented to show the performance of the optimal stochastic fault detection filter. The time-invariant system is from (White and Speyer, 1987).

$$
A = \begin{bmatrix} 0 & 3 & 4 \\ 1 & 2 & 3 \\ 0 & 2 & 5 \end{bmatrix} \quad , \quad C = \begin{bmatrix} 0 & 1 & 0 \\ 0 & 0 & 1 \end{bmatrix} \quad , \quad F_1 = \begin{bmatrix} 0 \\ 0 \\ 1 \end{bmatrix} \quad , \quad F_2 = \begin{bmatrix} 5 \\ 1 \\ 1 \end{bmatrix}
$$

F_1 is the target fault direction. F_2 is the nuisance fault direction. There is no process noise.

In the first case, the power spectral densities are chosen as $Q_1 = 1$, $Q_2 = 1$ and $V = I$. The steady-state solutions to the Riccati equation (12.13) when $\gamma = 10^{-4}$ and 10^{-6} are obtained, respectively. Figure 12.1 shows the frequency response from both faults to the residual (12.7). The left one is $\gamma = 10^{-4}$ and the right one is $\gamma = 10^{-6}$. In each figure, there are two solid lines representing the frequency response from the target fault to the residuals with projectors (12.18) and

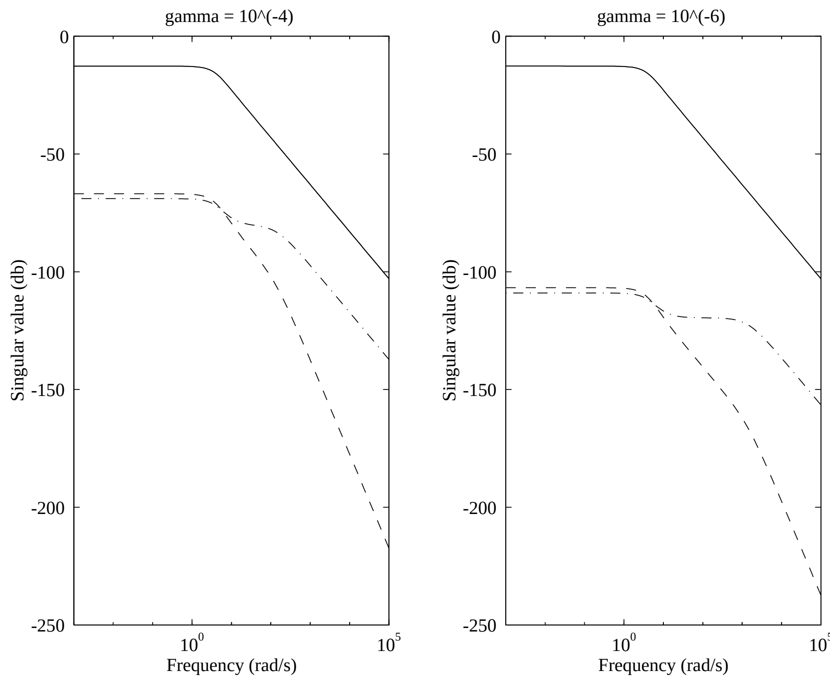

Figure 12.1: Frequency response from both faults to the residual

(12.23), respectively. Note that the two solid lines overlap. The dashdot line and the dashed line represent the frequency response from the nuisance fault to the residuals with projectors (12.18) and (12.23), respectively. This case shows that the nuisance fault transmission can be reduced by using a smaller γ while the target fault transmission is not affected. Further, the projector (12.18), derived from solving the minimization problem, is better than (12.23), used by other approximate unknown input observers (Chung and Speyer, 1998; Chen and Speyer, 2000), at low frequency. This suggests that (12.23) might not be the best choice for the approximate unknown input observer.

In the second case, $Q_2 = 1$, $V = I$ and $\gamma = 10^{-6}$. The steady-state solutions to the Riccati equation (12.13) when $Q_1 = 1$ and 10 are obtained, respectively. The left figure of Figure 12.2 shows the frequency response from the target fault to the residual. This case shows that the target fault transmission can be enhanced by using a larger Q_1.

In the third case, $Q_1 = 1$, $Q_2 = 1$ and $\gamma = 10^{-6}$. The steady-state solutions to the Riccati equation (12.13) when $V = I$ and $10I$ are obtained, respectively. The right figure of Figure 12.2 shows the frequency response from the sensor noise to the residual. This case shows that the sensor noise transmission can be reduced by using a larger V.

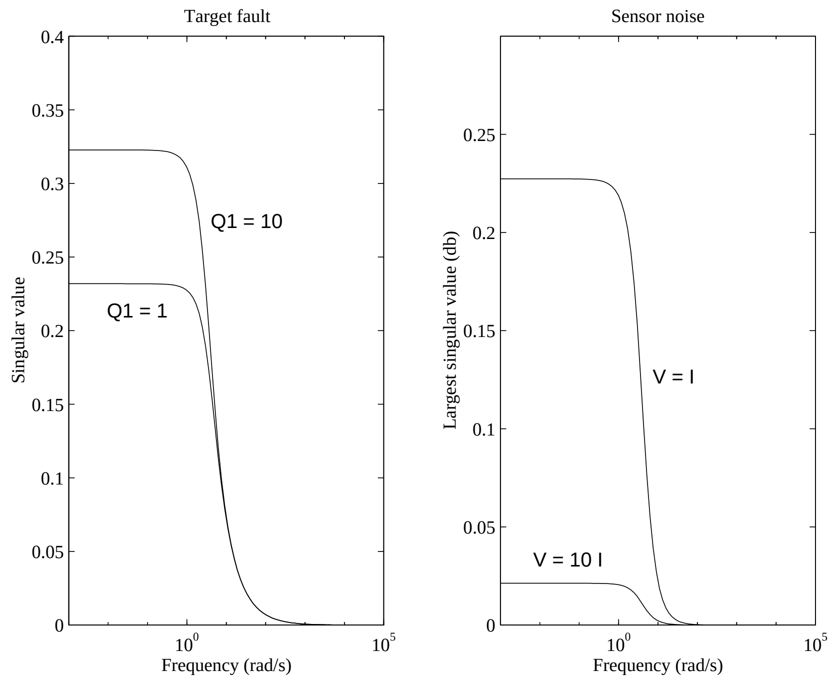

Figure 12.2: Frequency response from the target fault and the sensor noise to the residual

12.6.2 Example 2

A time-varying system is obtained by adding some time-varying elements to A and F_2 matrices of the time-invariant system in previous section. C and F_1 matrices are kept the same.

$$A = \begin{bmatrix} -cos(t) & 3+2sin(t) & 4 \\ 1 & 2 & 3-2cos(t) \\ 5sin(t) & 2 & 5+3cos(t) \end{bmatrix} \quad , \quad F_2 = \begin{bmatrix} 5-2cos(t) \\ 1 \\ 1+sin(t) \end{bmatrix}$$

The Riccati equation (12.13) is solved with $Q_1 = 1$, $Q_2 = 1$, $V = I$ and $\gamma = 10^{-5}$ for $t \in [0, 25]$. Figure 12.3 shows the time response of the residual (12.7) when there is no fault, a target fault and a nuisance fault, respectively. The left three figures use projector (12.18) and the right three figures use projector (12.25). In each case, there is no sensor noise. The faults are unit steps that occur at the fifth second. There is a transient response until about two seconds due to the initial condition error. This example shows that the filter works well for time-varying systems. Further, the projector (12.18), derived from solving the minimization problem, is better than (12.25), used by other approximate unknown input observers (Chung and Speyer, 1998; Chen and Speyer, 2000).

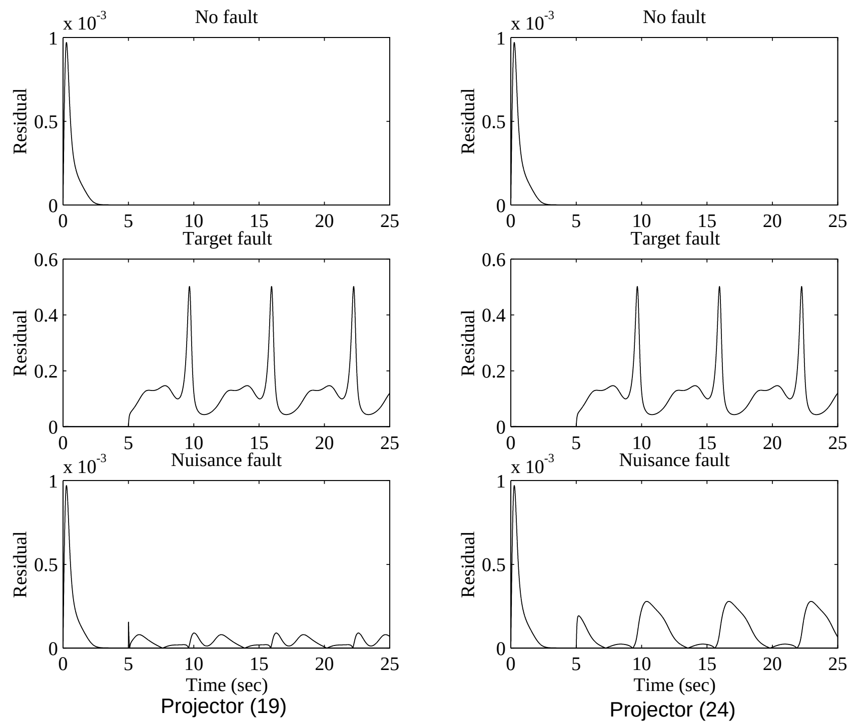

Figure 12.3: Time response of the residual

12.6.3 Example 3

In this section, four cases are presented to show the properties of the Riccati matrix Π in the limit. The first case shows that $\mathrm{Ker}(\Pi|_{\gamma=0})$ contains the nuisance fault direction and the invariant zero direction associated with the right-half plane invariant zero. One of the filter eigenvalues is near the mirror image of the invariant zero. The second case shows that none of the filter eigenvalues is near the mirror image of the invariant zero if the nuisance fault direction is modified. The third case shows that $\mathrm{Ker}(\Pi|_{\gamma=0})$ contains only the nuisance fault direction, but not the invariant zero direction associated with the left-half plane invariant zero. One of the filter eigenvalues is near the invariant zero. The fourth case shows that $\mathrm{Ker}(\Pi|_{\gamma=0})$ contains the nuisance fault direction and the invariant zero direction associated with the left-half plane invariant zero if the nuisance fault direction is modified. Further, none of the filter eigenvalues is near the invariant zero.

In the first case, A and C matrices are the same as the example in Section 12.6.1 and

$$F_1 = \begin{bmatrix} 1 \\ -0.5 \\ 0.5 \end{bmatrix} \quad , \quad F_2 = \begin{bmatrix} -3 \\ 1 \\ 0 \end{bmatrix}$$

(C, A, F_2) has an invariant zero at 3 and the invariant zero direction ν is $[1\ 0\ 0]^T$. The power spectral densities are chosen as $Q_1 = 1$, $Q_2 = 1$ and $V = I$. The steady-state solutions to the Riccati equation (12.27) when $\gamma = 10^{-6}$ and Lemma 12.4 when $\gamma = 0$ are

$$\Pi|_{\gamma=10^{-6}} = \begin{bmatrix} 0.0000 & -0.0000 & 0.0000 \\ -0.0000 & 0.0010 & -0.0002 \\ 0.0000 & -0.0002 & 0.0965 \end{bmatrix} \quad , \quad \Pi|_{\gamma=0} = \begin{bmatrix} 0 & 0 & 0 \\ 0 & 0 & 0 \\ 0 & 0 & 0.0965 \end{bmatrix}$$

This shows that $\mathrm{Ker}(\Pi|_{\gamma=0})$ contains the nuisance fault direction and the invariant zero direction associated with the right-half plane invariant zero. The filter has an eigenvalue near the mirror image of the invariant zero at -3.00002.

In the second case, the nuisance fault direction used for the filter design is changed to ν. The power spectral densities are the same. The steady-state solutions to the Riccati equation (12.27) when $\gamma = 10^{-6}$ and Lemma 12.5 when $\gamma = 0$ are

$$\Pi|_{\gamma=10^{-6}} = \begin{bmatrix} 0.0000 & -0.0000 & 0.0000 \\ -0.0000 & 0.0044 & -0.0009 \\ 0.0000 & -0.0009 & 0.0967 \end{bmatrix} \quad , \quad \Pi|_{\gamma=0} = \begin{bmatrix} 0 & 0 & 0 \\ 0 & 0 & 0 \\ 0 & 0 & 0.0965 \end{bmatrix}$$

This shows that $\mathrm{Ker}(\Pi|_{\gamma=0})$ contains F_2 and ν. The filter does not have any eigenvalue near the mirror image of the invariant zero.

The third case is obtained from modifying the first case such that the invariant zero is in the left-half plane instead of the right-half plane. The system matrices are the same except

$$C = \begin{bmatrix} 1 & 0 & 0 \\ 0 & 0 & 1 \end{bmatrix} \quad , \quad F_2 = \begin{bmatrix} 1.5 \\ 2 \\ 1 \end{bmatrix}$$

(C, A, F_2) has an invariant zero at -2 and the invariant zero direction ν is $[\,0\ 1\ 0\,]^T$. The power spectral densities are the same. The steady-state solutions to the Riccati equation (12.27) when $\gamma = 10^{-6}$ and Lemma 12.4 when $\gamma = 0$ are

$$\Pi|_{\gamma=10^{-6}} = \begin{bmatrix} 9.8610 & -6.1084 & -2.5869 \\ -6.1084 & 3.8176 & 1.5357 \\ -2.5869 & 1.5357 & 0.8127 \end{bmatrix} \quad , \quad \Pi|_{\gamma=0} = \begin{bmatrix} 9.7791 & -6.0530 & -2.5626 \\ -6.0530 & 3.7801 & 1.5192 \\ -2.5626 & 1.5192 & 0.8055 \end{bmatrix}$$

This shows that $\mathrm{Ker}(\Pi|_{\gamma=0})$ contains only the nuisance fault direction, but not the invariant zero direction associated with the left-half plane invariant zero. The filter has an eigenvalue near the invariant zero at -1.9999.

In the fourth case, the nuisance fault direction used for the filter design is changed to ν. The power spectral densities are the same. The steady-state solutions to the Riccati equation (12.27) when $\gamma = 10^{-6}$ and Lemma 12.5 when $\gamma = 0$ are

$$\Pi|_{\gamma=10^{-6}} = \begin{bmatrix} 0.0890 & -0.0000 & -0.1292 \\ -0.0000 & 0.0000 & -0.0000 \\ -0.1292 & -0.0000 & 0.1951 \end{bmatrix} \quad , \quad \Pi|_{\gamma=0} = \begin{bmatrix} 0.0866 & 0 & -0.1299 \\ 0 & 0 & 0 \\ -0.1299 & 0 & 0.1949 \end{bmatrix}$$

This shows that $\mathrm{Ker}(\Pi|_{\gamma=0})$ contains F_2 and ν. The filter does not have any eigenvalue near the invariant zero.

12.6.4 Example 4

This example shows how the target fault's power spectral density Q_1 affects the Riccati matrix P and the filter. The system matrices are

$$A = \begin{bmatrix} -3 & 2 \\ -5 & -1 \end{bmatrix} \quad , \quad C = \begin{bmatrix} 1 & 0 \\ 0 & 1 \end{bmatrix} \quad , \quad F_1 = \begin{bmatrix} 1 \\ 0 \end{bmatrix} \quad , \quad F_2 = \begin{bmatrix} 0 \\ 1 \end{bmatrix}$$

F_1 is the target fault direction. F_2 is the nuisance fault direction. There is no process noise.

The steady-state solutions to the Riccati equation (12.13) with $Q_2 = 1$, $V = I$ and $\gamma = 10^{-5}$ are obtained for Q_1 between 0 and 12. When Q_1 is larger than 12.99, there exists a finite escape time. The upper two figures of Figure 12.4 show how Q_1 affects the definiteness of P by plotting the eigenvalues of P versus Q_1. When Q_1 increases, one of the eigenvalues becomes smaller showing that P is less positive definite and eventually, P becomes indefinite. The lower two figures of Figure 12.4 show how Q_1 affects the filter eigenvalues. When Q_1 increases, one of the filter eigenvalues moves towards the imaginary axis. Note that it is possible that the filter is stable while P is indefinite. This is very different from (Chung and Speyer, 1998; Chen and Speyer, 2000) where Π, the inverse of P, is used because while P is indefinite and does not have a finite escape time, Π has a finite escape time. This implies that the optimal stochastic fault detection filter may be made more sensitive to the target fault than (Chen and Speyer, 2000).

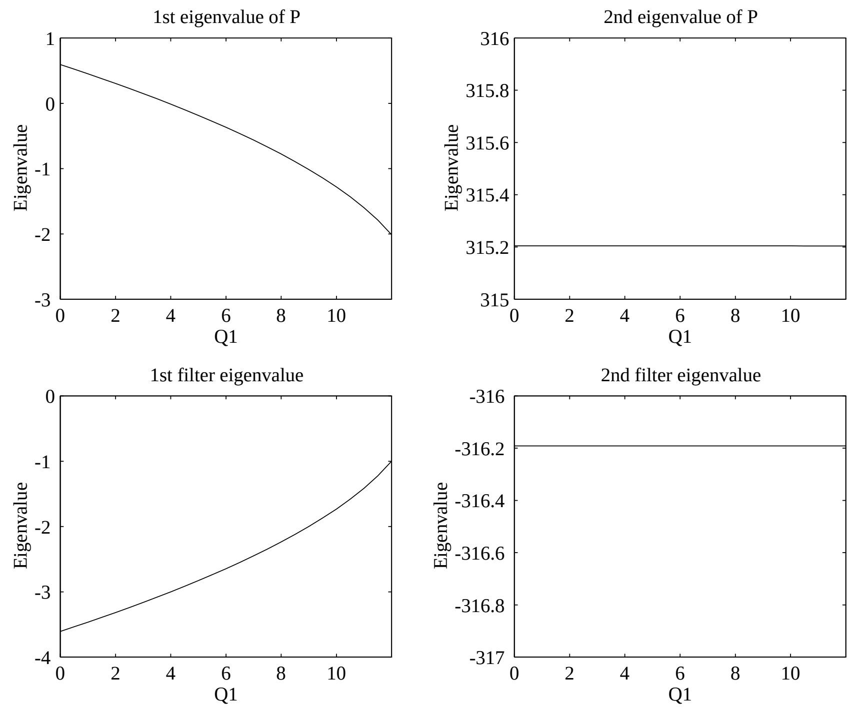

Figure 12.4: Eigenvalues of the Riccati matrix P and the filter for different Q_1

12.7 Appendix

12.7.1 Proof of Lemma 12.3

By substituting (12.33) into (12.27) and collecting terms of common power,

$$\gamma^{-1} \; : \quad 0 = \Pi_0 \bar{Q}_2 \Pi_0 \tag{12.42a}$$

$$\gamma^{-3/4} \; : \quad 0 = \Pi_1 \bar{Q}_2 \Pi_0 + \Pi_0 \bar{Q}_2 \Pi_1 \tag{12.42b}$$

$$\gamma^{-1/2} \; : \quad 0 = \Pi_2 \bar{Q}_2 \Pi_0 + \Pi_1 \bar{Q}_2 \Pi_1 + \Pi_0 \bar{Q}_2 \Pi_2 \tag{12.42c}$$

$$\gamma^{-1/4} \; : \quad 0 = \Pi_3 \bar{Q}_2 \Pi_0 + \Pi_2 \bar{Q}_2 \Pi_1 + \Pi_1 \bar{Q}_2 \Pi_2 + \Pi_0 \bar{Q}_2 \Pi_3 \tag{12.42d}$$

$$\begin{aligned} \gamma^{0} \; : \; -\dot{\Pi}_0 &= \Pi_0 A + A^T \Pi_0 - C^T V^{-1} C + \Pi_4 \bar{Q}_2 \Pi_0 + \Pi_3 \bar{Q}_2 \Pi_1 + \Pi_2 \bar{Q}_2 \Pi_2 + \Pi_1 \bar{Q}_2 \Pi_3 + \Pi_0 \bar{Q}_2 \Pi_4 \\ &\quad - \Pi_0 \bar{Q}_1 \Pi_0 \end{aligned} \tag{12.42e}$$

$$\begin{aligned} \gamma^{1/4} \; : \; -\dot{\Pi}_1 &= \Pi_1 A + A^T \Pi_1 + \Pi_5 \bar{Q}_2 \Pi_0 + \Pi_4 \bar{Q}_2 \Pi_1 + \Pi_3 \bar{Q}_2 \Pi_2 + \Pi_2 \bar{Q}_2 \Pi_3 + \Pi_1 \bar{Q}_2 \Pi_4 + \Pi_0 \bar{Q}_2 \Pi_5 \\ &\quad - \Pi_1 \bar{Q}_1 \Pi_0 - \Pi_0 \bar{Q}_1 \Pi_1 \end{aligned} \tag{12.42f}$$

$$\begin{aligned} \gamma^{1/2} \; : \; -\dot{\Pi}_2 &= \Pi_2 A + A^T \Pi_2 + \Pi_6 \bar{Q}_2 \Pi_0 + \Pi_5 \bar{Q}_2 \Pi_1 + \Pi_4 \bar{Q}_2 \Pi_2 + \Pi_3 \bar{Q}_2 \Pi_3 + \Pi_2 \bar{Q}_2 \Pi_4 + \Pi_1 \bar{Q}_2 \Pi_5 \\ &\quad + \Pi_0 \bar{Q}_2 \Pi_6 - \Pi_2 \bar{Q}_1 \Pi_0 - \Pi_1 \bar{Q}_1 \Pi_1 - \Pi_0 \bar{Q}_1 \Pi_2 \end{aligned} \tag{12.42g}$$

$$\vdots$$

where $\bar{Q}_2 = F_2 Q_2 F_2^T$ and $\bar{Q}_1 = F_1 Q_1 F_1^T - B_w Q_w B_w^T$.

From (12.42a), $\mathrm{Ker}\,\Pi_0$ contains F_2. Then, Π_0 can be written as

$$\Pi_0 = \begin{bmatrix} u_1 & u_2 \end{bmatrix} \begin{bmatrix} 0 & 0 \\ 0 & \Pi_{022} \end{bmatrix} \begin{bmatrix} u_1^T \\ u_2^T \end{bmatrix} = u_2 \Pi_{022} u_2^T \tag{12.43}$$

where Π_{022} is to be determined. (12.42b) is trivially satisfied because of (12.43). By substituting (12.43) into (12.42c), Π_1 can be written as

$$\Pi_1 = \begin{bmatrix} u_1 & u_2 \end{bmatrix} \begin{bmatrix} 0 & 0 \\ 0 & \Pi_{122} \end{bmatrix} \begin{bmatrix} u_1^T \\ u_2^T \end{bmatrix} = u_2 \Pi_{122} u_2^T \tag{12.44}$$

where Π_{122} is to be determined. (12.42d) is trivially satisfied because of (12.43) and (12.44).

By using (12.43) and (12.44), (12.42e) becomes

$$-\dot{\Pi}_0 = \Pi_0 A + A^T \Pi_0 - C^T V^{-1} C + \Pi_2 \bar{Q}_2 \Pi_2 - \Pi_0 \bar{Q}_1 \Pi_0 \tag{12.45}$$

Let

$$\Pi_2 = \begin{bmatrix} u_1 & u_2 \end{bmatrix} \begin{bmatrix} \Pi_{211} & \Pi_{212} \\ \Pi_{212}^T & \Pi_{222} \end{bmatrix} \begin{bmatrix} u_1^T \\ u_2^T \end{bmatrix} \tag{12.46}$$

By multiplying (12.45) by $[u_1\ u_2]^T$ from the left and $[u_1\ u_2]$ from the right and substituting (12.43) and (12.46), (12.34) is obtained. Note that (12.34) is solved for Π_{022}, Π_{211} and Π_{212}.

By using (12.43) and (12.44), (12.42f) becomes

$$-\dot{\Pi}_1 = \Pi_1 (A - \bar{Q}_1 \Pi_0) + (A - \bar{Q}_1 \Pi_0)^T \Pi_1 + \Pi_2 \bar{Q}_2 \Pi_3 + \Pi_3 \bar{Q}_2 \Pi_2 \tag{12.47}$$

Let

$$\Pi_3 = \begin{bmatrix} u_1 & u_2 \end{bmatrix} \begin{bmatrix} \Pi_{311} & \Pi_{312} \\ \Pi_{312}^T & \Pi_{322} \end{bmatrix} \begin{bmatrix} u_1^T \\ u_2^T \end{bmatrix} \tag{12.48}$$

By multiplying (12.47) by $[u_1\ u_2]^T$ from the left and $[u_1\ u_2]$ from the right and substituting (12.43), (12.44), (12.46) and (12.48), (12.35) is obtained. Note that (12.35) is solved for Π_{122}, Π_{311} and Π_{312}.

By using (12.43) and (12.44), (12.42g) becomes

$$-\dot{\Pi}_2 = \Pi_2 (A - \bar{Q}_1 \Pi_0 + \bar{Q}_2 \Pi_4) + (A - \bar{Q}_1 \Pi_0 + \bar{Q}_2 \Pi_4)^T \Pi_2 + \Pi_3 \bar{Q}_2 \Pi_3 - \Pi_1 \bar{Q}_1 \Pi_1 \tag{12.49}$$

Let

$$\Pi_4 = \begin{bmatrix} u_1 & u_2 \end{bmatrix} \begin{bmatrix} \Pi_{411} & \Pi_{412} \\ \Pi_{412}^T & \Pi_{422} \end{bmatrix} \begin{bmatrix} u_1^T \\ u_2^T \end{bmatrix} \tag{12.50}$$

By multiplying (12.49) by $[\, u_1 \ u_2 \,]^T$ from the left and $[\, u_1 \ u_2 \,]$ from the right and substituting (12.43), (12.44), (12.46), (12.48) and (12.50),

$$0 = \Pi_{411}\sigma\Pi_{211} + \Pi_{211}\sigma\Pi_{411} + \Pi_{311}\sigma\Pi_{311} + \Pi_{211}A_{11} + A_{11}^T\Pi_{211} + \Pi_{212}A_{21} + A_{21}^T\Pi_{212}^T + \dot{\Pi}_{211} \tag{12.51a}$$

$$\begin{aligned} 0 &= \Pi_{211}\sigma\Pi_{412} + A_{21}^T\Pi_{222} + \Pi_{411}\sigma\Pi_{212} + A_{11}^T\Pi_{212} + \Pi_{212}A_{22} + \Pi_{211}A_{12} \\ &\quad - \Pi_{212}Q_{22}\Pi_{022} - \Pi_{211}Q_{12}\Pi_{022} + \Pi_{311}\sigma\Pi_{312} + \dot{\Pi}_{212} \end{aligned} \tag{12.51b}$$

$$\begin{aligned} -\dot{\Pi}_{222} &= \Pi_{222}(A_{22} - Q_{22}\Pi_{022}) + (A_{22} - Q_{22}\Pi_{022})^T\Pi_{222} + \Pi_{212}^T(A_{12} - Q_{12}\Pi_{022} + \sigma\Pi_{412}) \\ &\quad + (A_{12} - Q_{12}\Pi_{022} + \sigma\Pi_{412})^T\Pi_{212} + \Pi_{312}^T\sigma\Pi_{312} - \Pi_{122}Q_{22}\Pi_{122} \end{aligned} \tag{12.51c}$$

Note that (12.51) is solved for Π_{222}, Π_{411} and Π_{412}. In (12.51a) and (12.51b), $\dot{\Pi}_{211}$ and $\dot{\Pi}_{212}$ are known by taking the derivative of (12.34a) and (12.34b). The same procedure can be done for the higher-order terms if needed.

Remark 8. For time-invariant systems, $[\, u_1 \ u_2 \,]$ can be obtained from the singular value decomposition of $F_2Q_2F_2^T$ and $[\, \dot{u}_1 \ \dot{u}_2 \,] = 0$. For time-varying systems, u_1 and u_2 have to be formed differently. Since $\operatorname{Im} u_1 = \operatorname{Im} F_2$, u_1 can be chosen as $F_2(F_2^TF_2)^{-1/2}$. Since $[\, u_1 \ u_2 \,]$ is unitary, u_2 has to satisfy $u_1^Tu_2 = 0$ and $u_2^Tu_2 = I$. Define $U_1 = I - u_1u_1^T$. Since $u_1^TU_1 = 0$, the first column of u_2, called u_{21}, can be chosen as $u_{21} = U_{1i}(U_{1i}^TU_{1i})^{-1/2}$ where U_{1i} is any nonzero column of U_1. Note that $u_1^Tu_{21} = 0$ and $u_{21}^Tu_{21} = 1$. Next, define $U_2 = I - [\, u_1 \ u_{21} \,][\, u_1 \ u_{21} \,]^T$. Since $[\, u_1 \ u_{21} \,]^TU_2 = 0$, the second column of u_2, called u_{22}, can be chosen as $u_{22} = U_{2i}(U_{2i}^TU_{2i})^{-1/2}$ where U_{2i} is any nonzero column of U_2. Note that $u_1^T[\, u_{21} \ u_{22} \,] = 0$ and $[\, u_{21} \ u_{22} \,]^T[\, u_{21} \ u_{22} \,] = I$. Other directions of u_2 can be obtained similarly. Note that u_1 and u_2 are not unique. The derivative of u_1 and u_2 can also be obtained since u_1 and u_2 are explicitly written as functions of time. ◀

12.7.2 Proof of Lemma 12.4

When $CF_2 \neq 0$, R_{11} is positive definite because $\operatorname{Im} u_1 = \operatorname{Im} F_2$. Then, from (12.34a),

$$\Pi_{211} = R_{11}^{1/2}(R_{11}^{1/2}\sigma R_{11}^{1/2})^{-1/2}R_{11}^{1/2}$$

Note that Π_{211} is positive definite. From (12.34b),

$$\Pi_{212} = \sigma^{-1}\Pi_{211}^{-1}(R_{12} - A_{21}^T\Pi_{022}) \tag{12.52}$$

By substituting (12.52) into (12.34c) and using (12.34a),

$$-\dot{\Pi}_{022} = \Pi_{022}(A_{22} - A_{21}R_{11}^{-1}R_{12}) + (A_{22} - A_{21}R_{11}^{-1}R_{12})^T\Pi_{022} + \Pi_{022}(A_{21}R_{11}^{-1}A_{21}^T - Q_{22})\Pi_{022}$$
$$- (R_{22} - R_{12}^T R_{11}^{-1}R_{12}) \quad (12.53)$$

Therefore, the zeroth-order term Π_0 (12.43) can be obtained by solving (12.53). Part of the second-order term Π_2 (12.46) can be obtained from (12.34a) and (12.52).

From (12.35a),

$$\Pi_{311} = 0 \quad (12.54)$$

because σ and Π_{211} are positive definite. By substituting (12.54) into (12.35b),

$$\Pi_{312} = -\sigma^{-1}\Pi_{211}^{-1}A_{21}^T\Pi_{122} \quad (12.55)$$

By substituting (12.55) into (12.35c),

$$\dot{\Pi}_{122} = \Pi_{122}(-A_{22} + Q_{22}\Pi_{022} + A_{21}\Pi_{211}^{-1}\Pi_{212}) + (-A_{22} + Q_{22}\Pi_{022} + A_{21}\Pi_{211}^{-1}\Pi_{212})^T\Pi_{122} \quad (12.56)$$

Since (12.56) is a homogeneous equation and the initial condition is zero,

$$\Pi_{122} = 0 \quad (12.57)$$

By substituting (12.57) into (12.55),

$$\Pi_{312} = 0 \quad (12.58)$$

Therefore, the first-order term Π_1 (12.44) is zero from (12.57). Part of the third-order term Π_3 (12.48) is also zero from (12.54) and (12.58).

By substituting (12.54) into (12.51a) and (12.51b),

$$0 = \Pi_{411}\sigma\Pi_{211} + \Pi_{211}\sigma\Pi_{411} + \Pi_{211}A_{11} + A_{11}^T\Pi_{211} + \Pi_{212}A_{21} + A_{21}^T\Pi_{212}^T + \dot{\Pi}_{211} \quad (12.59)$$

$$\Pi_{412} = -\sigma^{-1}\Pi_{211}^{-1}[A_{21}^T\Pi_{222} + \Pi_{411}\sigma\Pi_{212} + A_{11}^T\Pi_{212} + \Pi_{212}A_{22} + \Pi_{211}A_{12}$$
$$- \Pi_{212}Q_{22}\Pi_{022} - \Pi_{211}Q_{12}\Pi_{022} + \dot{\Pi}_{211}] \quad (12.60)$$

Define $\bar{\Pi}_{222} \triangleq \Pi_{222} - \Pi_{212}^T\Pi_{211}^{-1}\Pi_{212}$. By substituting (12.57), (12.58) and (12.60) into (12.51c) and using (12.59),

$$\dot{\bar{\Pi}}_{222} = \bar{\Pi}_{222}(-A_{22} + Q_{22}\Pi_{022} + A_{21}\Pi_{211}^{-1}\Pi_{212}) + (-A_{22} + Q_{22}\Pi_{022} + A_{21}\Pi_{211}^{-1}\Pi_{212})^T\bar{\Pi}_{222} \quad (12.61)$$

Therefore, the second-order term Π_2 (12.46) can be obtained from (12.34a), (12.52) and (12.61). Part of the fourth-order term Π_4 (12.50) can be obtained from (12.59) and (12.60). In (12.59) and (12.60), $\dot{\Pi}_{211}$ and $\dot{\Pi}_{212}$ are known by taking the derivative of (12.34a) and (12.52). The same procedure can be done for the higher-order terms if needed, i.e., obtaining Π_{322} and Π_{422}.

Remark 9. Since Π_{211} and Π_{212}, the lowest-order terms of the (1,1) and (1,2) elements of the expansion of Π, are obtained from the algebraic equations (12.34a) and (12.52), the initial condition $\Pi(t_0) = P_0^{-1}$ cannot be completely satisfied. This is because the dimension of the differential Riccati equation (12.27) is reduced in the limit as $\gamma \to 0$. This leads to the occurrence of a boundary layer (Nayfeh, 1973). Note that the expansion of Π (12.36) is valid everywhere except near $\tau = 0$ and is called the outer expansion. The inner expansion, which is only valid near $\tau = 0$ and approximates the boundary layer, can be obtained by using fast time scales (Nayfeh, 1973). Since the inner expansion is only valid for a very short period of time, the focus will be placed on generating the boundary layer which will be used as the initial condition of the outer expansion. Note that only the (2,2) element of the outer expansion needs an initial condition. By applying a new fast time scale $\zeta = \tau/\gamma$ to (12.27) and substituting

$$\Pi = \Pi_0^{IN} + \gamma^{1/2}\Pi_2^{IN} + \gamma\Pi_4^{IN} + \cdots$$

where the superscript IN denotes the inner expansion, the collection of terms of common power yields the asymptotic boundary layer dynamics as

$$\begin{aligned}
\gamma^{-1} &: -\frac{d}{d\zeta}\Pi_0^{IN} = \Pi_0^{IN}\bar{Q}_2\Pi_0^{IN} &&, \quad \Pi_0^{IN}(t_0) = \Pi(t_0) \\
\gamma^{-1/2} &: -\frac{d}{d\zeta}\Pi_2^{IN} = \Pi_2^{IN}\bar{Q}_2\Pi_0^{IN} + \Pi_0^{IN}\bar{Q}_2\Pi_2^{IN} &&, \quad \Pi_2^{IN}(t_0) = 0 \\
&\vdots
\end{aligned}$$

The initial condition of the outer expansion is obtained by matching it with the steady-state solution of the inner expansion (Nayfeh, 1973) as

$$\Pi_{022}|_{\tau=t_0} = \Pi_{022}^{IN}|_{\zeta\to\infty}$$
$$\Pi_{222}|_{\tau=t_0} = \Pi_{222}^{IN}|_{\zeta\to\infty}$$

Since $\bar{Q}_2 = F_2 Q_2 F_2^T$ is apriori known, $\Pi_{022}(t_0)$ and $\Pi_{222}(t_0)$ can be obtained apriori. The initial condition of the higher-order terms can be obtained similarly. Note that in the limit as

$\gamma \to 0$, the fast time scale $\zeta \to \infty$ and there is an instant jump at the initial time. This is consistent with the Goh transformation (Chung and Speyer, 1998; Bell and Jacobson, 1975).

Remark 10. By using (12.52) and (12.53),

$$\begin{aligned} -A_{22} + Q_{22}\Pi_{022} + A_{21}\Pi_{211}^{-1}\Pi_{212} &= -(A_{22} - A_{21}R_{11}^{-1}R_{12}) - (A_{21}R_{11}^{-1}A_{21}^T - Q_{22})\Pi_{022} \\ &= (A_{22} - A_{21}R_{11}^{-1}R_{12}) - \Pi_{022}^{-1}(R_{22} - R_{12}^T R_{11}^{-1}R_{12}) \end{aligned} \tag{12.62}$$

For the time-invariant and infinite-time case, given that $(A_{22} - A_{21}R_{11}^{-1}R_{12}) - \Pi_{022}^{-1}(R_{22} - R_{12}^T R_{11}^{-1}R_{12})$, the closed-loop A matrix of (12.53), is stable. Then, from (12.61),

$$\bar{\Pi}_{222} = 0$$

12.7.3 Proof of Lemma 12.5

When $CF_2 = 0$, $R_{11} = 0$ and $R_{12} = 0$ because $\operatorname{Im} u_1 = \operatorname{Im} F_2$. From (12.34a),

$$\Pi_{211} = 0 \tag{12.63}$$

because σ is positive definite. By substituting (12.63) into (12.34b),

$$\Pi_{022}A_{21} = 0 \tag{12.64}$$

Then, Π_{022} can be written as

$$\Pi_{022} = \begin{bmatrix} v_1 & v_2 \end{bmatrix} \begin{bmatrix} 0 & 0 \\ 0 & \Pi_{02222} \end{bmatrix} \begin{bmatrix} v_1^T \\ v_2^T \end{bmatrix} \tag{12.65}$$

and

$$\Pi_{212} = \begin{bmatrix} \Pi_{2121} & \Pi_{2122} \end{bmatrix} \begin{bmatrix} v_1^T \\ v_2^T \end{bmatrix} \tag{12.66}$$

where $[\, v_1 \;\; v_2 \,]$ is unitary and $\operatorname{Im} v_1 = \operatorname{Im} A_{21}$. By multiplying (12.34c) by $[\, v_1 \;\; v_2 \,]^T$ from the left and $[\, v_1 \;\; v_2 \,]$ from the right and substituting (12.65) and (12.66),

$$0 = \Pi_{2121}^T \sigma \Pi_{2121} - R_{2211} \tag{12.67a}$$

$$0 = \Pi_{2121}^T \sigma \Pi_{2122} + A_{2221}^T \Pi_{02222} - R_{2212} \tag{12.67b}$$

$$-\dot{\Pi}_{02222} = \Pi_{02222}A_{2222} + A_{2222}^T\Pi_{02222} - \Pi_{02222}Q_{2222}\Pi_{02222} - R_{2222} + \Pi_{2122}^T\sigma\Pi_{2122} \tag{12.67c}$$

where

$$\begin{bmatrix} A_{2211} & A_{2212} \\ A_{2221} & A_{2222} \end{bmatrix} \triangleq \begin{bmatrix} v_1^T \\ v_2^T \end{bmatrix} A_{22} \begin{bmatrix} v_1 & v_2 \end{bmatrix} + \begin{bmatrix} \dot{v}_1^T v_1 & \dot{v}_1^T v_2 \\ \dot{v}_2^T v_1 & \dot{v}_2^T v_2 \end{bmatrix}$$
$$\begin{bmatrix} Q_{2211} & Q_{2212} \\ Q_{2212}^T & Q_{2222} \end{bmatrix} \triangleq \begin{bmatrix} v_1^T \\ v_2^T \end{bmatrix} Q_{22} \begin{bmatrix} v_1 & v_2 \end{bmatrix}$$
$$\begin{bmatrix} R_{2211} & R_{2212} \\ R_{2212}^T & R_{2222} \end{bmatrix} \triangleq \begin{bmatrix} v_1^T \\ v_2^T \end{bmatrix} R_{22} \begin{bmatrix} v_1 & v_2 \end{bmatrix}$$

Note that Π_{2121} cannot be determined uniquely from (12.67a) because it is not symmetric. However, additional constraints will be obtained later to determine Π_{2121} with (12.67a). Since $\operatorname{Im} u_1 = \operatorname{Im} F_2$, $Cu_1 = 0$ and $C(Au_1 - \dot{u}_1) \neq 0$. Since $R_{2211} = v_1^T u_2^T C^T V^{-1} C u_2 v_1$ and $\operatorname{Im} v_1 = \operatorname{Im} A_{21}$, R_{2211} is positive definite because

$$\begin{aligned} &A_{21}^T u_2^T C^T V^{-1} C u_2 A_{21} = (u_1^T A^T u_2 - \dot{u}_1^T u_2) u_2^T C^T V^{-1} C u_2 (u_2^T A u_1 - u_2^T \dot{u}_1) \\ &= (u_1^T A^T - \dot{u}_1^T)(I - u_1 u_1^T) C^T V^{-1} C (I - u_1 u_1^T)(A u_1 - \dot{u}_1) = (A u_1 - \dot{u}_1)^T C^T V^{-1} C (A u_1 - \dot{u}_1) > 0 \end{aligned}$$

Therefore, , Π_{2121} is invertible. Then, from (12.67b),

$$\Pi_{2122} = \sigma^{-1} \Pi_{2121}^{-T} (R_{2212} - A_{2221}^T \Pi_{02222}) \tag{12.68}$$

By substituting (12.68) into (12.67c) and using (12.67a),

$$\begin{aligned} -\dot{\Pi}_{02222} = &\Pi_{02222}(A_{2222} - A_{2221} R_{2211}^{-1} R_{2212}) + (A_{2222} - A_{2221} R_{2211}^{-1} R_{2212})^T \Pi_{02222} \\ &+ \Pi_{02222}(A_{2221} R_{2211}^{-1} A_{2221}^T - Q_{2222}) \Pi_{02222} - (R_{2222} - R_{2212}^T R_{2211}^{-1} R_{2212}) \end{aligned} \tag{12.69}$$

Therefore, the zeroth-order term Π_0 (12.43) can be obtained from (12.65) and (12.69). Part of the second-order term Π_2 (12.46) can be obtained from (12.63).

By substituting (12.63) into (12.35a), the equation becomes trivial. By substituting (12.63) into (12.51a),

$$0 = \Pi_{311} \sigma \Pi_{311} + \Pi_{212} A_{21} + A_{21}^T \Pi_{212}^T \tag{12.70}$$

By substituting (12.66) into (12.70),

$$0 = \Pi_{311} \sigma \Pi_{311} + \Pi_{2121} v_1^T A_{21} + A_{21}^T v_1 \Pi_{2121}^T \tag{12.71}$$

because $v_2^T A_{21} = 0$. Let

$$\Pi_{122} = \begin{bmatrix} v_1 & v_2 \end{bmatrix} \begin{bmatrix} \Pi_{12211} & \Pi_{12212} \\ \Pi_{12212}^T & \Pi_{12222} \end{bmatrix} \begin{bmatrix} v_1^T \\ v_2^T \end{bmatrix} \tag{12.72}$$

and

$$\Pi_{312} = \left[\begin{array}{cc} \Pi_{3121} & \Pi_{3122} \end{array}\right] \left[\begin{array}{c} v_1^T \\ v_2^T \end{array}\right] \tag{12.73}$$

By multiplying (12.35b) by $[\, v_1 \;\; v_2 \,]$ from the right and substituting (12.63), (12.66) and (12.72),

$$\Pi_{12211} = -(A_{21}^T v_1)^{-1} \Pi_{311} \sigma \Pi_{2121} \tag{12.74a}$$

$$\Pi_{12212} = -(A_{21}^T v_1)^{-1} \Pi_{311} \sigma \Pi_{2122} \tag{12.74b}$$

Note that $v_1^T A_{21}$ is invertible because $\operatorname{Im} A_{21} = \operatorname{Im} v_1$. Since Π_{12211} is symmetric,

$$(A_{21}^T v_1)^{-1} \Pi_{311} \sigma \Pi_{2121} = \Pi_{2121}^T \sigma \Pi_{311} (v_1^T A_{21})^{-1} \tag{12.75}$$

By combining (12.75) with (12.67a) and (12.71), Π_{2121} and Π_{311} can be determine uniquely. By multiplying (12.35c) by $[\, v_1 \;\; v_2 \,]^T$ from the left and $[\, v_1 \;\; v_2 \,]$ from the right and substituting (12.65), (12.66) (12.72) and (12.73),

$$\begin{aligned} 0 = {} & \Pi_{2121}^T \sigma \Pi_{3121} + \Pi_{3121}^T \sigma \Pi_{2121} + \Pi_{12211} A_{2211} + \Pi_{12212} A_{2221} + A_{2211}^T \Pi_{12211} + A_{2221}^T \Pi_{12212}^T \\ & + \dot{\Pi}_{12211} \end{aligned} \tag{12.76a}$$

$$\begin{aligned} 0 = {} & \Pi_{2121}^T \sigma \Pi_{3122} + \Pi_{3121}^T \sigma \Pi_{2122} + A_{2221}^T \Pi_{12222} + A_{2211}^T \Pi_{12212} + \Pi_{12211} A_{2212} + \Pi_{12212} A_{2222} \\ & - \Pi_{12211} Q_{2212} \Pi_{02222} - \Pi_{12212} Q_{2222} \Pi_{02222} + \dot{\Pi}_{12212} \end{aligned} \tag{12.76b}$$

$$\begin{aligned} -\dot{\Pi}_{12222} = {} & \Pi_{12222}(A_{2222} - Q_{2222}\Pi_{02222}) + (A_{2222} - Q_{2222}\Pi_{02222})^T \Pi_{12222} \\ & + \Pi_{12212}^T (A_{2212} - Q_{2212}\Pi_{02222}) + (A_{2212} - Q_{2212}\Pi_{02222})^T \Pi_{12212} \\ & + \Pi_{2122}^T \sigma \Pi_{3122} + \Pi_{3122}^T \sigma \Pi_{2122} \end{aligned} \tag{12.76c}$$

From (12.76b),

$$\begin{aligned} \Pi_{3122} = {} & -\sigma^{-1} \Pi_{2121}^{-T} (\Pi_{3121}^T \sigma \Pi_{2122} + A_{2221}^T \Pi_{12222} + A_{2211}^T \Pi_{12212} + \Pi_{12211} A_{2212} + \Pi_{12212} A_{2222} \\ & - \Pi_{12211} Q_{2212} \Pi_{02222} - \Pi_{12212} Q_{2222} \Pi_{02222} + \dot{\Pi}_{12212}) \end{aligned} \tag{12.77}$$

By substituting (12.77) into (12.76c) and using (12.76a),

$$
\begin{aligned}
-\dot{\Pi}_{12222} &= \Pi_{12222}(A_{2222} - Q_{2222}\Pi_{02222} - A_{2221}\Pi_{2121}^{-1}\Pi_{2122}) \\
&\quad + (A_{2222} - Q_{2222}\Pi_{02222} - A_{2221}\Pi_{2121}^{-1}\Pi_{2122})^T\Pi_{12222} \\
&\quad + \Pi_{12212}^T(A_{2212} - Q_{2212}\Pi_{02222}) + (A_{2212} - Q_{2212}\Pi_{02222})^T\Pi_{12212} \\
&\quad + \Pi_{2122}^T\Pi_{2121}^{-T}(\Pi_{12211}A_{2211} + A_{2211}^T\Pi_{12211} + \Pi_{12212}A_{2221} + A_{2221}^T\Pi_{12212}^T + \dot{\Pi}_{12211})\Pi_{2121}^{-1}\Pi_{2122} \\
&\quad - \Pi_{2122}^T\Pi_{2121}^{-T}(\Pi_{12211}A_{2212} - \Pi_{12211}Q_{2212}\Pi_{02222} + \Pi_{12212}A_{2222} - \Pi_{12212}Q_{2222}\Pi_{02222} \\
&\qquad\qquad + A_{2211}^T\Pi_{12212} + A_{2221}^T\Pi_{12222} + \dot{\Pi}_{12212}) \\
&\quad - (\Pi_{12211}A_{2212} - \Pi_{12211}Q_{2212}\Pi_{02222} + \Pi_{12212}A_{2222} - \Pi_{12212}Q_{2222}\Pi_{02222} + A_{2211}^T\Pi_{12212} \\
&\qquad + A_{2221}^T\Pi_{12222} + \dot{\Pi}_{12212})^T\Pi_{2121}^{-1}\Pi_{2122}
\end{aligned} \tag{12.78}
$$

Therefore, part of the second-order term Π_2 (12.46) and part of the third-order term Π_3 (12.48) can be obtained by solving (12.67a), (12.71) and (12.75) and using (12.66) and (12.68). The first-order term Π_1 (12.44) can be obtained from (12.72), (12.74) and (12.78). Part of the third-order term Π_3 (12.48) can be obtained from (12.73), (12.76a) and (12.77). The same procedure can be done for the higher order terms if needed, i.e., obtaining Π_{222} and Π_{322}.

Therefore, Π can be expressed as

$$
\begin{aligned}
\Pi &= \begin{bmatrix} u_1 & u_2 \end{bmatrix} \begin{bmatrix} \gamma^{3/4}\Pi_{311} & \gamma^{1/2}\Pi_{212} \\ \gamma^{1/2}\Pi_{212}^T & \begin{bmatrix} v_1 & v_2 \end{bmatrix} \begin{bmatrix} \gamma^{1/4}\Pi_{12211} & \gamma^{1/4}\Pi_{12212} \\ \gamma^{1/4}\Pi_{12212}^T & \Pi_{02222} + \gamma^{1/4}\Pi_{12222} \end{bmatrix} \begin{bmatrix} v_1^T \\ v_2^T \end{bmatrix} \end{bmatrix} \begin{bmatrix} u_1^T \\ u_2^T \end{bmatrix} + \cdots \\
&= \begin{bmatrix} u_1 & u_2 v_1 & u_2 v_2 \end{bmatrix} \begin{bmatrix} \gamma^{3/4}\Pi_{311} & \gamma^{1/2}\Pi_{2121} & \gamma^{1/2}\Pi_{2122} \\ \gamma^{1/2}\Pi_{2121}^T & \gamma^{1/4}\Pi_{12211} & \gamma^{1/4}\Pi_{12212} \\ \gamma^{1/2}\Pi_{2122}^T & \gamma^{1/4}\Pi_{12212}^T & \Pi_{02222} + \gamma^{1/4}\Pi_{12222} \end{bmatrix} \begin{bmatrix} u_1^T \\ v_1^T u_2^T \\ v_2^T u_2^T \end{bmatrix} + \cdots
\end{aligned}
$$

Note that only the lowest-order term for each element is kept for simplicity.

Remark 11. By multiplying (12.64) by u_2 from the left and substituting $\dot{u}_2^T u_1 = -u_2^T \dot{u}_1$,

$$\Pi_0(Au_1 - \dot{u}_1) = 0$$

Since $\operatorname{Im} u_1 = \operatorname{Im} F_2$, $\Pi_0(AF_2 - \dot{F}_2) = 0$. Therefore, $\operatorname{Ker}\Pi_0$ contains F_2 and AF_2.

Remark 12. The initial condition of Π_{02222} and Π_{12222} can be obtained by using a fast time scale similarly as Lemma 12.4.

12.7.4 Proof of Lemma 12.7

By using Lemma 12.5 and matrix inversion lemma,

$$P = \Pi^{-1} = \begin{bmatrix} u_1 & u_2 v_1 & u_2 v_2 \end{bmatrix} \begin{bmatrix} \gamma^{3/4}\Pi_{311} & \gamma^{1/2}\Pi_{2121} & \gamma^{1/2}\Pi_{2122} \\ \gamma^{1/2}\Pi_{2121}^T & \gamma^{1/4}\Pi_{12211} & \gamma^{1/4}\Pi_{12212} \\ \gamma^{1/2}\Pi_{2122}^T & \gamma^{1/4}\Pi_{12212}^T & \Pi_{02222} \end{bmatrix}^{-1} \begin{bmatrix} u_1^T \\ v_1^T u_2^T \\ v_2^T u_2^T \end{bmatrix} + \cdots$$

$$= \begin{bmatrix} \begin{bmatrix} u_1 & u_2 v_1 \end{bmatrix} & u_2 v_2 \end{bmatrix} \begin{bmatrix} \bar{\Pi}_{11} & \bar{\Pi}_{12} \\ \bar{\Pi}_{12}^T & \Pi_{02222}^{-1} \end{bmatrix} \begin{bmatrix} \begin{bmatrix} u_1^T \\ v_1^T u_2^T \end{bmatrix} \\ v_2^T u_2^T \end{bmatrix} + \cdots$$

where

$$\bar{\Pi}_{11} = \begin{bmatrix} \gamma^{-3/4}(\Pi_{311} - \Pi_{2121}\Pi_{12211}^{-1}\Pi_{2121}^T)^{-1} & -\gamma^{-1/2}\Pi_{311}^{-1}\Pi_{2121}(\Pi_{12211} - \Pi_{2121}^T\Pi_{311}^{-1}\Pi_{2121})^{-1} \\ -\gamma^{-1/2}(\Pi_{12211} - \Pi_{2121}^T\Pi_{311}^{-1}\Pi_{2121})^{-1}\Pi_{2121}^T\Pi_{311}^{-1} & \gamma^{-1/4}(\Pi_{12211} - \Pi_{2121}^T\Pi_{311}^{-1}\Pi_{2121})^{-1} \end{bmatrix}$$

$$\bar{\Pi}_{12} = \begin{bmatrix} \gamma^{-1/4}[\Pi_{311}^{-1}\Pi_{2121}(\Pi_{12211} - \Pi_{2121}^T\Pi_{311}^{-1}\Pi_{2121})^{-1}\Pi_{12212} - (\Pi_{311} - \Pi_{2121}\Pi_{12211}^{-1}\Pi_{2121}^T)^{-1}\Pi_{2122}] \\ (\Pi_{12211} - \Pi_{2121}^T\Pi_{311}^{-1}\Pi_{2121})^{-1}(\Pi_{2121}^T\Pi_{311}^{-1}\Pi_{2122} - \Pi_{12212}) \end{bmatrix}$$

Note that Π_{311}, Π_{12211} and Π_{02222} are invertible from Appendix 12.7.3. By using (12.74a) and (12.71),

$$\Pi_{12211} - \Pi_{2121}^T\Pi_{311}^{-1}\Pi_{2121} = \Pi_{2121}^T\Pi_{311}^{-1}(A_{21}^T v_1)\Pi_{2121}^T(v_1^T A_{21})^{-1}$$

Since Π_{2121} is invertible, $\Pi_{12211} - \Pi_{2121}^T\Pi_{311}^{-1}\Pi_{2121}$ is invertible. By using matrix inversion lemma,

$$(\Pi_{311} - \Pi_{2121}\Pi_{12211}^{-1}\Pi_{2121}^T)^{-1} = \Pi_{311}^{-1} + \Pi_{311}^{-1}\Pi_{2121}(\Pi_{12211} - \Pi_{2121}^T\Pi_{311}^{-1}\Pi_{2121})^{-1}\Pi_{2121}^T\Pi_{311}^{-1}$$

Then, $\Pi_{311} - \Pi_{2121}\Pi_{12211}^{-1}\Pi_{2121}^T$ is also invertible.

By using matrix inversion lemma and substituting (12.74) and (12.75), the coefficient of the $\gamma^{-1/4}$ term in $(1,1)$-element of $\bar{\Pi}_{12}$ is zero.

$$\begin{aligned} &\Pi_{311}^{-1}\Pi_{2121}(\Pi_{12211} - \Pi_{2121}^T\Pi_{311}^{-1}\Pi_{2121})^{-1}\Pi_{12212} - (\Pi_{311} - \Pi_{2121}\Pi_{12211}^{-1}\Pi_{2121}^T)^{-1}\Pi_{2122} \\ =&\Pi_{311}^{-1}\Pi_{2121}(\Pi_{12211} - \Pi_{2121}^T\Pi_{311}^{-1}\Pi_{2121})^{-1}(\Pi_{12212} - \Pi_{2121}^T\Pi_{311}^{-1}\Pi_{2122}) - \Pi_{311}^{-1}\Pi_{2122} \\ =&0 \end{aligned}$$

Then, $\bar{\Pi}_{12}$ remains finite in the limit.

Chapter 13

Conclusion

Analytical redundancy is a viable approach to vehicle health monitoring. The vehicle health monitoring system including residual generator and residual processor is evaluated in real-time on a PATH Buick LeSabre at Crow's Landing. The health monitoring system can detect and identify vehicle actuator and sensor failures with probability under various disturbances and uncertainties including sensor noise, road noise, system parameter variations, unmodeled dynamics and nonlinearities. The design as presented is intended to be packaged as a module to be used by the vehicle health management system under development by the UC Berkeley team.

Acknowledgement

We would like to thank Xiao-Yun Lu for helping us to carry out the experiments at Crow's Landing and Paul Kretz for helping us to develop the input/output interface between our laptop and PATH computer. In addition, we would like to thank Gurprit Hansra and Hassan Aboukhadijeh at California Department of Transportation, and Dan Empey and Chin-Woo Tan from PATH for their guidance and support.

Appendix A

Vehicle Dynamics Data

A.1 Linear Vehicle Model at 20 m/s

The reduced-order longitudinal model derived when the vehicle is traveling at 20 m/s is

$$\dot{x} = Ax + Bu$$

$$y = Cx$$

where

$$A = \left[\begin{array}{rrrrrrrrrr}
-9.1179 & -0.0737 & 0 & 0 & 0 & 0 & 0 & 0 & 0 & 0 \\
378.1792 & -52.6035 & 542.0456 & -0.6104 & -36160.7905 & 38278.6530 & -273.5986 & 18078.5219 & 0 & -0.0549 \\
0 & 0.0539 & -0.5598 & 0.0006 & 27.1410 & -38.2600 & 0.3007 & -17.8643 & 0.1238 & -0.0019 \\
0 & -0.0001 & 0.0006 & -0.0000 & -448.3132 & -155.9259 & 20.0007 & 112.0907 & 112.0683 & 0.0000 \\
0 & 0 & 0.0011 & 1.0000 & 0 & -20.0010 & 0 & 0 & 0 & 0 \\
0 & 0 & 0 & 0 & 0 & 0 & 1.0000 & 0 & 0 & 0 \\
0 & -0.0257 & 0.2633 & -0.0003 & -106.5309 & -540.7918 & -0.1329 & -62.1835 & 117.3693 & 0.0009 \\
0 & 0 & 0 & 0 & 66.3437 & -70.2314 & 0 & -39.2622 & 0 & 0 \\
0 & 0 & 0 & 0 & 48.6827 & 85.4589 & 0 & 0 & -32.6411 & 0 \\
0 & 0 & 0 & 0 & 0 & 0 & 0 & 0 & 0 & -1.2500
\end{array}\right]$$

$$B = \begin{bmatrix} 2.6048 & 0 \\ 0 & 0 \\ 0 & 0 \\ 0 & 0 \\ 0 & 0 \\ 0 & 0 \\ 0 & 0 \\ 0 & 0 \\ 0 & 0 \\ 0 & 1.2500 \end{bmatrix}$$

$$C = \left[\begin{matrix} 19.3272 & 0 & 0 & 0 & 0 \\ 0 & 1.0000 & 0 & 0 & 0 \\ 0 & 0.0539 & -0.5598 & 0.0006 & 27.1410 \\ 0 & 0.0372 & 6.3838 & -0.0072 & -425.8747 \\ 0 & 0 & 6.5305 & -0.0074 & -426.4547 \end{matrix}\right.$$
$$\left.\begin{matrix} 0 & 0 & 0 & 0 & 0 \\ 0 & 0 & 0 & 0 & 0 \\ -38.2600 & 0.3007 & -17.8643 & 0.1238 & -0.0019 \\ 450.8173 & -3.2222 & 212.9153 & 0 & -0.0006 \\ -748.6173 & -3.2294 & 0 & 213.1967 & -0.0010 \end{matrix}\right]$$

The actuator fault directions are

$$F_{u_\alpha} = \begin{bmatrix} 2.6048 \\ 0 \\ 0 \\ 0 \\ 0 \\ 0 \\ 0 \\ 0 \\ 0 \\ 0 \end{bmatrix}, \quad F_{u_{T_b}} = \begin{bmatrix} 0 \\ 0 \\ 0 \\ 0 \\ 0 \\ 0 \\ 0 \\ 0 \\ 0 \\ 1.2500 \end{bmatrix}$$

The sensor fault directions are

$$F_{y_{m_p}} = \begin{bmatrix} 0.0517 & -0.4718 \\ 0 & 19.5672 \\ 0 & 0 \\ 0 & 0 \\ 0 & 0 \\ 0 & 0 \\ 0 & 0 \\ 0 & 0 \\ 0 & 0 \\ 0 & 0 \end{bmatrix}, \quad F_{y_{w_e}} = \begin{bmatrix} 0 & -0.0737 \\ 1.0000 & -55.7626 \\ 0.0010 & -0.0000 \\ -0.0000 & -0.0404 \\ 0.0068 & 0.0217 \\ -0.0011 & -0.0006 \\ -0.0006 & 0.0064 \\ 0.0157 & -0.0889 \\ 0.0098 & -0.0805 \\ 0.0000 & -0.0000 \end{bmatrix}, \quad F_{y_{a_x}} = \begin{bmatrix} 0 & -0.0000 \\ 0.0000 & -0.0000 \\ -0.0171 & 1.0000 \\ 0.0000 & 0.3660 \\ -0.1198 & -0.3738 \\ 0.0187 & 0.0011 \\ 0.0108 & 0.3736 \\ -0.2784 & 1.6743 \\ -0.1732 & 1.4217 \\ -0.0002 & 0.0003 \end{bmatrix}$$

$$F_{y_{\bar{w}_f}} = \begin{bmatrix} 0 & -0.0000 \\ 0.0000 & 84.9095 \\ -0.0012 & 0.0000 \\ 0.0000 & 0.5530 \\ -0.0100 & -0.0425 \\ 0.0021 & 0.0008 \\ 0.0008 & -0.3221 \\ -0.0199 & -0.0364 \\ -0.0126 & 0.1033 \\ -0.0000 & 0.0000 \end{bmatrix}, \quad F_{y_{\bar{w}_r}} = \begin{bmatrix} 0 & 0.0000 \\ -0.0000 & 0.0000 \\ 0.0001 & -0.0000 \\ -0.0000 & 0.5226 \\ 0.0001 & 0.0187 \\ -0.0009 & -0.0001 \\ -0.0001 & 0.5477 \\ 0.0021 & -0.0127 \\ 0.0015 & -0.1268 \\ 0.0000 & -0.0000 \end{bmatrix}$$

The modified brake actuator fault direction is

$$F_{u_{T_b}} = \begin{bmatrix} 0 & 0 \\ 0 & -0.0549 \\ 0 & -0.0019 \\ 0 & 0.0000 \\ 0 & 0 \\ 0 & 0 \\ 0 & 0.0009 \\ 0 & 0 \\ 0 & 0 \\ 1.2500 & 0 \end{bmatrix}$$

The reduced-order lateral model derived when the vehicle is traveling at 20 m/s is

$$\dot{x} = Ax + Bu$$

$$y = Cx + Du$$

where

$$A = \begin{bmatrix} -8.3608 & 0.0006 & -4.2079 & -19.4511 & 0 & 0 \\ 0 & 0 & 1.0000 & -0.0011 & 0 & 0 \\ -22.7746 & -841.1438 & -11.4010 & 1.4370 & 285.9465 & 285.9420 \\ 0.2925 & 0.3148 & 0.1065 & -8.4241 & -0.2052 & -0.0490 \\ 0 & 49.7578 & 0 & 0 & -39.2622 & 0 \\ 0 & 36.5121 & 0 & 0 & 0 & -32.6411 \end{bmatrix}$$

$$B = \begin{bmatrix} 100.6752 \\ 0 \\ 274.6695 \\ 56.3547 \\ 0 \\ 0 \end{bmatrix}$$

$$C = \begin{bmatrix} -8.3608 & 0.0006 & -4.2079 & -19.4511 & 0 & 0 \\ 0 & 0 & 0 & 1.0000 & 0 & 0 \\ 0 & -338.4411 & -0.0058 & -5.0733 & 225.6041 & 0 \\ 0 & -319.8411 & -0.0056 & -4.8979 & 0 & 213.1967 \end{bmatrix}$$

$$D = \begin{bmatrix} 100.6752 \\ 0 \\ 0 \\ 0 \end{bmatrix}$$

The steering actuator fault direction is

$$F_{u_\gamma} = \begin{bmatrix} -9.6077 & 0.0000 \\ 0.0002 & 4.8354 \\ -4.8354 & 0.7967 \\ 0.0000 & 59.6801 \\ 0.0002 & -0.0030 \\ 0.0002 & -0.0016 \end{bmatrix}$$

The sensor fault directions are

$$F_{y_{a_y}} = \begin{bmatrix} -0.0954 & 1.0000 \\ 0.0000 & -0.0480 \\ -0.0480 & 2.7204 \\ 0.0000 & -0.0330 \\ 0.0000 & 0.0000 \\ 0.0000 & 0.0000 \end{bmatrix}, \quad F_{y_r} = \begin{bmatrix} -1.8563 & 0.0000 \\ -0.0124 & -0.9354 \\ -0.9342 & 67.1423 \\ 1.0000 & -9.0716 \\ 0.0039 & -0.7690 \\ 0.0044 & -0.5951 \end{bmatrix},$$

$$F_{y_{\tilde{\omega}_f}} = \begin{bmatrix} -0.0000 & -0.0000 \\ -0.0012 & -0.0000 \\ -0.0000 & 1.2472 \\ 0.0000 & -0.0008 \\ 0.0026 & -0.1630 \\ -0.0018 & 0.0151 \end{bmatrix}, \quad F_{y_{\tilde{\omega}_r}} = \begin{bmatrix} -0.0000 & 0.0000 \\ -0.0013 & -0.0000 \\ -0.0000 & 1.3197 \\ -0.0000 & -0.0001 \\ -0.0019 & 0.0117 \\ 0.0028 & -0.1372 \end{bmatrix}$$

The modified reduced-order lateral model derived when the vehicle is traveling at 20 m/s is

$$\dot{x} = Ax + Bu$$

$$y = Cx + Du$$

where

$$A = \begin{bmatrix} -8.3608 & 0.0006 & -3.3663 & -19.4511 & 0 & 0 \\ 0 & 0 & 0 & -0.0011 & 0 & 0 \\ -22.7746 & -841.1438 & -9.1208 & 1.4370 & 285.9465 & 285.9420 \\ 0.2925 & 0.3148 & 0.1065 & -8.4241 & -0.2052 & -0.0490 \\ 0 & 49.7578 & 0 & 0 & -39.2622 & 0 \\ 0 & 36.5121 & 0 & 0 & 0 & -32.6411 \end{bmatrix}$$

$$B = \begin{bmatrix} 398.0182 \\ 0 \\ 511.0140 \\ 52.4230 \\ 0 \\ 0 \end{bmatrix}$$

$$C = \begin{bmatrix} --8.3608 & 0.0006 & -3.3663 & -19.4511 & 0 & 0 \\ 0 & 0 & 0 & 1.0000 & 0 & 0 \\ 0 & -338.4411 & -0.0058 & -5.0733 & 225.6041 & 0 \\ 0 & -319.8411 & -0.0056 & -4.8979 & 0 & 213.1967 \end{bmatrix}$$

$$D = \begin{bmatrix} 234.1285 \\ 0 \\ 0 \\ 0 \end{bmatrix}$$

The steering actuator fault direction is

$$F_{u_\gamma} = \begin{bmatrix} -24.0967 & 163.8898 \\ 0.0005 & -0.0000 \\ -9.7020 & -126.1342 \\ -0.0000 & 60.5048 \\ 0.0005 & -0.0054 \\ 0.0005 & -0.0024 \end{bmatrix}$$

The sensor fault directions are

$$F_{y_{a_y}} = \begin{bmatrix} -0.1029 & 1.0000 \\ 0.0000 & 0.0000 \\ -0.0414 & 2.7214 \\ -0.0000 & -0.0345 \\ 0.0000 & 0.0000 \\ 0.0000 & 0.0000 \end{bmatrix}, \ F_{y_r} = \begin{bmatrix} -2.0019 & 0.0000 \\ -0.0124 & -0.0011 \\ -0.8060 & 67.1617 \\ 1.0000 & -9.1005 \\ 0.0039 & -0.7691 \\ 0.0044 & -0.5953 \end{bmatrix},$$

$$F_{y_{\tilde{w}_f}} = \begin{bmatrix} -0.0000 & 0.0000 \\ -0.0012 & 0.0000 \\ -0.0000 & 1.2472 \\ -0.0000 & -0.0008 \\ 0.0026 & -0.1630 \\ -0.0018 & 0.0151 \end{bmatrix}, \ F_{y_{\tilde{w}_r}} = \begin{bmatrix} -0.0000 & -0.0000 \\ -0.0013 & -0.0000 \\ -0.0000 & 1.3197 \\ 0.0000 & -0.0001 \\ -0.0019 & 0.0117 \\ 0.0028 & -0.1372 \end{bmatrix}$$

A.2 Linear Vehicle Model at 24 m/s

The reduced-order longitudinal model derived when the vehicle is traveling at 24 m/s is

$$\dot{x} = Ax + Bu$$

$$y = Cx$$

where

$$A = \begin{bmatrix} -10.4692 & -0.1177 & 0 & 0 & 0 \\ 327.7406 & -53.2410 & 552.4915 & -0.7238 & -44121.7763 \\ 0 & 0.0550 & -0.5721 & 0.0007 & 43.3440 \\ 0 & -0.0001 & 0.0007 & -0.0000 & -448.3575 \\ 0 & 0 & 0.0013 & 1.0000 & 0 \\ 0 & 0 & 0 & 0 & 0 \\ 0 & -0.0263 & 0.2684 & -0.0004 & -114.1535 \\ 0 & 0 & 0 & 0 & 66.3436 \\ 0 & 0 & 0 & 0 & 48.6827 \\ 0 & 0 & 0 & 0 & 0 \end{bmatrix}$$

$$\begin{bmatrix} 0 & 0 & 0 & 0 & 0 \\ 46710.0274 & -278.9203 & 22058.6614 & 0 & -0.0672 \\ -46.7168 & 0.3150 & -21.8174 & 0.1475 & -0.0019 \\ -155.8232 & 23.9996 & 112.0991 & 112.0787 & 0.0000 \\ -24.0000 & 0 & 0 & 0 & 0 \\ 0 & 1.0000 & 0 & 0 & 0 \\ -536.7500 & -0.1355 & -60.2901 & 117.3615 & 0.0009 \\ -70.2379 & 0 & -39.2621 & 0 & 0 \\ 85.4543 & 0 & 0 & -32.6411 & 0 \\ 0 & 0 & 0 & 0 & -1.2500 \end{bmatrix}$$

$$B = \begin{bmatrix} 2.6100 & 0 \\ 0 & 0 \\ 0 & 0 \\ 0 & 0 \\ 0 & 0 \\ 0 & 0 \\ 0 & 0 \\ 0 & 0 \\ 0 & 0 \\ 0 & 1.2500 \end{bmatrix}$$

$$C = \begin{bmatrix} 19.3272 & 0 & 0 & 0 & 0 \\ 0 & 1.0000 & 0 & 0 & 0 \\ 0 & 0.0550 & -0.5721 & 0.0007 & 43.3440 \\ 0 & 0.0456 & 6.2989 & -0.0083 & -503.0252 \\ 0 & 0 & 6.5316 & -0.0086 & -511.6989 \end{bmatrix}$$

$$\begin{bmatrix} 0 & 0 & 0 & 0 & 0 \\ 0 & 0 & 0 & 0 & 0 \\ -46.7168 & 0.3150 & -21.8174 & 0.1238 & -0.0019 \\ 532.5334 & -3.1799 & 251.4872 & 0 & -0.0008 \\ -898.2125 & -3.2312 & 0 & 255.8137 & -0.0013 \end{bmatrix}$$

The actuator fault directions are

$$F_{u_\alpha} = \begin{bmatrix} 2.6100 \\ 0 \\ 0 \\ 0 \\ 0 \\ 0 \\ 0 \\ 0 \\ 0 \\ 0 \end{bmatrix}, \quad F_{u_{T_b}} = \begin{bmatrix} 0 \\ 0 \\ 0 \\ 0 \\ 0 \\ 0 \\ 0 \\ 0 \\ 0 \\ 1.2500 \end{bmatrix}$$

The sensor fault directions are

$$F_{y_{mp}} = \begin{bmatrix} 0.0517 & -0.5417 \\ 0 & 16.9575 \\ 0 & 0 \\ 0 & 0 \\ 0 & 0 \\ 0 & 0 \\ 0 & 0 \\ 0 & 0 \\ 0 & 0 \\ 0 & 0 \end{bmatrix}, F_{y_{we}} = \begin{bmatrix} 0 & -0.1177 \\ 1.0000 & -57.2411 \\ 0.6802 & -0.0000 \\ -0.0006 & -29.3339 \\ 0.0131 & 0.0031 \\ -0.0001 & -0.9488 \\ -0.9488 & -1.4008 \\ -0.0027 & 0.9856 \\ -0.0035 & 0.7435 \\ 0.0452 & -0.0564 \end{bmatrix}, F_{y_{a_x}} = \begin{bmatrix} 0 & 0.0000 \\ -0.0000 & 0.0000 \\ -11.5368 & 1.0000 \\ 0.0096 & 497.1906 \\ -0.2217 & -0.0415 \\ 0.0015 & 16.0924 \\ 16.0925 & 23.4975 \\ 0.0458 & -16.6123 \\ 0.0596 & -12.6107 \\ -0.7659 & 0.9573 \end{bmatrix}$$

$$F_{y_{\bar{w}_f}} = \begin{bmatrix} 0 & -0.0000 \\ 0.0000 & 87.7128 \\ -1.0008 & -0.0000 \\ 0.0008 & 43.5788 \\ -0.0203 & -0.0190 \\ 0.0008 & 1.3961 \\ 1.3961 & 1.8008 \\ 0.0044 & -1.5758 \\ 0.0053 & -1.0948 \\ -0.0664 & 0.0831 \end{bmatrix}, F_{y_{\bar{w}_r}} = \begin{bmatrix} 0 & -0.0000 \\ 0.0000 & 0.0000 \\ 0.0067 & -0.0000 \\ -0.0000 & 0.1513 \\ -0.0005 & 0.0160 \\ -0.0007 & -0.0093 \\ -0.0093 & 0.4433 \\ 0.0000 & 0.0090 \\ 0.0002 & -0.0899 \\ 0.0004 & -0.0006 \end{bmatrix}$$

The modified brake actuator fault direction is

$$F_{u_{T_b}} = \begin{bmatrix} 0 & 0 \\ 0 & -0.0672 \\ 0 & -0.0019 \\ 0 & 0.0000 \\ 0 & 0 \\ 0 & 0 \\ 0 & 0.0009 \\ 0 & 0 \\ 0 & 0 \\ 1.2500 & 0 \end{bmatrix}$$

Appendix B

Fault Detection Filter Design Data

B.1 Fault Detection Filter Set No. 1

For the unknown input observer that detects the engine speed sensor fault,

$$
P = \left[\begin{array}{rrrrrr}
1350.3961 & 0.8773 & -0.0314 & -0.0002 & -0.0006 & -0.0000 \\
0.8773 & 5.8668 & -2.8248 & 0.6544 & -0.0557 & 0.0257 \\
0.0109 & -2.8069 & 1331282.9651 & -902.0962 & 255849.7988 & -166.3382 \\
-0.0002 & 0.6556 & -902.3711 & 135375.0589 & -33.8725 & 4381.7814 \\
0.0002 & -0.0554 & 25584.9799 & -33.8672 & 491.7016 & -3.7318 \\
-0.0000 & 0.0257 & -166.3452 & 4381.7813 & -3.7319 & 141.8424 \\
-0.0152 & 4.0639 & -1856976.7902 & 8035.9323 & -35688.7429 & 451.3924 \\
-0.0000 & -0.0176 & -5289.7022 & -4518.5004 & -101.1068 & -145.7055 \\
-0.0001 & 0.0250 & -6881.4187 & -3427.5537 & -131.8300 & -110.2308 \\
0.0007 & -0.1905 & 8.8376 & 182.6973 & 1698.4032 & -3.1905
\end{array}\right.
$$

$$
\left.\begin{array}{rrrr}
0.0437 & 0.0001 & 0.0002 & -0.0021 \\
4.0901 & -0.0174 & 0.0250 & -0.1917 \\
-1856976.7777 & -5289.7133 & -6881.4257 & 88375.8659 \\
8036.3158 & -4518.4993 & -3427.5533 & 182.6791 \\
-35689.7427 & -101.1070 & -131.8301 & 1698.4033 \\
451.4023 & -145.7055 & -110.2308 & -3.1910 \\
2590594.7134 & 7152.1045 & 9426.9054 & -123261.3718 \\
7152.0890 & 172.0752 & 141.9931 & -359.2548 \\
9426.8972 & 141.9931 & 122.5893 & -462.9663 \\
-123261.3702 & -3.5926 & -462.9667 & 5867.1766
\end{array}\right]
$$

$$
L = \left[\begin{array}{rrrrr}
26099.3883 & 0.8773 & 0.0512 & 0.0380 & 0.0082 \\
16.9551 & 5.8668 & -0.0004 & 6.7545 & -19.8160 \\
0.2101 & -2.8069 & -115554.4186 & 1794.9442 & -7332.2410 \\
-0.0046 & 0.6556 & -1049548.0051 & 11817831.2556 & -4828272.2753 \\
0.0040 & -0.0554 & -2207.9335 & -109.8110 & 448.6574 \\
-0.0002 & 0.0257 & -3384.9513 & 38250.6225 & -156276.0811 \\
-0.2932 & 4.0639 & 155926.0255 & 56663.5647 & -231504.3714 \\
-0.0007 & -0.0176 & 3967.4685 & -39483.7585 & 161314.1750 \\
-0.0010 & 0.0250 & 3260.0915 & -29971.6775 & 122451.7627 \\
0.0139 & -0.1905 & -7859.1627 & 2236.8301 & -9138.6951
\end{array}\right]
$$

$$\hat{H} = \begin{bmatrix} 0 & 0 & 0 & 0 & 0 \\ 0 & 1.0000 & -0.0000 & -0.0000 & 0.0000 \\ 0 & -0.0000 & -0.0000 & -0.0000 & -0.0000 \\ 0 & -0.0000 & -0.0000 & 0.9435 & 0.2309 \\ 0 & 0.0000 & -0.0000 & 0.2309 & 0.0565 \end{bmatrix}$$

The system matrices of the reduced-order unknown input observer that detects the engine speed sensor fault are

$$A_r = \begin{bmatrix} -2.6112 & -13.6803 & -0.2067 & -0.1206 & -0.0183 & -0.0030 & -0.0000 \\ 20.3806 & -10.9582 & -0.7697 & -0.4295 & -0.0628 & -0.0102 & -0.0000 \\ -32.7359 & -20.4715 & -5.0764 & -4.4745 & -0.7705 & -0.1241 & -0.0005 \\ 133.7180 & 182.1011 & 4.2746 & -1.8293 & -0.8600 & -0.1396 & -0.0006 \\ 960.2666 & 1181.2292 & 46.4167 & 14.4348 & -4.5592 & -2.0047 & -0.0082 \\ 38277.7073 & 46879.1449 & 1782.9267 & 571.5788 & 102.7921 & -84.9319 & 0.1250 \\ -21.9061 & -27.7164 & -1.0695 & -0.2475 & 0.0475 & 0.0410 & -1.2499 \end{bmatrix}$$

$$B_r = \begin{bmatrix} -0.0000 & 0.0000 & -0.0014 & -0.0046 & 0.0000 & -0.0034 & 0.0040 \\ -0.0000 & -0.0000 & -0.0052 & 0.0002 & 0.0000 & -0.0000 & 0.0036 \\ -0.0000 & 0.0002 & -0.0390 & -0.0669 & 0.0000 & -0.0561 & -0.1214 \\ -0.0000 & -0.0006 & -0.0327 & 0.0357 & 0.0000 & 0.0206 & 0.2972 \\ -0.0000 & 0.0024 & -0.4472 & -0.1386 & 0.0001 & -0.1654 & 0.3921 \\ -0.0000 & -0.0007 & -16.9515 & -5.8652 & 0.0003 & -6.7523 & 19.8120 \\ -0.0000 & -1.2491 & 0.0083 & 0.0046 & 0.0150 & 0.0043 & -0.0253 \end{bmatrix}$$

$$C_r = \begin{bmatrix} 0 & 0 & 0 & 0 & 0 & 0 & 0 \\ 0.0001 & 0.0003 & 0.0023 & 0.0019 & 0.0264 & 0.9996 & -0.0005 \\ -0.0000 & -0.0000 & -0.0000 & -0.0000 & -0.0000 & 0.0000 & -0.0000 \\ 446.2229 & 546.4967 & 20.7866 & 6.6644 & 1.2155 & -0.2549 & 0.0011 \\ 109.2189 & 133.7622 & 5.0878 & 1.6312 & 0.2975 & -0.0624 & 0.0003 \end{bmatrix}$$

$$D_r = \begin{bmatrix} 0 & 0 & 0 & 0 & 0 & 0 & 0 \\ 0 & 0 & 0 & 1.0000 & -0.0000 & -0.0000 & 0.0000 \\ 0 & 0 & 0 & -0.0000 & -0.0000 & -0.0000 & -0.0000 \\ 0 & 0 & 0 & -0.0000 & -0.0000 & 0.9435 & 0.2309 \\ 0 & 0 & 0 & 0.0000 & -0.0000 & 0.2309 & 0.0565 \end{bmatrix}$$

For the unknown input observer that detects the longitudinal accelerometer fault,

$$P = \begin{bmatrix} 1350.8879 & 266.5854 & -0.0262 & 136.1869 & -0.0151 & 4.4049 \\ 266.5896 & 170262.8626 & 6508.9493 & 82334.9066 & 116.7117 & 2662.1720 \\ -0.0260 & 6508.9882 & 21565.8418 & -5005.6858 & 429.3945 & -213.0742 \\ 136.1887 & 82334.8973 & -5007.0999 & 43838.5483 & -104.0390 & 1433.1659 \\ -0.0151 & 116.7125 & 429.3825 & -104.3586 & 8.5587 & -4.3975 \\ 4.4049 & 2662.1716 & -213.1327 & 1433.1652 & -4.3988 & 47.0093 \\ 6.5408 & -5153.6161 & -25211.8273 & 7446.3521 & -502.2644 & 295.7731 \\ -4.5756 & -2792.8924 & 384.8176 & -1545.7284 & 7.8439 & -51.2852 \\ -3.4520 & -2120.2920 & -389.1013 & -962.6821 & -7.6575 & -29.9582 \\ 0.2603 & 590.5793 & 1382.2166 & -233.6655 & 27.5243 & -10.7759 \end{bmatrix}$$

$$\begin{bmatrix} 6.5411 & -4.5755 & -3.4519 & 0.2603 \\ -5153.5707 & -2792.8931 & -2120.2913 & 590.5768 \\ -25214.1916 & 384.6827 & -389.0190 & 1382.2609 \\ 7448.5812 & -1545.7239 & -962.6738 & -233.7682 \\ -502.2990 & 7.8409 & -7.6555 & 27.5244 \\ 295.8664 & -51.2850 & -29.9579 & -10.7802 \\ 30223.9170 & -470.2072 & 372.5092 & -1620.9983 \\ -470.4125 & 58.3283 & 26.7537 & 21.3192 \\ 372.6527 & 26.7547 & 35.8833 & -26.6255 \\ -1621.1002 & 21.3095 & -26.6193 & 88.8944 \end{bmatrix}$$

$$L = \begin{bmatrix} 26108.8944 & 266.5854 & -9028.2973 & 1.1927 & -0.0485 \\ 5152.4336 & 170262.8626 & -5461121.3601 & 721.0816 & -29.3485 \\ -0.5031 & 6508.9882 & 18815.2750 & -16.3659 & 0.9452 \\ 2632.1475 & 82334.8973 & -2812414.1365 & 375.1583 & -15.3728 \\ -0.2922 & 116.7125 & 664.3428 & -0.3671 & 0.0204 \\ 85.1349 & 2662.1716 & -90968.1199 & 12.1755 & -0.5000 \\ 126.4147 & -5153.6161 & -160603.2483 & 36.6987 & -1.7576 \\ -88.4328 & -2792.8924 & 94413.8281 & -12.7828 & 0.5294 \\ -66.7171 & -2120.2920 & 71191.3966 & -9.0980 & 0.3627 \\ 5.0310 & 590.5793 & -41617.7673 & -0.3347 & 0.0305 \end{bmatrix}$$

$$\hat{H} = \begin{bmatrix} 0.0000 & 0.0000 & -0.0000 & 0.0000 & -0.0000 \\ 0.0000 & 0.0000 & 0.0000 & -0.0000 & -0.0000 \\ -0.0000 & 0.0000 & 0.9997 & 0.0043 & -0.0175 \\ 0.0000 & -0.0000 & 0.0043 & 0.9431 & 0.2316 \\ -0.0000 & -0.0000 & -0.0175 & 0.2316 & 0.0572 \end{bmatrix}$$

The system matrices of the reduced-order unknown input observer that detects the longitudinal accelerometer fault are

$$A_r = \begin{bmatrix} -0.8716 & -2.1026 & -0.0197 & -0.8059 & 0.1152 & -0.0596 & 0.0026 \\ 2.1086 & -11.5261 & 0.0381 & -11.1299 & 1.3875 & -0.6876 & 0.0539 \\ 0.0969 & -1.1612 & -0.2064 & -16.0272 & 0.0812 & -0.1561 & -0.0959 \\ -0.8065 & 11.1390 & 17.5935 & -16.6956 & 4.5415 & -2.3691 & 0.1428 \\ 0.1154 & -1.3878 & -0.4960 & 4.5432 & -8.2802 & 5.9691 & -0.7275 \\ -0.0646 & 0.7740 & 0.2778 & -2.6154 & 7.3702 & -8.1520 & -0.8765 \\ -0.0235 & 0.2809 & 0.1005 & -0.9619 & 3.4008 & -5.8070 & -7.9312 \end{bmatrix}$$

$$B_r = \begin{bmatrix} -0.0000 & 0.0252 & -0.4438 & 0.0001 & 25.7333 & -0.0173 & -0.0053 \\ 0.0000 & -0.0494 & 0.4764 & -0.0003 & -23.4140 & 0.2238 & -0.0134 \\ -0.0000 & 0.1250 & 0.0131 & 0.0001 & -3.9325 & -0.1427 & 0.0083 \\ -0.0000 & 0.0149 & -0.2193 & -0.0001 & 1.9300 & -0.0772 & 0.0044 \\ -0.0000 & -0.7810 & 0.0383 & 0.0008 & 0.2800 & -0.1165 & 0.0067 \\ 0.0000 & -0.8874 & -0.0229 & -0.0011 & -0.3206 & 0.0091 & -0.0005 \\ -0.0000 & 0.3714 & -0.0077 & 0.0014 & -0.2179 & -0.6073 & 0.0343 \end{bmatrix}$$

$$C_r = \begin{bmatrix} -0.0000 & -0.0000 & 0.0000 & -0.0000 & 0.0000 & 0.0000 & -0.0000 \\ -0.0000 & -0.0000 & 0.0000 & -0.0000 & 0.0000 & -0.0000 & 0.0000 \\ -1.8112 & -4.2680 & 1.3514 & -1.2805 & 0.2243 & 0.2975 & 0.3400 \\ 24.4450 & 26.6033 & 0.3603 & 11.4006 & -1.6085 & 0.8633 & -0.0113 \\ 6.0410 & 6.6158 & 0.0634 & 2.8250 & -0.3994 & 0.2066 & -0.0091 \end{bmatrix}$$

$$D_r = \begin{bmatrix} -0.0000 & -0.0000 & -0.0000 & -0.0000 & -0.0000 & 0.0000 & -0.0000 \\ 0.0000 & 0.0000 & 0.0000 & 0.0000 & 0.0000 & -0.0000 & 0.0000 \\ 0.0000 & 0.0000 & 0.0000 & 0.0002 & 0.0005 & -0.0000 & 0.0000 \\ -0.0000 & -0.0000 & -0.0000 & -0.0010 & -0.0026 & 0.0000 & -0.0000 \\ -0.0000 & -0.0000 & -0.0000 & -0.0003 & -0.0007 & 0.0000 & -0.0000 \end{bmatrix}$$

B.2 Fault Detection Filter Set No. 2

For the unknown input observer that detects the front wheel speed sensor fault,

$$P = \left[\begin{array}{cccccc} 1347.7387 & 1.0123 & 0.0000 & 0.0002 & 0.0000 & -0.0000 \\ 1.0123 & -2.4387 & -0.0042 & -0.1867 & -0.0004 & 0.0009 \\ 0.0000 & -0.0042 & -0.0006 & 0.0051 & 0.0002 & -0.0004 \\ 0.0002 & -0.1867 & 0.0051 & 7.5352 & 0.2726 & -0.0038 \\ 0.0000 & -0.0004 & 0.0002 & 0.2726 & 0.0099 & -0.0016 \\ -0.0000 & 0.0009 & -0.0004 & -0.0381 & -0.0016 & 0.0027 \\ 0.0002 & -0.0456 & 0.0058 & 7.9014 & 0.2855 & -0.0395 \\ 0.0000 & 0.0012 & 0.0008 & -0.0997 & -0.0032 & -0.0052 \\ -0.0000 & 0.0019 & -0.0007 & -1.7695 & -0.0636 & 0.0047 \\ 0.0000 & -0.0000 & 0.0000 & 0.0000 & 0.0000 & -0.0000 \end{array}\right.$$

$$\left.\begin{array}{cccc} 0.0002 & 0.0000 & -0.0000 & 0.0000 \\ -0.0456 & 0.0011 & 0.0019 & -0.0000 \\ 0.0058 & 0.0008 & -0.0007 & 0.0000 \\ 7.9014 & -0.1000 & -1.7695 & 0.0000 \\ 0.2855 & -0.0032 & -0.0636 & 0.0000 \\ -0.0395 & -0.0052 & 0.0047 & -0.0000 \\ 8.2765 & -0.1056 & -1.8541 & 0.0000 \\ -0.1056 & 0.0143 & 0.0330 & 0.0000 \\ -1.8541 & 0.0330 & 0.4220 & -0.0000 \\ 0.0000 & 0.0000 & -0.0000 & 0.0000 \end{array}\right]$$

$$L = \begin{bmatrix} 26048.0282 & 1.0123 & 0.0549 & 3.2197 & -0.9448 \\ 19.5648 & -2.4387 & -0.2085 & 84.7913 & 0.02829 \\ 0.0000 & -0.0042 & -0.0090 & -12.7643 & 4.6570 \\ 0.0044 & -0.1867 & 12.7854 & -17998.00250 & -49056.6664 \\ 0.0002 & 0.0004 & 0.4626 & -650.6146 & -1753.1573 \\ -0.0001 & 0.0009 & -0.0637 & 90.6121 & -24.3381 \\ 0.0046 & 0.0456 & 13.4050 & -18857.1396 & -51423.1919 \\ 0.0002 & 0.0012 & -0.1697 & 238.7449 & 1264.2107 \\ -0.0009 & 0.0019 & -3.0025 & 4223.0119 & 11958.0119 \\ 0.0000 & -0.0944 & -0.0001 & -0.0869 & 0.2596 \end{bmatrix}$$

$$\hat{H} = \begin{bmatrix} 0 & 0 & 0 & 0 & 0 \\ 0 & 1.0000 & -0.0000 & 0.0000 & -0.0000 \\ 0 & -0.0000 & 0.9925 & 0.0864 & 0.0000 \\ 0 & 0.0000 & 0.0864 & 0.0075 & 0.0000 \\ 0 & -0.0000 & 0.0000 & 0.0000 & -0.0000 \end{bmatrix}$$

The system matrices of the reduced-order unknown input observer that detects the front wheel speed sensor fault are

$$A_r = \begin{bmatrix} -2.1028 & -3.1445 & -3.8435 & -0.9076 & 0.0212 & 0.0715 & 0.0004 \\ 16.9287 & -9.9509 & -7.3819 & 7.1109 & 0.1709 & 0.4484 & 0.0035 \\ 38.8452 & -12.4570 & -9.5425 & 7.3856 & 0.1856 & 0.4893 & 0.0037 \\ 40.2722 & -18.8316 & -16.6111 & -0.0022 & 0.0204 & 0.1108 & 0.0001 \\ -2.5487 & 0.1844 & 0.1947 & -0.1674 & -53.3130 & 0.1881 & 0.0002 \\ -406.7329 & 188.9516 & 149.2547 & -74.4922 & 0.8518 & -14.6838 & -0.8940 \\ -7.8120 & 3.7123 & 2.9350 & -1.4360 & 0.0135 & -0.2657 & -1.2538 \end{bmatrix}$$

$$B_r = \begin{bmatrix} -0.0000 & 0.0003 & -0.0190 & 0.0033 & 0.0003 & -0.1548 & 0.0000 \\ -0.0000 & 0.0009 & -0.0629 & 0.0104 & 0.0010 & -0.3825 & -0.0000 \\ -0.0000 & -0.0002 & -0.0947 & 0.0139 & 0.0001 & -0.4225 & -0.0000 \\ -0.0000 & -0.0010 & -0.0321 & -0.0114 & -0.0006 & -0.1332 & 0.0000 \\ 0.0000 & 0.0001 & 19.5666 & -2.4382 & -0.2085 & 84.8923 & 0.0001 \\ -0.0000 & 0.0249 & -0.0842 & 0.1146 & 0.0072 & -0.2197 & 0.0000 \\ -0.0000 & -1.2498 & -0.0003 & 0.0021 & 0.0001 & 0.0009 & 0.0001 \end{bmatrix}$$

$$C_r = \begin{bmatrix} 0 & 0 & 0 & 0 & 0 & 0 & 0 \\ 0.0010 & 0.0032 & 0.0048 & 0.0016 & -1.0000 & 0.0043 & 0.0000 \\ 6.0940 & 3.1614 & 2.8522 & 0.0294 & -0.0267 & -0.0865 & -0.0006 \\ 0.4333 & 0.2248 & 0.2028 & 0.0021 & -0.0019 & -0.0061 & -0.0000 \\ -0.0000 & -0.0000 & -0.0000 & -0.0000 & -0.0000 & 0.0000 & 0.0000 \end{bmatrix}$$

$$D_r = \begin{bmatrix} 0 & 0 & 0 & 0 & 0 & 0 & 0 \\ 0 & 0 & 0 & 1.0000 & -0.0000 & 0.0000 & -0.0000 \\ 0 & 0 & 0 & -0.0000 & 0.9950 & 0.0707 & 0.0000 \\ 0 & 0 & 0 & 0.0000 & 0.0707 & 0.0050 & -0.0000 \\ 0 & 0 & 0 & -0.0000 & -0.0000 & 0.0000 & -0.0000 \end{bmatrix}$$

For the unknown input observer that detects the rear wheel speed sensor fault,

$$P = \left[\begin{array}{rrrrrr}
13.4776 & 0.0000 & 0.0000 & -0.0000 & 0.0000 & -0.0000 \\
0.0000 & 8400.1741 & -0.0004 & 54.7112 & -4.2124 & 0.0779 \\
0.0000 & -0.0000 & 0.4801 & -0.0001 & 3.9154 & -0.8289 \\
-0.0000 & 54.7112 & -0.0005 & 0.3564 & -0.0316 & 0.0014 \\
0.0000 & -4.2124 & 3.9154 & -0.0316 & 31.9373 & -6.7603 \\
-0.0000 & 0.0779 & -0.8289 & 0.0014 & -6.7603 & 1.4311 \\
0.0000 & -31.8670 & -0.3041 & -0.2072 & -2.4646 & 0.5248 \\
0.0000 & -3.6057 & 7.7377 & -0.0316 & 63.1125 & -13.3597 \\
-0.0000 & 10.2121 & 4.9023 & 0.0614 & 39.9791 & -8.4640 \\
-0.0000 & 0.0021 & 0.0068 & 0.0000 & 0.0553 & -0.0117
\end{array}\right.$$

$$\left.\begin{array}{rrrr}
0.0000 & 0.0000 & -0.0000 & -0.0000 \\
-31.8670 & -3.6057 & 10.2121 & 0.0021 \\
-0.3041 & 7.7377 & 4.9023 & 0.0068 \\
-0.2072 & -0.0316 & 0.0614 & 0.0000 \\
-2.4646 & 63.1124 & 39.9791 & 0.0553 \\
0.5248 & -13.3597 & -8.4640 & -0.0117 \\
0.3136 & -4.8884 & -3.1445 & -0.0043 \\
-4.8884 & 124.7212 & 79.0127 & 0.0109 \\
-3.1445 & 79.0127 & 50.0742 & 0.0692 \\
-0.0043 & 0.1093 & 0.0693 & 0.0001
\end{array}\right]$$

$$L = \left[\begin{array}{rrrrr}
2604849.5282 & 0.3267 & 0.2260 & -0.0000 & -0.0000 \\
6.3144 & 84001740.8773 & 39155631.5773 & 1.4762 & 0.4018 \\
0.0000 & -3.7417 & -1.7494 & -0.3896 & -0.0000 \\
-0.0863 & 54711.2396 & 255025.3875 & 0.0100 & 0.0026 \\
0.0066 & -42124.4425 & -19635.3896 & -3.1786 & -0.0002 \\
-0.0001 & 77.8761 & 362.9996 & 0.6727 & 0.0000 \\
0.0503 & -318670.3016 & -148541.4335 & 0.2412 & -0.0015 \\
0.0057 & -36056.6519 & -16807.0133 & -6.2807 & -0.0002 \\
-0.0161 & 102121.0951 & 47601.6248 & -3.9770 & 0.0005 \\
-0.0000 & 21.4675 & 10.0066 & -0.0055 & 0.0000
\end{array}\right]$$

$$\hat{H} = \left[\begin{array}{rrrrr}
0 & 0 & 0 & 0 & 0 \\
0 & 0.9967 & 0.0010 & 0.0000 & 0.0571 \\
0 & 0.0010 & 0.9997 & 0.0000 & -0.0172 \\
0 & 0.0000 & 0.0000 & -0.0000 & -0.0000 \\
0 & 0.0571 & -0.0172 & -0.0000 & 0.0036
\end{array}\right]$$

The system matrices of the reduced-order unknown input observer that detects the rear wheel speed sensor fault are

$$A_r = \left[\begin{array}{rrrrrrr}
-18.3467 & 13.8343 & -1.4128 & -0.3169 & 0.0812 & 0.0180 & -0.0000 \\
-60.2398 & -37.5142 & 8.6861 & 2.4465 & -0.4625 & -0.1612 & 0.0002 \\
-311.3778 & 108.6538 & -25.2552 & -6.8195 & 1.1422 & 0.5294 & -0.0006 \\
288.6782 & -125.3455 & 22.4069 & -1.2544 & 2.2319 & -0.1410 & -0.0004 \\
-336.7032 & 84.3614 & -11.1076 & -5.8561 & -0.1796 & 0.1124 & 0.0004 \\
315.3908 & -125.6428 & 9.9671 & 17.2843 & -1.9060 & -2.2633 & -0.0017 \\
1.5395 & -0.5169 & 0.0403 & 0.0694 & -0.0074 & -0.0032 & -1.2500
\end{array}\right]$$

$$B_r = \begin{bmatrix} 0.0000 & -0.0000 & 0.0070 & -0.0056 & -0.0020 & -0.0000 & -0.0000 \\ -0.0000 & 0.0000 & -0.0067 & 0.0151 & 0.0141 & 0.0000 & 0.0000 \\ 0.0000 & 0.0001 & 0.0361 & 0.0499 & 0.0440 & 0.0000 & -0.0000 \\ -0.0000 & -0.0002 & -0.0569 & 0.0026 & 0.0201 & 0.0000 & 0.0000 \\ 0.0000 & -0.0014 & -0.0147 & 0.2132 & 0.2690 & -0.0000 & 0.0000 \\ -0.0000 & 0.0046 & 0.1328 & -0.4160 & -0.7034 & -0.0000 & -0.0000 \\ -0.0000 & -1.2500 & 0.0005 & 0.0020 & -0.0011 & 0.0000 & 0.0000 \end{bmatrix}$$

$$C_r = \begin{bmatrix} 0 & 0 & 0 & 0 & 0 & 0 & 0 \\ -330.6442 & 98.2020 & -21.8516 & -1.7461 & 0.3541 & 0.1728 & -0.0003 \\ 16.6875 & 42.6023 & -7.5703 & -0.4180 & -0.3162 & 0.7839 & 0.0008 \\ -0.0000 & 0.0000 & -0.0000 & -0.0000 & 0.0000 & 0.0000 & -0.0000 \\ 689.6625 & -209.4661 & 46.4236 & 3.6914 & -0.7096 & -0.4377 & 0.0006 \end{bmatrix}$$

$$D_r = \begin{bmatrix} 0 & 0 & 0 & 0 & 0 & 0 & 0 \\ 0 & 0 & 0 & 0.1876 & -0.0379 & 0.0000 & -0.3886 \\ 0 & 0 & 0 & -0.0379 & 0.9982 & -0.0000 & -0.0181 \\ 0 & 0 & 0 & 0.0000 & -0.0000 & -0.0000 & -0.0000 \\ 0 & 0 & 0 & -0.3886 & -0.0181 & -0.0000 & 0.8141 \end{bmatrix}$$

B.3 Fault Detection Filter Set No. 3

For the unknown input observer that detects the brake actuator fault,

$$P = \begin{bmatrix} 2882.0135 & 12267.5367 & 37.9168 & -21.0952 & 1.9693 & -0.6396 \\ 12267.5354 & 308056.8520 & 1246.1188 & -4060.5875 & -569.2969 & 183.2128 \\ 37.9167 & 1246.1182 & 116.2326 & -2.6276 & 1.6775 & 0.1538 \\ -21.0952 & -4060.5876 & -2.6276 & 1222.3514 & 123.3366 & -71.1718 \\ 1.9693 & -569.2969 & 1.6775 & 123.3365 & 14.1664 & -7.5745 \\ -0.6396 & 183.2128 & 0.1538 & -71.1718 & -7.5745 & 4.3888 \\ -4.2081 & -11375.3235 & 23.7973 & 3439.7259 & 371.4223 & -208.9489 \\ 4.1640 & -564.8578 & 1.9465 & 68.2810 & 9.0706 & -4.4122 \\ -0.4248 & 2015.0954 & -2.7923 & -697.5179 & -74.1246 & 42.3463 \\ -0.0912 & 20.0209 & 0.8768 & -4.4715 & -0.4510 & 0.2503 \end{bmatrix.$$
$$\begin{bmatrix} -4.2080 & 4.1640 & -0.4248 & -0.0911 \\ -11375.3233 & -564.8578 & 2015.0954 & 20.0214 \\ 23.7973 & 1.9465 & -2.7923 & 0.8768 \\ 3439.7260 & 68.2810 & -697.5179 & -4.4715 \\ 371.4223 & 9.0706 & -74.1245 & -0.4510 \\ -208.9489 & -4.4122 & 42.3463 & 0.2503 \\ 10117.1559 & 220.7461 & -2038.9690 & -12.5519 \\ 220.7461 & 6.7152 & -4.3140 & -0.2420 \\ -2038.9690 & -43.1397 & 412.1722 & 2.5195 \\ -12.5519 & -0.2420 & 2.5195 & -937.4862 \end{bmatrix}$$

$$L = \begin{bmatrix} 0.1393 & 0.0031 & 0.0169 & 0.0264 & -0.0140 \\ 0.5927 & 0.0770 & -0.1992 & 14.9994 & 34.3581 \\ 0.0018 & 0.0003 & 0.0008 & 0.0220 & -0.0514 \\ -0.0010 & -0.0010 & 0.1985 & -4.6960 & -9.4380 \\ 0.0000 & -0.0001 & 0.0211 & -0.5038 & -1.0299 \\ -0.0000 & 0.0000 & -0.0122 & 0.2856 & 0.5722 \\ -0.0002 & -0.0003 & 0.5823 & -13.7581 & -27.8268 \\ 0.0002 & -0.0001 & 0.0121 & -0.2970 & -0.6208 \\ -0.0000 & 0.0005 & -0.1180 & 2.7776 & 5.5954 \\ -0.0000 & 0.0000 & -0.0007 & 0.0173 & 0.0349 \end{bmatrix}$$

$$\hat{H} = \begin{bmatrix} -0.0000 & 0.0000 & -0.0000 & 0.0000 & 0.0000 \\ 0.0000 & 0.0048 & -0.0554 & -0.0373 & 0.0162 \\ 0.0000 & -0.0554 & 0.9954 & 0.0153 & 0.0357 \\ 0.0000 & -0.0373 & 0.0153 & 0.7992 & -0.3986 \\ -0.0000 & 0.0162 & 0.0357 & -0.3986 & 0.2007 \end{bmatrix}$$

The system matrices of the reduced-order unknown input observer that detects the brake actuator fault are

$$A_r = \left[\begin{array}{rrrrr} -0.2101 & -0.4176 & -0.4361 & -0.3321 & 0.2321 \\ 0.3644 & -1.3266 & -3.0620 & -2.3952 & 1.5825 \\ 0.3008 & 0.6353 & -5.2125 & -11.1865 & 6.1338 \\ -0.2641 & 0.8994 & 11.1054 & -12.3121 & 13.5706 \\ 0.1597 & -0.2630 & -6.1323 & 13.3667 & -23.2125 \\ 0.0464 & -0.1982 & -1.0395 & 3.5386 & -10.2716 \\ 0.0133 & -0.0641 & -0.2670 & 0.8970 & -2.2092 \\ -0.0101 & 0.0553 & 0.1738 & -0.6078 & 1.4545 \\ 0.0002 & -0.0056 & 0.0166 & -0.0363 & 0.1297 \end{array} \right.$$

$$\left. \begin{array}{rrrr} -0.0486 & 0.0135 & 0.0100 & -0.0010 \\ -0.3386 & 0.0884 & 0.0696 & -0.0061 \\ -1.1834 & 0.3321 & 0.2466 & -0.0251 \\ -3.7134 & 0.9678 & 0.7384 & -0.0709 \\ 11.1814 & -2.6657 & -2.0059 & 0.2023 \\ -7.1829 & 4.1513 & 2.9411 & -0.2784 \\ -4.2447 & -7.9414 & -12.4384 & 1.2485 \\ 2.8240 & 12.5710 & -57.9262 & 11.0403 \\ 0.0453 & 0.0183 & 1.3175 & -14.5622 \end{array} \right]$$

$$B_r = \begin{bmatrix} -2.3144 & 0.07317 & -0.2337 & -0.0196 & -0.0463 & -1.5175 & 1.7636 \\ 1.2777 & -0.1003 & 0.0773 & 0.01122 & -0.0212 & 2.0307 & 11.1707 \\ 2.0502 & 0.0168 & 0.2419 & 0.0295 & -0.0744 & 5.7161 & 22.0243 \\ -4.4776 & 0.0040 & -0.2773 & 0.0293 & -0.2106 & 8.8028 & 17.5472 \\ -4.0121 & 0.0074 & -0.0963 & -0.1245 & 0.2643 & -23.0380 & -79.0805 \\ 5.6995 & -0.0048 & 0.3514 & -0.0189 & 0.1744 & -6.5611 & -5.1904 \\ -2.9563 & -0.0017 & -0.3300 & 0.0017 & 0.0997 & -2.0123 & 4.3232 \\ 8.9208 & 0.0017 & -0.0326 & -0.1093 & 0.4666 & -25.5619 & -67.1329 \\ -30.6514 & -0.0003 & -1.6000 & -0.0299 & -0.2153 & 0.9092 & 4.10178 \end{bmatrix}$$

$$C_r = \left[\begin{array}{cccccc} 0.0000 & 0.0000 & 0.0000 & 0.0000 & -0.0000 & 0.0000 \\ -0.0044 & -0.0025 & -0.0045 & -0.0030 & 0.0024 & -0.0004 \\ -0.0050 & -0.0284 & -0.0031 & -0.0121 & 0.0028 & -0.0022 \\ 0.1021 & 0.0887 & 0.1031 & 0.0810 & -0.0565 & 0.0117 \\ -0.0512 & -0.0455 & -0.0516 & -0.0410 & 0.0284 & -0.0060 \end{array}\right.$$

$$\left.\begin{array}{ccc} -0.0000 & 0.0000 & -0.0000 \\ 0.0002 & 0.0001 & -0.0000 \\ -0.0003 & 0.0004 & 0.0001 \\ -0.0033 & -0.0024 & 0.0003 \\ 0.0016 & 0.0012 & -0.0001 \end{array}\right]$$

$$D_r = \begin{bmatrix} 0 & 0 & 0.0000 & 0.0000 & -0.0000 & 0.0000 & 0.0000 \\ 0 & 0 & 0.0000 & 0.0048 & -0.0554 & -0.0373 & 0.0162 \\ 0 & 0 & 0.0000 & -0.0554 & 0.9954 & 0.0153 & 0.0357 \\ 0 & 0 & 0.0000 & -0.0373 & 0.0153 & 0.7992 & -0.3986 \\ 0 & 0 & -0.0000 & 0.0162 & 0.0357 & -0.3986 & 0.2007 \end{bmatrix}$$

For the unknown input observer that detects the rear wheel speed sensor fault,

$$P = \left[\begin{array}{cccccc} 1377.4072 & -1345.1875 & 0.0002 & -0.0000 & 0.0000 & -0.0000 \\ -1345.1877 & 167089.6647 & -0.2455 & -0.0097 & 0.0000 & -0.0006 \\ 0.0002 & -0.2455 & 1.6555 & -0.0900 & 0.0007 & -0.0040 \\ -0.0000 & -0.0097 & -0.0900 & 0.0287 & -0.0004 & 0.0013 \\ 0.0000 & 0.0001 & 0.0007 & -0.0004 & 0.0000 & -0.0000 \\ -0.0000 & -0.0006 & -0.0038 & 0.0013 & -0.0000 & 0.0001 \\ -0.0001 & 0.1266 & -0.7585 & 0.0274 & 0.0003 & 0.0011 \\ -0.0000 & 0.0012 & 0.0031 & -0.0022 & 0.0000 & -0.0001 \\ 0.0000 & -0.0017 & -0.0020 & 0.0018 & -0.0000 & 0.0001 \\ -0.0053 & 763.3994 & 518.1478 & -152.7053 & 0.9950 & -7.2292 \end{array}\right.$$

$$\left.\begin{array}{cccc} -0.0001 & 0.0000 & 0.0000 & -0.0015 \\ 0.1266 & 0.0012 & -0.0017 & 763.3981 \\ -0.7585 & 0.0031 & -0.0020 & 518.1476 \\ 0.0274 & -0.0022 & 0.0018 & -152.7053 \\ 0.0003 & 0.0001 & -0.0000 & 0.9950 \\ 0.0011 & -0.0001 & 0.0001 & -7.2292 \\ 0.3734 & 0.0009 & -0.0004 & -153.9051 \\ 0.0009 & 0.0003 & -0.0002 & 8.9745 \\ -0.0004 & -0.0002 & 0.0002 & -9.6547 \\ -153.9052 & 8.9745 & -9.6547 & 6032527.4369 \end{array}\right]$$

$$L = \begin{bmatrix} 26621.4377 & -1345.1875 & -73.9881 & -61.3445 & 0.0018 \\ -25998.7245 & 167089.6647 & 9189.0096 & 7617.4060 & -2.8878 \\ 0.0042 & -0.2455 & -2.0381 & 10.8594 & 15.1291 \\ -0.0000 & -0.0097 & 0.3155 & -0.1735 & -1.0195 \\ 0.0000 & 0.0000 & -0.0022 & 0.0013 & -0.0011 \\ -0.0000 & -0.0006 & 0.0146 & -0.0043 & -0.0442 \\ -0.0020 & 0.1266 & 0.7897 & -5.1712 & -7.1746 \\ -0.0000 & 0.0012 & -0.0170 & -0.0060 & 0.0134 \\ 0.0000 & -0.0017 & 0.0174 & 0.0159 & -0.0227 \\ -0.1021 & 763.3994 & -11487.2358 & -2928.1231 & -235.4026 \end{bmatrix}$$

$$\hat{H} = \begin{bmatrix} 0 & 0.0000 & -0.0000 & 0.0000 & 0.0000 \\ 0.0000 & 0.0017 & -0.0068 & -0.0298 & 0.0282 \\ 0.0000 & -0.0068 & 0.0270 & 0.1175 & -0.1113 \\ 0.0000 & -0.0298 & 0.1175 & 0.5118 & -0.4850 \\ -0.0000 & 0.0282 & -0.1113 & -0.4850 & 0.4596 \end{bmatrix}$$

The system matrices of the reduced-order unknown input observer that detects the rear wheel speed sensor fault are

$$A_r = \begin{bmatrix} -0.9982 & -7.7591 & 5.5083 & 0.9952 & 0.3757 & -0.1203 & -0.0074 \\ 7.7591 & -5.4436 & 24.6241 & 2.8246 & 1.1972 & -0.3759 & -0.0234 \\ 5.5083 & -24.6241 & -80.1984 & -36.0645 & -9.4182 & 3.1685 & 0.1938 \\ -0.9952 & 2.8246 & 36.0645 & -6.3110 & -5.8000 & 1.5135 & 0.0980 \\ 0.3757 & -1.1972 & -9.4182 & 5.8000 & -6.8531 & 6.3056 & 0.2702 \\ 0.1203 & -0.3759 & -3.1685 & 1.5135 & -6.3056 & -2.2406 & -0.2780 \\ -0.0074 & 0.0234 & 0.1938 & -0.0980 & 0.2702 & 0.2780 & -23.6762 \end{bmatrix}$$

$$B_r = \begin{bmatrix} -0.0000 & 0.0001 & -0.0000 & 0.0289 & -0.2484 & -0.3089 & 0.3257 \\ -0.0000 & 0.0001 & -0.0000 & 0.0920 & -2.4295 & 0.9907 & 4.9794 \\ 0.0000 & 0.0001 & 0.0000 & 0.0789 & 1.4367 & -3.5826 & -10.7436 \\ -0.0000 & 0.0002 & -0.0000 & 0.0093 & -1.6499 & 1.8957 & 3.5332 \\ 0.0000 & -0.0001 & 0.0000 & 0.0593 & -0.6791 & -0.5000 & 1.7267 \\ 0.0000 & 0.0000 & 0.0000 & 0.0437 & -0.4816 & -0.3826 & 1.0912 \\ -0.0000 & 0.0002 & -0.0000 & 0.1085 & -1.6908 & -0.3271 & 0.2197 \end{bmatrix}$$

$$C_r = \begin{bmatrix} 0.0000 & 0.0000 & -0.0000 & -0.0000 & -0.0000 & 0.0000 & -0.0000 \\ -0.0454 & -0.0788 & 0.1400 & 0.0218 & 0.0086 & -0.0027 & -0.0002 \\ 0.1788 & 0.3106 & -0.5520 & -0.0859 & -0.0338 & 0.0108 & 0.0007 \\ 0.7793 & 1.3535 & -2.4051 & -0.3743 & -0.1474 & 0.0469 & 0.0029 \\ -0.7385 & -1.2826 & 2.2791 & 0.3547 & 0.1397 & -0.0444 & -0.0028 \end{bmatrix}$$

$$D_r = \begin{bmatrix} 0 & 0 & 0 & 0.0000 & -0.0000 & 0.0000 & 0.0000 \\ 0 & 0 & 0.0000 & 0.0017 & -0.0068 & -0.0298 & 0.0282 \\ 0 & 0 & 0.0000 & -0.0068 & 0.0270 & 0.1174 & -0.1113 \\ 0 & 0 & 0.0000 & -0.0298 & 0.1174 & 0.5118 & -0.4850 \\ 0 & 0 & -0.0000 & 0.0282 & -0.1113 & -0.4850 & 0.4596 \end{bmatrix}$$

B.4 Fault Detection Filter Set No. 4

For the unknown input observer that detects the steering actuator fault,

$$P = \begin{bmatrix} 0.4566 & 0.1082 & -3.9693 & -0.0040 & 0.1621 & 0.2027 \\ 0.1082 & 0.2782 & -8.0408 & 0.0029 & 0.4171 & 0.3493 \\ -3.9693 & -8.0408 & 276.5833 & -0.1030 & -17.5830 & -9.7187 \\ -0.0040 & 0.0029 & -0.1030 & 0.0002 & 0.0080 & 0.0022 \\ 0.1621 & 0.4171 & -17.5830 & 0.0080 & 1.348 & 0.4569 \\ 0.2027 & 0.3493 & -9.7187 & 0.0022 & 0.4569 & 0.4574 \end{bmatrix}$$

$$L = \begin{bmatrix} 1.2963 & -403.5655 & 0.0728 & 0.8656 \\ 3.2874 & 287.9682 & -3.8561 & -1.4483 \\ -112.8641 & -10296.6743 & -124652.3578 & 49.8742 \\ 0.0464 & 16.8030 & 82.8647 & -0.0455 \\ 7.2476 & 799.4134 & 16298.0087 & -3.5934 \\ 3.9158 & 218.5103 & -1510.6887 & -1.4182 \end{bmatrix}$$

$$\hat{H} = \begin{bmatrix} 27315.1981 & -11.5185 & -0.0000 & 44557.8234 \\ -1.1518 & 99999.9982 & -0.0000 & 7.0612 \\ 0.0000 & -0.0000 & -0.0000 & -0.0000 \\ 44557.8234 & 7.0612 & 0.0000 & 72684.8037 \end{bmatrix}$$

The system matrices of the reduced-order unknown input observer that detects the steering actautor fault are

$$A_r = \begin{bmatrix} -0.0916 & 9.2243 & -0.0616 & 0.0075 \\ -42.8837 & -51.0755 & 3.3547 & -1.1327 \\ 40.9895 & 2.6069 & -4.5341 & 3.3056 \\ -410.8559 & -282.8797 & -1.4552 & -23.3848 \end{bmatrix}$$

$$B_r = \begin{bmatrix} -57.2253 & -0.0370 & 8.0859 & 0.0001 & -0.0274 \\ -22.1764 & 0.1920 & -36.5915 & -0.0004 & 0.0516 \\ -19.7201 & -0.1053 & 40.3448 & -0.0000 & -0.0280 \\ -60.5278 & 1.5424 & -384.9448 & -0.0020 & 0.7706 \end{bmatrix}$$

$$C_r = \begin{bmatrix} -13.8394 & -169.0823 & 5.6062 & -2.0210 \\ 0.9990 & -0.0647 & 0.0293 & 0.0513 \\ -0.0000 & 0.0000 & -0.0000 & -0.0000 \\ -22.5751 & -275.8149 & 9.1452 & -3.2967 \end{bmatrix}$$

$$D_r = \begin{bmatrix} -27.4996 & 0.2732 & -0.0001 & -0.0000 & 0.4456 \\ 0.0116 & -0.0001 & 1.0000 & -0.0000 & 0.0001 \\ -0.0000 & 0.0000 & -0.0000 & -0.0000 & -0.0000 \\ -44.8587 & 0.4456 & 0.0001 & 0.0000 & 0.7268 \end{bmatrix}$$

For the unknown input observer that detects the front wheel speed sensor fault,

$$P = \begin{bmatrix} 0.6621 & -67.4219 & 5021.0610 & -830.2164 & -0.1382 & -0.1560 \\ -67.4219 & 0.6349 & -20.6563 & 995.1970 & -0.0482 & -0.0250 \\ 5021.0611 & -0.6563 & 2525.3198 & -253.8937 & -0.0937 & -0.0967 \\ -830.2165 & 995.1970 & -253.8937 & 12283.1550 & -0.6022 & -0.3145 \\ -0.1382 & -0.0482 & -0.0937 & -0.6022 & 0.0007 & 0.0006 \\ -0.1560 & -0.0250 & -0.0967 & -0.3145 & 0.0006 & 0.0005 \end{bmatrix}$$

$$L = \begin{bmatrix} -88593.2489 & -830.2164 & 26970.1918 & 25569.4854 \\ -18707.0275 & 995.1970 & -32349.8415 & -30669.9902 \\ -47667.9716 & -253.8937 & 8243.3226 & 7815.6314 \\ -230910.8929 & 12283.1550 & -399265.9380 & -378532.6968 \\ 13.2634 & -0.6022 & 19.5180 & 18.4837 \\ 7.8275 & -0.3145 & 10.1843 & 9.6383 \end{bmatrix}$$

$$\hat{H} = \begin{bmatrix} -0.0000 & -0.0000 & 0.0000 & 0.0000 \\ -0.0000 & 99950.1836 & 1619.3239 & 1535.2350 \\ 0.0000 & 1619.3239 & 47362.4973 & -49904.1218 \\ 0.0000 & 15352.3497 & -49904.1218 & 52687.3190 \end{bmatrix}$$

The system matrices of the reduced-order unknown input observer that detects the front wheel speed sensor fault are

$$A_r = \begin{bmatrix} -36.2342 & -1.5478 & -1.8193 & 0.1206 \\ 0.3156 & -1.9216 & 2.8453 & 0.5286 \\ 1.4167 & -53.4111 & -5.7035 & 0.7588 \\ -51.1979 & -694.5874 & -1.4598 & -2.2517 \end{bmatrix}$$

$$B_r = \begin{bmatrix} -0.0000 & 0.0002 & -0.0008 & -0.0116 & -0.0144 \\ 0.0000 & 0.0474 & 0.0224 & -0.0424 & -0.0288 \\ -0.0000 & -0.1701 & 0.0145 & 0.0541 & 0.0459 \\ -0.0000 & -1.9733 & 0.0374 & 0.0047 & -0.4128 \end{bmatrix}$$

$$C_r = \begin{bmatrix} -0.0000 & 0.0000 & -0.0000 & 0.0000 \\ -0.0667 & -11.5203 & -0.1195 & -0.0281 \\ -150.7044 & -3.3634 & -3.7735 & 0.2457 \\ 158.9567 & 3.1738 & 3.9763 & -0.2601 \end{bmatrix}$$

$$D_r = \begin{bmatrix} 0.0000 & -0.0000 & -0.0000 & 0.0000 & 0.0000 \\ 0.0000 & -0.0000 & 0.9995 & 0.0162 & 0.0154 \\ -0.0002 & 0.0000 & 0.0162 & 0.4736 & -0.4990 \\ -0.0000 & 0.0000 & 0.0154 & -0.4990 & 0.5269 \end{bmatrix}$$

B.5 Fault Detection Filter Set No. 5

For the unknown input observer that detects the yaw rate sensor fault,

$$P = \begin{bmatrix} 1.8444 & -0.4528 & -5.4053 & -0.0031 & -0.4915 & 0.6633 \\ -0.4528 & 0.2772 & 1.0655 & 0.0001 & 0.3698 & -0.4871 \\ -5.4053 & 1.0655 & 966.8507 & -0.0431 & 8.9698 & -100.4749 \\ -0.0031 & 0.0001 & -0.0431 & 0.0002 & -0.0013 & 0.0040 \\ -0.4915 & 0.3698 & 8.9698 & -0.0013 & 0.5756 & -1.4838 \\ 0.6633 & -0.4871 & -100.4749 & 0.0040 & -1.4838 & 11.2129 \end{bmatrix}$$

$$L = \begin{bmatrix} 738.3307 & -306495.9332 & 4.2419 & 28.6286 \\ -69.9443 & 10626.7607 & -1.0411 & -19.2518 \\ -402234.5298 & -4314889.5003 & 165.7673 & -2176.6879 \\ 20.3817 & 17345.0267 & -0.0327 & 0.0814 \\ -3360.9379 & -128749.8721 & 0.4666 & -43.4654 \\ 41716.1602 & 398204.9094 & -16.935 & 254.6869 \end{bmatrix}$$

$$\hat{H} = \begin{bmatrix} 0.1835 & -0.0000 & 0.3871 & 0 \\ -0.0000 & 1.0000 & 0.0000 & 0.0000 \\ 0.3871 & 0.0000 & 0.8165 & -0.0000 \\ -0.0000 & 0.0000 & -0.0000 & 0.0000 \end{bmatrix}$$

The system matrices of the reduced-order unknown input observer that detects the yaw rate sensor fault are

$$A_r = \begin{bmatrix} -1.0867 & 717.8472 & 34.9830 & 21.7380 & 0.1384 \\ -3841.6339 & -3922.5524 & -345.7994 & -398.3940 & -15.3762 \\ -12088.6422 & -2205.24279 & -593.8635 & -1329.9928 & -48.1155 \\ -23279.2039 & -6720.9252 & -44.4418 & -2521.9813 & -178.4867 \\ -17646.7938 & 3814.4279 & 259.8930 & -655.6364 & -1400.9598 \end{bmatrix}$$

$$B_r = \begin{bmatrix} -5660.0838 & -05.3948 & 928.3968 & -0.0288 & -0.0370 \\ -2464.5993 & 13.1114 & -3689.2901 & 0.0114 & 0.2585 \\ 1296.0719 & 13.1969 & -12242.3063 & -0.0470 & -0.5114 \\ -1220.1517 & 70.1672 & -23927.9759 & 0.2824 & -0.0647 \\ 2879.7364 & 48.4944 & -17499.7027 & 0.3369 & 5.1328 \end{bmatrix}$$

$$C_r = \begin{bmatrix} -6.2726 & -157.0056 & -7.6044 & -8.6010 & -0.3069 \\ 0.9938 & 0.0659 & -0.0028 & 0.0935 & 0.0076 \\ 13.2318 & -331.1921 & -16.0409 & -18.1431 & -0.6474 \\ 0.0000 & 0.0000 & 0.0000 & 0.0000 & -0.0000 \end{bmatrix}$$

$$D_r = \begin{bmatrix} -18.4736 & 0.1835 & -0.0000 & 0.3871 & 0 \\ 0.0021 & -0.0000 & 1.0000 & 0.0000 & 0.0000 \\ -38.9687 & 0.3871 & 0.0000 & 0.8165 & -0.0000 \\ 0.0000 & -0.0000 & 0.0000 & -0.0000 & 0.0000 \end{bmatrix}$$

For the unknown input observer that detects the rear wheel speed sensor fault,

$$P = \begin{bmatrix} 34479.1400231.302317208.8498 - 18554.5722 - 71.2631 - 80628.3736 \\ 231.302330.1262 - 1935.9129152.688123.016817642.6319 \\ 17208.8478 - 1935.9129155906.7618 - 29166.0175 - 1722.7413 - 13460.2818 \\ -18554.5719152.6881 - 29166.018512674.5209266.314321982.2834 \\ -71.263123.0168 - 1722.7412266.314219.470515121.8121 \\ -80.628417.6426 - 1346.0282219.822815.121811763.0985 \end{bmatrix}$$

$$L = \begin{bmatrix} 0.7383 & -306.4959 & 0.0042 & 0.0286 \\ -0.0699 & 10.6268 & -0.0010 & -0.0193 \\ -402.23458 & -4314.8895 & 0.1658 & -2.1767 \\ 0.0204 & 17.34503 & -0.0000 & 0.0001 \\ -3.3609 & -128.7499 & 0.0005 & -0.0435 \\ 41.7162 & 398.2049 & -0.0169 & 0.2547 \end{bmatrix}$$

$$\hat{H} = \begin{bmatrix} 0.8799 & -0.0000 & 0.2137 & 0.2450 \\ -0.0000 & -0.0000 & -0.0000 & -0.0000 \\ 0.2137 & -0.0000 & 0.6198 & -0.4359 \\ 0.2450 & -0.0000 & -0.4359 & 0.5003 \end{bmatrix}$$

The system matrices of the reduced-order unknown input observer that detects the rear wheel speed sensor fault are

$$A_r = \begin{bmatrix} -37.2964 & 0.5502 & 0.0616 & -1.6673 \\ 51.1162 & -97.5659 & 7.1571 & -1.0081 \\ 99.8539 & -159.1525 & -1.3655 & 2.8679 \\ -16.3390 & 37.0212 & -3.8432 & -6.5857 \end{bmatrix}$$

$$B_r = \begin{bmatrix} -1.8235 & 0.0210 & -0.0000 & -0.0084 & -0.0165 \\ 101.4597 & -0.8214 & 0.0000 & -0.2048 & 0.0783 \\ 39.0193 & -1.6040 & 0.0000 & -0.6445 & -0.1063 \\ -55.8282 & 0.2969 & -0.0000 & 0.1335 & 0.0394 \end{bmatrix}$$

$$C_r = \begin{bmatrix} -11.1209 & 167.5528 & 2.0900 & 1.3049 \\ 0.0000 & -0.0000 & -0.0000 & -0.0000 \\ -170.4509 & 63.9043 & 4.2904 & -3.6219 \\ 143.2289 & 26.4103 & -2.7177 & 3.7991 \end{bmatrix}$$

$$D_r = \begin{bmatrix} -88.5816 & 0.8799 & -0.0000 & 0.2137 & 0.2450 \\ 0.0000 & -0.0000 & -0.0000 & -0.0000 & -0.0000 \\ -21.5151 & 0.2137 & -0.0000 & 0.6198 & -0.4359 \\ -24.6653 & 0.2450 & -0.0000 & -0.4359 & 0.5003 \end{bmatrix}$$

B.6 Fault Detection Filter Set No. 6

For the unknown input observer that detects the lateral accelerometer fault,

$$P = \begin{bmatrix} 0.0465 & 0.0003 & -0.1191 & 0.0001 & 0.0004 & 0.0005 \\ 0.0003 & 0.1640 & -0.0261 & -0.0000 & 0.2458 & -0.3526 \\ -0.11912 & -0.0261 & 391.7060 & -0.0431 & 3.4291 & -40.6287 \\ 0.0001 & -0.0000 & -0.0431 & 0.0000 & -0.0004 & 0.0044 \\ 0.0004 & 0.2458 & 3.4291 & -0.0004 & 0.3991 & -0.9000 \\ 0.0005 & -0.3526 & -40.6287 & 0.0044 & -0.9000 & 4.9868 \end{bmatrix}$$

$$L = \begin{bmatrix} 0.9973 & 99.9993 & -0.0000 & -0.0001 \\ 8.5174 & -1.4610 & -0.0000 & -1.2763 \\ -131677.4456 & -43078.4862 & 0.0781 & -86.5552 \\ 14.4073 & 5.5108 & -0.0000 & 0.0095 \\ -1153.9430 & -381.3118 & 0.0007 & -2.6816 \\ 13667.8461 & 4448.4573 & -0.0081 & 11.7616 \end{bmatrix}$$

$$\hat{H} = \begin{bmatrix} 0.2599 & -0.0000 & 0.4386 & 0.0000 \\ -0.0000 & 1.0000 & 0.0000 & -0.0000 \\ 0.4386 & 0.0000 & 0.7401 & 0.0000 \\ 0.0000 & -0.0000 & 0.0000 & -0.0000 \end{bmatrix}$$

The system matrices of the reduced-order unknown input observer that detects the lateral accelerometer fault are

$$A_r = \begin{bmatrix} -38.3795 & 4.8261 & 0.4187 & -0.0384 \\ 9.2680 & -5.6671 & -0.9146 & 0.0882 \\ 3.4650 & -0.6965 & -4.6438 & 0.3187 \\ -8.8154 & -62.1846 & 80.8520 & -5.8822 \end{bmatrix}$$

$$B_r = \begin{bmatrix} -12.1973 & -0.0180 & 0.3565 & 0.0000 & -0.0000 \\ -65.7380 & -0.1581 & 2.2749 & 0.0000 & 0.0000 \\ 11.9367 & -0.2361 & -4.5318 & 0.0000 & 0.0000 \\ -162.0592 & -0.9589 & -101.6535 & 0.0000 & -0.0000 \end{bmatrix}$$

$$C_r = \begin{bmatrix} -178.1637 & 11.8465 & 0.9742 & -0.0891 \\ 0.0717 & 0.6160 & -0.7829 & 0.0570 \\ -300.6254 & 19.9892 & 1.6438 & -0.1504 \\ -0.0000 & 0.0000 & 0.0000 & -0.0000 \end{bmatrix}$$

$$D_r = \begin{bmatrix} --60.8574 & 0.2599 & -0.0000 & 0.4386 & 0.0000 \\ 0.0056 & -0.0000 & 1.0000 & 0.0000 & -0.0000 \\ -102.6880 & 0.4386 & 0.0000 & 0.7401 & 0.0000 \\ -0.0000 & 0.0000 & -0.0000 & 0.0000 & -0.0000 \end{bmatrix}$$

For the unknown input observer that detects the rear wheel speed sensor fault,

$$P = \begin{bmatrix} 18775.6157 & -1.3587 & -44271.4224 & 107.9244 & -1.7258 & -1.5188 \\ -1.3587 & 0.0001 & 3.4201 & -0.0080 & 0.0001 & 0.0001 \\ -44271.4207 & 3.4201 & 120294.7856 & -392.5539 & 4.4205 & 3.8564 \\ 107.9241 & -0.0080 & -392.5532 & 3.8499 & -0.0114 & -0.0094 \\ -1.7258 & 0.0001 & 4.4204 & -0.0114 & 0.0002 & 0.0002 \\ -1.5188 & 0.0001 & 3.8564 & -0.0094 & 0.0001 & 0.0001 \end{bmatrix}$$

$$L = \begin{bmatrix} -10047.3215 & 107.9244 & -222.1551 & -171.7619 \\ 0.0015 & -0.0080 & 0.0152 & 0.0113 \\ -27169.0369 & -392.5539 & 1138.7238 & 982.3336 \\ 344.2394 & 3.8499 & -17.1592 & -16.1408 \\ -0.2289 & -0.0114 & 0.0257 & 0.0204 \\ -0.0999 & -0.0094 & 0.0196 & 0.0151 \end{bmatrix}$$

$$\hat{H} = \begin{bmatrix} 0.0000 & 0.0000 & -0.0000 & -0.0000 \\ 0.0000 & 0.9774 & 0.1079 & 0.1023 \\ -0.0000 & 0.1079 & 0.4853 & -0.4880 \\ -0.0000 & 0.1023 & -0.4880 & 0.5374 \end{bmatrix}$$

The system matrices of the reduced-order unknown input observer that detects the rear wheel speed sensor fault are

$$A_r = \begin{bmatrix} -0.1545 & -0.2594 & -0.0831 & 0.0006 \\ 6.4215 & -35.6815 & 3.1008 & -0.0252 \\ -57.7884 & 1.6073 & -34.2507 & 0.2877 \\ 340.0360 & -252.9324 & 169.7429 & -1.6481 \end{bmatrix}$$

$$B_r = \begin{bmatrix} -0.0179 & -0.0000 & 0.0028 & -0.0010 & 0.0009 \\ -0.0108 & 0.0000 & 0.0000 & 0.0005 & 0.0006 \\ -0.4381 & 0.0000 & 0.0186 & -0.0110 & -0.0001 \\ -57.5668 & -0.0000 & 2.7229 & -1.3337 & 0.3131 \end{bmatrix}$$

$$C_r = \begin{bmatrix} 0.0000 & 0.0000 & 0.0000 & -0.0000 \\ -69.2553 & 0.3726 & -32.4236 & 0.1944 \\ -8.1664 & 150.6730 & -10.1719 & 0.0860 \\ -6.6996 & -158.8483 & 3.5600 & -0.0476 \end{bmatrix}$$

$$D_r = \begin{bmatrix} 0.0000 & 0.0000 & 0.0000 & -0.0000 \\ -69.2553 & 0.3726 & -32.4236 & 0.1944 \\ -8.1664 & 150.6730 & -10.1719 & 0.0859 \\ -6.6996 & -158.8483 & 3.5600 & -0.0476 \end{bmatrix}$$

B.7 Fault Detection Filter Set No. 1’

For the redesigned unknown input observer that detects the longitudinal accelerometer fault,

The fault directions are

$$F_{n_1} = \begin{bmatrix} 1 & 0 \\ 0 & 1 \\ 0 & 0 \\ 0 & 0 \\ 0 & 0 \\ 0 & 0 \\ 0 & 0 \\ 0 & 0 \\ 0 & 0 \\ 0 & 0 \\ 0 & 0 \\ 0 & 0 \\ 0 & 0 \end{bmatrix}, \quad F_{n_2} = \begin{bmatrix} 0 \\ 0 \\ 0 \\ 0 \\ 0 \\ 0 \\ 0 \\ 0 \\ 0 \\ 0 \\ 1 \\ 0 \\ 0 \end{bmatrix}, \quad F_{y_{w_e}} = \begin{bmatrix} 0 \\ 0 \\ 0 \\ 0 \\ 0 \\ 0 \\ 0 \\ 0 \\ 0 \\ 0 \\ 0 \\ 1 \\ 0 \end{bmatrix}, \quad F_{y_{a_x}} = \begin{bmatrix} 0 \\ 0 \\ 0 \\ 0 \\ 0 \\ 0 \\ 0 \\ 0 \\ 0 \\ 0 \\ 0 \\ 0 \\ 1 \end{bmatrix}$$

$$P = \left[\begin{array}{rrrrrrrrrrrrr}
517.3771 & 0.4986 & 0.0000 & 0.0000 & -0.0000 & 0.0000 & 0.0000 & -0.0000 & 0.0000 & 0.0000 & -0.0020 & 0.0035 & -0.0000 \\
0.4986 & 10172.7115 & -22.1266 & -33.2601 & 0.7575 & -1.5775 & -7.7329 & 3.5912 & -2.6146 & 0.0000 & -588.3614 & -9067.1113 & -0.0000 \\
0.0000 & -22.1266 & 0.0673 & 0.0608 & -0.0012 & 0.0030 & 0.0208 & -0.0061 & 0.0050 & -0.0000 & 1.5057 & 20.8433 & 0.0000 \\
0.0000 & -33.2601 & 0.0608 & 0.1427 & -0.0036 & 0.0065 & 0.0218 & -0.0162 & 0.0107 & -0.0000 & 1.9624 & 32.1731 & 0.0000 \\
-0.0000 & 0.7575 & -0.0012 & -0.0036 & 0.0001 & -0.0002 & -0.0004 & 0.0004 & -0.0003 & 0.0000 & -0.0447 & -0.7363 & -0.0000 \\
0.0000 & -1.5775 & 0.0030 & 0.0065 & -0.0002 & 0.0003 & 0.0011 & -0.0007 & 0.0005 & -0.0000 & 0.0931 & 1.5237 & 0.0000 \\
0.0000 & -7.7329 & 0.0208 & 0.0218 & -0.0004 & 0.0011 & 0.0076 & -0.0022 & 0.0018 & -0.0000 & 0.4563 & 7.3609 & 0.0000 \\
-0.0000 & 3.5912 & -0.0061 & -0.0162 & 0.0004 & -0.0007 & -0.0022 & 0.0019 & -0.0012 & 0.0000 & -0.2119 & -3.4824 & -0.0000 \\
0.0000 & -2.6146 & 0.0050 & 0.0107 & -0.0003 & 0.0005 & 0.0018 & -0.0012 & 0.0008 & -0.0000 & 0.1543 & 2.5237 & 0.0000 \\
0.0000 & -0.0000 & 0.0000 & 0.0000 & -0.0000 & 0.0000 & 0.0000 & -0.0000 & 0.0000 & 0.0000 & 0.0000 & 0.0000 & -0.0000 \\
-0.0020 & -588.3614 & 1.5057 & 1.9624 & -0.0447 & 0.0931 & 0.4563 & -0.2119 & 0.1543 & -0.0000 & 4506.6414 & 535.1276 & 0.0000 \\
0.0035 & -9067.1113 & 20.8433 & 32.1731 & -0.7363 & 1.5237 & 7.3609 & -3.4824 & 2.5237 & -0.0000 & 535.1276 & 998740.8566 & -0.0000 \\
0 & 0 & 0 & 0 & 0 & 0 & 0 & 0 & 0 & 0 & 0 & 0 & 0
\end{array}\right]$$

$$L = \begin{bmatrix} 9999.4557 & 0.0001 & 0.1273 & 2290.2008 & -0.0001 \\ 9.6361 & 0.1106 & 45.7446 & 3142966.8551 & 241.2583 \\ 0.0002 & -0.0001 & 0.9990 & 43.5684 & -0.4253 \\ 0.0002 & -0.0001 & -0.0003 & 62.6422 & -0.9757 \\ -0.0000 & 0.0000 & 0.0000 & -1.4150 & 0.0235 \\ 0.0000 & -0.0000 & -0.0000 & 2.9786 & -0.0458 \\ 0.0001 & -0.0000 & -0.0000 & 14.3553 & -0.1821 \\ -0.0000 & 0.0000 & 0.0000 & -6.7362 & 0.1086 \\ 0.0000 & -0.0000 & -0.0000 & 4.9422 & -0.0756 \\ 0.0000 & -0.0000 & -0.0000 & 0.0000 & -0.0000 \\ -0.0378 & -0.0053 & 22359.6217 & -5319.1705 & -12.9277 \\ 0.0671 & 98.9674 & 0.4417 & 15118.1258 & -234.1377 \\ 0 & 0 & 0 & 0 & 0 \end{bmatrix}$$

$$\hat{H} = \begin{bmatrix} 0 & 0 & 0 & 0 & 0 \\ 0 & -0.0000 & -0.0000 & -0.0000 & 0 \\ 0 & 0 & 0.0000 & -0.0000 & 0 \\ 0 & -0.0000 & -0.0000 & -0.0000 & 0 \\ 0 & 0 & 0 & 0 & 1.0000 \end{bmatrix}$$

The system matrices of the reduced-order unknown input observer that detects the longitudinal accelerometer fault are

$$A_r = \left[\begin{matrix} -19.5509 & 4.3863 & -1.4104 & -1.0042 & 0.3063 \\ -26.7579 & -0.1929 & 1.2247 & -0.6414 & 0.1392 \\ -290.1396 & -1.5247 & -23.31397 & -7.1116 & 2.7413 \\ 299.6871 & 84.5110 & 4.7030 & -2.8455 & 2.9147 \\ 262.8337 & -53.3404 & 52.2409 & 4.6176 & -6.7242 \\ 693.7508 & 277.7750 & -12.7216 & 10.1496 & 8.0912 \\ -576.1701 & -191.4395 & -4.6230 & -8.4284 & -5.2343 \\ 1233.6486 & 286.2598 & 45.7112 & 23.5827 & -2.4035 \\ -6.2362 & 47.5666 & -17.2031 & -0.9607 & 3.5865 \end{matrix} \right.$$

$$\left. \begin{matrix} -0.2919 & 0.1424 & 0.0085 & -0.0000 \\ -0.1158 & 0.0441 & 0.0015 & -0.0000 \\ -2.7874 & 1.4705 & 0.0971 & -0.0000 \\ -2.9201 & 1.4236 & 0.0839 & -0.0000 \\ 7.4792 & -4.2246 & -0.3096 & 0.0000 \\ -15.5154 & 11.6344 & 1.0537 & -0.0001 \\ 10.6074 & -10.1904 & -1.3603 & 0.0001 \\ 2.7809 & -0.9357 & -4.4433 & 0.0005 \\ -4.6237 & 3.2850 & 0.5849 & -1.2498 \end{matrix} \right]$$

$$B_r = \begin{bmatrix} 0.0000 & -0.0000 & 0.0000 & 0.0000 & -0.0004 & -0.0031 & 0.0042 \\ -0.0000 & 0.0000 & -0.0000 & -0.0000 & -0.0005 & -0.0200 & -0.0148 \\ 0.0000 & -0.0000 & 0.0000 & 0.0000 & 0.1292 & 0.1250 & 0.0569 \\ -0.0000 & 0.0000 & -0.0001 & -0.0000 & 0.0991 & -0.2435 & -0.1667 \\ -0.0000 & 0.0001 & -0.0002 & -0.0000 & 0.9266 & 0.0735 & -0.2972 \\ -0.0000 & 0.0000 & -0.0001 & 0.0000 & -0.1001 & -0.3536 & -0.3245 \\ 0.0000 & -0.0002 & 0.0001 & -0.0000 & -0.3109 & 0.3072 & 0.2947 \\ -0.0000 & 0.0005 & -0.0003 & -0.0000 & 0.0904 & 0.1635 & -0.9424 \\ -0.0000 & -1.2500 & -0.0000 & 0.0030 & 0.0002 & -0.0683 & -0.0076 \end{bmatrix}$$

$$C_r = \left[\begin{matrix} 0 & 0 & 0 & 0 & 0 \\ 0.0000 & -0.0000 & 0.0000 & 0.0000 & -0.0000 \\ -0.0000 & 0.0000 & -0.0000 & -0.0000 & 0.0000 \\ 0.0000 & -0.0000 & 0.0000 & 0.0000 & -0.0000 \\ -1056.9562 & -50.9139 & -112.1932 & -15.3710 & 10.1939 \end{matrix} \right.$$

$$\left. \begin{matrix} 0 & 0 & 0 & 0 \\ 0.0000 & -0.0000 & -0.0000 & -0.0000 \\ -0.0000 & 0.0000 & 0.0000 & 0.0000 \\ 0.0000 & -0.0000 & -0.0000 & -0.0000 \\ -6.8800 & 3.5132 & 0.2362 & -0.0000 \end{matrix} \right]$$

$$D_r = \begin{bmatrix} 0 & 0 & 0 & 0 & 0 & 0 & 0 \\ 0 & 0 & 0 & -0.0000 & -0.0000 & -0.0000 & 0 \\ 0 & 0 & 0 & 0 & 0.0000 & -0.0000 & 0 \\ 0 & 0 & 0 & -0.0000 & -0.0000 & -0.0000 & 0 \\ 0 & 0 & 0 & 0 & 0 & 0 & 1.0000 \end{bmatrix}$$

B.8 Fault Detection Filter Set No. 3'

The reduced-order longitudinal model derived when the vehicle is traveling at 24 m/s with modified dynamical equation for brake state is

$$\dot{x} = Ax + Bu$$
$$y = Cx$$

where

$$
A = \left[\begin{matrix}
-10.4692 & -0.1177 & 0 & 0 & 0 \\
327.7406 & -53.2410 & 552.4915 & -0.7238 & -44121.7763 \\
0 & 0.0550 & -0.5721 & 0.0007 & 43.3440 \\
0 & -0.0001 & 0.0007 & -0.0000 & -448.3575 \\
0 & 0 & 0.0013 & 1.0000 & 0 \\
0 & 0 & 0 & 0 & 0 \\
0 & -0.0263 & 0.2684 & -0.0004 & -114.1535 \\
0 & 0 & 0 & 0 & 66.3436 \\
0 & 0 & 0 & 0 & 48.6827 \\
0 & 0 & 0 & 0 & 0
\end{matrix}\right.
$$

$$
\left.\begin{matrix}
0 & 0 & 0 & 0 & 0 \\
46710.0274 & -278.9203 & 22058.6614 & 0 & -0.0672 \\
-46.7168 & 0.3150 & -21.8174 & 0.1475 & -0.0019 \\
-155.8232 & 23.9996 & 112.0991 & 112.0787 & 0.0000 \\
-24.0000 & 0 & 0 & 0 & 0 \\
0 & 1.0000 & 0 & 0 & 0 \\
-536.7500 & -0.1355 & -60.2901 & 117.3615 & 0.0009 \\
-70.2379 & 0 & -39.2621 & 0 & 0 \\
85.4543 & 0 & 0 & -32.6411 & 0 \\
0 & 0 & 0 & 0 & -10.0000
\end{matrix}\right]
$$

$$
B = \begin{bmatrix}
2.6100 & 0 \\
0 & 0 \\
0 & 0 \\
0 & 0 \\
0 & 0 \\
0 & 0 \\
0 & 0 \\
0 & 0 \\
0 & 0 \\
0 & 10.0000
\end{bmatrix}
$$

$$
C = \left[\begin{matrix}
19.3272 & 0 & 0 & 0 & 0 \\
0 & 1.0000 & 0 & 0 & 0 \\
0 & 0.0550 & -0.5721 & 0.0007 & 43.3440 \\
0 & 0.0456 & 6.2989 & -0.0083 & -503.0252 \\
0 & 0 & 6.5316 & -0.0086 & -511.6989
\end{matrix}\right.
$$

$$
\left.\begin{matrix}
0 & 0 & 0 & 0 & 0 \\
0 & 0 & 0 & 0 & 0 \\
-46.7168 & 0.3150 & -21.8174 & 0.1238 & -0.0019 \\
532.5334 & -3.1799 & 251.4872 & 0 & -0.0008 \\
-898.2125 & -3.2312 & 0 & 255.8137 & -0.0013
\end{matrix}\right]
$$

The actuator fault directions are

$$F_{u_\alpha} = \begin{bmatrix} 2.6100 \\ 0 \\ 0 \\ 0 \\ 0 \\ 0 \\ 0 \\ 0 \\ 0 \\ 0 \end{bmatrix}, \quad F_{u_{T_b}} = \begin{bmatrix} 0 \\ 0 \\ 0 \\ 0 \\ 0 \\ 0 \\ 0 \\ 0 \\ 0 \\ 10.0000 \end{bmatrix}$$

The sensor fault directions are

$$F_{y_{mp}} = \begin{bmatrix} 0.0517 & -0.5417 \\ 0 & 16.9575 \\ 0 & 0 \\ 0 & 0 \\ 0 & 0 \\ 0 & 0 \\ 0 & 0 \\ 0 & 0 \\ 0 & 0 \\ 0 & 0 \end{bmatrix}, F_{y_{we}} = \begin{bmatrix} 0 & -0.1177 \\ 1.0000 & -57.2411 \\ 0.6802 & -0.0000 \\ -0.0006 & -29.3339 \\ 0.0131 & 0.0031 \\ -0.0001 & -0.9488 \\ -0.9488 & -1.4008 \\ -0.0027 & 0.9856 \\ -0.0035 & 0.7435 \\ 0.0452 & -0.4515 \end{bmatrix}, F_{y_{ax}} = \begin{bmatrix} 0 & 0.0000 \\ -0.0000 & 0.0000 \\ -11.5368 & 1.0000 \\ 0.0096 & 497.1906 \\ -0.2217 & -0.0415 \\ 0.0015 & 16.0924 \\ 16.0925 & 23.4975 \\ 0.0458 & -16.6123 \\ 0.0596 & -12.6107 \\ -0.7659 & 7.6585 \end{bmatrix}$$

The modified brake actuator fault direction is

$$F_{u_{T_b}} = \begin{bmatrix} 0 & 0 \\ 0 & -0.0672 \\ 0 & -0.0019 \\ 0 & 0.0000 \\ 0 & 0 \\ 0 & 0 \\ 0 & 0.0009 \\ 0 & 0 \\ 0 & 0 \\ 10.0000 & 0 \end{bmatrix}$$

For the unknown input observer that detects the brake actuator fault designed using the linear model with modified dynamical equation for brake state,

$$P = \left[\begin{array}{rrrrr} 3029.8460 & 13098.0031 & 39.2427 & -18.3812 & 1.5599 \\ 13098.0030 & 125187.7641 & 574.8844 & -558.5685 & -46.0205 \\ 39.2427 & 574.8844 & 32.5714 & -4.3349 & 0.4952 \\ -18.3812 & -558.5685 & -4.3349 & 382.2027 & 39.5097 \\ 1.5599 & -46.0205 & 0.4952 & 39.5097 & 4.3184 \\ -0.8136 & 13.9658 & -0.0257 & -22.8439 & -2.4349 \\ -2.2580 & -1166.7878 & 4.8896 & 1098.4626 & 117.2042 \\ 3.3723 & -31.7878 & 0.8587 & 21.8940 & 2.5604 \\ -1.7024 & 195.6650 & -0.5278 & -222.7192 & -23.6436 \\ -0.3362 & 14.4783 & 1.24950 & -11.4279 & -1.1264 \end{array} \right.$$

$$\left. \begin{array}{rrrrr} -0.8136 & -2.2580 & 3.3723 & -1.7024 & -0.3360 \\ 13.9658 & -1166.7878 & -31.7878 & 195.6650 & 14.4800 \\ -0.0258 & 4.8896 & 0.8587 & -0.5278 & 1.2495 \\ -22.8439 & 1098.4626 & 21.8940 & -222.7192 & -11.4279 \\ -2.4349 & 117.2042 & 2.5604 & -23.6436 & -1.1264 \\ 1.4098 & -67.1895 & -1.3964 & 13.6227 & 0.6469 \\ -67.1895 & 3224.9157 & 67.3384 & -652.5464 & -32.0163 \\ -1.3964 & 67.3384 & 1.6460 & -13.4906 & -0.5830 \\ 13.6227 & -652.5464 & -13.4906 & 132.1769 & 6.4332 \\ 0.6469 & -32.0163 & -0.5830 & 6.4332 & -7499.6938 \end{array} \right]$$

$$L = \left[\begin{array}{rrrrr} 0.0015 & 0.3275 & 0.0182 & 0.2410 & -0.1196 \\ 0.0063 & 3.1297 & 0.1066 & 17.8188 & 34.2939 \\ 0.0000 & 0.0144 & 0.0005 & 0.0845 & -0.0842 \\ -0.0000 & -0.0140 & 0.0647 & -15.0412 & -30.1270 \\ 0.0000 & -0.0012 & 0.0069 & -1.5985 & -3.2234 \\ -0.0000 & 0.0003 & -0.0040 & 0.9194 & 1.8408 \\ -0.0000 & -0.0292 & 0.1901 & -44.0445 & -88.4754 \\ 0.0000 & -0.0008 & 0.0039 & -0.9140 & -1.8596 \\ -0.0000 & 0.0049 & -0.0386 & 8.9188 & 17.8910 \\ -0.0000 & 0.0004 & -0.0015 & 0.4403 & 0.8811 \end{array} \right]$$

$$\hat{H} = \left[\begin{array}{rrrrr} 0 & -0.0000 & -0.0000 & 0.0000 & 0.0000 \\ -0.0000 & 0.0048 & -0.0554 & -0.0373 & 0.0162 \\ -0.0000 & -0.0554 & 0.9954 & 0.0153 & 0.0357 \\ -0.0000 & -0.0373 & 0.0153 & 0.7992 & -0.3986 \\ -0.0000 & 0.0162 & 0.0357 & -0.3986 & 0.2007 \end{array} \right]$$

The system matrices of the reduced-order unknown input observer that detects the brake actuator fault are

$$A_r = \begin{bmatrix} -0.6173 & 1.6771 & 0.9911 & -0.7484 & 0.8287 \\ -1.9168 & -4.8550 & -4.9491 & 7.0811 & -4.3788 \\ 0.5425 & 6.6218 & -8.3009 & 5.8250 & -8.8322 \\ -0.4944 & -3.8323 & -9.4218 & -12.5601 & 10.2690 \\ 0.2643 & 1.3993 & 8.1516 & 16.5017 & -26.5402 \\ 0.1554 & 0.8923 & -0.1307 & 3.6062 & -10.6877 \\ 0.0561 & 0.3551 & -0.5282 & 0.2861 & -0.0154 \\ 0.0685 & 0.4335 & -0.6502 & 0.3543 & -0.1194 \\ 0.0007 & -0.0010 & 0.0918 & 0.1892 & -0.5395 \end{matrix}$$

$$\begin{matrix} -0.1728 & 0.0587 & -0.0713 & 0.0086 \\ 0.8304 & -0.3106 & 0.3922 & -0.0481 \\ 1.7406 & -0.5371 & 0.6211 & -0.0737 \\ -3.1357 & 1.0962 & -1.4045 & 0.1729 \\ 13.2808 & -3.7502 & 4.5709 & -0.5536 \\ -5.2437 & 3.8582 & -4.2631 & 0.5214 \\ -2.9807 & -5.9883 & 17.1450 & -1.7760 \\ -3.0900 & -17.1675 & -60.9010 & 14.6327 \\ -0.2726 & 0.4117 & 2.4421 & -14.6185 \end{bmatrix}$$

$$B_r = \begin{bmatrix} -1.5314 & 0.0770 & -0.0018 & -0.8848 & -0.0338 & -3.9863 & 5.7606 \\ -2.1386 & 0.1082 & -0.0021 & -0.7426 & -0.0278 & -3.7044 & -19.6021 \\ 0.9830 & -0.1145 & -0.0001 & -0.2975 & 0.0045 & -5.0506 & -14.3739 \\ -3.9311 & -0.0265 & -0.0027 & -0.5007 & -0.0502 & 4.7696 & 9.2081 \\ -3.0635 & 0.0338 & -0.0009 & -1.3081 & 0.0242 & -23.3705 & -77.8112 \\ 5.2283 & -0.0048 & 0.0034 & 0.5248 & 0.0604 & -6.7955 & -11.9278 \\ -2.8043 & -0.0046 & -0.0026 & -0.6927 & -0.0339 & -1.5568 & 2.3557 \\ -4.6428 & -0.0057 & 0.0004 & 1.1522 & 0.0076 & 13.8596 & 33.9203 \\ 11.1815 & 0.0005 & 0.0058 & 1.2087 & 0.0714 & -0.0712 & -3.6028 \end{bmatrix}$$

$$C_r = \begin{bmatrix} 0.0000 & 0.0000 & -0.0000 & 0.0000 & -0.0000 \\ 0.0049 & -0.0006 & -0.0080 & -0.0004 & -0.0031 \\ -0.0064 & -0.0758 & 0.0791 & 0.0605 & 0.0005 \\ -0.0990 & 0.1056 & 0.0805 & -0.0638 & 0.0668 \\ 0.0492 & -0.0560 & -0.0368 & 0.0345 & -0.0333 \end{matrix}$$

$$\begin{matrix} -0.0000 & -0.0000 & -0.0000 & -0.0000 \\ 0.0007 & -0.0002 & 0.0002 & -0.0000 \\ -0.0014 & -0.0001 & 0.0005 & -0.0001 \\ -0.0138 & 0.0047 & -0.0057 & 0.0007 \\ 0.0068 & -0.0024 & 0.0029 & -0.0004 \end{bmatrix}$$

$$D_r = \begin{bmatrix} -0.0000 & -0.0000 & -0.0000 & 0.0000 & -0.0000 & 0.0000 & 0.0000 \\ 0.0000 & 0.0000 & 0.0000 & -0.0000 & 0.0000 & -0.0000 & -0.0000 \\ 0.0000 & 0.0000 & 0.0000 & -0.0000 & 0.0000 & -0.0000 & -0.0000 \\ -0.0000 & -0.0000 & -0.0000 & 0.0000 & -0.0000 & 0.0000 & 0.000 \\ 0.0000 & 0.0000 & 0.0000 & -0.0000 & 0.0000 & -0.0000 & -0.0000 \end{bmatrix}$$

Bibliography

Beard, R. V. (1971). *Failure Accomodation in Linear Systems through Self-Reorganization*, Ph.D. thesis, Massachusetts Institute of Technology.

Bell, D. J. and D. H. Jacobson (1975). *Singular Optimal Control Problems*, Academic Press.

Brinsmead, T. S., J. S. Gibson, G. C. Goodwin, G. H. Lee, and D. L. Mingori (1997). "Fault detection: A quadratic optimization approach," in *Proceedings of the 36th IEEE Conference on Decision and Control*, pp. 3970–3975.

Chen, C.-T. (1984). *Linear system theory and design*, Holt, Rinehart, and Winston.

Chen, R. H. (2000). *Fault Detection Filters for Robust Analytical Redundancy*, Ph.D. thesis, University of California at Los Angeles.

Chen, R. H., D. L. Mingori, and J. L. Speyer (2002). "Optimal stochastic fault detection filter," *Automatica*, **39**, pp. 377–390.

Chen, R. H. and J. L. Speyer (1999a). "Optimal stochastic fault detection filter," in *Proceedings of the American Control Conference*, pp. 91–96.

Chen, R. H. and J. L. Speyer (1999b). "Residual-sensitive fault detection filter," in *Proceedings of the 7th IEEE Mediterranean Conference on Control and Automation*, pp. 835–851.

Chen, R. H. and J. L. Speyer (2000). "A generalized least-squares fault detection filter," *International Journal of Adaptive Control and Signal Processing - Special Issue: Fault Detection and Isolation*, **14**, no. 7, pp. 747–757.

Chen, R. H. and J. L. Speyer (2002). "Robust multiple-fault detection filter," *The special issue of condition monitoring, fault detection and isolation in the International Journal of Robust and Nonlinear Control*, **12**, no. 8, pp. 377–390.

Chung, W. H. and J. L. Speyer (1998). "A game theoretic fault detection filter," *IEEE Transactions on Automatic Control*, **AC-43**, no. 2, pp. 143–161.

Douglas, R. K. (1993). *Robust Fault Detection Filter Design*, Ph.D. thesis, The University of Texas at Austin.

Douglas, R. K., R. H. Chen, and J. L. Speyer (2004). "Linear system input-order reduction by hankel norm maximization," *AIAA Journal of Guidance, Control, and Dynamics*, **27**, no. 1.

Douglas, R. K., W. H. Chung, D. P. Malladi, R. H. Chen, J. L. Speyer, and D. L. Mingori (1997). *Integration of Fault Detection and Identification into a Fault Tolerant Automated Highway System*, California PATH Research Report UCB-ITS-PRR-97-52.

Douglas, R. K. and J. L. Speyer (1996). "Robust fault detection filter design," *AIAA Journal of Guidance, Control, and Dynamics*, **19**, no. 1, pp. 214–218.

Douglas, R. K. and J. L. Speyer (1999). "$\mathcal{H}_\infty$ bounded fault detection filter," *AIAA Journal of Guidance, Control, and Dynamics*, **22**, no. 1, pp. 129–138.

Douglas, R. K., J. L. Speyer, D. L. Mingori, R. H. Chen, D. P. Malladi, and W. H. Chung (1996). *Fault Detection and Identification with Application to Advanced Vehicle Control Systems*, California PATH Research Report UCB-ITS-PRR-96-25.

Frank, P. M. (1990). "Fault diagnosis in dynamic systems using analytical and knowledge-based redundancy - a survey and some new results," *Automatica*, **26**, no. 3, pp. 459–474.

Jones, H. L. (1973). *Failure Detection in Linear Systems*, Ph.D. thesis, Massachusetts Institute of Technology.

Kwakernaak, H. (1976). "Asymptotic root loci of multivariable linear optimal regulators," *IEEE Transactions on Automatic Control*, **AC-21**, no. 3, pp. 378–382.

Kwakernaak, H. and R. Sivan (1972a). *Linear Optimal Control Systems*, Wiley-Interscience.

Kwakernaak, H. and R. Sivan (1972b). "The maximally achievable accuracy of linear optimal regulators and linear optimal filters," *IEEE Transactions on Automatic Control*, **AC-17**, no. 1, pp. 79–86.

Lee, G. H. (1994). *Least-Squares and Minimax Methods for Filtering, Identification and Detection*, Ph.D. thesis, University of California at Los Angeles.

Malladi, D. P. and J. L. Speyer (1999). "A generalized shiryayev sequential probability ratio test for change detection and isolation," *IEEE Transactions on Automatic Control*, **AC-44**, no. 8, pp. 1522–1534.

Massoumnia, M.-A. (1986). "A geometric approach to the synthesis of failure detection filters," *IEEE Transactions on Automatic Control*, **AC-31**, no. 9, pp. 839–846.

Massoumnia, M.-A., G. C. Verghese, and A. S. Willsky (1989). "Failure detection and identification," *IEEE Transactions on Automatic Control*, **AC-34**, no. 3, pp. 316–321.

Moore, B. C. (1981). "Principal component analysis in linear systems: Controllability, observability, and model reduction," *IEEE Transactions on Automatic Control*, **AC-26**, no. 1, pp. 17–32.

Moylan, P. J. and J. B. Moore (1971). "Generalizations of singular optimal control theory," *Automatica*, **7**, no. 5, pp. 591–598.

Nayfeh, A. H. (1973). *Perturbation Methods*, Wiley-Interscience.

Patton, R. J. and J. Chen (1992). "Robust fault detection of jet engine sensor systems using eigenstructure assignment," *AIAA Journal of Guidance, Control, and Dynamics*, **15**, no. 6, pp. 1491–1497.

Prakash, R. (1994). "Properties of a low-frequency approximation balancing method of model reduction," *IEEE Transactions on Automatic Control*, **AC-39**, no. 5, pp. 1135–1141.

Shiryayev, A. N. (1977). *Optimal Stopping Rules*, Springer-Verlag.

Speyer, J. L. (1986). "Linear-quadratic control problem," *Control and Dynamic Systems*, **13**, pp. 241–293. Edit by C.T. Leondes, Academic Press.

Speyer, J. L. and J. E. White (1984). "Shiryayev sequential probability ratio test for redundancy management," *AIAA Journal of Guidance, Control, and Dynamics*, **7**, no. 5, pp. 588–595.

White, J. E. and J. L. Speyer (1987). "Detection filter design: Spectral theory and algorithms," *IEEE Transactions on Automatic Control*, **AC-32**, no. 7, pp. 593–603.

Wonham, W. M. (1985). *Linear Multivariable Control: A Geometric Approach*, Springer-Verlag.